Improvement of breast cancer diagnosis through microfluidics

THÈSE N° 8459 (2018)

PRÉSENTÉE LE 20 AVRIL 2018
À LA FACULTÉ DES SCIENCES ET TECHNIQUES DE L'INGÉNIEUR
LABORATOIRE DE MICROSYSTÈMES 2
PROGRAMME DOCTORAL EN MICROSYSTÈMES ET MICROÉLECTRONIQUE

ÉCOLE POLYTECHNIQUE FÉDÉRALE DE LAUSANNE

POUR L'OBTENTION DU GRADE DE DOCTEUR ÈS SCIENCES

PAR

Huu Tuan NGUYEN

acceptée sur proposition du jury:

Prof. L. G. Villanueva Torrijo, président du jury
Prof. M. Gijs, directeur de thèse
Prof. E. Laurenceau, rapporteuse
Dr A. T. Ciftlik, rapporteur
Dr J. Sordet-Dessimoz, rapporteuse

ÉCOLE POLYTECHNIQUE
FÉDÉRALE DE LAUSANNE

Suisse
2018

Acknowledgment

Doing research at the laboratory of microsystem 2 in EPFL was one of the best experiences in my life. I received here unconditional supports from professor Martin Gijs and other colleagues who helped me grow up intellectually and personally. Therefore, I would like to express sincere gratitude to them, in particular my supervisor Prof. Gijs. He is a brilliant scientist with a strong critical thinking and a true leader with a deterministic vision. I learnt from him to express my ideas more clearly and simply. More than that, he is a teacher and a motivator. During the most difficult time in my 2nd year of PhD, Martin did not give me any pressure for the results but instead he brought me smiles and encouragements. Our close student-professor relationship passed a wonderful moment when Martin and his family attended my wedding. I was very lucky to be his student.

I also would like to thank the jury members: Dr. Ata Tuna Ciftlik, Dr. Jessica Sordet-Dessimoz, Prof. Emmanuelle Laurenceau for reading and evaluating my thesis, and Prof. Luis Guillermo Villanueva for accepting to be the president of the jury. Finally, I acknowledge European Research Council for funding my research.

I would like to thank all my co-authors. The difficulty at the beginning of my thesis could not be surpassed if I did not get precious help from Dr. Raphaël Trouillon. Thanks to his vast experience and knowledge in several fields of science, he trained young scientists like me to perform research rigorously. His mentorship assisted me throughout my research mission at EPFL. I would like to thank him very much and wish him all the best for his scientific career. I thank again Dr. Ciftlik for introducing me to the microfluidic system created by him, giving me some initial ideas to develop new applications from the existing system. I also thank Prof. Emmanuelle Laurenceau (again) and Yann Chevolot from the Institute of Nanotechnology of Lyon for performing a joint-project with me and revise our manuscripts. I also thank Dr. Bettina Bisig and Prof. Laurence de Leval from the Institute of Pathology in Lausanne for stimulating scientific discussion during our collaboration and revising our manuscripts. My special thanks go to my students Seiya Matsuoka, Laurène Dupont, Léa Bernier, Estelle Cuttaz and Antoine Jean, also my colleague Daniel Migliozzi for their important experimental contributions. We learned, worked but also enjoyed a good time together.

I am grateful to work with my colleagues of LMIS2. I would like to thank Melis for her help in my endless paperwork requests and Dr. Abdeljalil Sayah for his unwavering supports for my teaching assistantship. Many thanks go to my lab-mates Christina, Li, Roger, Matteo, Yang, Xiaopeng, Baris, Vittorio, Fabien, Diego, Gergely, Rima for joyful discussions during lunch times and lab trips. My colleagues made my life more colorful and enjoyable. The most remarkable moment was when I host Cristina and her boyfriend Luca, Raphaël and his wife Melissa during my wedding time in Viet Nam. I will never forget that wonderful moment. Finally, I also thank experienced researchers in our lab such as Thomas, Hui, Axel, Virendra for their scientific advices and staffs in the CMI and the BIOP for their support during my stay.

I would like to thanks all Vietnamese association in Lausanne (VNLausanne) members: Manh Tinh, Hieu, Thanh, Khanh, Minh, Thu, Bang, Viet Anh, Dat, Khoa, Kim and many others, with whom I worked with to organize associative activities and leisure trips. I also thank Linh Phong association who accepted me as a part of the big family and taught me a lot about sharing and meditation. I would like to thank my friends: Thinh, Khoa, Cuong, Elise, Emile, Margot and many others for their emotional supports throughout my studies. Last but not least, my deepest gratitude to my family: my wife Khanh, my parents Lien and Manh

and my brother Thanh for their unconditional support and encouragement during my PhD. My wife Khanh had to live alone in the USA during her pregnancy, so that I could finalize my works in Switzerland. Fortunately, I could assist her on the due day and her effort was finally recompensed as we welcome now the newest member of our family, Alex. I owe her a very big "thank you" for all happiness she brings to my life.

Huu Tuan Nguyen,

Worcester, USA, 30th March 2018

Abstract

In breast cancer, 15-20% of cases are reported with overexpression of human epidermal growth factor receptor 2 (HER2) that causes rapid cancer progression and poor prognosis. Fortunately, HER2-targeted therapy using specific antibodies such as Trastuzumab is effective for treating these cases. In situ hybridization (ISH) is a standard technique used for HER2 assessment. This technique locates the *HER2* gene by using complementary DNA probes. Two main ISH methods are fluorescence in situ hybridization (FISH) and chromogenic in situ hybridization (CISH). However, both FISH and CISH are expensive and laborious. Moreover, they can only be assessed in a small area of the tissue and thus are prone to errors in case of HER2 intra-tumoral heterogeneity (ITH). This thesis aims to improve HER2 assessment in breast cancer through various techniques related to microfluidics. The main component of our technology is a microfluidic tissue processor. This micro-fabricated chip is clamped to a microscope slide carrying a human tissue slice, creating a chamber that accommodates the tissue and delivering reagents to stain it. Five applications of this microfluidic technology to breast cancer diagnostics are presented in the three chapters of this thesis. In chapter 1, we present a microfluidic FISH protocol for *HER2* gene assessment using a standard FISH probe and demonstrate that, when applying an oscillatory flow within the chip, hybridization efficiency is increased thanks to molecular replenishment. This back-and-forth motion of the diluted FISH probe inside a thin chamber above the tissue slide is the principle of microfluidic-assistance for ISH. We thereby succeed in drastically reducing the experimental time from 2 days to 1, and the amount of the expensive probe used per test by a factor of 10. We highlight the performance and reliability of microfluidic-assistance FISH by comparing the FISH scores obtained by this method to standard FISH technique scores using several clinical tissue samples. The principle of microfluidic assistance in FISH is also applicable to other types of ISH probes, including fast FISH based on Ethylene Carbonate and CISH. In chapter 2, we describe a new microfluidic method allowing the quantification of HER2 expression levels from formalin-fixed breast cancer tissues. After partial extraction of proteins from the tissue slide, the extract is routed to an antibody microarray for HER2 titration by fluorescence. HER2-negative and positive samples can be distinguished using this simple test, and the obtained results agree with the FISH scores. In chapter 3, we establish a method allowing high content, cell-by-cell analysis of both protein overexpression and gene amplification using successive microfluidic immunofluorescence (IF) and FISH staining combined with image processing. We demonstrate that by using high-content automatic analysis, the HER2 status of the sample can be precisely assessed using both a quantitative IF technique based on HER2 and cytokeratin protein quantification and automatic scoring of *HER2* loci and centromere of chromosome 17 signals in a FISH image. Furthermore, this method characterizes HER2 ITH quantitatively. In particular, heterogeneous clusters and individual cells are visualized in a reconstructed map of the tissue. We conclude that high-content IF/FISH analysis is a powerful tool that can assist clinical diagnostics in the future.

Key words: Breast cancer, fluorescence in situ hybridization (FISH), chromogenic in situ hybridization (CISH), immunofluorescence (IF), human epidermal growth factor receptor - 2 (HER2), protein microarrays, microfluidics, tissue slides, protein extraction, tissue biomarkers, HER2 assessment, intratumoral heterogeneity, automatic analysis, high-content analysis.

Version abrégée

15 à 20% des cas du cancer du sein sont associés à une surexpression du récepteur 2 pour les facteurs de croissance épidermiques humains (HER2) qui induit une progression rapide du cancer et un mauvais pronostic. Heureusement, la thérapie HER2-ciblée utilisant des anticorps spécifiques tels que le Trastuzumab est efficace pour traiter ces cas. L'hybridation in situ (ISH) est une technique conventionnelle utilisée pour l'évaluation de HER2. Cette technique localise le gène *HER2* en utilisant des sondes d'ADN complémentaires. Les deux principales méthodes d'ISH sont l'hybridation in situ en fluorescence (FISH) et l'hybridation chromogénique in situ (CISH). Cependant, FISH et CISH sont des méthodes onéreuses et longues. De plus, elles ne peuvent être utilisées que sur une petite zone de l'échantillon et sont donc sujettes à des erreurs en cas d'hétérogénéité intra-tumorale (HIT). Cette thèse vise à améliorer l'évaluation de HER2 dans le cancer du sein à travers différentes techniques basées sur la microfluidique. Nous utilisons une puce microfluidique de traitement du tissu qui est montée sur une lame de microscope portant une coupe de tissu humain pour créer une chambre qui contient l'échantillon et délivrer des réactifs pour le marquer. Dans le chapitre 1, nous présentons un protocole de FISH microfluidique pour l'évaluation du gène *HER2* à l'aide d'une sonde de FISH conventionnelle et démontrons qu'en utilisant un flux oscillant créé par la puce, l'efficacité d'hybridation augmente grâce aux réapprovisionnements moléculaires. Nous avons ainsi réussi à réduire drastiquement le temps d'expérimentation de 2 jours à 1, et la quantité de la sonde utilisée par test d'un facteur de 10. Nous mettons en évidence la performance et la fiabilité du FISH microfluidique en le comparant avec le FISH conventionnel sur 17 échantillons de tissus humains. Ce principe d'assistance microfluidique est ensuite utilisé pour étudier une sonde HER2 FISH à réaction rapide basée sur des solutions tampons de carbonate d'éthylène et une sonde HER2 CISH. Dans le chapitre 2, nous mettons en œuvre une nouvelle méthode pour quantifier des protéines HER2 dans des lames de tissu. En appliquant une incubation à haute température sur le tissu dans une solution à base de détergent, nous extrayons les protéines solubles dans le tissu et les détectons sur puce de protéines HER2 en les acheminant dans une seconde puce dans laquelle sont placées des sondes d'anticorps immobilisées capturant des protéines HER2. Enfin, nous démontrons que des échantillons HER2 négatifs et positifs peuvent être distingués en utilisant ce simple test, et les résultats obtenus sont en accord avec des scores de FISH. Dans le chapitre 3, nous développons une analyse HER2 à haute densité pour caractériser à la fois la surexpression de la protéine HER2 et l'amplification du gène *HER2* dans une lame entière. Nous démontrons le statut HER2 de l'échantillon peut être évalué avec précision en utilisant d'une part une technique immunofluorescence (IF) quantitative basée sur la quantification des protéines HER2 et de la cytokératine et d'autre part le comptage automatique des loci de *HER2* et des centromères du chromosome 17 dans une image de FISH. De plus, cette méthode caractérise quantitativement l'HIT de HER2. En particulier, des clusters hétérogènes et des cellules individuelles sont visualisés par une image reconstruite du tissu en utilisant des indicateurs locaux d'association spatiale.

Mots clés: Cancer du sein, hybridation in situ à fluorescence (FISH), hybridation chromogénique in situ (CISH), immunofluorescence (IF), récepteur du facteur de croissance épidermique humain 2 (HER2), biopuces à protéine, microfluidiques, lames tissulaires, extraction de protéines, cancer biomarqueurs tissulaires, évaluation HER2, hétérogénéité intratumorale, analyse automatique, analyse à haute densité.

Table of content

List of figures

hybridization steps (t_h). (b) Optimization of the diameter for HER2 (in red) and CEN17 (in green) signals. The plot shows linear regression coefficients of the HER2 and CEN17 signal diameter, corresponding to the same 7 parameters as (a). From our analysis, we find as optimal condition: post-fixation step present, discontinuous flow, 4× dilution, no denaturation ($t_d = t_h = 45°C$), 12 µl probe volume and 35-minute hybridization._____75

Figure 2.14 - Comparison of ESIMA-FISH and standard IQ-FISH (a) Deconvoluted z-stack (0.2 µm-step) from an ESIMA-FISH-treated tissue slide. (b) Deconvoluted z-stack (0.2 µm-step) from a standard IQ-FISH-treated tissue slide adjacent to that in (b). The HER2 signal obtained from ESIMA-FISH tends to have a weaker intensity than that of the standard IQ-FISH technique. The images were acquired using a fluorescence microscope with a 63× objective. Scale bars: 5 µm. _____76

Figure 2.15 - Comparison of standard IQ FISH, ESIMA-FISH and "off-chip" IQ FISH obtained from a cell line slide (SKBR3). Standard IQ FISH (non-diluted probe and 1h hybridization) and off-chip IQ FISH (8× diluted probe and 15 minute hybridization) were performed using the coverslip technique (see the standard IQ FISH protocol in section 2.2.4.2). ESIMA-FISH and off-chip IQ FISH were implemented using the same probe concentration (8×) and hybridization time (15 min). (a) Image of a single focal plane of: (ai) an off-chip IQ FISH image stack (aii) an ESIMA-FISH image stack and (aiii) a standard IQ FISH image stack. Scale bar: 10 µm. (b) Quantitative analysis of HER2 signal in standard IQ FISH, ESIMA-FISH and "off-chip" IQ FISH images shown in (a): (bi) Contrast measurements (bii) Diameter measurements. The datasets were compared using an ANOVA test followed by a Tukey multiple comparison test:* for $p<0.05$, ** for $p<0.01$, *** for $p<0.001$._____77

Figure 2.16 - Comparison between ESIMA-FISH and standard IQ-FISH obtained from 2 adjacent tissue slides. Two adjacent slides from the same breast cancer sample were processed with ESIMA-FISH (4× diluted, 35 min incubation) and the standard IQ-FISH protocol, respectively, after which they were imaged using the same exposition conditions and then assessed using an automatic image processing routine. (a) Contrast of the red and green signal (dots) from two methods. (b) Diameter comparison of red and green signals from the two FISH methods. The red signal diameter of ESIMA-FISH is strongly decreased in comparison to the standard method. However, this did not affect the interpretation of the signal. The different datasets (ESIMA-FISH vs. standard IQ-FISH) were compared using a Student's t-test: * for $p <0.05$; ** for $p <0.01$;*** for $p <0.001$._____78

Figure 2.17 - Comparison between ESIMA-FISH and standard IQ-FISH on human tissue slides. (a) Plots of *HER2* copies per cell (*HER2*/cell) obtained by ESIMA-FISH *versus* standard IQ-FISH in a set of clinical breast cancer samples with *HER2*/cell ranging (ai) from 0 to 15 and (aii) from 0 to 5. The dotted lines represent the threshold for negative, equivocal or positive HER2 classifications. (b) Plots of the *HER2*/CEN17 ratio (*HER2*/CEN17) obtained by ESIMA-FISH *versus* standard IQ-FISH in the same set of clinical samples than in (b) with *HER2*/CEN17 ranging (bi) from 0 to 5 and (bii) from 0 to 2. The data shown here are mean ± SD obtained from the scores measured in 3 different clusters of 20 cells in each slide. The dotted lines represent the threshold for negative/equivocal or positive HER2 classifications._____79

Figure 2.18 - (a) Optimization of the hybridization step using FISH images of a series of cell lines. The plot shows linear regression coefficients of the two HER2 signal outputs (contrast and diameter), corresponding to 3 experimental parameters, namely the hybridization time, the probe dilution, and the type of flow regime used. The signal quality is assessed by measuring the diameter and contrast of the red and green fluorescence signals (dots). From our analysis (see section 2.5.1.1), we find as optimal conditions a 2 hours hybridization time, a 4 × probe dilution and the application of discontinuous flow. (b) Result of an optimal microfluidic-assisted FISH protocol applied on a cell line. The cell is marked with 3 colors corresponding to the 2 probes

protein quantity in the protein extraction solutions obtained from two adjacent sections from the same breast cancer tissue patient, measured by the two methods (P8-S1, P9-S1, P9-S2, P11-S1 in table 3.3).

List of tables

1. INTRODUCTION TO CANCER DIAGNOSIS AND MICROFLUIDICS

1.1. Overview of breast cancer

1.1.1. Epidemiology

The World Health Organization reported about 14.1 million new breast cancer cases and 8.2 million deaths worldwide in 2012, making breast cancer one of the main causes of death in women [1]. Multiple factors are associated with the incidence risk of breast cancer. Unhealthy nutrition, consumption of alcohol, smoking, excess body weight, and lack of physical activity are associated with a high risk of breast cancer. In the mid-1990s, the cancer mortality rate in some high-risk countries such as the United States was dramatically decreased due to modern screening and adjuvant hormonal treatments (figure 1.1) [2].
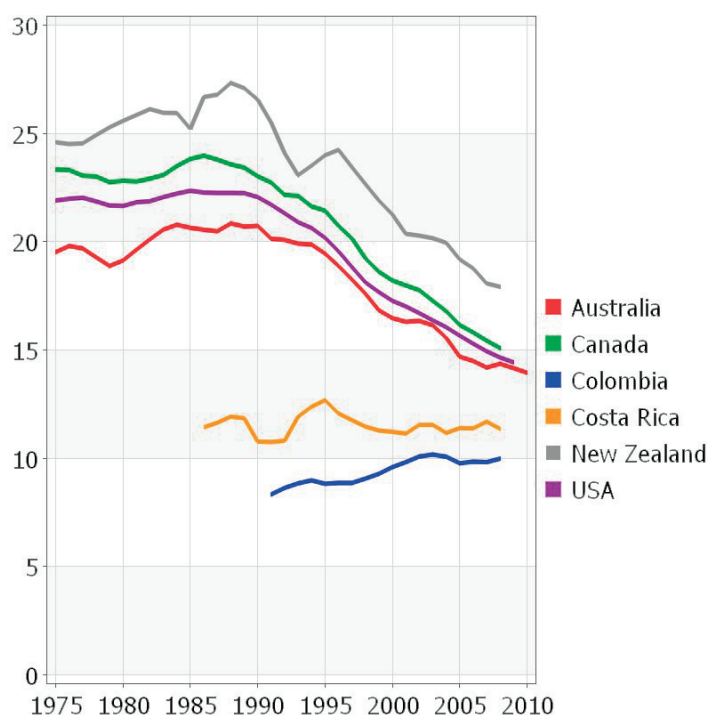
Figure 1.1 - Women's breast cancer mortality rate in selected countries [1]. In y axis: Rate per 100,000.

Early diagnosis of breast cancer is essential if the disease is to be treated efficiently. Detection of all symptoms such as breast lumps, nipple abnormalities (discharge, retraction, distortion, or eczema) suggests a need for clinical examination, imaging techniques (mammography, ultrasound) and needle biopsy. In case of strong indications of breast cancer, the lump is removed by surgery and evaluated by pathologists. Breast cancer is classified by type, grade, stage and gene expression. The latter has recently been added to histopathological assessment routine as a part of modern personalized medicine. In particular, the treatment of each patient is based on the gene expression classification. In this chapter, histopathological techniques for gene expression classification and some current personalized treatments are presented.

1.1.2. Cancer classification

Cancer is traditionally classified by the tissue from which it is originated. It can be either carcinoma or sarcoma. For carcinoma, cancer cells are generated from epithelial cells while for sarcoma, cancer originates from connective cells such as adipocytes. Breast carcinoma was the most common type of cancer in women worldwide in 2012 [1]. Breast carcinoma is further classified based on its location inside the breast and its aggressiveness. For example, a carcinoma can be classified as invasive ductal carcinoma, ductal carcinoma *in situ* (DCIS), and other rarer types such as inflammatory breast cancer [3]. For a DCIS case, tumor cells (TCs) are contained inside milk ducts, while for an invasive ductal carcinoma TCs invade adjacent tissues and often metastasize to distant sites. Invasive ductal carcinoma is the most common form of breast carcinoma [2].
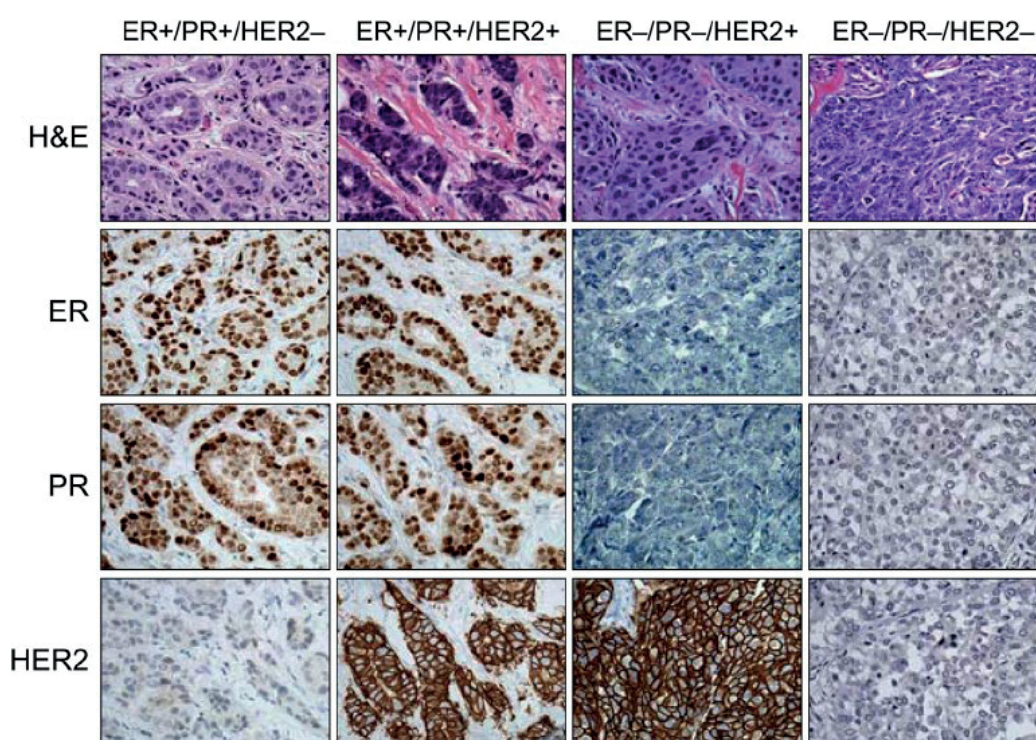
Figure 1.2 - Molecular classification panels for breast cancer. In lines: hematoxylin & eosin (HE), estrogen receptor (ER), progesterone receptor (PR) and human epithelial growth factor receptor (HER2) staining of tissue slides, respectively. In columns: different subtypes of breast cancer. In all slides, nuclei are stained blue using hematoxylin. In the HE image, cytoplasm is stained pink with eosin. In the ER, PR, and HER2 images, these biomarkers are tagged with a brown compound. This brown staining is stronger in positive (+, i.e. overexpressed of protein) than in negative (-) cases. Figure is adopted from [4].

Concerning the state of the disease, cancer is classified by grade and stage. Grade 1 to 3 are based on the appearance of TCs in a tissue biopsy (assessment of tubule/gland formation, nuclear pleomorphism, and mitotic counts). A high grade implies high metastatic activity. The stage of breast cancer (1 to 4) indicates the progression of the disease and is evaluated according to the size of the tumor and the invasion of TCs

from the tumor to near lymph nodes. The higher the stage, the smaller the survival rate and treatment efficiency.

Breast cancer can also be classified according to its gene expression [5]. Based on some indicative molecules (biomarkers), breast carcinoma is divided into four groups: luminal A, luminal B, HER2 positive and triple negative (basal type). These groups are characterized by different expression levels of 3 proteins ER, PR and human epithelial growth factor receptor (HER2), see table 1.1 and figure 1.2. Because each group has a specific prognosis and clinical characteristics, treatments are tailored to each (see section 1.1.4).

Table 1.1 - Subtypes of breast cancer based on molecular classifications [4].

	ER	PR	HER2
Luminal A & B A: low grade B: high grade	+	+	-
HER2 positive	- or +	- or +	+
Triple negative (Basal)	-	-	-

After being removed from a patient, the tumor is sliced into thin sections. To enhance the contrast of the tissue to observe its morphology, hematoxylin and eosin (HE) staining are performed (figure 1.2, the first row). Nuclei are stained blue with hematoxylin and cytoplasm is stained pink with eosin. By observing the morphology of the HE-stained tissue, assessment of tumor malignancy, type of cancer tissue and cancer grade can be performed by a pathologist. Therefore, HE staining is considered an essential step in current cancer diagnostic practice.

Several treatments are recommended for breast cancer patients. Classical treatment such as surgery, radiotherapy, and chemotherapy are three principle methods applied for most cancer cases worldwide. However, cancer often relapses and patients suffer from the side effects of radio- and chemo-therapies. Personalized medicine such as adjuvant hormonal therapy and targeted therapy in breast cancer have had a considerable impact on cancer treatment, increasing the survival rate of cancer patients while triggering less-important side-effects. Personalized treatments, based on gene expression characterization, carefully select patients eligible for a hormonal or targeted therapy. For example, hormone therapies such as Tamoxifen are used to treat Luminal A & B patients while HER2-positive patients are treated with Trastuzumab (HERCEPTIN®) [6]. Trastuzumab is a humanized monoclone antibody (Ab) that binds to the domain IV of the extracellular segment of the HER2 receptor, activating several pathways which leads to cell proliferation inhibition and immune destruction of TCs.

More recently, immunotherapy has been approved by the United States Food and Drug Administration to treat certain types of cancer such as melanoma. Immunotherapy involves boosting the patients' immune system using engineered T-cells and immune checkpoint blockade [7]. Contrary to classical methods,

immunotherapy can pursue TCs long after treatment, thus preventing cancer relapse. Clinical trials are currently being conducted to prove its efficiency to treat breast cancer [8].

1.1.3. Intratumoral heterogeneity (ITH)

Heterogeneity is an important feature of cancer. It is characterized by distinct morphologies, phenotypes or genes in different TCs, existing either in two different cancer patients (intertumoral heterogeneity) or in the same tumor (ITH). Intertumoral heterogeneity causes different responses to a given treatment for different patients having the same type of cancer. Recently, personalized medicine has improved patients' survival rate by adjusting cancer treatments according to the genetic and phenotypic characteristics of each patient. However, current personalized treatment is less efficient for patients with ITH, which is characterized by genetic or phenotypic differences among different subclones in different regions of the tumor [9]. While the cause of ITH is still being debated, two models are widely accepted: the tumor stem cell model and the clonal evolution model. The former indicates that a cancer stem cell (CSC) can differentiate into different cancer phenotypes, suggesting a hierarchical development of the tumor. The latter represents different genetic and epigenetic changes during tumor development. In reality, both scenarios can take place in complex developments of the tumor [10]. Several factors influence CSC differentiation and clonal evolution, such as genetic instability, stochastic processes, cell and tissue plasticity, and, in particular, adaptation to the tumor microenvironment (TME). The TME mainly consists of blood vessels, extracellular matrix, stromal cells such as fibroblasts, adipocytes and immune cells and other signaling molecules that surround a tumor. During the development, TCs can acquire several new mutations. However, only some of these mutations can survive after undergoing selective pressures (*e.g.* hypoxia or immune attacks) generated by the TME, as the basis of Darwinian evolution. When the TME conditions change, some subclones might gain or lose survival and proliferation advantages. Continuous mutations and selections during cancer evolution are the sources of tumor heterogeneity. Furthermore, cancer treatments may enhance selective pressure that aggravates ITH [11]. Regarding the consequence of ITH, different subclones can have different phenotypes exhibiting varied proliferation rates, motility, and protein expression, thus contributing to cancer resistance to certain treatments, *e.g.* chemotherapy [12], targeted therapy [13] and immunotherapy [14]. As a result, developing a tool for intratumoral analysis is an urgent need for personalized cancer treatment.

1.2.   Molecular analysis methods for cancer prognostics

Accurate biomarker assessment is essential for cancer diagnosis and treatment. Some biomarkers have a prognostic value indicating patient survival information and others can predict the likelihood that a patient will benefit from a specific cancer treatment. Validated techniques for protein biomarker analyses in breast cancer are enzyme-linked immunosorbent assay (ELISA) and immunohistochemistry (IHC). For gene biomarkers, ISH and gene (DNA and RNA) assays and arrays are approved for clinical diagnostics. All mentioned methods have a common working principle: the detection of target biomarkers (either protein or gene) using probe molecules that have an affinity to the targets. Fluorescence or chromogenic tags can be used to reveal the probe/target position. In the following, some techniques for histopathological assessment are presented.

1.2.1.   ELISA and microarrays

ELISA is a popular tool that uses antibodies (Abs) and an enzymatic reaction to identify a substance, usually an antigen. Two ELISA configurations exist: either the target protein is immobilized on a glass surface and captures the probe mixed in a solution, or it is diluted in a solution from which is captured by a probe

immobilized on a surface. In both configurations, the probe-target structure is detected using a reporter Ab that is linked directly or indirectly to an enzyme, in most cases horseradish peroxidase (HRP) (figure 1.3ai, ii, iii). In the presence of an appropriate substrate, the enzymatic reaction by HRP creates a color change at the probe-target site, which can be visible in a bright-field microscope (figure 1.3aiv). In breast cancer, ELISA is used for the detection of a urokinase plasminogen activator (uPA) and plasminogen activator inhibitor 1 (PAI1) [15]. These are two new validated biomarkers predicting the recurrence likelihood in negative lymph node breast cancers [16]. These biomarkers are extracted from a tissue and quantified by ELISA.
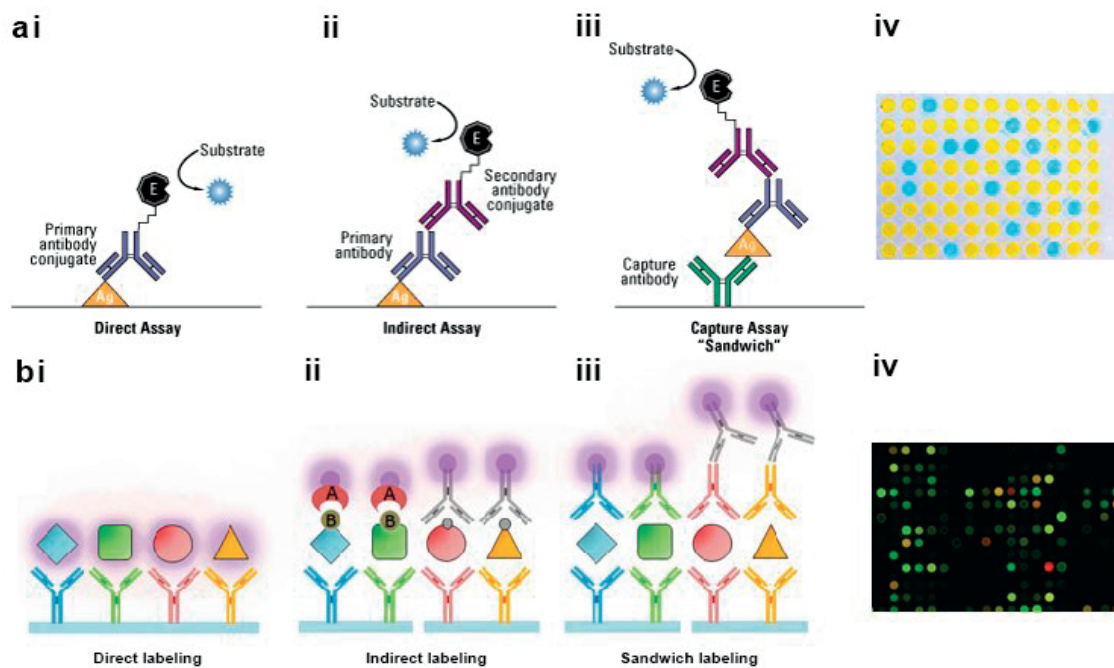
Figure 1.3 - Principle of enzyme-linked immunosorbent assay (ELISA) and microarrays. (a) ELISA. (i) Direct assay. The target antigen (Ag) is immobilized on a surface and recognized by an enzyme-linked Antibody (Ab). In the presence of an adaptive substrate, a color change caused by an enzymatic reaction reveals the position of the Ag-Ab structures. (ii) Indirect assay. The immobilized target Ag binds to a primary Ab that is linked to another secondary Ab. The secondary Ab has an enzyme label that creates color changes when a substrate is presented. (iii) "Sandwich" capture assay. The target Ag is first captured by an immobilized Ab, then is detected by primary and enzyme-linked secondary Abs. The revelation is performed by an enzymatic reaction of the substrate. (iv) Final image of an ELISA test taken from a bright-field camera. Images are taken from www.thermofisher.com and www.enzolifesciences.com. (b) Different protein microarrays. (i) Direct labeling. The target Ag is labeled before introducing to the microarrays, then binds to an antibody immobilized on a surface. (ii) Indirect assay. The target Ag is labeled with biotin or small haptens, then binds to immobilized Ab. The Ag is then detected with labeled avidin or hapten-specific Ab. (iii) Capture assay "Sandwich". The target Ag is unmodified, first captured by an immobilized Ab, and is then detected by either tagged-primary Ab or via a primary Ab/tagged-secondary Ab. (iv) Final image of

microarrays recorded by fluorescence scanner. Figures are adapted from [17] and www.gesundheitsindustrie-bw.de.

Protein microarrays are also based on probe-target binding such as ELISA but use a fluorescence-tagged Ab for revelation instead of chromogenic labels (see figure 1.3b). Furthermore, protein microarrays use a smaller quantity of probe and target solution for each test (~100nl compared to ~100 µl for ELISA). The positions in which proteins are immobilized (spots) are organized into arrays. Thus, the throughput of the tests is improved compared to ELISA. The detection of protein microarrays is performed using a fluorescence scanner.

DNA microarrays are similar to protein microarrays. In a common configuration, DNA probe fragments are immobilized on a substrate surface and bind to DNA or RNA in a lysate solution [18]. The DNA probes are spotted on the surface by arrays. The DNA-RNA binding is revealed by fluorescent tags. DNA microarrays provide prognostic information for newly cancer-diagnosed patients. In breast cancer, DNA microarray tests such as MammaPrint help assess the recurrence risk and identify patients who might benefit chemotherapy [19].

1.2.2. Immunohistochemistry (IHC) and immunofluorescence (IF)

Table 1.2 - Criteria for HER2 assessment by IHC [20].

Criteria	Class
No staining or incomplete staining that is faint or hardly distinguishable and within less than or equal to 10% of the invasive TCs	0
Incomplete membrane staining that is faint or hardly distinguishable and within more than 10% of the invasive TCs	1+
Circumferential membrane staining that is incomplete and/or weak or moderate and within more than 10% of the invasive TCs Complete and circumferential membrane staining that is intense and within less than or equal to 10% of the invasive TCs	2+
Strong and complete circumferential membrane staining	3+

IHC is the most popular method for histopathological assessment of biomarkers. While ELISA detects targeted Abs dissolved in a solution, IHC identifies proteins at their specific location inside a tissue. When Ab probes are applied to a tissue section, they can diffuse into the tissue and recognize the specific target proteins. Similar to the revelation step of ELISA, the IHC probe-target binding is revealed using a secondary Ab that binds to the primary Ab probe. The secondary Ab binds to an HRP molecule (figure 1.4a) or a polymer bone possessing several HRP molecules (see figure 1.4b) for enzymatic revelation. Using 3,3'-diaminobenzidine (DAB), the enzymatically-reactive sites are revealed by a colored compound originating from oxidized DAB. Therefore, the locations of target Abs in the tissue are detected and assessed in a bright-field microscope (figure 1.4c). In breast cancer, as part of the clinical practice, three main biomarkers ER, PR and HER2 are assessed using IHC. In addition, assessment of some other prognosis biomarkers, such as a marker of cell proliferation Ki-67 and a marker of differentiation Cytokeratin (CK) are also performed using

IHC [21]. Nevertheless, IHC is a semi-quantitative method that relies on subjective assessment of staining intensity and the number of positive cells (see table 1.2 and figure 1.4c). In particular, for HER2 assessment, a second test using in situ hybridization (ISH) is required if the IHC test results are equivocal (IHC 2+, see figure 1.4ciii).
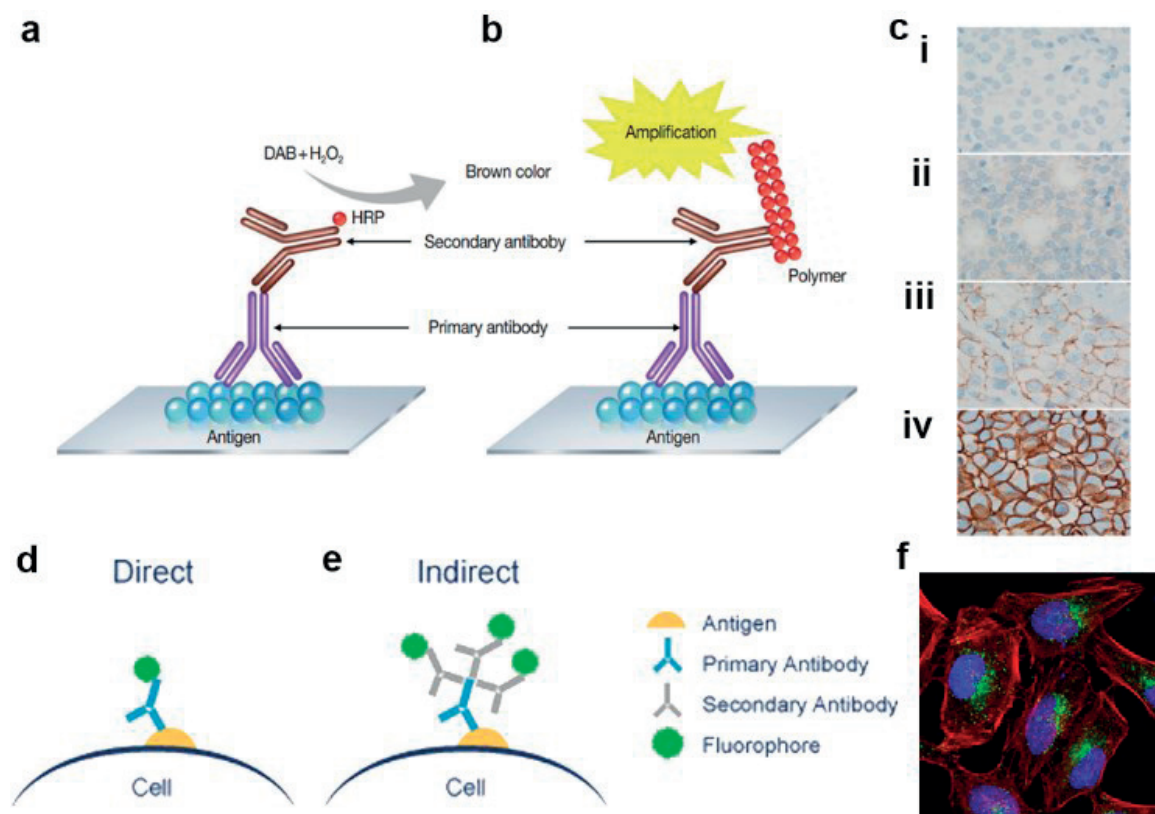
Figure 1.4 - The principle of immunohistochemistry (IHC) and immunofluorescence (IF). (a) Indirect IHC: detection of Ag using primary Ab and horseradish peroxidase (HRP)-tagged secondary Ab. Figures are obtained from [22]. (b) Indirect IHC with an additional amplification step using a polymer carrying several HRP labels that binds to secondary Ab/primary Ab/Ag structures [23]. (c) Image of cells with HER2 IHC staining having different classes: (i) 0 : negative (ii) 1+: negative (iii) 2+: equivocal (iv) 3+: positive. (d) Direct and (e) and indirect immunofluorescence staining. i. In a direct-IF configuration, an Ag in one cell is tagged by a fluorescent primary Ab. In an indirect-IF configuration, the Ag/primary Ab structure is labeled by fluorescent secondary Abs. f. A typical IF image. Images are adopted from www.abcam.com and www.cellsignal.com.

Similar to IHC, IF uses a specific Ab to recognize the target Ab. However, the techniques differ in the revelation phase. While IHC uses enzymatic reaction to mark the protein locations, IF uses a fluorescence-labeled secondary Ab and fluorescence microscope to detect the probe-target binding (figure 1.4d,e,f). IF has many applications in biology, such as living organism imaging and flow sorting. In breast cancer, recent studies have proved that IF signals are more quantitative than those of IHC [24], as they reflect better the

protein quantity in the probe-target binding sites. Although quantitative IF is not yet a validated method, it can be considered a promising alternative method of IHC.

1.2.3. Fluorescence in situ hybridization FISH and chromogenic in situ hybridization (CISH)
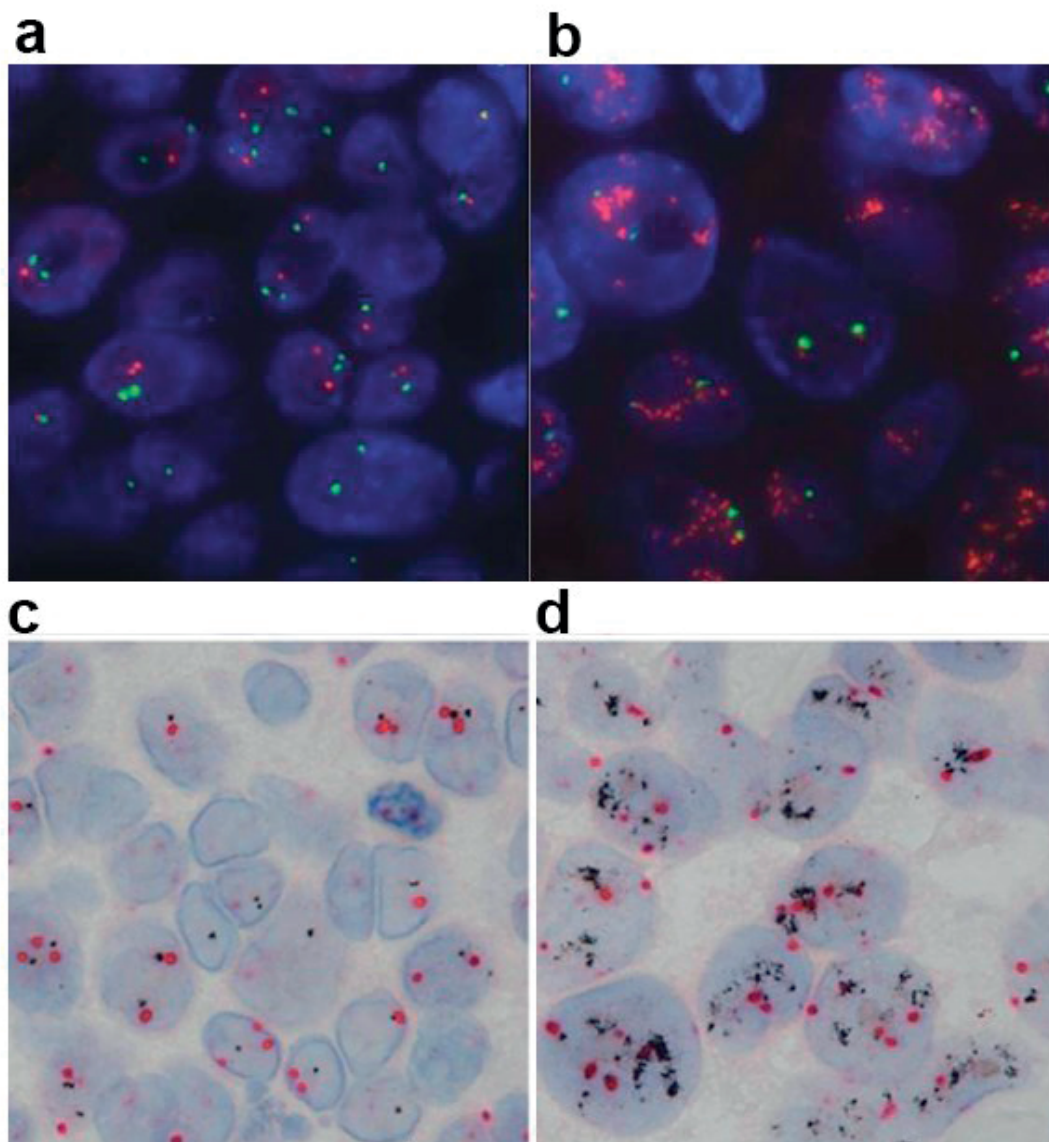
Figure 1.5 - Fluorescence in situ hybridization (FISH) images for HER2 assessment. (a) A HER2-negative case. (b) A HER2-positive case. In blue: nuclei; red: *HER2* gene; green: centromere of chromosome 17 (CEN17). Chromogenic in situ hybridization (CISH) images for HER2 assessment. (c) A HER2-negative case. (d) A HER2-positive case. In light blue: nuclei; black: *HER2* gene; magenta: CEN17. Figures are obtained from [25].

FISH is a cytogenetic technique for detecting and locating a specific DNA sequence on a chromosome. A DNA probe, labeled with a fluorescent molecule, is applied to the cell and binds to the target-complementary

sequence of a specific chromosome within the nuclei. Both target and probe DNA segments are denatured at high temperature and recombined at lower temperature. The position of the interested gene can be located when the chromosome is observed by a fluorescence microscope. This technique can therefore be used to build a genetic map for analysis of chromosomal aberrations and genetic abnormalities in various organisms such as animals and plants. In pathology, FISH is one of today's most important diagnostic, prognostic tools for genetic alteration-related diseases, like cancer or detection of congenital disorders. In particular, in breast cancer FISH is used for detecting the *HER2* gene amplification responsible for HER2 protein overexpression (figure 1.5a, b). In particular, as FISH is quantitative and accurate, it is used for reassessing cases with an HER2-equivocal status in an IHC test (classified as 2+ in table 1.2). Similar to FISH, CISH is designed to detect a chromosome aberration. The main difference is that CISH uses an enzymatic label leading to a chromatic signal visible in a bright-field microscope. CISH is an alternative validated method for HER2 amplification assessment in breast cancer (figure 1.5c, d).

1.3. Introduction of microfluidics: technology and theory

1.3.1. Overview of microfluidics

Microfluidic systems, also known as lab-on-a-chip (LOC) systems, have attracted much research attention since the mid-1990s. The domain has a wide range of applications, but most importantly in analytic biology and chemistry. In particular, microfluidic systems use miniaturized fluidic channels to implement biological and chemical reactions. The main advantages of microfluidics are that, in these narrow channels, the surface-to-volume ratio is very high and the diffusion time is shortened. Therefore, the kinetics of reaction that takes place on a surface can be increased thanks to fast-fluidic exchanges of molecules in the presence of flows. Besides, miniaturization lowers consumption of reagents, which is essential when dealing with biological samples. Moreover, integration of electronic and optical components allows precise monitoring of fluids, molecules, and particles. Finally, the possibility of multiplexing is also an advantage of microfluidic systems towards performing high-throughput analyses. Research advances in microfluidics resulted in several industrial applications. Several multinational companies and startups have commercialized microfluidic-related products in different fields of technology. For example, Illuminia Inc. and Fluidigm Corp are leading companies in the gene sequencing domain, and Agilents and the Abbott Laboratory are key players in point-of-care diagnostics. In 2013, the microfluidics market value was estimated at $1.6 billion and will be extended to reach $3.6-5.7 billion by 2018 [26].

In most applications presented in this thesis, hydrodynamic flows are used for increasing molecular exchanges, shortening reaction time and decreasing the reagents needed. Below, we explain the role of hydrodynamic flows in biological reactions by providing some microfluidic background and hypothesis. First, we study a model for a biosensor configuration (protein or DNA microarrays) and then generalize the principle for biological reactions in a tissue such as FISH or IHC. Biosensors are detection devices based on a biological interface that interacts with target molecules and characterizes them by a biochemical reaction. The literature shows that biosensors become more sensitive with down-scaling [27]. However, when the biosensors are too small, the target molecules have difficulty encountering with the sensor's probe molecules, thus increasing the time needed for detection. Microfluidics help create an effective mass transport that facilitates the capture of target molecules on the surface of biosensors. In addition, the high surface-to-volume ratio in microfluidics systems is inherently adapted for integration of biosensors, which requires a large solid-liquid interface area.

1.3.2.   Convection, diffusion and reaction theory

1.3.2.1.   Reaction-induced and diffusion-induced flows in a biosensor

We consider a typical chamber used in microfluidics for biological detection, as described in figure 1.6, where W_C is the width of the channel, H the channel height, Q the flow rate, L the sensor length along the fluid and a W_s the width in the perpendicular direction to the fluid flow.
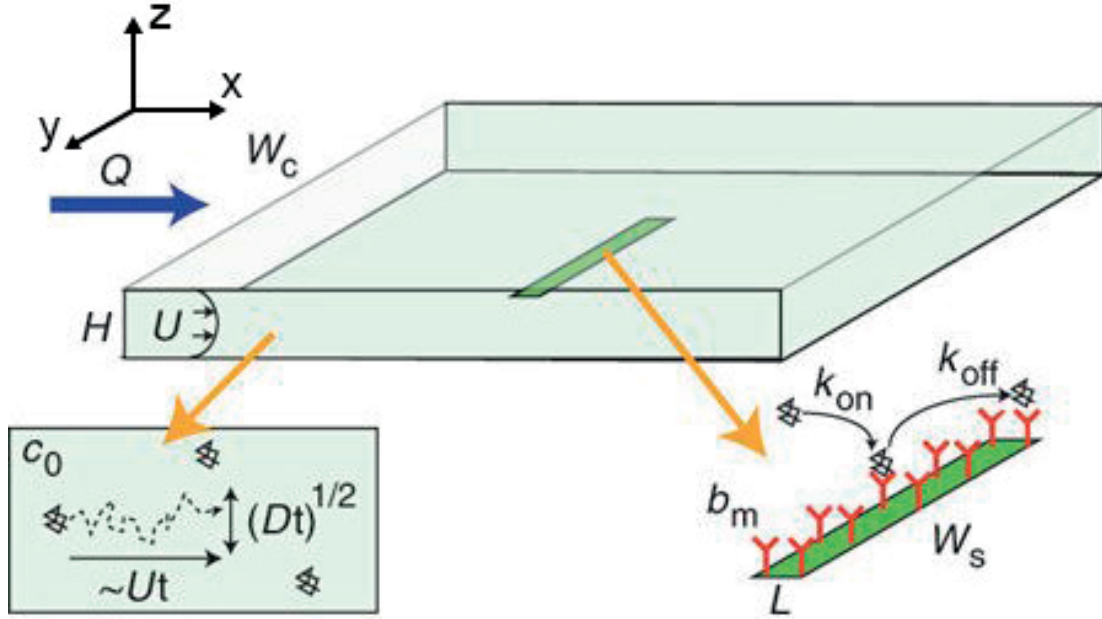
Figure 1.6 - A typical reaction chamber for biosensor-based detection of molecules. Figure is adapted from [28].

A biosensor with immobilized probes on top (for example, Ab or DNA) is placed inside the chamber filled with fluids containing target molecules. During the biological assay, solutions containing the target molecules are injected into the chamber and flow above the biosensor surface. Some target molecules arrive at a location close enough to the probes and bind with them thanks to the probe-target affinity. As the target molecules are consumed in the vicinity of the biosensor, a depletion volume surrounding the biosensor appears, which enlarges with the reaction time. This volume is characterized by a depletion layer thickness (δ_s). At the same time, a concentration gradient of the target molecules $grad(c)$, is created due to the presence of the depletion layer. c is the concentration of the target molecules inside the solution. The first Fick law suggests that when there is a concentration gradient, a diffusion flow $j_D = -Dgrad(c)$ is present, where D is the diffusion coefficient, to counterbalance this gradient. j_D is a flow density, *i.e.* flow per surface unity. In a set up as presented in figure 1.6, we can assume that the surface of the biosensor is much larger compared to the size of a probe molecule. Therefore, the concentration is the same for all points having the same z. Therefore j_D can be rewritten as:

$$j_D = -Dgrad(c) = -D\frac{\partial c}{\partial z} \tag{1.1}$$

Furthermore, at the surface of the sensor we have $j_D = j_R$, where j_R is the reaction flow-density created by the biosensor by adsorbing molecules from the solution. To calculate j_R, we use a Langmuir isotherm model, a classical model for the reaction of two species (here is probe P and target T) as follows:

Given a reaction

$$P + T \leftrightarrow PT$$
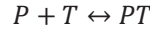
Then the reaction rate j_R is presented as follows:

$$j_R = \frac{\partial [PT]}{\partial t} = -\frac{\partial [T]}{\partial t} = -\frac{\partial [P]}{\partial t} = k_f[P][T] - k_b[PT] \tag{1.2}$$

where $[T]$ is the concentration of the target in the solution at the vicinity of the biosensor, $[P]$ is the density of the non-combined probe available on the sensor, $[PT]$ is the density of the combined probe-target on the sensor, k_f is the forward reaction coefficient representing the association of probe and target and k_f is the backward reaction coefficient representing the dissociation of probe and target. If the initial density of the biosensor is known as b_0, $[T]$ is presented as c, and $[PT]$ is presented as b, the equation (1.1) is represented as follows.

$$j_R = \frac{\partial b}{\partial t} = k_f(b_0 - b)c - k_b b \tag{1.3}$$

Combining equation (1.1) and (1.3), we obtain:

$$j_R = j_D = \frac{\partial c(z=0,t)}{\partial z} = \frac{\partial b(t)}{\partial t} = k_f\big(b_0 - b(t)\big)c(z=0,t) - k_b b(t) \tag{1.4}$$

This equation is a reaction-diffusion differential equation containing two variables, c and b. Now we apply some assumptions to simplify this equation.

In the case of molecular transportation to the surface being faster than the probe-target binding rate, the transport is 'reaction limited'. In this case we can assume that $c_s = c_o$. Therefore, an analytic solution of equation (1.4) can be obtained:

$$\frac{b(t)}{b_0} = \frac{c_o k_f}{k_b + c_o k_f}\left(1 - e^{(-k_b + c_o k_f)t}\right) \tag{1.5}$$

The reaction rate is:

$$j_R = \frac{\partial b(t)}{\partial t} = -\frac{c_o k_f\big(-k_b + c_o k_f\big)}{k_b + c_o k_f} e^{(-k_b + c_o k_f)t} \tag{1.6}$$

We would normally require a forward reaction to occur. Therefore the coefficient related to the forward reaction $c_o k_f$ should be superior to that of the backward reaction k_b: $\big(-k_b + c_o k_f\big) > 0$. This reaction rate then decreases with time and is independent to the diffusion.

To establish a threshold between the diffusion- and reaction-limited regime, we consider the diffusive and reactive flux at the beginning of the reaction. If we consider that all probes are still available at t=0, then $b(t = 0) = 0$. The reactive flux is written as

$$j_R(t = 0) = \frac{\partial b(t = 0)}{\partial t} = k_f b_0 c(z = 0, t = 0) \sim k_f b_0 c_0 \qquad (1.7)$$

In the beginning, only a tiny depletion layer $\delta_s \ll H$ is formed, which means the gradient of c can be written as

$$\frac{\partial c(z = 0, t)}{\partial z} \sim \frac{c_0}{\delta_s} \qquad (5) \qquad (1.8)$$

The diffusive flux is then given as

$$j_D(t = 0) = -D \frac{\partial c}{\partial z} = -D \frac{c_0}{\delta_s} \qquad (1.9)$$

Thus,

$$\left| \frac{j_R(t = 0)}{j_D(t = 0)} \right| \sim \frac{k_f b_0 \delta_s}{D} = Da \qquad (1.10)$$

Da is the Damkohler number, the ratio between reactive and diffusive flux. When Da>>1, the consumption of molecules by the reaction is higher than the number of molecules that the diffusion can supply. Therefore, the mass transport is rate-limiting. When Da<<1, the mass transport is reaction-limited. To switch from reaction-limited to diffusion-limited, the only parameter that can be changed is the depletion-layer thickness δ_s. Therefore, we use microfluidics to create convective flows that enhance transportation by shrinking δ_s (*vide infra*).

1.3.2.2. *Diffusion-convection interplay*

In a diffusion-limited regime (Da>>1), we are interested in knowing how fast a molecule immigrate from the bulk to the surface of the biosensor to supply the molecular consumption. Imagine that a molecule is traveling above the detection area with a velocity u, it has only a time of $t_c = \frac{L}{u}$, where L the length of the detection area along the flow, where molecules can diffuse to the surface of the biosensor, before being washed away. t_c is the convection time or the time-of-flight of the molecule. Therefore, during t_c, a molecule at a depletion layer is created above the surface of the biosensor, with a thickness $\delta_s = \sqrt{Dt_c}$. Thus, on the molecular level, the shorter the convection time, the smaller the depletion layer δ_s. Now we consider a chamber with an initial concentration c_0 and a flow rate Q. From the conservation equation, we obtain the following equation:

$$\frac{\partial c(z, t)}{\partial t} = \nabla . j_c + \nabla . j_D = u \frac{\partial c(z, t)}{\partial z} - D \frac{\partial c^2(z, t)}{\partial^2 z} \qquad (1.11)$$

Where the convective molecular flow $j_c = u.c(z, t)$, thus $\nabla . j_c = u \frac{\partial c(z,t)}{\partial z}$ (we suppose that the concentration do not depend on x and y axis in this configuration).

In this equation, we see the two terms 'convection' and 'diffusion' interplay and create the variation on the concentration. To understand whether the system is diffusion or convection limited, we define a Peclet number, Pe_H, as the ratio between the convective and diffusive flows:

$$Pe_H = \frac{uc(z,t)}{D\frac{\partial c(z,t)}{\partial z}} \tag{1.12}$$

Using the following approximations:

$$\frac{\partial c(z,t)}{\partial z} \sim \frac{c_0}{H} \tag{1.13}$$

$$u \sim \frac{Q}{HW_C} \tag{1.14}$$

we obtain

$$Pe_H = \frac{u\frac{\partial c(z,t)}{\partial z}}{D\frac{\partial c^2(z,t)}{\partial^2 z}} = \frac{Q}{DW_C} \tag{1.15}$$

This Pe_H number considers only the dimension of the channel, not the sensor itself. It reflects the balance between the diffusive and convective-limit regime at the channel level. However, at the sensor level, we define a shear Peclet number, Pe_S, which takes in account the length of the sensor and defines the balance between the diffusive and convective flow at the sensor. From the literature [28], we have

$$Pe_s = \frac{\frac{\delta u}{\delta v}L^2}{D} = 6\,\lambda^2 Pe_H \tag{1.16}$$

Where λ is the ratio between the length of the sensor and the chamber height

$$\lambda = \frac{L}{H} \tag{1.17}$$

From Pe_H and Pe_S, simulations allow calculation of the depletion layer inside a diffusive-convective system (see figure 1.7) [28].

$$\delta_s = LPe_S^{1/3} \tag{1.18}$$

From equation (1.9) and (1.18), the rate in a diffusion-limited system is written as

$$j_D \sim D(c_0 - c_s)LPe_S^{1/3} \sim Dc_0 L.Pe_S^{1/3} \qquad (1.19)$$

From equation (1.16), (1.17) and (1.19), we obtain the reaction rate j_D in function of flowrate Q:

$$j_D \sim Const * c_0 Q^{1/3}$$

Where $Const$ is the constant representing the dimensions of the channel and sensor.

$$Const = 1.82 W_c^{-1/3} D^{2/3} L^{5/3} H^{-2/3} \qquad (1.20)$$

We use equation (1.20) to show that in a diffusion-limited system, if we want to detect a low concentration of the target solution (c_0) and maintain the same rate j_D, we need to increase the Pe_S. An increase of flow Q is thus required.

For tissue staining, the principle of convection-diffusion is similar to that used in biosensor applications. The difference is that the molecule in the solution is the probe and the target is immobilized inside the tissue. If we suppose that the tissue is thin enough to be considered as surface, the diffusion-convection-reaction theory can thus be applied to tissue staining. In this case, we use the equation (1.20) to explain that by applying microfluidic flows, we can reduce the concentration of the probe needed, while performing the same reaction rate.
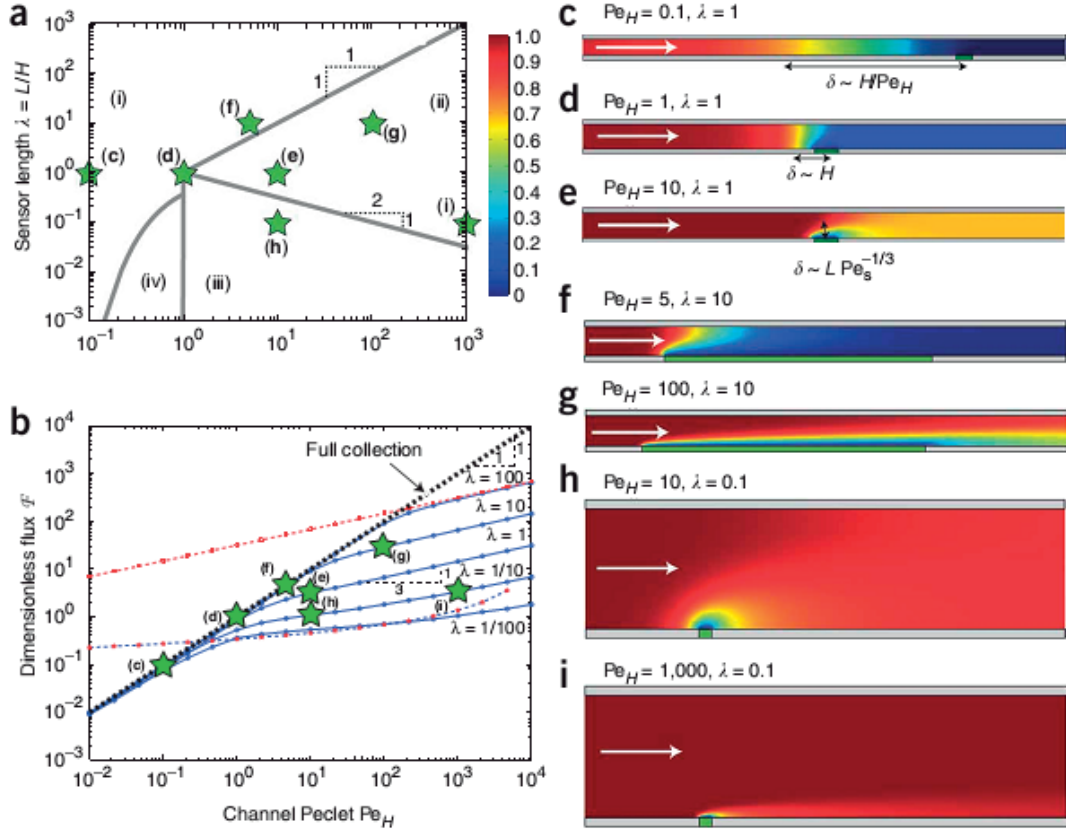
Figure 1.7 - Modeling of the depletion layer δ for different channel geometries and flow conditions. (a) Phase diagram by the ratio of the sensor length relative to the channel height $\lambda = \frac{L}{h}$ and the channel Peclet number Pe_H. Each green star corresponds to a flow profile represented in figure c-i. (b) Dependency of dimension less flux F and Pe_H in different channel geometry. The green stars indicate the same flow regime as in a. c-i) Different flow regimes corresponding to an increasing Pe_H and various values of λ. Figures are adopted from [28].

1.3.3. Microfabrication technology

Microfluidics has benefited from the progress in microtechnologies, especially in the field of micro-electro-mechanical systems. In particular, the manufacturing of structures on a micrometer scale and smaller allows the fabrication of fully-functional miniaturized devices. Microfluidic systems can be fabricated by several microfabrication techniques such as milling, hot embossing, stereolithography, injection molding, 3D-printing and silicon-based microfabrication [29]. The latter is based on the same concept as the microelectronic fabrication, in which the major principles are microlithography, etching, thin films, bonding, and polishing. As our microfluidic chip is fabricated using a silicon technology-based process, here we focus only on this method.

1.3.3.1. Materials choice

Microfluidic chips require microstructured patterns on a supporting substrate. Silicon is widely used as a substrate in microelectronics thanks to its excellent thermal and electrical characteristics. In particular, silicon is inert to most common solvents and reagents used in biological assays, and is stable at high temperature (melting temperature is more than 1400°C). Such features make it a suitable material for our microfluidic applications, in which biological reagents and high temperature (up to 95°C, the denaturation temperature in ISH applications) are involved. Besides this, glass is also a material highly adapted to use in microfluidic applications thanks to its transparency and stability to temperature and solvents. Glass and silicon substrates are usually supplied in the form of a wafer for facilitating the handling during successive microfabrication steps.

1.3.3.2. Photolithography

Photolithography is a technique which uses ultra-violet (UV) light to pattern a photoresist layer. A photoresist is a photosensitive polymer whose solubility in a particular solvent changes after being exposed to a UV light beam. In a standard photolithography protocol, there are three main steps: resist coating on the substrate, UV exposure and development. Two types of photoresist exist: positive and negative resists. After the development step, the exposed parts of a positive photoresist are dissolved in a solution while the exposed parts of a negative photoresist stay on the substrate wafer. Therefore, if light is exposed through a micro-structured mask, features of the photoresist layer can be formed on the substrate. Photolithography is one of the most important steps in microfabrication, involving mask fabrication and pattern transfer from a mask to a wafer.

1.3.3.3. Mask fabrication

A mask is based on a thick glass plate (order of mm of thickness) on which thin layers (order of μm) of Chromium (Cr) and Chromium oxide (Cr_2O_3) are deposited. To create a pattern for a mask, a layer of photoresist is deposited on the surface of the Cr_2O_3/Cr/glass structure. Design from a layout is transferred to the photoresist layer using a computer-controlled laser beam. Positions, where the Cr_2O_3 and Cr layers are not covered by the photoresist are then etched by potassium hydroxide (KOH). After the etching step, the photoresist is removed from the plate by a resist-stripping protocol using an adaptive solvent.

1.3.3.4. Patterns transfer to wafers

Patterns of the mask can be transferred to wafers using photolithography. First, photoresists are deposited on the surface of the silicon wafers by spin-coating and then baked and annealed. The wafer makes then contact with the mask and receives the UV light through the mask. After development, the patterns from the mask are transferred to the wafer. Depending on the type of photoresist, either positive or negative, the patterns of the wafer are identical or complementary to those of the mask. The resolution of photolithography is limited by the wavelength of UV light used, around 400 nm for a typical mercury lamp. This resolution is sufficient for our application. If multiple layers of microstructures are needed, the relative position of the wafer compared to the mask is adjusted. This step is called alignment.

1.3.3.5. Etching

Once the patterns are printed on the photoresist layer, microstructures on the surface of the wafers are created by removing materials at the specific positions defined by the photoresist layer. The etching can be done in a solution (wet etching) or in a plasma (dry etching). For plasma etching, the materials are removed

anisotropically while the materials are removed isotropically for wet etching. Dry etching using high-energy plasma to create high-aspect ratio features, is called deep reactive-ion etching (DRIE). For DRIE processing, as high-energy plasma is used, the photoresist layer used as etching mask can be replaced by a "hard mask" originating from more stable materials such as metal or silicon dioxide.

1.3.3.6. Thin film deposition

In some applications, a nanometric layer of materials can be deposited on the surface of wafers using chemical vapor deposition (CVD) or physical vapor deposition (PVD). For PVD, materials are transformed to a vapor phase, then condense on the surface of a wafer where they create a thin film. For CVD, with the presence of a volatile precursor in a chamber, a chemical reaction occurs and creates a layer of materials on the surface of the wafer. CVD and PVD techniques help create a heterogeneous stack of different materials on the wafer. In our protocol, PVD of Parylene-C polymer is used for making an intermediate adhesion layer for the bonding process (see section 1.3.3.7).

1.3.3.7. Bonding

In microfluidics, a bonding process is mostly required to create fluidic channels. Bonding of two wafers can be performed using either direct adhesion of two pieces or an intermediate adhesion layer such as Parylene-C polymer. Temperature, pressure and reactive plasma can be used to create bonds between different layers [29].

1.4. Microfluidic tissue processor (MTP)

1.4.1. Design and fabrication of the MTP

Considerable research on how using microfluidics for diagnostic applications has been performed. Most research and commercial products in this field are related to genetic and proteomic screening, biomarker analysis, and gene sequencing [30]. Our applications focus on cancer diagnostics, especially tissue biomarker characterization. In particular, Ciftlik et al. performed IF staining of breast cancer tissue using a MTP, a device of ~1 mm thickness consisting of a micromachined silicon wafer bonded to a glass slide (see figure 1.8a,b). The silicon side has "tree-like" channels on one face which are connected to the other face via "feed-through" holes. When the MTP is clamped to a microscope slide, on which a tissue is mounted, together with a plastic o-ring, it creates a reaction chamber above the tissue. Using a high flow rate, the MTP flushes reagents uniformly, and thus produces a homogenous probe concentration above the tissue in a large reaction chamber of 16×16 mm^2 [31].

The MTP is fabricated by a low-temperature polymer/polymer interface-free Parylene–C bonding step (figure 1.8c 1-6). A MTP consists of 2 main wafers: a silicon wafer and a pyrex (borosilicate glass) wafer. The silicon wafer was micropatterned by performing multi-step deep reactive-ion etching (DRIE). The hard mask used for DRIE was obtained by etching silicon oxides with a resist mask made by photolithography. They are bonded via a thin Parylene-C layer. The Parylene-C layer is deposited on the glass wafer by using a layer of Parylene monomers. Afterwards, both silicon and glass wafers are exposed to an O$_2$ plasma for surface activation of the Parylene-C layer before being bonded. Finally, the bonding is performed at 280°C during 40 min with a tool pressure of 1 bar [31, 32].
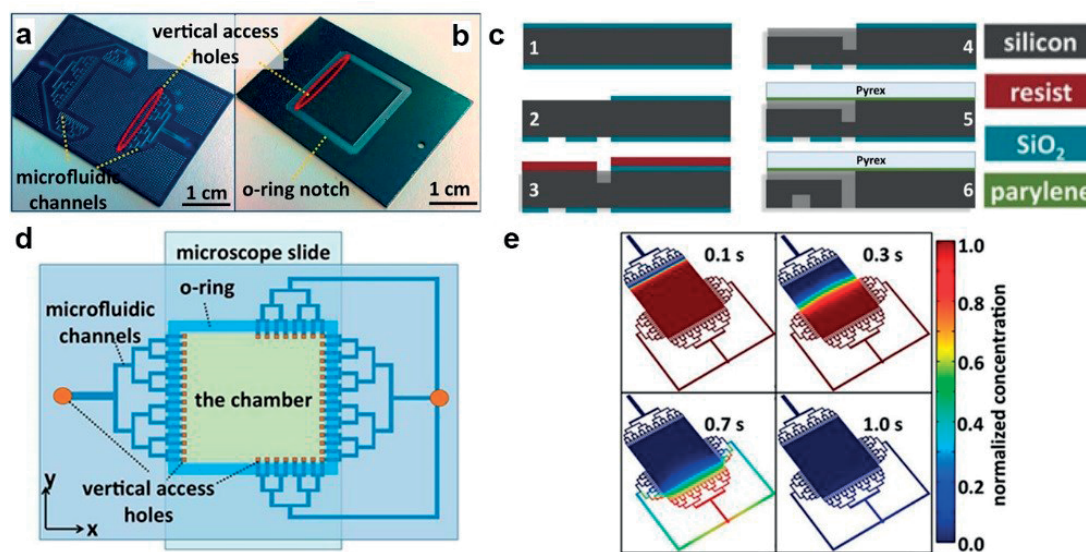
Figure 1.8 - (a), (b) Two faces of the silicon slide: (a) the face structured with microfluidic channels, bonded to a glass slide via a thin Parylene-C layer; (b) the face that has an o-ring notch in order to make a chamber with an opposite microscope slide (c) Microfabrication process of the microfluidic chip. (1) 550 µm silicon (Si) wafer coated by 2 µm wet silicon oxide on two sides. (2) Micropatterning of a SiO_2 layer using deep reactive ion etching (DRIE) through photoresist masks on both two sides. (3) DRIE of Si substrate via a resist mask created by a photolithography step to structure fit-through holes and in/outlets. (4) Resist stripping, followed by DRIE of the Si substrate through SiO_2 hard mask to create microchannels. (5) A 500 µm pyrex glass substrate, with 2 µm Parylene-C on the pyrex substrate, is bonded to the Si wafer. (6) Additional DRIE of the Si side of the bonded glass-Si stack to finalize the fit-through holes. (d) An assembly of the MTP and a microscope slide. The microscope slide is clamped against the silicon slide using a sealing o-ring to form a chamber. Microfluidic channel networks were designed to distribute the bioreagents uniformly within the chamber. (e) Modeling of the reagent concentration in the chamber, showing the rapid concentration change of the fluid thanks to convection. Figures are adapted from [31].

1.4.2. Effect of flows to immunostaining

The MTP was previously used to perform IHC staining. Multiple steps of reagent injection and washing were applied to the sample via the microfluidic processor. The tissue slide is clamped against the MTP half-chamber, together with a plastic o-ring to form a complete chamber (figure 1.8d). Ab probes were injected from the inlet, passed through the "tree like channels", entered the chamber and evacuated via the exit channels and the outlet on the right. Thanks to the MTP, the tissue was exposed to Abs with a precise control of time and concentration. As the chamber is thin, molecular exchange in the chamber during the injection was fast and homogeneous (see figure 1.8e). After incubation time of fluorescent probes, the fluids were flushed away. A result of the immunostaining is reported in figure 1.9a. The immunostaining signal was then characterized in function of the incubation time. The signal and background intensity of the immunostaining were measured in the inverted image (dark field) of figure 1.9a, shown in figure 1.9b. It was demonstrated that, during immunostaining, both the IF HER2 signal and background intensity increased with time with different rate (figure 1.9c). The background intensity increased due to non-specific adsorption of fluorescent

molecules. Therefore, the signal to background ratio is a linear function of the time only at the beginning of the incubation (figure 1.9d). To avoid the non-specific adsorption causing non-linearity, the incubation time was fixed at 2 min for all microfluidic immunostaining. Thanks to fast fluidic exchange, the immunostaining signal obtained was accurate and had a high contrast thanks to the low presence of non-specific adsorption of fluorescent molecules. The fluorescent signal strength resulting from the test was shown to be proportional to HER2 biomarker concentration and helped reduce ambiguous diagnostic outcomes [31]. In my thesis, the MTP is mainly used for other applications, such as FISH and protein extraction.
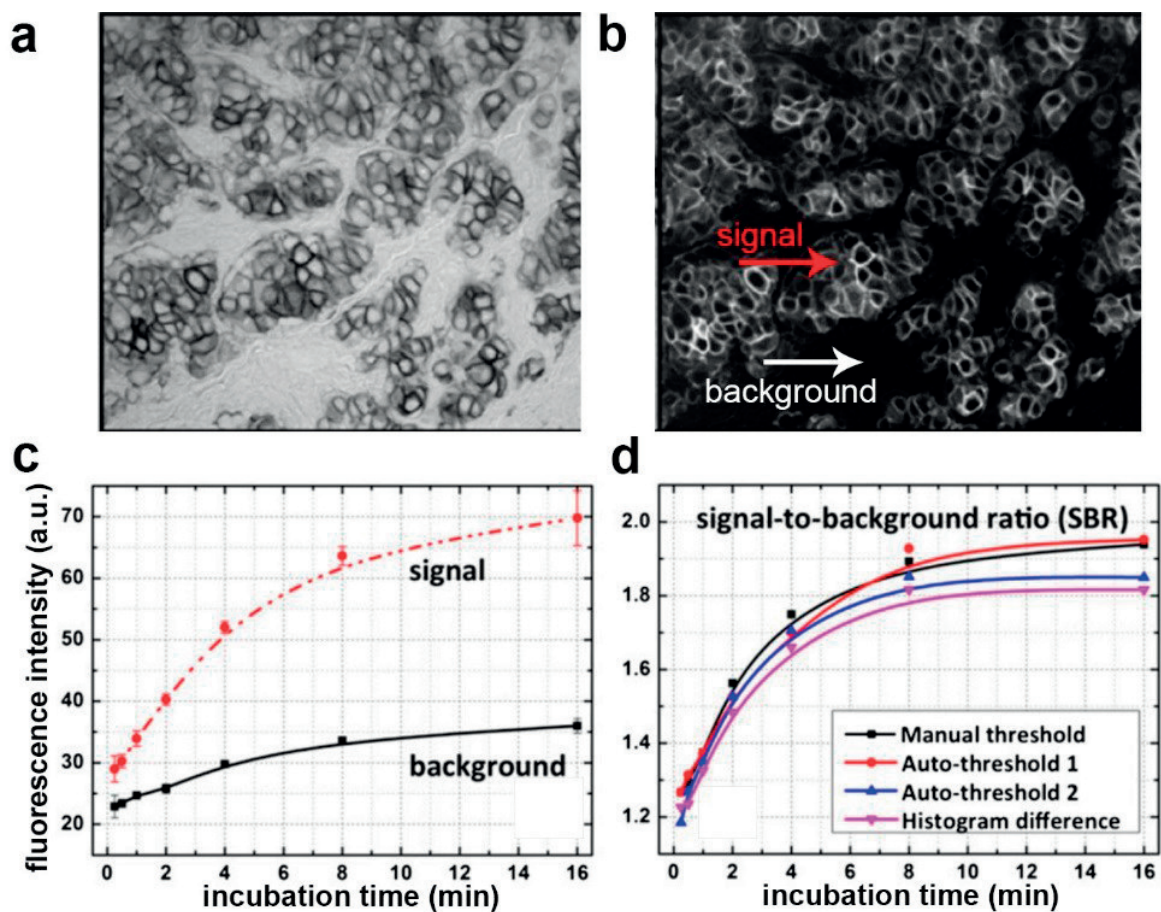
Figure 1.9 - Microfluidic immunostaining intensity in relation with time and assessment method. (a) IHC image of a slide obtained from microfluidic staining. (b) Inverted image of figure a. From figure b, the signals and background intensity were obtained using an image processing program. (c) The HER2 biomarker signal intensity and the background intensity measured in the IF image. Both signal and background intensity increase during the incubation time with different rates. The background intensity increases due to non-specific adsorption of fluorescent molecules. (d) The ratio between HER2 signal and the background obtained by different assessment method. The signal-to-noise ratio is a linear function of the time at the beginning of the staining (t<2 min) [31].

1.4.3. Reliability of the MTP

As we will use the MTP for applications involving high-temperature incubation of different kinds of reactants, we would like to know its reliability during long-term exposure to thermal shocks and solvents. The fabrication and working principle of the MTP is therefore presented here for the understanding of some potential problems related to the reliability of the device.

In an experiment, the chip can be in direct contact with different types of reagents: organic (alcohol, detergent), inorganic (acid, salt and phosphate etc.) and biological (DNA, proteins) substances. Could these factors influence the reliability of the chip? The selected materials are in fact chemically and biologically inert. Indeed, Si and glass are very stable materials, even in a low pH environment or at a high temperature; and Parylene-C is usually used as a barrier or encapsulation material. Some research shows that Parylene-C is stable for a long-term contact with the saline solution and no organic solution, acid or alkaline materials could attack it in any significant manner [33]. We do not expect reactions between reagents and microchannels.

The contact between the chip and the tissue slide is made by a mechanical clamp, which is either a magnetic or a screw-nut system, which exerts a vertical force on the chip. The chip is relatively thin (order of mm). The stresses in the chip can be thus considered as planar. Therefore, in the case of human error, this force could not significantly affect the chip. If the chip is not well placed, however, it could be bent or broken.

Due to the fabrication method, the chip could be subjected to some thermal stress. Indeed, the dilatation coefficients of the composed materials of the chip are quite different: Parlylene-C's thermal expansion coefficient of 3.5×10^{-5}/K is ten times higher than the pyrex and silicon's coefficient (around 3×10^{-6}/K). In the worst case, the stress could break the bond at the Parylene-Pyrex or Parylene-Silicon interface to relieve the stress after some thermal cycles and decrease the adhesion between them. Moreover, Pyrex has a constant thermal expansion coefficient, while Parylene-C has a variable one. Thus, the thermal stress in these layers should be studied as well. Moreover, compared to IHC, FISH requires a heating step. The temperature is increased from room temperature (RT) to 75°C and then maintained at 37°C. The chip is then cooled down for the next use. Therefore, we would need an investigation into the reliability of the chip under these thermal cycles. We study the impact of the thermal stress by layer. To simplify the problem, because the thickness of Parylene-C is too small compared to that of silicon and glass, we consider that the stress in the silicon layer is due to the glass layer and conversely. In contrast, the stress in Parylene-C depends on both the silicon and glass layer.

First, we study the stress in the glass and silicon layer. In fact, the fabrication process has already resolved a part of this issue which links to the thermal characteristic difference between glass and silicon. Indeed, the bonding temperature is about 280°C. The glass and silicon wafers were heated up from RT. This bonding temperature is interesting because when the temperature of the stack decreases to the RT, the thermal stress in both layers decreases to approximately zero. The linear thermal expansion coefficients of glass and silicon are presented in the graph below, which explains this phenomenon:
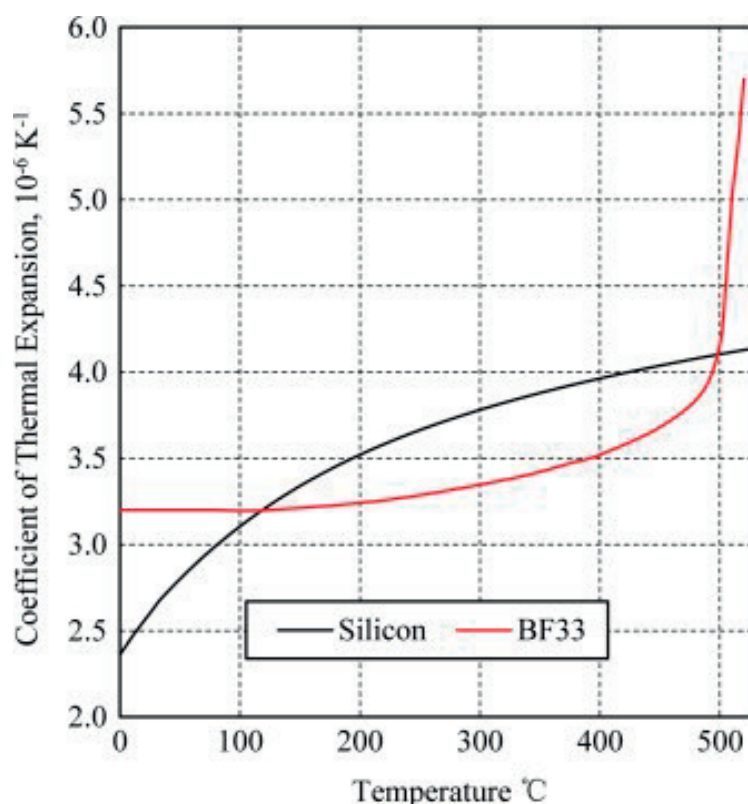
Figure 1.10 - Thermal expansion coefficient of Silicon and glass [34]

Indeed, figure 1.10 shows the thermal expansion coefficient of silicon and Pyrex as a function of temperature. We notice that at about 125°C, the thermal expansion coefficients of silicon and glass are equal. Above this temperature, silicon dilates more than Pyrex and below, it dilates less than glass. This means that if the bonding temperature is about 280°C, when the structure cooled down to RT, the tensile stress that develops in the silicon at higher temperatures will be compensated by the compressive stress that develops at lower temperatures. Therefore there is almost no stress in both the silicon and glass layer at RT. At some extreme conditions, the chip can be cooled down to 0°C and heated to 95°C (protein extraction protocol, chapter 3). During a cycle, the silicon slide is always in compression and the Pyrex slide is always in tension. However, these stresses are in the working stress interval of Silicon and Pyrex. Indeed, the compressive yield strength of single crystal silicon has range of GPa [35], and the tensile strength of glass is between 27 Mpa and 62 MPa (obtained from the website http://www.roymech.co.uk/). These are very high compared to the stress developed in the Silicon and glass layer that is estimated in the range of 100kPa (calculation not shown). Thus, the glass and silicon layers can withstand thermal stress.

Concerning the Parylene-C layer, when the whole system is cooled down from 280°C to RT, it first goes through the rubber-like state (T°C>110°C) where no stress is generated. The thermal stress in the Parylene-C layer appears when the temperature is decreased from the glass transition temperature of about 110°C to RT. We estimate that at the RT the Parylene-C layer undergoes tensile stress that is 5 times smaller than the yield strength of Parlene-C of 55 MPa and thus still in the elastic domain. On the other hand, during a FISH

procedure, when the temperature increases up to 95°C, the tensile stress in Parylene-C layer decreases. Therefore, the Parylene-C layer is expected stable when the temperature changes in the range of temperatures used in the FISH experiment. In the protein extraction protocol, we apply even more extreme temperature to the MTP (down to 0°C or up to 95°C). The experiment proved that the chip is still reliable in these temperatures. However, at a higher of temperature than 110°C, the Parylene-C can melt and cause chip destruction [31, 32]. To conclude, the temperature conditions used in our experiment do not influence the reliability of the MTP.

To create a homogenous distribution of reagents on the tissue, the liquid need to be pumped with a high velocity into the chamber. As the channels are small, the hydrodynamic resistance is increased as is the pressure to reach the desired velocity. However, if the pressure is too high, the chip could collapse (figure 1.11). Mechanical tests of the MTP indicated that the burst pressure, *i.e.* the pressure just before the occurrence of a sharp pressure decrease, had a mean value of 7.6 MPa and a standard deviation (SD) of 1.7 MPa [32]. Compared to a bonding strength of 10±3 MPa, the burst pressure is slightly lower but still in the same range. This burst pressure could occur due to the geometry of the chip, where stress was concentrated in some areas. Finally, the working pressure typically used for injecting IHC reagents to create a high flow rate of 10-100 μL/s is only in the range of 10 kPa [31]. This pressure is 100 times less than the range of bonding strength and burst pressure (MPa) [32]. It ensures the reliability of the chip for long-term use. If we want to study further the effect of both the hydraulic pressure and thermal cycle on the chip, we need to study further by modeling them with a computational tool.
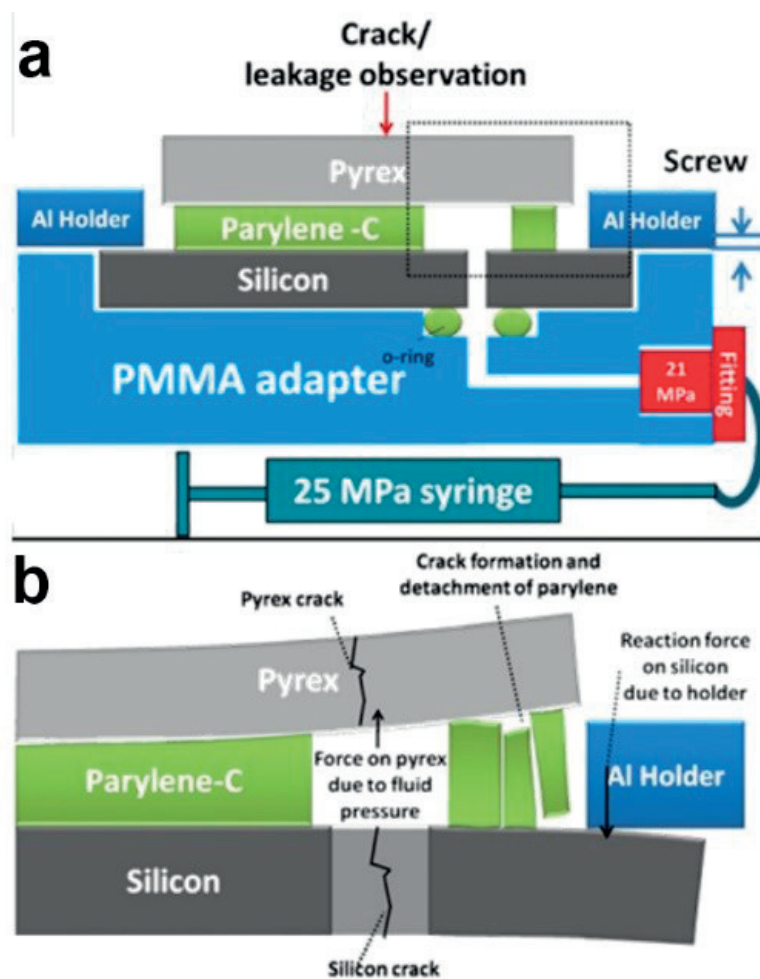
Figure 1.11- Diagram of (a) the burst pressure measurement setup, where the Pyrex part of the device is neither clamped nor assembled by any force other than that due to the Parylene–SiO$_2$ bonding process. (b) Diagram showing of possible burst pressure failure events. The image is adopted from [32].

This study shows that the bonding strength, the burst pressure and failure mode are important criteria for studying the reliability of this system. After examining different reliability factors, we can conclude that MTP is totally adapted for experiments that require high-temperature heating, up to 100°C, such as FISH and protein extraction (*vide infra*). It is chemically stable, resistant to high hydraulic pressure and is not affected by thermal stress during the experiment.

1.5.   Statistical background for intratumoral heterogeneity study

In the following section, I will present the basis for spatial autocorrelation analysis that is used in chapter 4.

In many fields, scientists need to define a relationship between locations and values of selected variables at these locations. For example, in biology a number of species like cells, plants or human in adjacent and distant sites can interact. If there is a correlation between distances of samples and properties of samples, this reveals that spatial locations can affect the distribution of properties at these locations. This phenomenon is

called spatial auto-association, in which there are two tendencies. First, similar values of a property tend to be situated close to each other. In this case, the site property has a positive autocorrelation with its neighbors. Second, different values can be located next to each other, meaning this site property has a negative autocorrelation with its neighbors. To quantify these events, we use global and local Moran's indicator (Moran's I). Global Moran's I (or Moran's I in short)was developed by Patrick Alfred Pierce Moran [36]. It is calculated as follow

$$I = \frac{N}{W} \sum_i \sum_j w_{ij} \, z_i z_j$$

where

N: number of spatial units indexed from i to j

$$W = \sum_i \sum_j w_{ij}$$

w_{ij}= weight matrix which defines neighborhood. $w_{ij} = 0$ if i and j are not neighbors of each other. $w_{ij} = 1$ if i and j are neighbors of each other. The unit j is the neighbor of each unit i when distance between i and j is lower than a threshold distance

x= variable value at the considered location

$\bar{x}$= mean of x

$$\sigma \, (standard \; deviation) = \sqrt{\frac{(x_i - \bar{x})^2}{N}}$$

σ^2: variance

$$z_i = \frac{x_i - \bar{x}}{\sigma}$$

$$z_j = \frac{x_j - \bar{x}}{\sigma}$$

Moran's I has a value between -1 and 1. A positive Moran's I hints that samples with high-value property is clustered together. A negative Moran's I suggests that data is more scattered and high- and low- value samples are mixed.

Local Moran's I is one of local indicators of spatial association proposed by Luc Anselin [37]. It is in fact the indicator of Moran's I computed at each unit i with its neighbor j. Moran's I aims to test whether the data in the whole study area is more clustered or scattered, while local Moran's I intends to identify elements within a homogeneous and heterogeneous cluster (local level). Without a specification, Moran's I means global Moran's I. The local Moran's I is calculated at each sample position as follows:

$$I_i = z_i \times \sum_j W_{ij} z_j$$

Local's Moran I provides a classification of the sample of interest with 5 types of clusters, which are "high-high" (high value of unit i next to high value of neighbor j z_i>0 and $\sum_j W_{ij} z_j$>0), "low-low"(low value of unit i next to low value of neighbor j, z_i<0 and $\sum_j W_{ij} z_j$<0), "low-high" (low value of unit i next to high value of neighbor j, z_i<0 and $\sum_j W_{ij} z_j$>0), "high-low" (high value of unit i next to low value of neighbor j, z_i>0 and $\sum_j W_{ij} z_j$<0), and "no significance" where there is no spatial association. If I_i>0 the sample has a positive spatial autocorrelation and If I_i<0 the point has a negative spatial autocorrelation.

Here is an example of using five-cluster classification to locate low and high risk of Japanese Encephalitis (JE) incidence in Nepal (figure 1.12) [38].
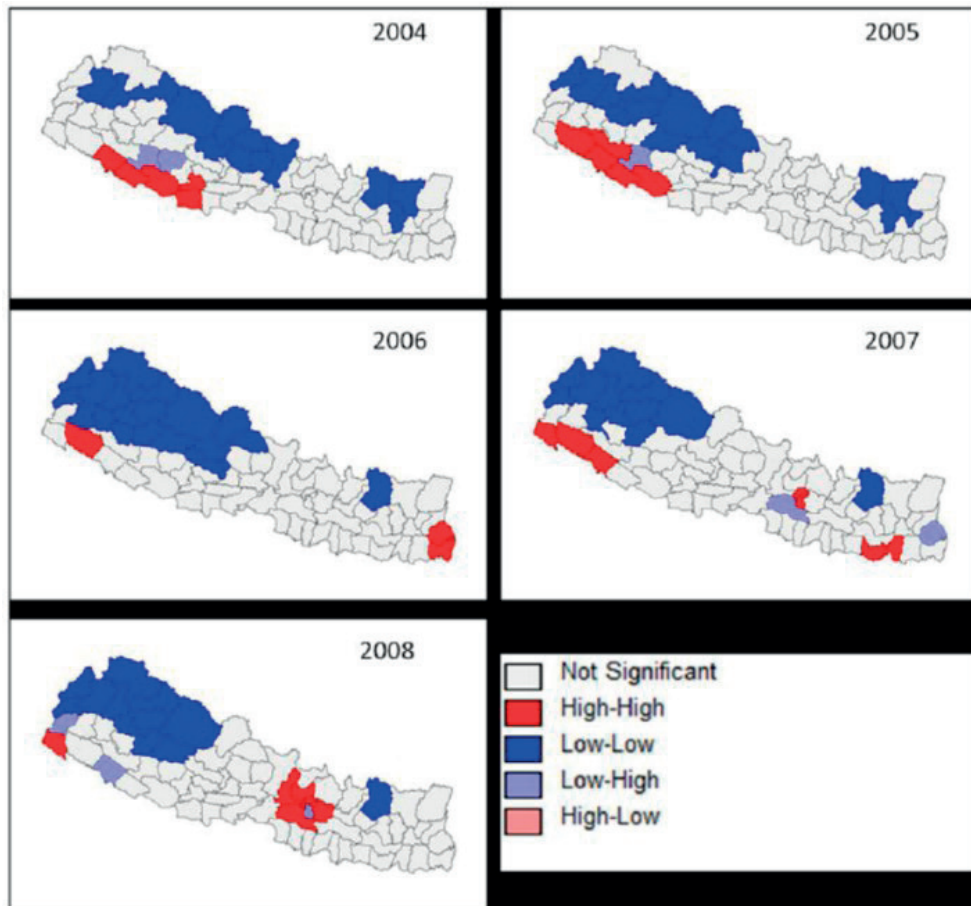
Figure 1.12 - The map of five local Moran'I clusters for Japanese Encephalitis incidence from 2004 to 2008. The 5-cluster classification was obtained from local indication of spatial association (LISA) analysis. In all years, there is a local association of homogeneously low (low-low) and homogeneously high (high-high) clusters that are marked in blue and red respectively. In some years, heterogeneously low (low-high) clusters are observed (light blue). Figure is adopted from [38].

From the local Moran's I map of JE incidence in Nepal from 2004 to 2008, we found different clusters of regions: the red regions represent locations where there are high values of JE incidence, while the blue ones display low values of JE incidence. Light red areas (not shown) are sites with high values of JE incidence and located nearby low-JE-incidence regions. Reversely, for light blue regions, low-JE-incidence areas are close to areas with high values of JE incidence. Finally, in grey areas, it is not significant to define a relationship between locations and values of JE incidence at these locations. In Nepal, JE virus concentrated in the Far-west and Mid-west regions in 2004-2005 (red clusters in the map). In 2006, it transmitted to the Far-east and then to the center in 2007-2008. Besides, it is found that values of JE incidence are often low in the North-west and North-east locations, shown by blue area. Further explanations for global and local Moran's I as well as their relation are described in Appendix A.

My research interest is to identify cancer heterogeneity where tumor areas have different HER2 protein expression or gene amplification classifications. Therefore, the local Moran's I is used as an indicator to pinpoint these tumor areas.

1.6. Thesis motivation

We have seen several state-of-the-art techniques for cancer classifications and treatments. Nowadays, cancer can be cured if the right treatment is applied at the right time. However, everything comes at a cost. The price for cancer diagnostics and treatments are increasing every year, provoking a rise in health insurance fees and financial burden for cancer patients. Personally, the author believes that cancer should not be a disease of the "rich". Instead, medicine should become affordable for every person who needs it. In this thesis, several applications for cancer diagnostics are presented. The motivation is all about making the current cancer screening methods cheaper and faster, while maintaining good quality in the tests. To achieve this aim, biological detections of biomarkers in tissue such as FISH or CISH are performed using the MTP. Thanks to efficient mass transport hydrodynamic flow, the reagent and time requirements for the tests can be decreased, thus lowering costs (see chapter 2). A proof-of-concept for protein biomarker quantification by combining microfluidic extraction and microarray detection is presented in chapter 3. Finally, a high-content analysis of quantitative IF and automatic FISH scoring techniques for accurate cancer heterogeneity detection is presented in chapter 4. We hope that this research can advance the field of cancer diagnostics. We also anticipate that in the future, personalized medicine will become more precise and affordable for cancer patients worldwide.

2. MICROFLUIDIC-ASSISTED IN SITU HYBRIDIZATION

FISH and CISH are well-recognized techniques for evaluating the human epidermal growth factor receptor 2 (*HER2*) gene status in breast cancer, despite their traditionally long and costly experimental procedure. Here we develop microfluidic-assisted principle for ISH, in which hybridization of the FISH probes with their target DNA strands is obtained by applying oscillatory flows of diluted probe solutions in a thin microfluidic chamber of 5 µl volume. We found that microfluidics helps reducing the experimental duration and decreasing the consumption of the expensive probe solution by improving the mass transport of the reactants. The study was done in 3 phases.

First, microfluidic-assisted FISH (MA-FISH) decreased the consumption of a standard HER2 FISH probe (Pathvysion®) by a factor 10 with respect to the standard technique, and reduced the hybridization time to 4 hours, which is 4 times faster than in the standard protocol, at the expense of a weaker *HER2* gene signal. To validate the method, we blindly conducted HER2 MA-FISH on 51 formalin-fixed paraffin-embedded (FFPE) tissue slides of 17 breast cancer samples, and compared the results with standard HER2 FISH testing. HER2 status classification was determined according to published guidelines, based on average number of *HER2* copies per cell and average *HER2*/CEP17 ratio (CEP17: Chromosome Enumeration Probe 17). Excellent agreement was observed between the two methods, supporting the validity of MA-FISH and further promoting its short hybridization time and reduced reagent consumption.

While microfluidics was found to help improving the mass transport of the reactants, the hybridization time of a standard FISH probe could not be decreased further because the use of formamide, serving as a double-helix destabilizing agent, slowed down the hybridization. Therefore, we combined a different, highly reactive probe solution containing ethylene carbonate buffer for fast double-helix destabilization (HER2 IQ-FISH pharmDx^{TM} probe), with a microfluidic system for improved reactant delivery. As this fast FISH probe is radically different from the ones used in any previous microfluidic FISH studies, a complete redesign of the protocol is required. Therefore, we used a fractional factorial design of experiments to optimize the microfluidic, ethylene carbonate buffer-based FISH protocol. After optimization, the incubation time required for performing FISH can be as short as 15 min for a cell line sample and 30 min for a human tissue slide, corresponding respectively to a fourth and a half of the duration of the corresponding step in the classical IQ-FISH protocol. Extra-short incubation microfluidic-assisted FISH (ESIMA-FISH) is overall the fastest and most economic microfluidic FISH technique for tissue analysis at the moment. The main drawback of ESIMA-FISH is that its HER2 signal is weaker than the one from the classical IQ-FISH technique. However, this limitation does not affect the scoring of the FISH signals, as the HER2 assessments of adjacent slides of human breast cancer tissue by ESIMA-FISH and standard IQ-FISH were similar.

Last, the microfluidic-assistance principle was applied to a CISH probe. The CISH probe used is diluted in a formamide–based hybridization solution and composed of a fluorescence that binds to enzymatic-labelled Ab. In this study, we achieve two aims: first we optimized MA-FISH using discontinuous-flow regime during hybridization step and apply the optimized MA-FISH parameter to perform Microfluidic-assisted CISH (MA-CISH). Hybridization time of MA-FISH and MA-CISH was then decreased from overnight down to 2 hours and 70% less probe solution is required for both tests, while achieving even a better signal quality than the corresponding standard techniques. Optimized MA-CISH was successfully tested for 6 breast cancer tissue samples and two cell lines, showing a good correlation with standard CISH results as

evaluated on adjacent slides. Finally, automatic scoring software was developed to facilitate CISH signal evaluation, and showed good agreement with the traditional counting protocol.

2.1. Introduction

FISH is a cytogenetic technique that targets a specific DNA or RNA location on a chromosome with a fluorophore-labeled oligonucleotide probe that is complementary to the target nucleic acid sequence [39]. In diagnostic and research laboratories, interphase FISH is widely used on FFPE tissue sections of cancer samples, to detect numerical and structural chromosomal alterations such as aneuploidies, amplifications, deletions and translocations [40]. However, its dissemination is impeded, among other factors such as its technical and analytical complexity, by the high cost of the probe and the long protocol times. Therefore, many studies focused on reducing the duration and reagent consumption of FISH tests through different approaches, including custom hybridization probes [41, 42], electric field mixing [43] and modification of the hybridization buffer composition [44]. In particular, microfluidic devices, where pl to μl volumes of fluid are manipulated, were used for implementing on-chip FISH on cells. Pioneering work was reported by Sieben et al. [45], who demonstrated that, by using recirculating hydrodynamic flow or electrokinetic transport, it was possible to decrease by ~90% the reagent volume and to reduce the hybridization time to few hours for FISH staining on adherent cells. The same group also reported a fully automatic cell-based microfluidic FISH, which consumed ~5% of the standard used probe volume [46], Recently, for implementing rapid, economical and multiplexed FISH for cell analysis, Huber et al. proposed scanning a vertically oriented capillary that creates a hydrodynamic flow of FISH probe on a small area (~0.096 mm^2) of the cell slide surface [47]. However, this technique can work only with fast hybridization centromere probes and has a small footprint due to the limited size of the capillary. While on-chip FISH analysis for immobilized cells is well-documented [47-54]. few examples of on-chip FISH analysis of FFPE tissue have appeared in the literature, partially because of the difficulty of miniaturizing the setup while preserving a large staining area.

About 15-20% of breast cancer patients have amplified and/or overexpressed human epidermal growth factor receptor 2 (*HER2*, also referred to as *ERBB2*) gene, which is associated with poor prognosis but predicts tumor response to HER2-targeted therapies, such as trastuzumab and other agents, which improve the patients' survival [55-58]. Reliable assessment of HER2 status is therefore of paramount importance and should be accomplished according to published guidelines [59, 60]. In a clinical perspective, immuno-histochemistry (IHC) can be used for HER2 detection, is cheaper (~100-300 $/test) and faster (2 h/test) than FISH (~300-800 $/test, 2 days/test with an overnight incubation) [56-58]. However, standard IHC is largely

qualitative, which may result in diagnostic ambiguities, whereas FISH is quantitative. In practice, in most pathology laboratories, HER2 status of a newly diagnosed breast cancer is first assessed by IHC, equivocal IHC cases are then elucidated by FISH [59, 60]. In this context, on-chip FISH for analysis of clinical tissue slides was recently reported for detecting *HER2* amplification [61]. In this design, a removable polydimethylsiloxane (PDMS) chip was clamped against a glass slide containing a tissue or immobilized cells to create a chamber. This chip could automatize the FISH process and consumed only 2 µl of probe solution, which is 1/5th of the classical probe volume per test, for a 5×5 mm^2 tissue surface. Also, no improvement of the hybridization time was reported. Nevertheless, and despite the high economic impact, FISH-on-a-chip for either cells or tissue was never clearly established in a pre-clinical study and its potential for routine diagnostic use not unambiguously demonstrated.

To address these challenges, in the first phase, we developed microfluidic-assisted FISH (MA-FISH), in which hybridization of the FISH probes with their target DNA strands is obtained by applying oscillatory flows of diluted probe solutions in a thin 16×16 mm^2 microfluidic chamber of 5 µl volume. The microfluidic system is based on a previously reported microfluidic chip used for the accurate IHC staining of breast carcinomas [31, 62]. The study consisted in two steps: optimization of MA-FISH experimental conditions, followed by validation of the optimized parameters by comparing MA-FISH with the standard FISH technique. Using the optimization parameter set, we show that MA-FISH can be performed on a tissue surface as large as 16×16 mm^2 and uses only 1 µl of the standard probe solution Locus Specific Identifier (LSI) *HER2*/CEP17 (PathVysion Kit, ABBOTT, IL, USA), which can be diluted, thus further decreasing the consumption of the expensive hybridization probe solution and the total duration of a test. In the validation step, we conducted *HER2* MA-FISH on 51 FFPE tissue slides of 17 breast cancer samples, and compared the results with those obtained from standard *HER2* FISH testing.

So far, despite fast fluidic exchanges, the incubation time was still relatively long (2 h to overnight), owing to the intrinsically slow probe-target hybridization kinetics, because of the presence of the formamide component in the probe solution [44]. Therefore, in the second phase of the study, we developed a new fast FISH technique, namely ESIMA-FISH to overcome the limitations of MA-FISH. This technique combines the confinement capability and fast mass transport of microfluidics with the highly reactive IQ-FISH probes. The unique reaction kinetics of the ethylene carbonate buffer-based probe called for a novel study aimed at designing a new, specific protocol. This approach reduces both the incubation time and the probe consumption. The staining protocol was optimized with a fractional factorial design of experiments combined to a multivariate linear regression analysis. The HER2 classification results obtained by ESIMA-FISH are compared to the standard IQ-FISH results using a series of tests ran on human breast cancer tissue samples.

In the third phase, the microfluidic-assistance principle was applied for improving Chromogenic ISH (CISH). CISH is emerging as a cheaper alternative to FISH, the latter requiring an expensive fluorescence microscope setup. Still, CISH usually require a high amount of the expensive probe solutions as well as long experimental times. No study has demonstrated a microfluidic CISH signal that is comparable to a standard ISH technique, while significantly reducing both the experimental time and the probe consumption. Therefore, we developed a microfluidic-assisted chromogenic in situ hybridization (MA-CISH) technique. The signal can be revealed either by directly observing the fluorescence image using MA-FISH as a control, or by bright-field microscopy (MA-CISH), after performing some additional immunohistochemical steps. Optimization of the protocol was carried out with an HER2-positive breast cancer cell line (SKBR3) by

analyzing different experimental conditions according to a fractional factorial design of experiments. The clinical performance of the optimized MA-CISH test was validated by comparing the results obtained from MA-CISH and standard CISH images originating from adjacent slides of 4 tissue samples and two SKBR3 cell line slides. Furthermore, an image processing software was developed to automatically score the HER2 and CEP17 signals, thus helping to reduce the analysis time. This study further improved microfluidic FISH and introduced MA-CISH as a promising tool for HER2 diagnostics.

2.2. Materials and methods

2.2.1. Chemicals and Materials

All the reactants were purchased from Sigma, unless stated otherwise. All the solutions in this work were made using 18 MΩ.cm water obtained from a Millipore purification system. All fluidic connectors, tubes, and fittings were purchased from ThermoFisher Scientific (MA, USA).

For the MA-FISH staining, the PathVysion HER-2 DNA Probe Kit (Abbott Molecular, IL, USA) was used and consisted of 2 differentially labeled probes focused at 2 different targets. The *HER2* gene locus (17q11.2-q12) is targeted by a 190 kb SpectrumOrange-labeled probe, which comprises several complementary DNA segments of the specific gene, and in our analysis was assigned a red color. The centromeric regions of chromosome 17 (CEN17) (17p11.1-q11.1) are localized by the 5.4kb SpectrumGreen-labeled CEP17 DNA probe, which comprises complementary DNA segments of the alpha-satellite region located at the CEN17, and in our analysis was assigned a green color. *HER2* probe and CEP17 are diluted in a formamide-based hybridization buffer.

ESIMA-FISH was performed using the reagents from the *HER2* instance quality FISH (IQ-FISH) pharmDx™ kit (Agilent Technologies Schweiz AG, Basel, Switzerland) and MA-CISH reagents were from the *HER2* Chromogenic in situ hybridization (CISH) pharmDX™ kit (Agilent Technologies Schweiz AG, Basel, Switzerland). *HER2* IQ-FISH pharmDx™ probe solution contains Texas Red-labeled DNA probes target the human epidermal growth factor receptor 2 (*HER2*) gene and fluorescein isothiocyanate (FITC)-labeled DNA probes target the CEN17. The probes are diluted in an ethylene carbonate-based hybridization buffer. HER2 CISH pharmDX™ kit is also consisted of Texas Red, and FITC-label reveal the position of *HER2* gene and CEN17, but diluted a classical formamide-based hybridization buffer. Texas Red and FITC labels are respectively bound to alkaline phosphatase (AP)- and HRP- conjugated secondary Abs to develop colored compounds for visualization.

2.2.2. Tissues and cell lines

FFPE invasive breast carcinoma samples, diagnosed between 2012 and 2015, were retrieved from the archives of the Institute of Pathology from the Vaud University Hospital (CHUV, Lausanne, Switzerland), selected in order to span a wide range of HER2 status. For each sample, 4 µm-thick tissue sections were cut from a representative FFPE block and mounted on Super Frost Plus slides (Menzel-Glaser, Germany). The invasive component of the carcinoma was located by a pathologist on adjacent hematoxylin and eosin (HE) stained slides. As part of an ethical convention (BB514/2012) with the Ethical Commission of Clinical Research of the state of Vaud, all tissues used in this study have been anonymized, codified and all patients have not expressed any objection to the use of their tissue. FFPE breast cancer cell lines (SKBR3) were produced by AMS Biotechnology (Europe) Limited, UK.

2.2.3. Microfluidic chip and setup
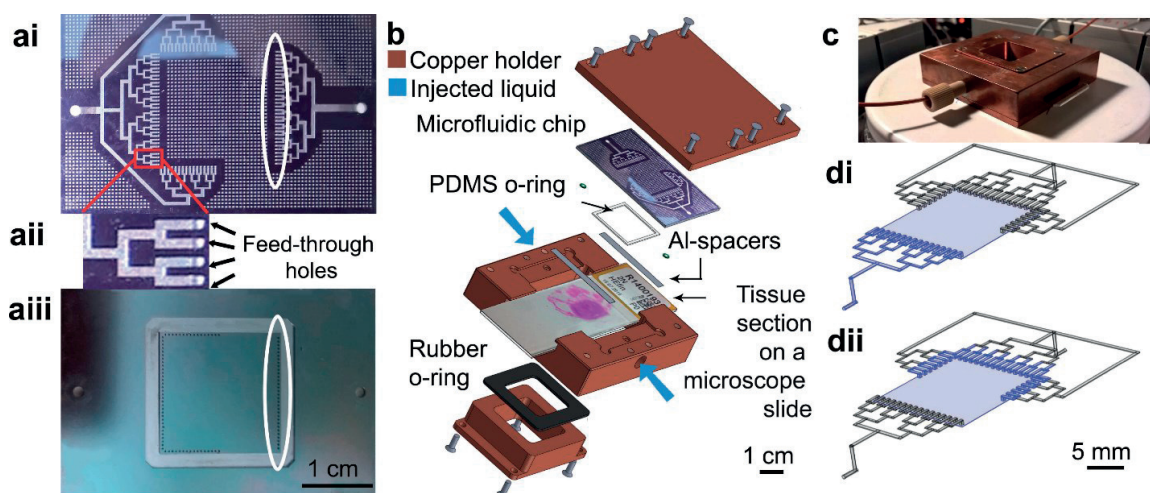
Figure 2.1 - Design of the microfluidic system. (a) The microfluidic chip consists of a bonded Pyrex-Si stack: (ai) view on the Pyrex side of the stack showing 'tree'-like channels on Si layer allowing a homogenous distribution of the liquid for uniform staining of the tissue; the flow is channelized via feedthrough holes, for example the array encircled in white, to (aii) the Si chip face that later will form the microfluidic chamber, together with the spacer strips, Polydimethylsiloxane (PDMS) o-ring and the tissue slide. (b) Exploded view of the setup. A microscope slide carrying a tissue section is mechanically clamped against a microfluidic chip and thereby forms the bottom of a thin 16×16 mm^2 size chamber. Two strips of Al foil serve as spacers controlling the chamber height to 20 µm, while a PDMS o-ring hermetically seals the chamber and the fluidic circuit that are placed in a thermostatic copper holder. (c) View of the upside-down assembly of the setup of (b) on a hot plate, which itself is to be positioned in a thermally insulating polystyrene chamber afterwards. (d) Three-dimensional representation of the channels and the 5 µl microfluidic chamber, in which square-wave oscillatory flow cycles are applied during the incubation step of a microfluidic-assisted in situ hybridization protocol. (di) and (dii) show the extreme situations of a cycle; the total staining solution volume (indicated in blue) is only 10-12 µl and is flanked by perfluorinated oil that fills the rest of the channels.

The microfluidic chip (see figure 2.1a) was micro-fabricated using the protocol illustrated in figure 1.8c in Chapter 1. The microfabrication process flow was adapted from reference [31]. Briefly, the chip consisted of a bonded Pyrex-Si stack: the Pyrex side showed 'tree'-like channels (figure 2.1ai) allowing a homogenous distribution of liquid for uniform staining of the tissue; the liquid was channelized via feedthrough holes (figure 2.1aii) to the Si side of the stack (figure 2.1aiii) that later formed, using mechanical clamping via screws, the microfluidic chamber together with the spacer strips, PDMS o-ring and the tissue slide (see figure 2.1b). A controlled screwing force during assembly was provided by a dynamometric screw driver (TorqueVario-S, Wiha Werkzeuge GmbH, Germany) for reproducibility. Two 20 µm thick aluminum strips served as spacers for fixing the chamber height at 20 µm, while a 350 µm thick PDMS o-ring (Shielding Solutions Ltd, Essex, UK) was inserted in a 275 µm deep notch to hermetically seal the chamber. A rubber o-ring distributed the clamping force homogeneously, and also contributed to a better thermal insulation of the chamber. If a cell line slide was inserted, two additional plastic film spacers of 10 µm-thickness were inserted inside the chamber in order to focus the flow stream on the pre-wetted surface of the cell pellet (Ø4

mm, not presented). The assembly of these elements was placed in a copper holder (figure 2.1b, c), the temperature of which was controlled by placing it on a hotplate (Scilogex MS-H280-Pro, Thomas Scientific, NJ, USA). Note that the assembly of figure 2.1b was presented upside-down for better visualization. Thermal stabilization was realized via read-out of an external thermometer probe (Fluke 54ii, Fluke, WA, USA) that was in contact with the microscope slide. During operation, the copper holder was also covered by a polystyrene foam-based thermal insulation chamber. Finally the copper holder was interfaced via commercial microfluidic fittings (see figure 2.1c) to 2 automated syringe pumps (Low Pressure Syringe Pump neMESYS V2 modules and base, code: A3921000102 and A3921000114, Cetoni GmbH, Germany). During the DNA hybridization step of the microfluidic FISH protocol, the pumps generated back-and-forth movements of the probe solution in the chamber (figure 2.1di-ii).

2.2.4. Standard FISH and CISH protocols

2.2.4.1. Standard HER2 Pathvysion FISH
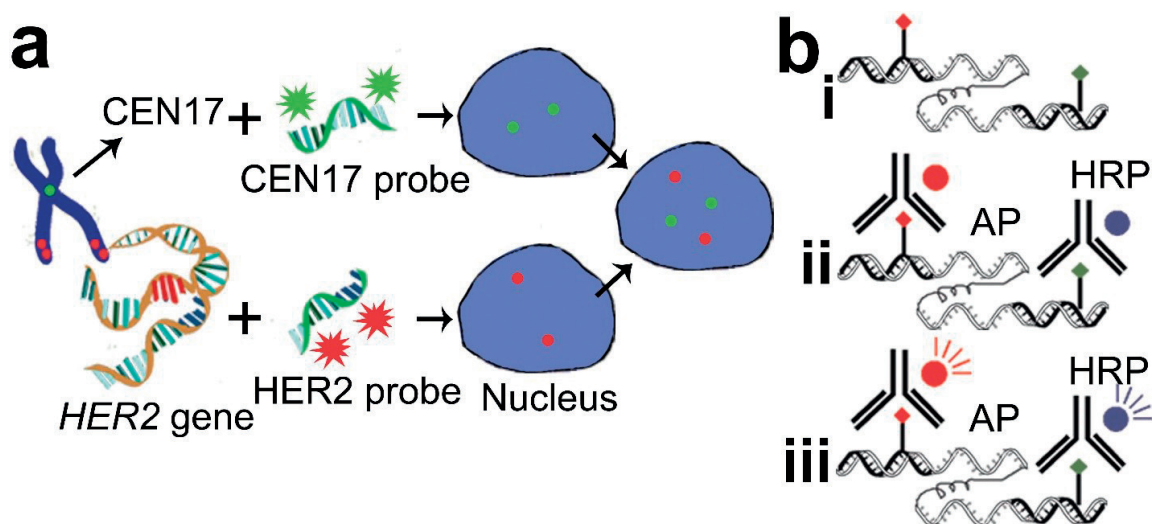
Figure 2.2 - Standard FISH and CISH technique illustration. (a) Schematic presentation of FISH method. After applying the probe solution via the microfluidic chip, probe-tissue incubation is performed under a hydrodynamic flow. The probe solution contains DNA probes that target the human epidermal growth factor receptor 2 (*HER2*) and the centromere of chromosome 17 (CEN17). During incubation, the DNA probes diffuse into the tissue where they combine with the denaturated single-stranded target DNA, revealing the different positions of *HER2* oncogene copies and CEN17 inside a nucleus. After FISH, counting the HER2 (in red) and CEN17 (in green) signals allows for HER2 scoring and classification. (b) Principle of DNA detection and chromogenic revelation in CISH. (bi) On-chip DNA hybridization between the two fluorescent probes and *HER2* gene and CEN17, respectively. HER2 probe is labeled with Texas Red (in red) and the CEN17 probe (CEP17) is labeled with fluorescein isothiocyanate (FITC) (in green). (bii) Off-chip binding of the Texas Red molecule to an alkaline phosphatase (AP)-conjugated secondary Ab and of the FITC molecule to a horseradish peroxidase (HRP)-conjugated secondary Ab, respectively. (biii) Off-chip development of the chromogenic HER2 signal by AP-induced precipitation of a red colored compound from a substrate and of the chromogenic CEN17 signal by HRP-induced precipitation of a dark blue colored compound from a substrate.

The standard Pathvysion FISH protocol was adopted from the standard practice used at the Institute of Pathology. For dehydration, a FFPE tissue section was first heated to 65°C during 5 min on a hot plate, and subsequently cooled down during 1 minute before being immersed 3 times in a Histoclear II (National Diagnostics, GA, USA) deparaffinization solution for 5 min. Next, the slide was rehydrated in a six-step protocol, using 100%, 100%, 95%, 70%, 40% ethanol, and Tris/HCl buffer (DAKO, Denmark) solutions, respectively, each step taking 2 min. The slide was then dipped into a Coplin jar containing MES (2-[N-morpholino] ethanesulphonic acid) 1× buffer (DAKO, Denmark) for 10 min at 95°C, and was then allowed to cool down in the same solution for 15 min. The slide was subsequently rinsed twice in Tris/HCl and treated by pepsin for 10 min at 37°C to remove any residual proteins from the tissue. After being washed twice in Tris/HCl, the slide was exposed to phosphate buffered saline (PBS, pH= 7.4) supplemented with 1% formaldehyde (Merck Millipore, Germany), 0.021 M $MgCl_2$ for 10 min and then rinsed in pure PBS. The slide was successively dehydrated in 40%, 70%, 95%, 100% ethanol using 2 minute sequences. The sample was retrieved from the ethanol bath and dried. After the complete ethanol evaporation, 10 μl of dual-labeled PathVysion DNA probe (HER2 and centromere of chromogene 17 probe) was applied on the tissue slide (figure 2.2a). The probe was spread evenly over the sample by depositing a 22×22 mm^2 coverslip on the slide and this stack was sealed by a thermoplastic rubber Coverslip Sealant (DAKO, Denmark). The sample was then exposed to 73°C for 5 min, on a hot plate, to denaturate the DNA and placed overnight (16 hours) in an oven at 37°C for hybridization. Upon completion of the hybridization step, the tissue slide was dipped in a stringent wash solution composed of 2× sodium-saline citrate (SSC), 0.3% Tween 20 (Bio Rad, CA, USA) at 73°C, followed by successive washing steps at room temperature in 2× SSC, 0.1% Tween 20 for 2 min, then in 2× SSC for 2 min, and finally in de-ionized (DI) water for 10 s. The sample was then successively rehydrated in 100%, 85%, 70% and 40% ethanol before being mounted with mounting solution containing 4',6-diamidino-2-phenylindole (DAPI) and anti-fading agent (Fluorescence Mounting Medium, DAKO), coverslipped and sealed with nail polish before imaging. A typical example of standard HER2 Pathvysion FISH image is detailed in figure 2.3.
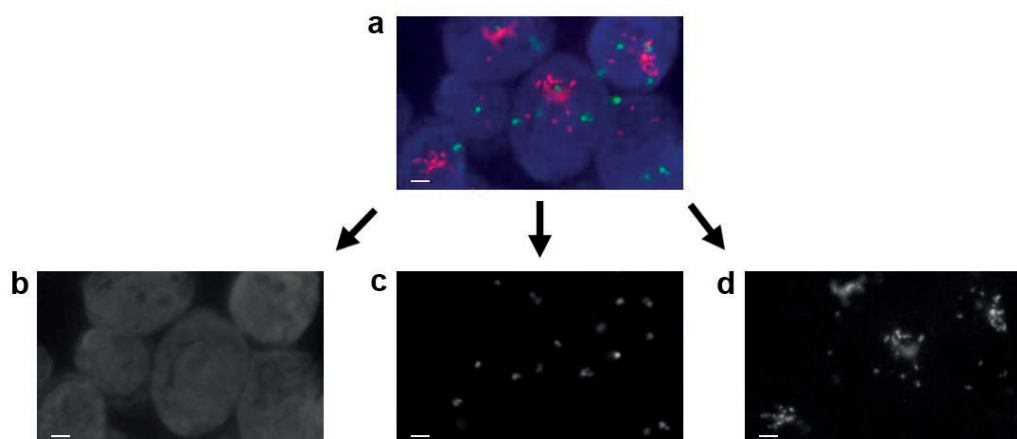
Figure 2.3 - Example of a fluorescence image obtained using the in-house standard FISH protocol. The image was acquired using a fluorescence microscope with high resolution objective (63×, NA=1.4, oil immersion). (a) Three-channel (blue, green and red) fluorescence microscopy image of a cluster of cells in a tissue. (b) Blue channel, locating the nuclei stained by DAPI. (c) Green channel, showing the centromere enumeration probe in chromosome 17 (CEP17). (d) Red channel, showing HER2 probe-labeled signals locating the *HER2* gene. Scale bar: 2 μm.

2.2.4.2. Standard HER2 IQ-FISH

For standard IQ-FISH, all pretreatment steps until the probe application step were similar as in standard Pathvysion FISH. During the probe application step, 10 μl of probe mix HER2 IQ-FISH FISH pharmDx^{TM} was applied on the tissue surface and the slide was subsequently covered with a glass coverslip and closed with rubber sealant. For standard IQ-FISH, the covered slide was put on a hot plate for denaturation at 66°C for 10 min (for IQ-FISH) and then incubated at 45°C for 1.2 hour on the hot plate (Scilogex MS-H280-Pro, Thomas Scientific, NJ, USA). For CISH, slides were then heated up to 73 °C for 5 min, then placed in a humid chamber (glass Petri dish, with humidified tissue, sealed with a plastic paraffin film) in the oven for overnight hybridization (45 °C). Once the hybridization step was completed, the rubber and coverslip were removed at room temperature. The slide was then processed with a stringent wash step, in which it was immersed in 1× stringent wash buffer (saline-sodium citrate (SSC) with Tween 20 detergent, respectively obtained from the standard IQ-FISH or CISH kit) at 63-65°C for 10 min, after which the specimens were washed twice with washing buffer for 3 min and dehydrated in a series of 70%, 85%, and 100% ethanol baths for 2 min each. For standard IQ-FISH, the slide was counterstained with DAPI (Agilent Technologies, CA, USA), covered with a glass coverslip and sealed with nail polish before imaging.

2.2.4.3. Standard CISH

All standard CISH pretreatment steps were similar to these of the standard FISH. 10 μl of the CISH pharmDX^{TM} probe is applied to the surface of the slide. 10 μl of dual-labeled PathVysion DNA probe was applied on the tissue slide. The slide is then coverslipped and sealed by the Coverslip Sealant thermoplastic rubber. The sample was then exposed to 73-82°C for 5 min, on a hot plate, to denaturate the DNA and placed overnight (16 hours) in an oven at 45°C for hybridization. Following overnight hybridization, the slide was washed in the same hot stringent wash bath (65±2 °C, 10 min), followed by 2 washing steps in tris(hydroxymethyl)aminomethane hydrochloride (Tris/HCl) from the kit for 3 min each. After 2 washing steps in Tris/HCl, named "1st wash buffer" for 3 min each, and after washing in Tris-buffered saline solution with 0.05% Tween 20, named "2nd wash buffer", for 3 min, tissues were covered with Peroxidase block for a 5±1 min incubation at room temperature (RT). After two 2nd wash buffer steps of 3 min each, tissues were covered with the CISH Ab mix (mix of HRP-conjugated Ab to FITC and AP-conjugated Ab to Texas Red, in 50 mmol/L Tris buffer with stabilizer, pH 7.5) and put in a humid chamber for incubation during 30±1 min at RT (figure 2.2bii). After two 2nd wash buffer steps of 3 min each, tissues were covered with the red chromogen solution for incubation in a humid chamber (10 min) (figure 2.2biii). After two 2nd wash buffer steps of 3 min each, tissues were covered with the blue chromogen solution for incubation (10 min) (figure 2.2biii). A 1:5 diluted hematoxylin solution was prepared, and put on the tissues after two 2nd wash steps using (3 min each) for counterstaining (5 min). Finally, tissues were rinsed with 2nd wash buffer, and left in it for 5 min, rinsed with distilled water and left to dry at 37 °C for approximately 30 min. After they had cooled down, slides were coverslipped with CISH-mounting medium, which was left to harden before inspection. Slides were then stored at RT.

2.2.5. MA-FISH protocol

The de-paraffinization, pre-treatment, protein digestion, post-fixation and washing steps were identical to that of the standard protocol and were done off-chip. However, the denaturation and hybridization steps were performed differently from the standard FISH protocol. In contrast with the standard FISH method, the PathVysion DNA probe solution was diluted with a solution consisting of 70% locus-specific identifier (LSI)

hybridization buffer (Abbott) and 30% DI water. Typically, the probe was diluted 10-fold, but other dilutions (5× and 20×) were also investigated. To run a MA-FISH protocol, a pre-treated and dehydrated tissue section was placed in the microfluidic system, which was then assembled (figure 2.1b). The spacer fixed the chamber height at h= 20 μm. Afterwards, two empty 100 μl syringes were partially loaded with ~30 μl perfluorinated oil (FC-40, Sigma-Aldrich Chemie GmbH, Buchs, Switzerland), degassed in a vacuum chamber and placed in an automatic syringe pump system (Nemesys, Cetoni GmbH, Germany). Each syringe was fitted with polyether ether ketone (PEEK) tubings (160 μm inner diameter, UpChurch Scientific, WA, USA). The probe was loaded in the system by aspirating a volume V= 10 μl of diluted probe in the tubing system attached to one of the syringes. The chamber was filled with the probe at 0.1 μl s^{-1} via fluidic connectors (UpChurch Scientific, WA, USA) until 5 μl of probe had been injected or until it reached the outlet, as presented in figure2.1di. The chamber has to be filled slowly to avoid bubble formation. After filling, the second syringe was connected to the outlet to close the microfluidic system. Great attention was given to avoid trapping of any bubble during the assembly. The denaturation was initiated by placing the microfluidic chip on a hotplate at T_d = 73°C for 5 min. The chip was then transferred to another hotplate, the temperature of which was fixed at T_h = 37°C. When the temperature was stabilized, the whole platform was thermally insulated by covering it with a polystyrene chamber, and a periodic flow was applied to the probe solution. The syringe pumps were programed to set a push-pull injection pattern, with one syringe injecting 5 μl of probe, and the other one aspirating the same volume, at the same flow rate. Once 5 μl of solution had been displaced (figure 2.1dii), the direction of the flow was reversed, thus allowing for repeated, cyclic flushes of 5 μl of probe over the sample. The flow rate Q was typically 1 nl s^{-1}, but other flow rates (0, 10, 100, 1000 nl s^{-1}) were also investigated. Each flow rate Q= 0, 1, 10, 100, 1000 nl s^{-1} has a corresponding push-pull cycle frequency f = 0, 10^{-4}, 10^{-3}, 10^{-2}, 10^{-1} Hz, respectively to keep exactly 5 μl of probe solution moving on the tissue surface. The cyclic square wave flow was applied inside the chamber for typically 4 h (but other hybrization time (2h and 8h) were also investigated), while the system was still maintained at 37˚C, to allow for hybridization. Hereafter, the slide was removed from the microfluidic setup, washed and prepared for imaging in the same manner as for the standard protocol. After being imaged, slides were stored at -25°C. The setup with the chip could be re-used after washing that was performed using a dummy slide, by injecting 2× SSC supplemented with 0.1 % Tween for ~2 min, rinsing it with 70 % ethanol, before drying the different components with compressed air. The MA-FISH protocol was optimized by comparing the fluorescence signal obtained from adjacent slides that were processed with series of different values of different experimental conditions (*vide infra*). The tissues that were used for the optimization process are different than the ones used in the validation phase.

2.2.6. ESIMA-FISH protocol

The ESIMA-FISH protocol was partially similar to the standard IQ-FISH protocol (*vide supra*), but the steps from the post-fixation to the end of the hybridization step were different. Here, several parameters can be adjusted, namely the absence or presence of a post-fixation step (*P*), the flow rate during hybridization (*Q*), the probe concentration (*C*), the denaturation temperature (*T*), the total volume of probe used (*V*), and the duration of the denaturation (t_d) and hybridization steps (t_h). We used a fractional factorial design of experiments to optimize these parameters, as described below in the optimization section. In our fractional factorial design, the post-fixation step could be present (*P*=1) or absent (*P*=-1). After the post-fixation step, a phosphate buffer saline (PBS) wash and a second dehydration in a series of 70%, 85%, and 100% ethanol, the denaturation and hybridization steps of ESIMA-FISH were implemented using the microfluidic setup. A syringe filled with FC-40 oil and 12 μl (*V* =-1) or 20 μl (*V* =1) of the diluted probe mix is mounted on a

pump and connected to the inlet of the microfluidic setup, see figure 2.1c. The probe solution is diluted 8× (*C=-1*) or 4× (*C=1*) in an ethylene carbonate-based hybridization buffer (reference G9415A, Agilent). The diluted probe solution was transferred to a microcentrifuge tube (Vaudaux-Eppendorf AG, Basel, Switzerland) and denatured at 66°C for 10 min. The probe solution is loaded in the microfluidic setup, and a second FC40 oil-flanked syringe is connected to the outlet of the setup. The device was put on a hot plate for denaturation (45 °C (*T=1*) or 66 °C (*T=-1*), 10 min (t_d =-1) or 20 min (t_d=1)). It was cooled down to 45 °C with an air flow in the case of the 66°C denaturation, and we used either a continuous (*Q* =1, see figure 2.4a) or discontinuous flow (*Q* =-1, see figure 2.4b) applied by two synchronized pumps placed at the inlet and outlet of the chip, until the end of the incubation step (45 °C during 15 min (t_h=1) or 30 (t_h=-1) min). The flow rates and the functions of the syringes were defined using the software supplied by Cetoni GmbH. All fractional factorial design of experiment combinations are presented in table 2.1.

Table 2.1 - Analysis of fractional factorial design of the experiments. The experimental conditions are summarized in the columns labeled with (1-8). For each of the parameters listed in the column on the left, two values are considered in columns (1-8), as reported between brackets, and associated to an arbitrary '-1' or '1' value. The regression coefficients for the 4 different signal outputs are listed in the last four columns, namely the average green and red signal diameter (D_{green} and D_{red}) and contrast (C_{green} and C_{red}), respectively. Here, the contrast is defined as $C = (I_s - I_b)/(I_s + I_b)$, with I_s the intensity of the signal and I_b the intensity of the background. The quality of the linear regression model is assessed with the least-square coefficient R^2 and the F-test p value.

Run #	Value of the parameter for this run							
	1	2	3	4	5	6	7	8
P	-1 (No)	-1 (No)	-1 (No)	-1 (No)	1 (Yes)	1 (Yes)	1 (Yes)	1 (Yes)
Q (nl/s)	-1 (10 nl/s discontinuous)	-1 (10 nl/s discontinuous)	1 (10 nl/s continuous)	1 (10 nl/s continuous)	-1 (10 nl/s discontinuous)	-1 (10 nl/s discontinuous)	1 (10 nl/s continuous)	1 (10 nl/s continuous)
C	-1 (8×)	-1 (8×)	1 (4×)	1 (4×)	1 (4×)	1 (4×)	-1 (8×)	-1 (8×)
T (°C)	-1 (66)	1 (45)	-1 (66)	1 (45)	-1 (66)	1 (45)	-1 (66)	1 (45)
V (µl)	-1 (10)	1 (20)	-1 (10)	1 (20)	1 (20)	-1 (10)	1 (20)	-1 (10)
t_d (min)	-1 (10)	1 (20)	1 (20)	-1 (10)	-1 (10)	1 (20)	1 (20)	-1 (10)
t_h (min)	-1 (30)	1 (15)	1 (15)	-1 (30)	1 (15)	-1 (30)	-1 (30)	1 (15)

Once the hybridization step was complete, the device was cooled down to room temperature using an air flow. The slide was then processed with a stringent wash step, in which the slide was immersed in a 1× stringent wash buffer obtained from the kit (SSC, buffer with Tween 20 detergent) at 63°C for 10 min, after which the specimens were washed twice with the washing buffer included in the kit for 3 min and dehydrated in a series of 70%, 85%, and 100% ethanol baths for 2 min each. Finally the slide was counterstained with mounting medium containing DAPI, covered with a glass coverslip and sealed with nail polish before imaging. In a FISH image, DAPI reveals the position of the nuclei, while Texas Red-labeled and FITC-labeled probes reveal the position of *HER2* gene and CEN17, respectively, see figure 2.2a.
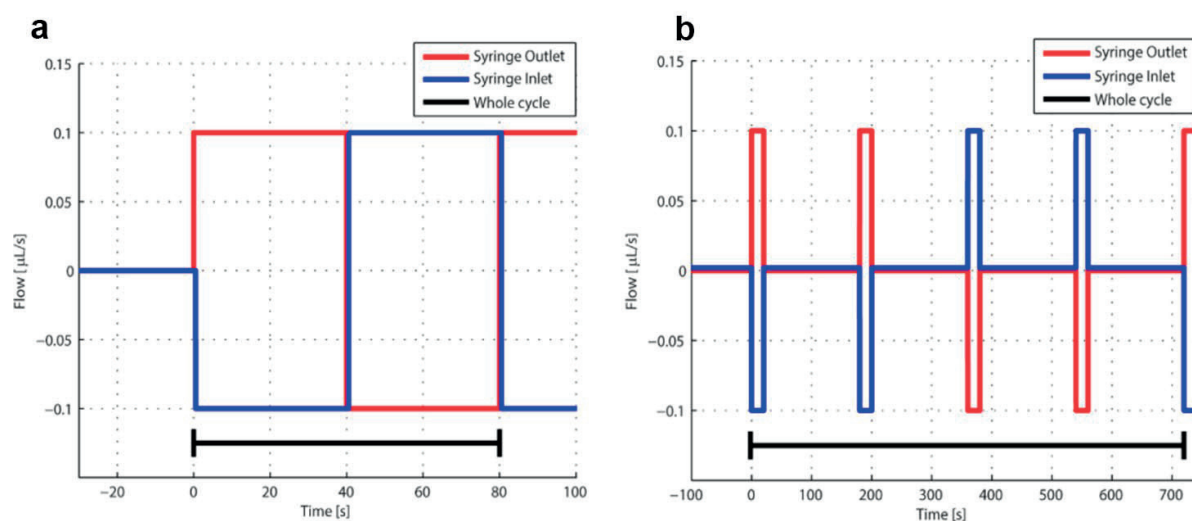
Figure 2.4 - Flow profiles applied during incubation, as actuated by two (inlet and outlet) syringe pumps. (a) For the continuous flow regime, the outlet syringe aspirated and the inlet syringe pump injected with a constant flow rate of ±0.1 µl/s until 4 µl was displaced, then the flow was reversed and 4 µl of solution was pumped back. The process was repeated until the end of the incubation. A period (one whole cycle) took 80 s. (b) For the discontinuous flow regime, the syringe pumps still aspirated/injected at the same flow rate, for the same displaced volume (4 µl) but each half period was split into 2 identical short regimes, characterized by a first ± 0.1 µl/s flow rate for 20 s followed by a quiescent phase for 160 s. Then the pumping directions of the two syringes were inverted. Here, the period was 720 s (4 min) and was repeated until the end of the incubation.

2.2.7. MA-CISH protocol

The pretreatment of slides before the hybridization step in the MA-CISH protocols is the same as in a standard CISH protocol from Agilent Technologies (*vide supra*). Only probe application, denaturation and hybridization differed from the standard procedure and were performed based on the microfluidic setup. Syringes were mounted on a neMESYS dosing system (Cetoni GmbH) and connected to the fluidic inlet and outlet, after being filled with FC-40 oil (Sigma-Aldrich Chemie GmbH, Buchs, Switzerland) and 12 µl of the diluted probe mix. The original probe solution was diluted in a solution based on SureFISH FFPE Hybridization Buffer from Agilent Technologies. The probe solution used in MA-CISH and MA-FISH protocol are identical. First, only the inlet was connected and the probe mix was injected until complete

filling of the chamber, after which the outlet syringe was connected. The device was put on a hot plate for denaturation (73 °C, 5 min). It was cooled down to 45 °C with compressed air, and a discontinuous flow regime, presented in figure 2.5a, was applied throughout hybridization (45 °C, 2 hours). The flow rates and the functions of the syringes were controlled using the software supplied by Cetoni. A volume of 4 µl oscillated at a flow rate of 0.01 µl/s. The probe was pushed for 100 s pulses (at a 0.01 µl/s rate), with 200 s intervals between each pulse. After 4 pulses, 4 µl had been moved forward, and the process was reversed, moving the 4 µl backwards. This cycle was repeated for the 2 hours of hybridization. The MA-CISH protocol can also be performed using a continuous flow regime (figure 2.5b) by applying 0.01 µl/s rate back-and-forth flow with any stop interval inserted. Once hybridization was over, the device was cooled down with compressed air, disassembled, and washed with stringent wash solution (SSC buffer with detergent) and ethanol. The IHC staining procedure for chromogenic revelation was performed. The staining procedure is identical to that of a standard CISH protocol as described in section 2.2.4. It is possible to perform MA-FISH first and thereafter MA-CISH, by removing the coverslip in the 2nd wash buffer then pursuing additional immunohistochemical staining.
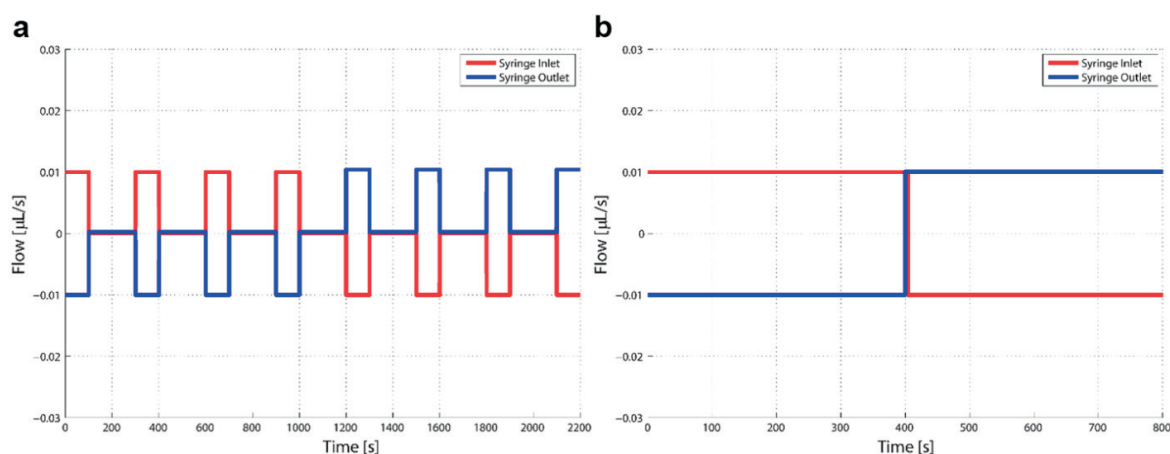
Figure 2.5 - Syringe-induced flow regimes that were used to induce back-and-forth movement of the probe solution during hybridization in a microfluidic-assisted chromogenic in situ hybridization (MA-CISH) experiment. (a) Discontinuous flow regime. A volume of 4 µl oscillated at a flow rate of 0.01 µl/s. The probe was pushed for 100 s pulses (at a 0.01 µl/s rate), with 200 s intervals between each pulse. After 4 pulses, 4 µl had been moved forward, and the process was reversed, moving the 4 µl backwards. This 220 s cycle was repeated during the hybridization time (2 or 4 h). (b) Continuous flow regime. During the hybridization time (2 or 4 h), a volume of 4 µl continuously oscillated at a flow rate of 0.01 µl/s without quiescent flow periods inserted between each back-and-forth flows.

2.2.8. Image acquisition

2.2.8.1. Fluorescence microscope for FISH:
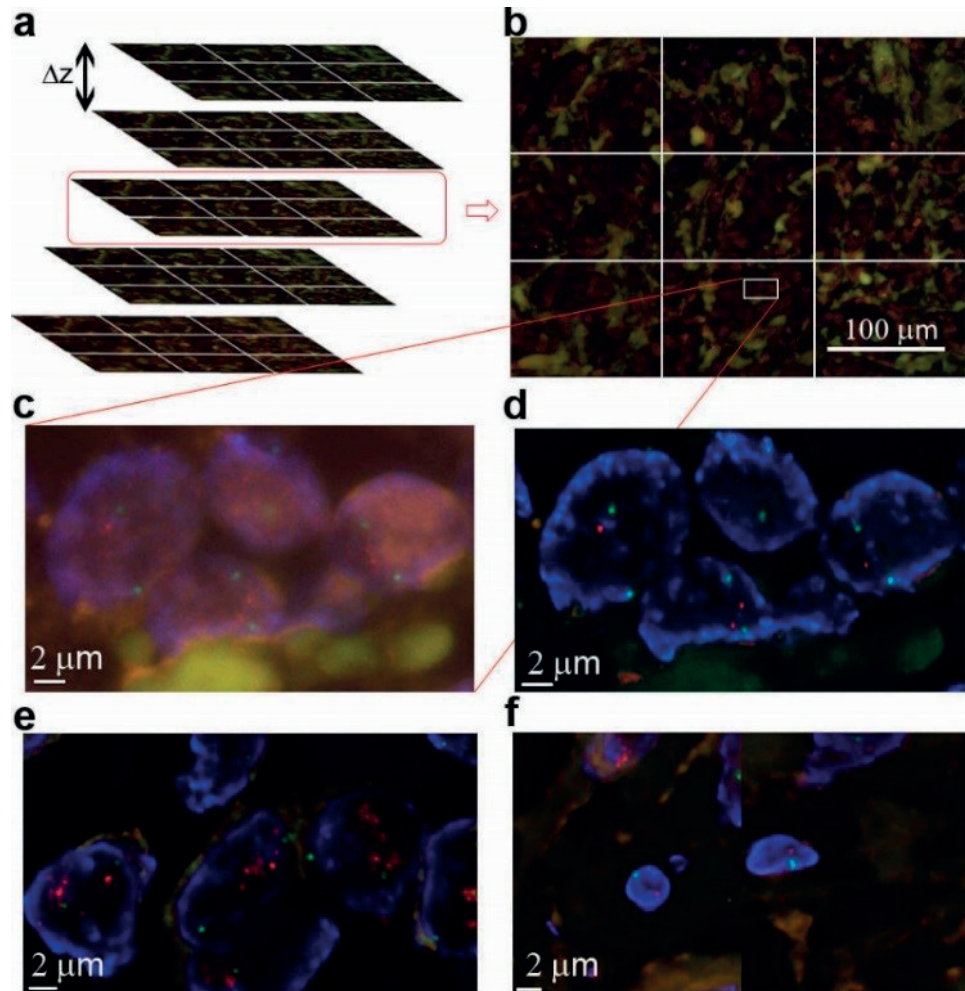
Figure 2.6 - FISH signal presentation. (a) Evaluation of the MA-FISH signal is based on a set of 3×3 mosaic z-stack images (typically 21 layers, Δz= 0.2 μm), recorded at different positions of the tumor area after the staining process. The recorded images span a tissue volume of $400 \times 300 \times 4$ μm^3. (b) The nine images of one layer of the z-stack. (c) Zoom on a region of interest of b, from which the FISH signal can be acquired. (d) Projected image of the 3-dimensional region of interest in a single plane, following deconvolution of all layers of the z-stack (HRM software, Scientific Volume Imaging B.V., Nertherlands) and three-dimensional reconstruction (IMARIS software, Bitplane, Switzerland) of the latter. This is a HER2-negative case (*i.e.* not amplified), which shows 1 to 2 copies of the *HER2* gene (corresponding to the red signals) per nucleus in the cancerous cells (their large nuclei can be appreciated thanks to the blue DAPI counterstain), and an approximately equivalent number of copies of centromere 17 (CEP17, corresponding to the green signals). (e) Projected image of a HER2-positive case (*i.e.* amplified), in which the cancer cells have large nuclei containing >6 *HER2* copies (red signals) per nucleus, while the number of CEP17 (green signals) is not increased, yielding a *HER2*/CEP17 ratio >2. (f) The same case as in e, but focusing on a region in the tissue of non-cancerous cells that have smaller nuclei and show no amplification of the *HER2* gene (internal negative control).

The same image acquisition and scoring method were applied for both MA-FISH, ESIMA-FISH, standard Pathvysion FISH and standard IQ-FISH. A fluorescence microscope (Carl Zeiss Axio Imager M2m) was used for the imaging. Three filter sets of Zeiss were used (02 High Efficiency (HE), 10 HE, and 43 HE) for imaging of DAPI, SpectrumGreen fluorophore (Abbott), and SpectrumOrange fluorophore (Abbott), respectively. A low magnification (10× objective) was first used to identify the areas of invasive carcinoma, which were then imaged at a higher magnification with a 63× oil immersion objective with 1.4 numerical aperture (Plan-Apochromat Oil DIC, Zeiss). The images were acquired through the Axiovision LE64 software to obtain multichannel images. The pixel size was 0.1 µm × 0.1 µm for all the images presented in this work. To allow high-quality imaging, z-stacks were obtained for n layers, with $n = h_{tissue}/\Delta z$, where h_{tissue} is the tissue thickness (~4 µm) and Δz is the axial increment step (figure 2.6a). This parameter could be tuned depending on the purpose of the analysis: for counting signals within a stack, Δz was 0.5 µm. For a 3D image reconstruction for a graphical presentation, Δz was fixed at 0.2 µm. The explanation of this choice is detailed in the section 2.2.8.2.

With these parameters, 3-channel (blue, green, red) z-stacks were recorded for the regions of interest of the slide, each corresponding to a volume of $300 \times 400 \times h_{tissue}$ µm³ of tissue. To facilitate the acquisition, each plane of the xy image was divided into a 3×3 mosaic (figure 2.6b, zoom to a region of interest in figure 2.6c), for which thereafter the whole 3D volume was reconstructed. The 0.2 µm step z-stack images were de-convoluted with the Huygens software (HRM software, AutoDeblur, BitPlane, Switzerland), followed by a 3-dimensional reconstruction with the software IMARIS (BitPlane, Switzerland). The fluorescence signal, for each channel, was then projected on the xy plane. Results for a HER2-negative case and a HER2-positive case were selected for the graphical representation in figures 2.6d and 2.6e, respectively. As an internal control of the technique, smaller non-cancerous nuclei with normal HER2 status, adjacent to HER2 positive cancer cells, are shown in figure 2.6f.

2.2.8.2. Choice of the z-stack and axial increment step Δz

FISH signals within a 4µm-thick tissue were recorded by analyzing a z-stack of high resolution (63× objective, 1.4 numerical aperture (NA)) images. The axial increment step Δz was chosen based on a calculation of the axial resolution (or depth of field) of the microscope. The latter can be computed as follows: $d_{tot} = \frac{\lambda_0 n}{NA^2} + \frac{n}{M.NA} e$,[1] with λ_0 the wavelength of the excitation light for the SpectrumGreen fluorophore (470 nm) or for the SpectrumOrange fluorophore (550 nm), n=1.515 the refractive index of the oil between the coverslip and the objective front lens element, and NA=1.4. The variable e is the resolution of the detector equal to 6.45 µm, and M=63× the lateral magnification. We obtain d_{tot}=0.474 µm for the green channel (SpectrumGreen) and d_{tot}=0.536 µm for the red channel (SpectrumOrange). For scoring signals, a z-stack composed of at least 9 layers with Δz=0.5 µm was chosen to record signals within the tissue volume. This sampling step Δz=0.5 µm < 0.536 µm is sufficiently small to observe all small red signals, whereas green signals which always span a much larger area (typically 1 µm in diameter) are easy to detect. Nevertheless, for getting high resolution representation of signals along the z direction, a deconvolution process applied to the z-stack images was needed and required a finer Δz=0.2 µm corresponding to the Nyquist criterion [63]. The latter states that the sampling frequency ~(1/Δz) should be at least twice the sample frequency ~(1/d_{tot}).

2.2.8.3. Bright-field microscope for CISH:

Slides were placed under a microscope (DM5500, Leica, Wetzlar, Germany) equipped with a motorized XY scanning stage, light source shutter and both optical and fluorescence functions. Images were acquired with a 63 × oil-immersion objective (LEICA HCX PL APO/ OIL).

2.2.9. Image analysis

An unbiased, quantitative and automated signal analysis based on an image processing pipeline, was developed using the open-access software Cell Profiler [64] (see figure 2.7 and table 2.2). The purpose of this analysis is to extract the diameter and intensities of each dot associated to the FISH signal, and allow for the comparison of different experimental conditions. Then, a contrast function, defined as $(I_{sg} - I_{bg})/(I_{sg} + I_{bg})$, with I_{sg} and I_{bg} the average intensities of the signals associated to either the green or red dot and the background, respectively, is computed. The numerical results for the different parameters were compared using a student t-test, or a one-way analysis of variance (ANOVA) test followed by a post-hoc Tukey's comparison test to justify our graphical observation, *vide infra*. The results were presented as mean ± SD, obtained by averaging diameter and contrast from 9 images in the selected 3×3 mosaic picture. Prism software (Graphpad Software Inc., CA, USA) was used to plot the results.
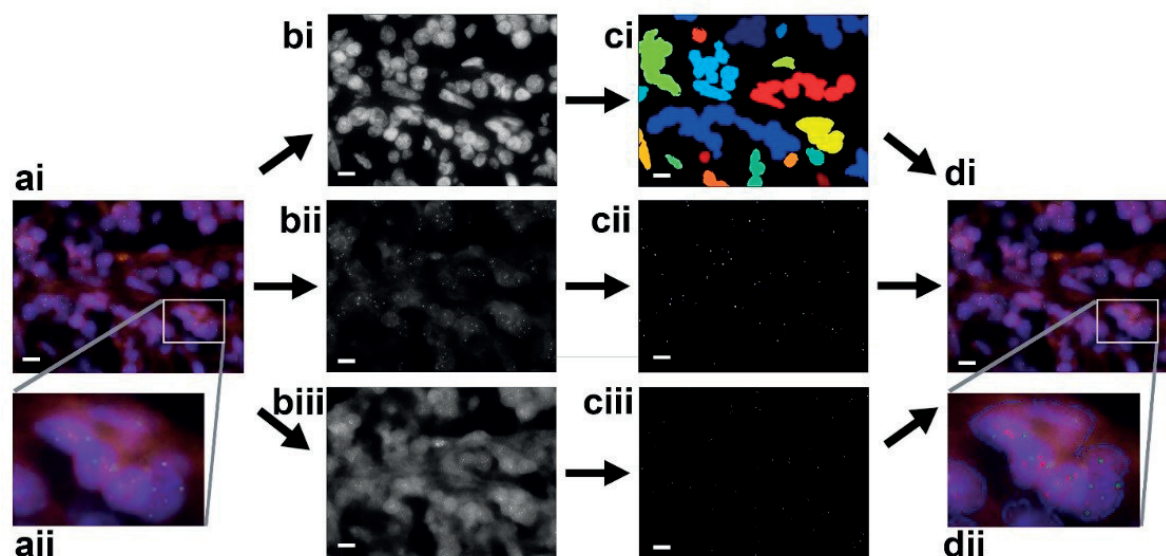
Figure 2.7 **-** Image processing performed on one focal plane of the z-stack in the MA-FISH protocol. (ai) One tile of the 3×3 mosaic picture. (aii) Zoom in one region of interest (ROI) of the picture in ai. (bi-iii) DAPI, green and red channel, respectively, of the picture in ai. (ci) Nuclei were identified by thresholding the signal in bi. A DAPI mask was created for allowing only selection of signals that are inside a nucleus. (cii) CEP17 signals, identified by thresholding the intensity in bii. (ciii) HER2 signals, identified by thresholding the intensity in biii. (di) Overlay of the outline of the identified nuclei, of the CEP17 signals, and of the HER2 signals with the original image. (dii) A zoom in one ROI of the picture di. Scale bar: 10 μm.

Table 2.2 - Different steps of the image processing protocol to measure the CEN17 (green) and HER2 (red) signal diameter (D_{green} and D_{red}) and contrast (C_{green} and C_{red}). Briefly, the original RGB (red, green, blue) image was split in 3 images, corresponding to the DAPI (blue), CEN17 (green), HER2 (red) signals, respectively. The HER2 image was thresholded with an appropriate automatic threshold method to define non-specific auto-fluorescence. Subsequently, the auto-fluorescence area was discarded in the DAPI image and the resulting image was called "DAPI masked". The area of nuclei was then detected in the "DAPI masked" image with an appropriate thresholding method. Afterwards, the background in HER2 and CEN17 image was suppressed and the images were called afterwards "HER2 filtered" and "CEN17 filtered". By using an appropriate threshold method, the "HER2 filtered" image was thresholded (named "HER2 filtered thresholded"). Then, "HER2 filtered thresholded" masked the "CEN17 filtered" image negatively (the outside of the "HER2 filtered thresholded" mask in the "CEN17 filtered" image is kept). The resulting image was called "CEN17 masked HER2", which contained only CEN17 signal without auto-fluorescence. By using an appropriate threshold method, the CEN17 signal was then detected in the "CEN17 masked HER2" image. The CEN17 signal was then transformed to a binary image that masked the "HER2 filtered" image negatively. Finally, the HER2 signal was detected in the "HER2 filtered masked" image using an appropriate threshold method. The backgrounds in CEN17 and HER2 images were defined as the area outside the CEN17 and HER2 signal areas. Afterwards, the program measured signal diameters (D_{green} and D_{red}) and intensities I_s of green and red signal, as well as the background intensity I_b of the HER2 and CEN17 image, in the original images based on the identified area to assess the signal quality.

Operation #	Input	Operation	Output
1	RGB (Red, green, blue) Image	Color to gray	images: DAPI (Blue), CEN17 (green), HER2 (Red)
2	HER2	Identify Primary Objects*	object: Auto-fluorescence
3	DAPI & Auto-fluorescence	Masking**	image: DAPI masked
4	DAPI	Identify Primary objects*	object: Nuclei
5	HER2	Enhance Or Suppress Features***	image: HER2 filtered
6	CEN17	Enhance Or Suppress Features	image: CEN17 filtered
7	HER2 filtered	Apply Threshold	HER2 filtered thresholded
8	CEN17 filtered& HER2 filtered thresholded	Masking	CEN17 masked HER2
9	CEN17 masked HER2	Identify Primary Objects	object: CEN17 dots
10	CEN17 filtered	Apply Threshold	Image: Binary CEN17
11	HER2 filtered& Binary CEN17	Masking	Image: HER2 filtered masked
12	HER2 filtered masked	Identify Primary Objects	object: HER2 dots
13	Nuclei& CEN17 dots	Masking+ Invert	Object:CEN17 background
14	Nuclei& HER2 dots	Masking+ Invert	Object:HER2 background
15	CEN17& CEN17 dots& CEN17 background	Measure intensity	CEN17 signal and background intensity
16	HER2& HER2 dots& HER2 background	Measure intensity	HER2 signal and background intensity
17	HER2	Measure size	HER2 dot size
18	CEN17	Measure size	CEN17 dot size

*Identify Primary Objects: Identification of nuclei, HER2 and CEN17 signals.
**Masking: Suppress the auto-fluorescence in one channel using another channel.
***Enhance or Suppress Features: similar to a high-pass filter that retains only speckle-like signal

2.2.10. Signal scoring

To assess MA-FISH and ESIMA-FISH scores, z-stacks (Δz= 0.5 µm) were obtained as detailed above, for three independent invasive locations of the sample. Axiovision software (Carl Zeiss, Germany) was used to inspect each layer of the z-stack (figure 2.8). For the *HER2* status assessment, the average number of HER2 dots per cell and the average *HER2*/CEN17 ratio in one or several cluster(s) of 20 cells were calculated. A ratio higher than 2, or a number of *HER2*/cell higher than 6 were considered positive; a number of *HER2*/cell higher than 4 and less than 6 with a ratio lower than 2 was considered equivocal, and anything lower than these thresholds was classified as negative, following the ASCO/CAP guidelines for FISH analysis [59]. According to these guidelines, two scores, the average *HER2* copy number/cell and the *HER2*/CEP17 ratio, should be reported for HER2 status assessment in clinical practice.

CISH scoring was performed using 2D images obtained from the bright-field microscope (z-stack not required). The image contrast was enhanced with FIJI [65], and blue and red signals were counted on clusters of 20 cells for each sample.
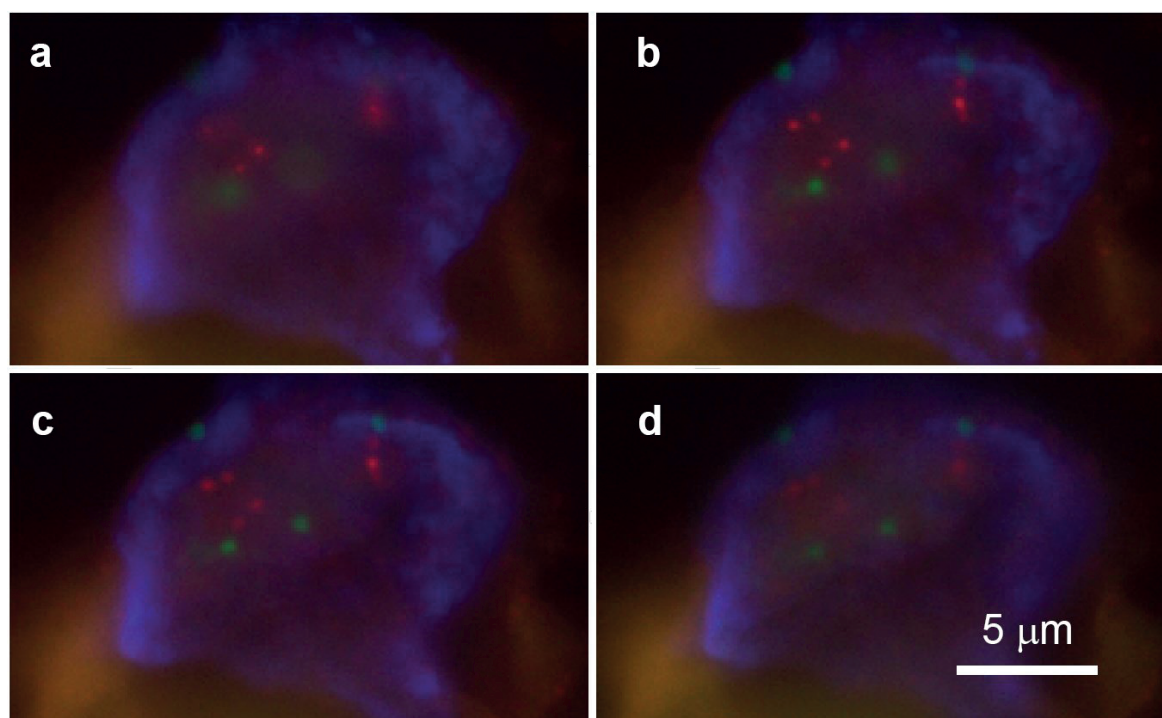
Figure 2.8 - Example of four consecutive images in a z-stack. For scoring signals in a FFPE tissue that was stained using a MA-FISH protocol, a zoom on consecutive images within a z-stack reveals several red and green signals that are identifiable in different focal planes. (a-d) 4 successive focal plans. In this example, 4 green CEP17 signals and 6 red HER2 signals are scored, as these are identifiable by the same signal pattern over the different images. To be counted as a signal, it should appear in at least two consecutive focal planes of the z-stack.

2.3. Microfluidic-assisted FISH (MA-FISH)

2.3.1. Results

2.3.1.1. Considerations on the system variables

To facilitate the analysis and guarantee an optimal diagnostic power, the FISH staining protocol should preserve the morphology of the tissue, result in a homogenous staining of nuclei with low auto-fluorescence from background materials, and feature well-defined, bright, DNA-specific FISH signals inside the nuclei. In a standard setup, DNA hybridization can be tuned by several experimental factors, such as the denaturation (T_d) and hybridization (T_h) temperatures, the denaturation (t_d) and hybridization (t_h) times, the composition of the buffers, the probe concentration C, etc. However, in the case where FISH is implemented in a microfluidic system, the flow rate Q and the microfluidic chamber height h will also all have an effect on the outcome of the test. Finally, the probe density d, *i.e.* the ratio of the total volume of undiluted probe solution used in the protocol V to the stained surface area of the section S is also introduced. The probe density can be seen as the cost, in terms of volume of undiluted probe solution, of the technique per unit of tissue surface, and has the dimension of a distance. This marker was used as a way to allow up-front comparison of different experimental techniques (for instance standard *vs.* MA-FISH) by normalizing the amount of probe used for each technique to the surface area of the target.

From these considerations, the analysis of the effects of the experimental parameters affecting the DNA-hybridization step in a MA-FISH protocol is a multi-parameter variational problem. However, some of these parameters are fixed according to the specificities of the standard protocol, such as T_d, T_h, or the buffer compositions, and others are not independent variables, such as d, and can be computed from other parameters (V, S and C). Furthermore, and in order to keep the dead volume to a minimum, h should be kept as low as technically possible. Therefore, to ensure that a total volume of probe solution could be used for each experiment, h was fixed at 20 μm and was not modified in this work. Finally, only 3 parameters were varied in the following analysis: t_h, C and Q. The other independent variables (T_d, T_h, t_d, V, S, etc.) were left unchanged throughout the experiments. For the off-chip standard protocol, a d value of ~21 μm (~0.021 μl mm^{-2}) had been used for the undiluted probe solution volume, following the recommendations of the manufacturer. The parameters t_h, C and Q were optimized. To ensure that the results for the different conditions, for a given parameter, were comparable, only adjacent slides from the same tissue block were used. As the tested material (human tissue sections) was limited, only one comparison test was performed for each condition for each parameter (t_h, C and Q). Furthermore, only conditions that were a priori expected to improve the technique (shorter times, diluted probes, etc.) and were also expected to not compromise dramatically the signal intensity were selected for this optimization.

2.3.1.2. *Optimization of the dilution factor*
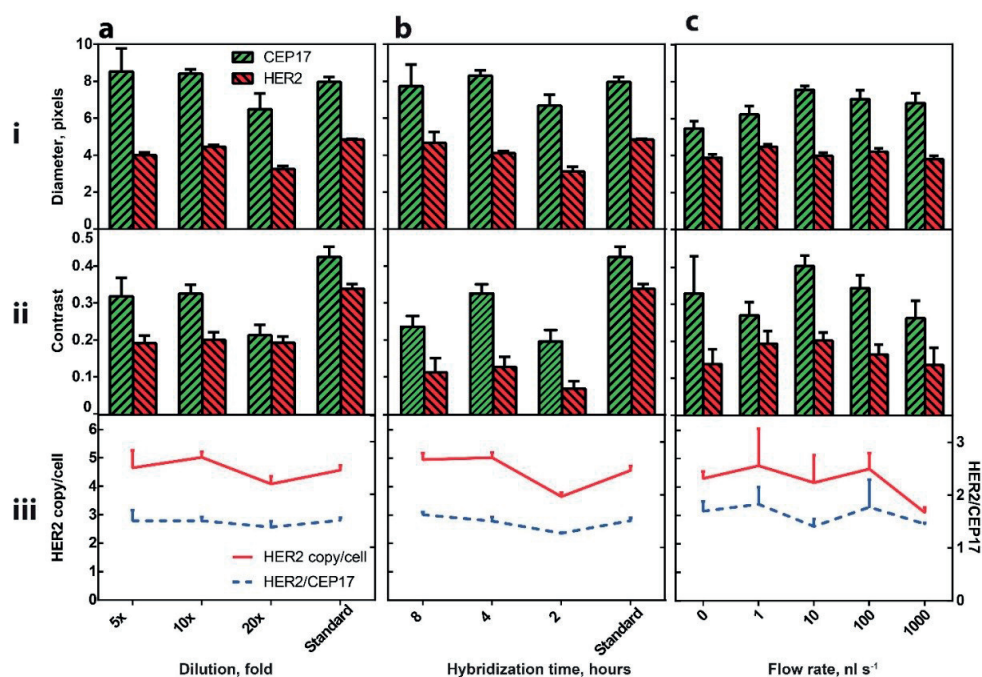
Figure 2.9 - Experimental parameter study of the MA-FISH protocol: Influence of probe dilution, hybridization time, and flow rate. (a) Optimization of the probe dilution. Four adjacent slides originating from the same tumor were incubated on-chip during 4 h with three different dilutions (5×, 10×, 20×) of a standard commercial probe solution, or off-chip using the standard protocol. The on-chip square-wave oscillatory flow was applied with an amplitude of 1 nl s^{-1} at a frequency of 10^{-4} Hz. The green bars were obtained by averaging the green signal diameter and contrast originating from the CEP17 and the red bars were obtained by averaging the red signal diameter and contrast originating from the HER2 probes from a mosaic image composed of 9 tiles. The last 2 bars correspond to standard off-chip overnight hybridization conditions with an undiluted solution. The different panels represent (ai) the average diameter of a signal, (aii) the average contrast of a signal (aiii) the average count of red signals (HER2) per nucleus of a cell (*HER2*/cell) for the three probe dilutions and the standard, obtained from 3 different positions for each slide (full line, left axis) and the *HER2*/CEP17 ratio (dashed line, right axis). (b) Optimization of the hybridization time. Four adjacent slides originating from the same tumor were incubated on-chip with a 10× diluted probe with a flow rate of 1 nl s^{-1} at a frequency of 10^{-4} Hz, using three different hybridization times (8, 4, and 2 h), respectively. The last 2 bars in each graph correspond to standard off-chip overnight hybridization conditions. (bi) The average diameter of a signal. (bii) The average contrast of a signal. (biii) *HER2*/cell number for the three hybridization times and the standard, obtained from 3 different positions for each slide (full line, left axis) and the *HER2*/CEP17 ratio (dashed line, right axis). (c) Optimization of the flow rate. Five adjacent slides originating from the same tumor were incubated on-chip during 4 hours using a 10× diluted probe, using five different flow rates of the on-chip square-wave oscillatory flow (0, 1, 10, 100, and 1000 nl s^{-1}) corresponding to push-pull cycle frequency f = 0, 10^{-4}, 10^{-3}, 10^{-2}, 10^{-1} Hz, respectively. (ci) The

average diameter of a signal. (cii) The average contrast of a signal (ciii) *HER2*/cell number for the five flow rate conditions and the standard, obtained from 3 different positions for each slide (full line, left axis) and the *HER2*/CEP17 ratio (dashed line, right axis).

To study the effect of C on the MA-FISH capabilities, three adjacent sections, obtained from the same tumor, were processed on-chip using the MA-FISH protocol with three different dilution factors (5×, 10×, 20×) of a standard commercial probe solution (PathVysion *HER*-2 DNA Probe Kit), with Q= 1 nl s^{-1}, f= 10^{-4} Hz and t_h= 4 h. These three sections were processed during three successive days and imaged with identical exposition conditions on the same day. A fourth adjacent section from the same sample was processed and imaged with the standard FISH method, which used a non-diluted probe, and served as a control. As detailed above, several numerical variables (signal diameter and contrast) were obtained to characterize the quality of the FISH staining, and are presented in figure 2.9. From the data shown in figure 2.9ai, the 20× dilution configuration resulted in smaller diameter of the red and green signals than the 10× dilution (p<0.0001 for red and <0.001 for green) and the 5× dilution (p<0.0001 for red and <0.0005 for green) (figure 2.9ai). An increased dilution yielded smaller green signal contrast for the 20× dilution than the 10× and 5× dilution (p<0.0001 for both), but did not significantly affect the red signal contrast (figure 2.9aii). Finally, the average number of *HER2*/cell and the *HER2*/CEP17 ratio in 3 clusters of 20 cells were also computed. As the sections were obtained from adjacent positions from the same tumor, similar scores are to be expected. Indeed, the 10× and 5× dilution yielded similar results as the standard FISH method (figure 2.9aiii), but a lower number of *HER2*/cell was found for the 20× dilution. Overall, these results indicated that the 10× dilution factor for the PathVysion probe was the preferable one, as it resulted for our MA-FISH setup into comparable results to the standard technique.

2.3.1.3. Optimization of the hybridization time t_h

As above, the effect of t_h was investigated by incubating 3 adjacent slides originating from the same tumor for 2 h, 4 h and 8 h, respectively, in a 10× diluted probe solution with Q= 1 nl s^{-1} and f= 10^{-4} Hz (see figure 2.9b). The sample corresponding to t_h= 4 h is the same as the one used in the dilution factor analysis for a 10× dilution, but was analyzed again alongside the other samples. The 4-h hybridization yielded the same type of response as for t_h = 8 h, as suggested from the values of the signal diameter in the red and green channels, but a noticeable degradation of the quality of the FISH staining was noticed for the 2-h hybridization. Indeed, from the data shown in figure 2.9b, the 2-h hybridization configuration resulted in smaller red signals (p<0.0001) and green signals than the 4 h (p=0.001) (figure 2.9bi). It also yielded weaker green and red signal contrast than the 4 h (p<0.005) (figure 2.9bii). The signal count on the 2-h hybridization MA-FISH slide resulted in a lower number of *HER2*/cell and lower *HER2*/CEP17 ratio comparing to the use of 4-h and 8-h hybridization times (p<0.0005 for *HER2*/cell number and <0.001 for the ratio), the latter times resulting in the same count than the standard technique (figure 2.9biii). From this analysis, an optimized hybridization time of 4 h was chosen, hereby resulting in a significant shortening of the experimental duration, in comparison to the standard protocol (16-h hybridization). The green signal in an 8-h hybridization MA-FISH test showed fluorescence intensity reduction due to photo-bleaching, possibly because of air exposure, which however did not affect the signal count. It proved to be difficult to decrease the hybridization time below 4 h, since probe diffusion in the tissue and small DNA hybridization rate in formamide solution require sufficient incubation time [44].

2.3.1.4. Optimization of the flow rate Q

In order to find an optimal Q for MA-FISH, five adjacent sections originating from the same tumor were incubated on-chip during 4 h in a 10× diluted probe, using five different Q for the on-chip square-wave oscillatory flow profile (Q= 0, 1, 10, 100, and 1000 nl s^{-1}). The characteristic parameters for each sample were computed and are reported in figure 2.9c. The Q= 1 nl s^{-1} configuration resulted in the largest red signal diameter with respect to the other flow rates used, while there is a noticeable variation of the green signal diameter as function of Q, which is however not critical for interpretation, due to the larger size and high intensity of a green signal that represents the centromere-specific probe (figure 2.9ci). The Q= 1 nl s^{-1} configuration resulted also in the largest contrast for the red signals with respect to the other flow rates used, while variation in the green signal contrast as function of Q again is not critical for interpretation (figure 2.9cii). The results for the number of *HER2*/cell and the *HER2*/CEP17 ratio (figure 2.9ciii) did not allow for clearly establishing which Q led to the best results, largely because of the signal variation induced in this specific sample by a high level of genetic heterogeneity. The variation induced by the heterogeneity depends on the position of the clusters studied, and has a more important impact on the experimental output than the variation due to change in flow rate. Therefore no significant difference between the flow rate conditions was found [66].

Summarizing, applying a flow of probe over the sample improves the reactant delivery with respect to the delivery by diffusion only and reduces depletion effects of the probe inside the chamber, as present with the quiescent flow condition, in which the tissue has consumed all local probes. On the other hand, if the flow rate is too high, it can affect the probe-target combination. It was demonstrated indeed that hybridization between target DNA and immobilized DNA on a surface of a DNA microarray could be impaired under a strong flow rate [67]. Therefore DNA hybridization on a tissue section can also be affected by a strong flow, probably because of the presence of shear stresses near the tissue surface that hinder the hybridization events. As a consequence, we have chosen to use Q= 1 nl s^{-1} for the final MA-FISH protocol. In conclusion, the final MA-FISH parameter set, chosen from the optimization study, are C= 10× dilution, t_h= 4h, Q= 1 nl s^{-1}.

2.3.1.5. Technical comparison between MA-FISH and standard-like coverslip technique but using the same 10× dilution and 4h hybridization time.

Chapitre 2 We compared the MA-FISH technique with a standard-like coverslip-based protocol, in which we exposed a slide to a 10× diluted probe (standard= 1×) and used a 4h hybridization time (standard= hybridization overnight, i.e. 16h). The probe density, presenting the probe solution used per footprint, was also kept the same as for MA-FISH (d=3.9 µm). This experiment was designed to show the signal enhancement granted by the hydrodynamic method. 17 sections from 17 different tissue blocs were processed with the coverslip method, were imaged by the same protocol than in MA-FISH slides and the resulting HER2 status was also compared to the in-house standard FISH and reported in table 2.3. As shown in figure 2.10, the MA-FISH results in much stronger signals compared to the coverslip-based technique, which showed a quasi-inexistent signal, even though the amount of probe introduced in the system and the image acquisition and processing were the same. Among them, 41% (7/17 cases) gave even no specific red signal for the scoring process. The reason of this difference is expected to arise from the constriction of the diffusion layer near the slide surface under hydrodynamic conditions, thus increasing the flux of probe towards the tissue and accelerating the hybridization. This confirmed the critical importance of the hydrodynamic conditions in improving the FISH signal.
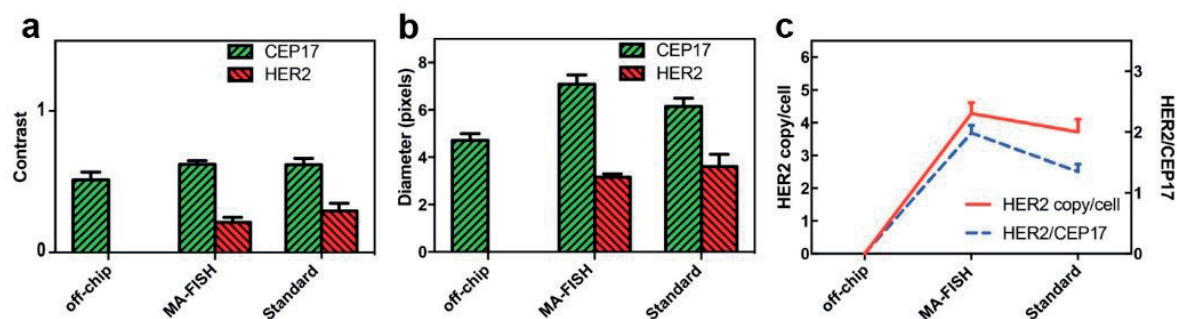
Figure 2.10 - Effect of microfluidics on hybridization. Three adjacent sections originating from the same tumor were incubated with a 10× diluted probe solution during 4 h under a coverslip (abbreviation in the graph: "off-chip"), with a 10× diluted probe solution during 4h according to the MA-FISH protocol ("MA-FISH") and with a standard probe concentration (1×) and long hybridization time (overnight) of probe under a coverslip ("standard"), respectively. The green bars were obtained by averaging the signal contrast and size originating from the CEP17 signals and the red bars were obtained by averaging the signal contrast and size originating from the HER2 probes, from a mosaic image composed of 9 tiles. (a) Average contrast of a signal. (b) Average diameter of a signal. (c) Average count of red signals (HER2) per nucleus of a cell (*HER2*/cell) (full line, left axis) and the *HER2*/CEP17 ratio (dashed line, right axis). The results were obtained from 3 different positions for each slide (20 cells evaluated for each position). In the "off-chip" results, images did not reveal any red signal, explaining the inexistent red signal contrast and diameter. The results were presented as mean ± standard deviation (SD).

Table 2.3- Comparison of the HER2 classification results between an off-chip FISH protocol with 10× diluted probe solution and the in-house standard FISH analysis, using HER2 assessment according to 2013 ASCO/CAP guidelines.

Concordance table		In-house standard FISH protocol			
		Negative	Equivocal	Positive	Sum
Off-chip FISH protocol with 10× diluted probe solution and 4 h hybridization time	No HER2 signal	4	2	1	7
	Negative	5	1	2	8
	Equivocal	0	0	0	0
	Positive	0	0	2	2
	Sum	9	3	5	17

2.3.1.6. Comparison of HER2/cell, HER2/CEP17 ratio and HER2 status between MA-FISH and standard FISH protocol

To test the diagnostic power of the MA-FISH technique, as optimized in the parameter study sections (*vide infra*), we performed a series of tests on a set of 17 breast cancer samples chosen to represent a wide spectrum of different *HER2* copy numbers per cell and different HER2 statuses. During the initial HER2 assessment performed at the Institute of Pathology using the standard off-chip protocol, 6 cases were classified as HER2-negative, 6 were equivocal and 5 were positive. However, to ensure a maximal consistency in the comparison of the MA-FISH technique with the standard protocol, the standard routine technique was repeated in our research laboratory to ensure that the use of other reactants, counting operators, and microscopic equipment, as well as the storage time of the biopsy sample in the tissue bank, did not introduce discrepancies with respect to the standard benchmark. To perform this study, several adjacent sections were used for each tissue sample. One section was processed according to the standard FISH protocol repeated in our laboratory, to provide the control dataset representing the current state of the art, further referred to as "in-house standard FISH". In parallel, 3 adjacent sections were processed with the MA-FISH system to address the question of technical reproducibility. Each slide was then blindly scored for i) the count of *HER2*/cell and ii) the *HER2*/CEP17 ratio. The counting routine used here based on z-stacks with $\Delta z = 0.5$ μm. For each slide, considering the biological variability issue, the average number of *HER2*/cell and the overall *HER2*/CEP17 ratio of a cluster of 20 cells were obtained for 3 clusters, corresponding to 3 separate locations on the tumor area. For the HER2 status assessment, the 2013 ASCO/CAP recommendations were used [59]. Briefly, the average *HER2* copy number/cell and the *HER2*/CEP17 ratio were obtained from 3 MA-FISH slides from the same patient. These scores were then averaged and compared to the cut-off values, for each parameter, reported in the 2013 ASCO/CAP recommendations to deduce the HER2 status of the patient. The variance among the 3 position scores for each slide was also computed, then averaged. The SD represents the scoring difference between clusters, and is different from the one obtained by pooling the average numbers of *HER2*/cell and the *HER2*/CEP17 ratio of the 3 cases and by then calculating the SD. The latter would incorporate slide-to-slide variability effects, which is represented by the coefficient of variation of triplicates, obtained by normalizing the SD of the triplicates to their mean. On the other hand, the former SD only describes the signal variability in the slide and was taken as a more reliable marker of data dispersion due to biological variability.
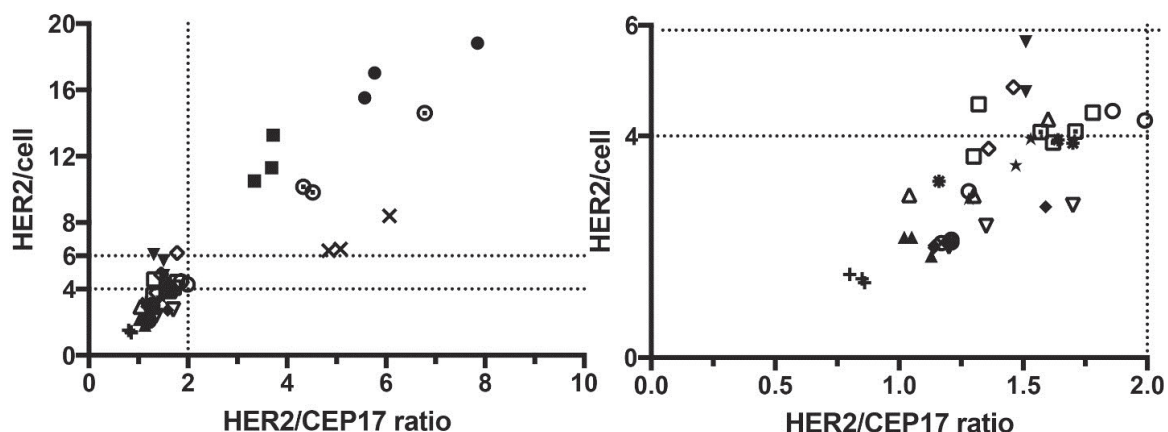
Figure 2.11 - Average number of HER2/cell and HER2/CEP17 ratio results from MA-FISH tests, in the full domain (left image) and in the sub-domain of HER2/cell number ≤6 and HER2/CEP17≤2 (right image). The test results that were obtained from slides of the same patient are represented by the same symbol in the graph. The dotted lines represent the cut-off values for HER2 status classification according to 2013 ASCO/CAP guidelines. In the right panel, some borderline cases, laying close to the dotted lines representing HER2/cell=4 and=6, are more likely to result in different clinical classifications, hence accounting largely for the assessment discrepancies discussed in the text. The total number of tissue slides analyzed here was N= 51 (17 tissues samples, analyzed in triplicates).

The final MA-FISH conditions using the optimized parameters described above were tested on 17 breast cancer samples, and the HER2 results were compared with the ones obtained with the standard protocol. The reproducibility of MA-FISH, shown by the consistency of the average number of *HER2*/cell and the average *HER2*/CEP17 ratio of triplicate slides are shown in figure 2.11. A good reproducibility of the MA-FISH results was demonstrated as the coefficient of variation among triplicates was 11.2% for the *HER2*/cell number (95% confidence interval (CI), 8.4 to 14%) and 10.6% for *HER2*/CEP17 ratio (95% CI, 7.5 to 13.7%).

The correlation between MA-FISH and in-house standard FISH scores with respect to the number of *HER2*/cell and the *HER2*/CEP17 ratio obtained from 17 patients is shown in figure 2.12a and figure 2.12b, respectively. The results of figure 2.12 demonstrate Pearson correlation coefficients (see appendix B for the explanation of the Pearson coefficient) between the MA-FISH and standard protocol datasets of r=0.98 (number of *HER2*/cell) and r=0.95 (*HER2*/CEP17 ratio), respectively. Also a linear regression was computed for these datasets, with a regression coefficient β=0.78 (R^2=0.97) and β= 0.93 (R^2=0.89), respectively. While the first regression coefficient may appear low, it mainly results from the lower fluorescence intensity for the highly amplified *HER2* cases due to the use of diluted probes. However, in these cases, the diagnostic outcome of the MA-FISH technique with respect to the standard protocol does not change (*vide infra*).
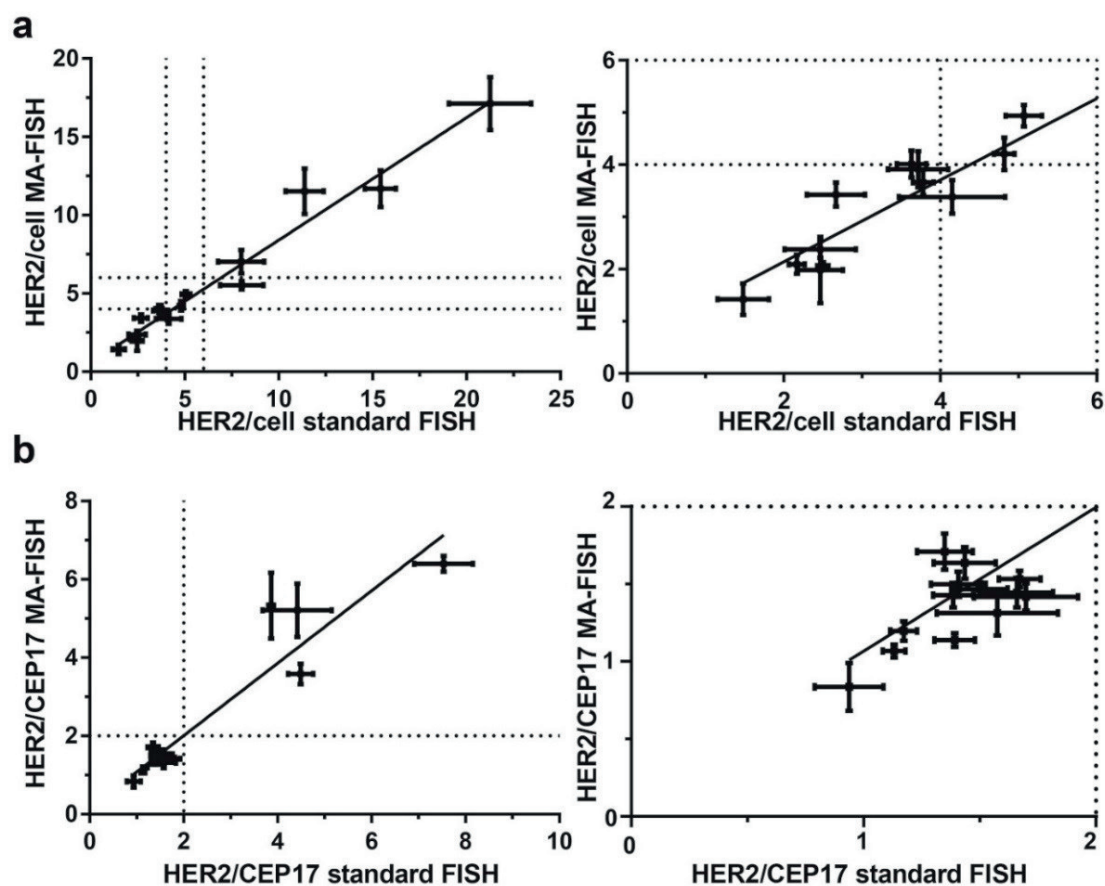
Figure 2.12 - Comparison of the MA-FISH with the in-house standard FISH protocol. Comparison between the results obtained for the MA-FISH and standard technique for (a) *HER2*/cell number in the full domain (left image) and in the 0 to 6 sub-domain (right image) and (b) the *HER2*/CEP17 ratio in the full domain (left image) and in the 0 to 2 sub-domain (right image). The results shown here correspond to 17 independent cases. The data represented for each point were the mean scores of 3 MA-FISH adjacent sections versus the mean scores of an in-house standard FISH adjacent section, obtained from the same tissue block. The vertical error bars represent the SD, with respect to the average of each specific slide, defined as the square root of the average of the variances obtained for each slide of the triplicates. The horizontal error bars are the SD of the scores among 3 positions in standard FISH slides. The dotted lines represent the cut-off values for HER2 status assessment according to 2013 ASCO/CAP guidelines. The linear fits show a good correlation of the FISH results (*HER2*/cell number and *HER2*/CEP17 ratio) between the MA-FISH and the standard FISH (Pearson's correlation coefficients were 0.98 and 0.95 respectively).

To compare the HER2 statuses obtained from MA-FISH with the ones from the standard FISH, the concordance between the average results of 17 MA-FISH triplicates from 17 independent tissue biopsies and standard FISH test results is reported in table 2.4. Table 2.4 also indicates that some of the borderline positive or negative slides, according to the standard test, became equivocal with the MA-FISH processing, and vice-versa. The likeliest explanation is that the biological variability is here critical, as most of the slides

were initially scored as equivocal, thus maximizing the risk for slide-to-slide variations (figure 2.11, right images). Nevertheless, no positive case was classified as negative and vice versa, which ruled out the risk for false positive or false negative HER2 status classification.

Table 2.4 - Comparison of the HER2 classification results of the MA-FISH protocol and the in-house standard FISH protocol based on a cut-off *HER2*/CEP17 ratio of 2.

		In-house standard FISH		
		Negative	Positive	Sum
MA-FISH protocol	Negative	13	0	13
	Positive	0	4	4
	Sum	13	4	17

The concordance between a FISH result and another method, such as IHC, or between two FISH methods was studied in the literature, solely based on the comparison of the *HER2*/CEP17 ratio, taking a cut-off value for the ratio of 2 or 2.2 [68-71]. A general strategy for comparing clinical outcomes involving two techniques makes use of Cohen's Kappa K, which is a parameter quantifying the agreement between two sets of qualitative ratings [72]. This analysis was applied to our MA-FISH and standard FISH datasets. By setting the *HER2*/CEP17 ratio cut-off at 2 and using it as a single criterion to separate the positive and negative FISH populations (*i.e.* there is no equivocal class), the concordance between the MA-FISH and in-house standard FISH results is evaluated with a score K=1.00 (100% concordance) (see table 2.4). The cut-off value for the HER2/CEP17 ratio was the one recommended in the 2013 ASCO/CAP recommendations [59].

Table 2.5 - Comparison of the HER2 classification results of the MA-FISH protocol and the standard initial FISH assessment done at the Institute of Pathology, based on a cut-off *HER2*/CEP17 ratio of 2. We observe that there is only one sample that is negative for the MA-FISH method but positive for the Institute of Pathology's standard FISH method. As our in-house standard FISH also indicated that this sample is negative, we think that this discordance is due principally to the HER2 intratumoral heterogeneity causing a variation of HER2 scores between different positions in the tissue.

		Institute of Pathology standard FISH		
		Negative	Positive	Sum
MA-FISH protocol	Negative	12	1	13
	Positive	0	4	4
	Sum	12	5	17

On the other hand, if the assessment is based on 3 classes described for the number of *HER2* copies per cell (negative, positive and equivocal) in the 2013 ASCO/CAP recommendations [59], the resulting Cohen's Kappa K is 0.71 (95% CI, 0.41 to 1.00), still showing a good concordance of MA-FISH and in-house

standard FISH clinical results [72]. A similar analysis comparing the MA-FISH results to the initial clinical HER2 assessments as obtained at the Institute of Pathology, showed that the results are highly consistent with the clinical standard methods (see table 2.5).

2.3.2. Discussion

The roughness of the tissue was considered as a possible source of inaccuracy by inducing different diffusion pathways for different tissue areas, resulting in non-uniform staining. However, the hydrodynamic flow was applied in a cycling fashion and helped mixing the probe inside the chamber, thus avoiding local depletions. Moreover, the diffusion distance of probe during the hybridization time of 4 hours is approximated by $x=2\sqrt{Dt}$ =0.88 mm, with D=1.33 10^{-7} cm^2/s [73]. The effect of this thickness variation, expected to be at most 10 nm [31], was therefore assessed as negligible. It was also investigated as a possible source of inaccuracy for FISH image readout. Here, the variation of the tissue thickness should be avoided because it might lead to a change of the average HER2 signals per cell, one of the two recommended scores for HER2 classification [59]. However, once again, comparing to the tissue thickness of 4 μm, the very limited roughness expected here should not dramatically alter the validity of the analysis.

From a technical standpoint, this study showed that MA-FISH is an advantageous, reliable technique to assess HER2 status on FFPE breast cancer tissue. On the one hand, by recirculating a diluted probe solution on the surface of the tissue during the hybridization time, the use of expensive probe can be optimized and the cost of a FISH experiment drastically reduced. Comparing to a standard FISH protocol using 10μl of probe per test, MA-FISH uses only 1 μl per test, reducing the cost by 10. If we consider the cost per footprint, the reduction is 5 times. Moreover, thanks to fast fluidic exchange within the microfluidic system [31], the diffusion of FISH probe from the probe solution to the targets situated in the tissue is also enhanced, resulting in short 4 h hybridization time (instead of an overnight incubation as in a standard FISH technique). The assay duration can be shortened to one working day (8 h) with the microfluidic method. The hybridization time can be further decreased by using a highly-reactive HER2 IQ-FISH PharmDx^{TM} probe (see section 2.4). However, the MA-FISH has a drawback is that the signals obtained are still weaker than that of a standard method, we demonstrate in section 2.5 that discontinuous flow regime can enhance the hybridization efficiency and increase the signal quality.

2.4. Extra-short incubation microfluidic-assisted FISH (ESIMA-FISH)

2.4.1. Results

2.4.1.1 Optimization of ESIMA-FISH protocol

The optimal experimental condition was chosen based on linear regression models of 4 different outputs (responses): the contrast (C_{red}) and diameter (D_{red}) of the red dots, and the contrast (C_{green}) and diameter (D_{green}) of the green dots, which were all required to be maximized to improve the quality of the images. These parameters were obtained and averaged for 3 different positions of the tissue for each combination of experimental conditions. At each position, a mosaic of 9 images (300 μm × 400 μm) was recorded. Each mosaic image displayed more than 20 cells. These outputs, and the array of input conditions, were then fitted to each other using a linear regression model:

$$\text{output} = \text{const} + a_P \times P + a_Q \times Q + a_C \times C + a_T \times T + a_V \times V + a_d \times t_d + a_h \times t_h \qquad (2.1)$$

where a_P, a_Q, a_C, a_T, a_V, a_d, a_h are the coefficients of the linear regression for the corresponding input variables presented above. The quality of the linear regression model was assessed with the least-square coefficient R^2 and the F-test p-value (see table 2.6).

Table 2.6 - Signal outputs and corresponding p-values. The top row represents the signal outputs: average green and red signal diameter (D_{green} and D_{red}) and contrast (C_{green} and C_{red}) with their p-values. The coefficients of the linear regression $a_{i=1, 2, ...7}$ are represented in the various columns for each signal output. In equation (2.1), the coefficients of the regression were normalized to *const*. The positive or negative sign of a coefficient indicates correlation or anti-correlation of an experimental variable with the output signal, respectively. The higher the contribution of an experimental variable to an output signal, the smaller the p-value; only a p-value < 0.05 (in **bold**) will be retained for interaction analysis between the important experimental variables.

	D_{green}	p-value D_{green}	D_{red}	p-value D_{red}	C_{green}	p value C_{green}	C_{red}	p-value C_{red}
Normalized const	1.000	**0.000**	1.000	**0.000**	1.000	**0.000**	1.000	**0.000**
a_P (P)	0.314	**0.000**	0.054	0.109	0.338	**0.001**	0.123	**0.012**
a_Q (Q)	-0.111	0.113	-0.038	0.248	-0.132	0.126	-0.016	0.721
a_C (C)	0.133	0.061	0.127	**0.001**	0.197	0.029	0.009	0.833
a_T (T)	0.110	0.115	-0.055	0.100	0.212	**0.020**	0.123	**0.012**
a_V (V)	0.002	0.979	0.001	0.986	-0.051	0.547	-0.019	0.673
a_d (t_d)	0.044	0.516	0.071	**0.040**	0.022	0.788	0.028	0.522
a_h (t_h)	0.072	0.291	0.081	**0.021**	0.067	0.427	0.047	0.297

The linear regressions corresponding to equation (2.1) resulted in R^2=0.53 (p=0.055), 0.67 (p=0.005), 0.686 (p=0.004) and 0.68 (p=0.004) for C_{red}, C_{green}, D_{red}, D_{green}, respectively. The product of an input variable to its corresponding coefficient (e.g. $a_h \times t_h$) is the contribution of this input to the output (diameter or contrast). Therefore, the optimal coded values for the inputs (*i.e.* -1 or 1, *vide supra*) should have the same signs as their coefficients in order to obtain a positive contribution, and an improvement of the signal output. The linear regression results is detailed in table 2.6. In this instance, each linear regression coefficient a_P, a_Q, a_C, a_V, a_d, and a_h had the same sign, when considering either contrast (see figure 2.13a) and diameter (see figure 2.13b) as output variable. Therefore, the optimized values of these parameters can be straightforwardly selected. The sole ambiguous case was for the parameter a_T, as the HER2 diameter indicated a negative sign (figure 2.13b): T, red) compared to 3 other positive coefficients (figure 2.13a: T, red and green, figure 2.13b: T, green), we chose the positive value of T, corresponding to 45°C.
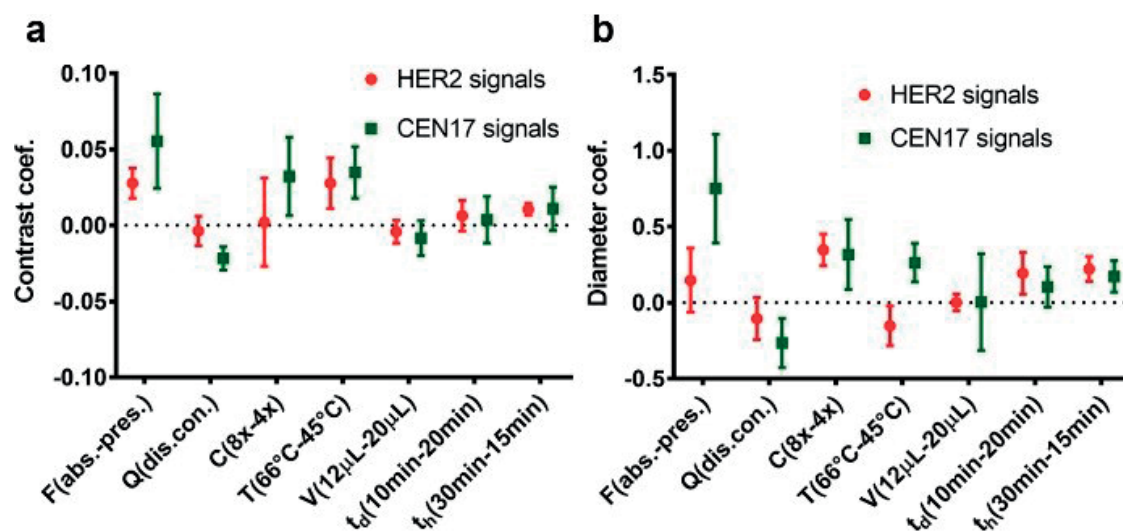
Figure 2.13 - ESIMA-FISH optimization protocol using human tissue samples (a) Optimization of the contrast for HER2 (in red) and CEN17 (in green) signals. The plot shows the linear regression coefficients of the HER2 and CEN17 signal contrasts, corresponding to 7 experimental parameters, namely the absence or presence of a post-fixation step (P), the flow rate during hybridization (Q), the probe concentration (C), the denaturation temperature (T), the total volume of probe used (V), and the duration of the denaturation (t_d) and hybridization steps (t_h). (b) Optimization of the diameter for HER2 (in red) and CEN17 (in green) signals. The plot shows linear regression coefficients of the HER2 and CEN17 signal diameter, corresponding to the same 7 parameters as (a). From our analysis, we find as optimal condition: post-fixation step present, discontinuous flow, 4× dilution, no denaturation ($t_d = t_h = $ 45°C), 12 µl probe volume and 35-minute hybridization.

Based on the results of this regression, an optimized set of parameters maximizing the signal while reducing both the probe consumption and the duration of the experiment was identified. Comparing to our MA-FISH technique, using a formamide-based probe, the flow rate for ESIMA-FISH was faster (0.1 vs 0.001 µl/s), quiescent flow periods were inserted between each back-and-forth probe flows (discontinuous flow), see figure 2.4b, and the denaturation step was skipped. Overall, the optimized microfluidic protocol (figure 2.14a) was twice faster (35 instead of 70 min of denaturation and hybridization) than the standard IQ-FISH assay (figure 2.14b) and the probe consumption was reduced by 70%.
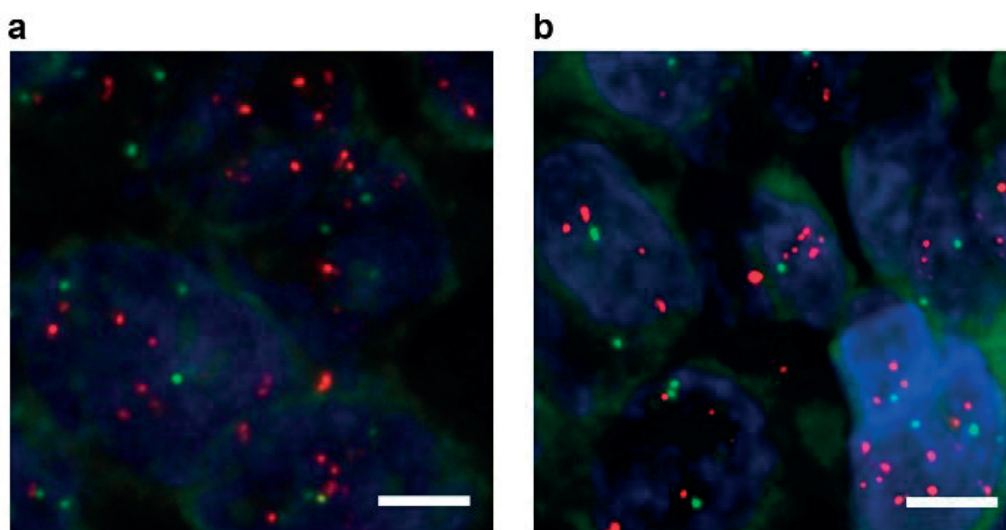
Figure 2.14 - Comparison of ESIMA-FISH and standard IQ-FISH (a) Deconvoluted z-stack (0.2 μm-step) from an ESIMA-FISH-treated tissue slide. (b) Deconvoluted z-stack (0.2 μm-step) from a standard IQ-FISH-treated tissue slide adjacent to that in (b). The HER2 signal obtained from ESIMA-FISH tends to have a weaker intensity than that of the standard IQ-FISH technique. The images were acquired using a fluorescence microscope with a 63× objective. Scale bars: 5 μm.

Based on the optimized protocol, ESIMA-FISH was performed on a SKBR3 cell line slide, resulting in further reduction of experimental time and probe consumption (post-fixation step present, continuous flow, 8× dilution, no denaturation, and 15 min hybridization, see figure 2.15 aii). In these conditions, quantitative comparison between signals obtained by the ESIMA-FISH and "off-chip IQ-FISH", using the standard coverslip method and the same probe dilution (8×) and hybridization time (15 min), performed on the same cell line is likely to show an improvement of HER2 signal (diameter and contrast) for the microfluidic method.

Figure 2.15 - Comparison of standard IQ FISH, ESIMA-FISH and "off-chip" IQ FISH obtained from a cell line slide (SKBR3). Standard IQ FISH (non-diluted probe and 1h hybridization) and off-chip IQ FISH (8× diluted probe and 15 minute hybridization) were performed using the coverslip technique (see the standard IQ FISH protocol in section 2.2.4.2). ESIMA-FISH and off-chip IQ FISH were implemented using the same probe concentration (8×) and hybridization time (15 min). (a) Image of a single focal plane of: (ai) an off-chip IQ FISH image stack (aii) an ESIMA-FISH image stack and (aiii) a standard IQ FISH image stack. Scale bar: 10 μm. (b) Quantitative analysis of HER2 signal in standard IQ FISH, ESIMA-FISH and "off-chip" IQ FISH images shown in (a): (bi) Contrast measurements (bii) Diameter measurements. The datasets were compared using an ANOVA test followed by a Tukey multiple comparison test:* for $p<0.05$, ** for $p<0.01$, *** for $p<0.001$.

2.4.1.2 ESIMA-FISH tests on clinical samples

The superiority of ESIMA-FISH over off-chip IQ-FISH was not, however, observed in ESIMA-FISH-treated tissue samples. These samples are less permeable to the probes and require a higher probe concentration and a longer hybridization time. Furthermore, for both tissue and cell line samples, the HER2 signals (dots) obtained by ESIMA-FISH using reduced concentration and time conditions typically show smaller diameters than that of the standard IQ-FISH in the conditions recommended by the manufacturer, i.e using an undiluted probe solution and 1 h incubation, see figure 2.16a, b for tissue and figure 2.15aii,iii and bi,ii for the cell lines. For CEN17, the dot diameter obtained by ESIMA-FISH is similar or slightly inferior to that of a standard IQ-FISH technique (see figure 2.15bii, iii for cell line and 2.16 for tissue).

Figure 2.16 - Comparison between ESIMA-FISH and standard IQ-FISH obtained from 2 adjacent tissue slides. Two adjacent slides from the same breast cancer sample were processed with ESIMA-FISH (4× diluted, 35 min incubation) and the standard IQ-FISH protocol, respectively, after which they were imaged using the same exposition conditions and then assessed using an automatic image processing routine. (a) Contrast of the red and green signal (dots) from two methods. (b) Diameter comparison of red and green signals from the two FISH methods. The red signal diameter of ESIMA-FISH is strongly decreased in comparison to the standard method. However, this did not affect the interpretation of the signal. The different datasets (ESIMA-FISH vs. standard IQ-FISH) were compared using a Student's t-test: * for $p < 0.05$; ** for $p < 0.01$; *** for $p < 0.001$.

Nevertheless, the signal quality obtained with the optimized ESIMA-FISH conditions is high and allows for the accurate scoring of *HER2* status using unprocessed z-stack images. Indeed, HER2 status assessments with ESIMA-FISH and standard IQ-FISH were compared by running the optimized ESIMA-FISH and standard IQ-FISH protocols on 2 adjacent sections of 9 different human breast cancer samples, after which the tissues were imaged and scored (figure 2.17). Quasi-identical FISH scores (*HER2*/cell number and *HER2*/CEN17 ratio) were obtained for these two techniques (see table 2.7).

Table 2.7 - Comparison of HER2 status assessment results of ESIMA-FISH and standard IQ-FISH. There is a good agreement between these methods. Only one sample was classified as negative with ESIMA-FISH and as equivocal with the standard IQ-FISH technique. This minor difference could be explained by the biological intratumoral heterogeneity of *HER2* copy numbers per cell. The results were obtained from 9 tissue blocks using a blind counting of FISH signals (number of *HER2* gene copies and the corresponding centromere CEN17 per cell).

| | | Standard IQ-FISH | | |
		Negative	Equivocal	Positive
ESIMA-FISH	Negative	3	1	0
	Equivocal	0	2	0
	Positive	0	0	3

The Pearson correlations between the two datasets were $r_{HER2/\text{cell}} = 0.99$ and $r_{HER2/\text{CEN17}} = 0.98$ and the regression coefficients of the ESIMA-FISH score as a function of the standard IQ-FISH score were $\beta_{HER2/\text{cell}}$

$=1$ ($R^2=0.98$) and $\beta_{HER2/CEN17} = 0.88$ ($R^2=0.96$), for *HER2*/cell and *HER2*/CEN17, respectively. Among the 9 cases considered in this study, only one discordance was reported (see table 2.7): a negative result with ESIMA-FISH was classified as equivocal with the standard IQ-FISH technique. This minor difference could be explained by the biological intratumor heterogeneity of *HER2* copy numbers per cell. For the SKBR3 cell line using 8× dilution and 15 min incubation, a *HER2*/CEN17 ratio of 3.66 is obtained using ESIMA-FISH, compared to a ratio of 3.67±0.22 found in the literature [74].

Figure 2.17 - Comparison between ESIMA-FISH and standard IQ-FISH on human tissue slides. (a) Plots of *HER2* copies per cell (*HER2*/cell) obtained by ESIMA-FISH *versus* standard IQ-FISH in a set of clinical breast cancer samples with *HER2*/cell ranging (ai) from 0 to 15 and (aii) from 0 to 5. The dotted lines represent the threshold for negative, equivocal or positive HER2 classifications. (b) Plots of the *HER2*/CEN17 ratio (*HER2*/CEN17) obtained by ESIMA-FISH *versus* standard IQ-FISH in the same set of clinical samples than in (b) with *HER2*/CEN17 ranging (bi) from 0 to 5 and (bii) from 0 to 2. The data shown here are mean ± SD obtained from the scores measured in 3 different clusters of 20 cells in each slide. The dotted lines represent the threshold for negative/equivocal or positive HER2 classifications.

2.4.2. Discussion

In comparison to other FISH techniques that use a formamide-based probe solution, the probe solution from the IQ-FISH assay used in this work is based on an ethylene carbonate hybridization buffer. This buffer promotes low-temperature denaturation of the target DNA strands and faster probe-target DNA hybridization [44]. Even though an ESIMA-FISH protocol is based on the same microfluidic-assistance principle developed in the MA-FISH method, the radically different protocols and incubation mechanisms used for the IQ-FISH probes required the development of specific hydrodynamic conditions and customized operation parameters. These considerations motivated the complete redesign of the assay protocol to accommodate the specificity of the IQ-FISH probes in a microfluidic format.

Hydrodynamic flows can improve the signal quality for FISH assays, as the microfluidic chamber allows for the continuous replenishment of the probe solution and improves mass transport. When the diffusion in the bulk liquid is not the bottle-neck for efficient hybridization, the hybridization rate at the DNA sites themselves is supposed to the rate-limiting factor. However, even when using a high-hybridization rate IQ-FISH solution combined to a hydrodynamic flow regime, the hybridization time for HER2 signal revelation cannot be reduced drastically. This might be because of the limited diffusion inside the tissue or cell itself, which is not influenced by hydrodynamic flows. Indeed, in figure 2.13a and b, post-fixation factors have the most impact on the outputs. This fact hints that post-fixation might influence the tissue structure, thus changing the probe permeability, and limiting diffusion inside the tissue.

2.5. Microfluidic-assisted chromogenic in situ hybridization (MA-CISH)

2.5.1. Results

2.5.1.1. MA-FISH and MA-CISH optimization results

The hybridization step in the MA-CISH protocol was optimized based on the FISH image of the tissue after hybridization and stringent wash steps (without the immunohistochemical steps for bright-field revelation).

Optimization was based on a FISH image rather than on a CISH image, because FISH signal provides a better contrast allowing a precise quantification of the signals. Only the diameter and contrast of HER2 dots were considered in the optimization process because the CEN17 signal is always strong thanks to abundant alpha-satellite DNA present in the centromere. Because of the preciousness of human tissue samples, the number of tests required for optimizing the procedure was reduced using a multivariate optimization process, combining fractional factorial design with linear regression analysis [75]. The values of each parameter are presented by a numerical number, either -1 or 1, corresponding to: 4× or 8× dilution for the probe concentration, 1 h or 2 h for the hybridization time and continuous or discontinuous for the flow regime. Signal outputs (diameter or contrast) were obtained and averaged at 3 different positions in the tissue for each experimental condition combination and represented as:

$$output = const + a_t \times t_h + a_C \times C + a_f \times Q \qquad (2.2)$$

where $a_{i=t,C,f}$ are the coefficients of the linear regression for the input variables hybridization time t_h, probe concentration C and flow regime Q, respectively. The chosen input values (-1 or 1) should be positively correlated to the coefficients in order to obtain a positive contribution to the signal output. The detailed experimental table representing all parameter combinations (Table 2.8) is presented as follows.

Table 2.8- Fractional factorial design of experiments used for MA-FISH optimization.

	Hybridization time	Probe dilution	Flow regime
Experiment 1	-1 (2 h)	-1 (4×)	1 (Discontinuous)
Experiment 2	1 (4 h)	-1 (4×)	-1 (Continuous)
Experiment 3	-1 (2 h)	1 (8×)	-1 (Continuous)
Experiment 4	1 (4 h)	1 (8×)	1 (Discontinuous)

Linear regression fittings of equation (2.2) resulted in a sum of square R^2=0.52 and 0.93 for contrast and diameter, respectively. Each linear regression coefficient a_t, a_C, a_f had the same sign, when considering either diameter or contrast as output variable (see figure 2.18a). Based on the results of this regression, the final configuration obtained from the optimization study was the following: hybridization time is 2 hours (8 times faster than standard CISH), the probe was diluted 4 times (resulting in a 70% probe consumption reduction, since 12 µl were used compared to 10 µl for standard CISH), and a discontinuous flow regime was used. Compared to our previous MA-FISH results, obtained by performing continuous back-and-forth flow at a flow rate of 0.001 µl/s, the flow regime applied for MA-CISH was faster (0.01 µl/s) and had quiescent flow periods inserted between each back-and-forth probe flow (see figure 2.5a and b). A fluorescence image of a SKBR3 cell line obtained with our microfluidic method is presented in figure 2.18b and 2.19a.

Figure 2.18 - (a) Optimization of the hybridization step using FISH images of a series of cell lines. The plot shows linear regression coefficients of the two HER2 signal outputs (contrast and diameter), corresponding to 3 experimental parameters, namely the hybridization time, the probe dilution, and the type of flow regime used. The signal quality is assessed by measuring the diameter and contrast of the red and green fluorescence signals (dots). From our analysis (see section 2.5.1.1), we find as optimal conditions a 2 hours hybridization time, a 4 × probe dilution and the application of discontinuous flow. (b) Result of an optimal microfluidic-assisted FISH protocol applied on a cell line. The cell is marked with 3 colors corresponding to the 2 probes (HER2 in red and CEN17 in green) and DAPI counterstaining for nucleus revelation (in blue). HER2 probe is labeled with Texas Red and the CEN17 probe is labeled with FITC. Scale bar: 5µm.
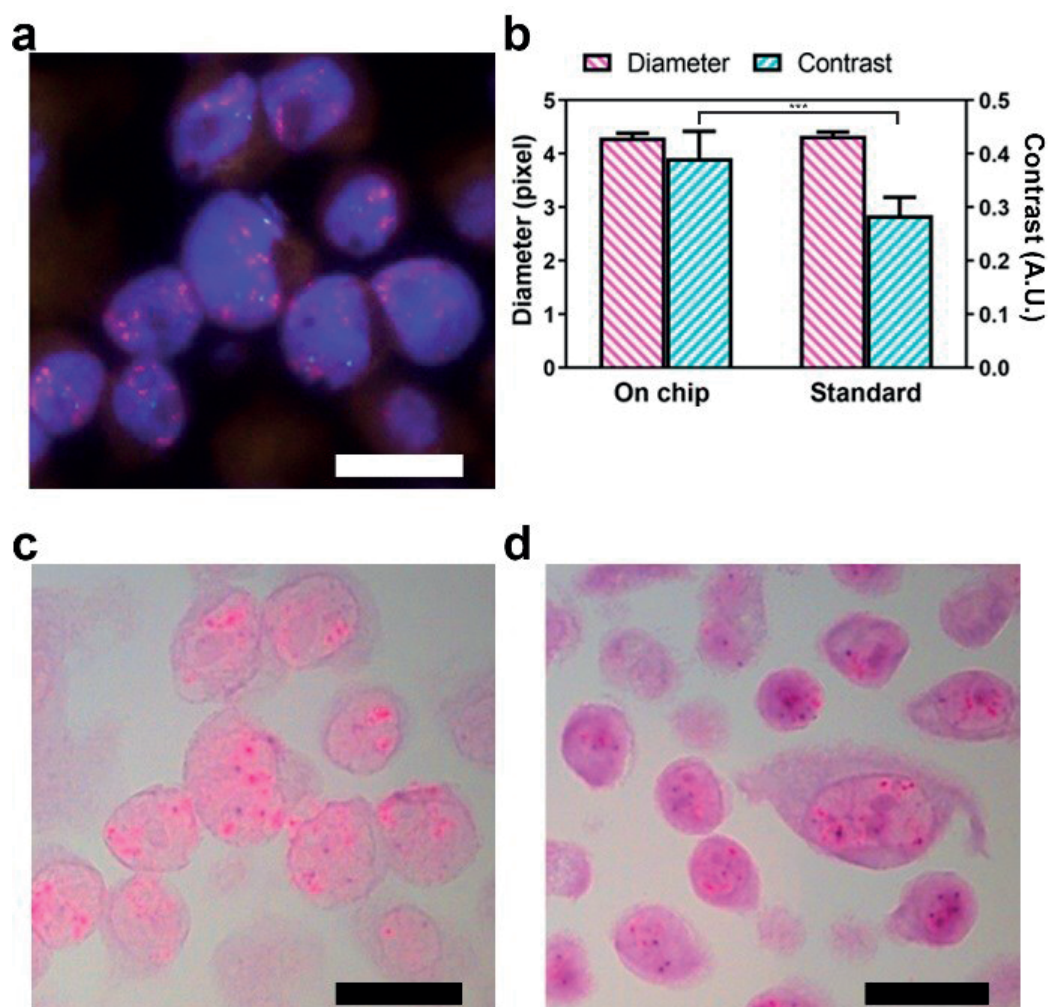
Figure 2.19 - Results of optimized microfluidic-assisted FISH (MA-FISH) and MA-CISH protocol using a discontinuous flow regime. (a) MA-FISH image of a cell line slide (SKBR3). (b) Comparison of HER2 signal output (diameter and contrast) in two SKBR3 cell line slides obtained by MA-FISH and standard FISH, respectively. The same dot diameter and a higher contrast are obtained by MA-FISH compared to standard FISH. The datasets (on chip *vs.* standard) were tested with a one-way ANOVA followed by a post-hoc Tukey test: p-value: ***<0.001. (c) MA-CISH image of the cell line slide shown in (a) after performing the protocol shown in figure 2.2b. The slide is marked with 3 colors corresponding to 2 probes (HER2 in red and CEN17 in dark blue) and hematoxylin in violet for nucleus revelation. (d) CISH image obtained using a standard CISH protocol performed on an SKBR3 cell line slide. Scale bars: 20 μm.

A quantitative comparison of signal quality between MA-FISH and standard FISH is presented in figure 2.19b, showing the same diameter and a better contrast of the obtained MA-FISH signal. This can be

explained by a reduction of non-specific DNA binding of the fluorophore to the nuclei. Following the optimization of MA-FISH, we started the MA-CISH protocol. Figure 2.19c shows the same cells as figure 2.19a. Moreover, MA-CISH allowed better visualization compared to a standard CISH image originating from same cell line (figure 2.19d). Overall, the optimized MA-CISH protocol was faster (1 day instead of 2) and cheaper (70% reduction of the probe consumption), while maintaining a good signal in comparison to standard CISH. Additionally, when performed using high probe dilution (8×) and short hybridization time (2 hours), MA-CISH still resulted in a recognizable signal while the traditional coverslip technique did not give any HER2 signal in these extreme conditions (see figure 2.20).
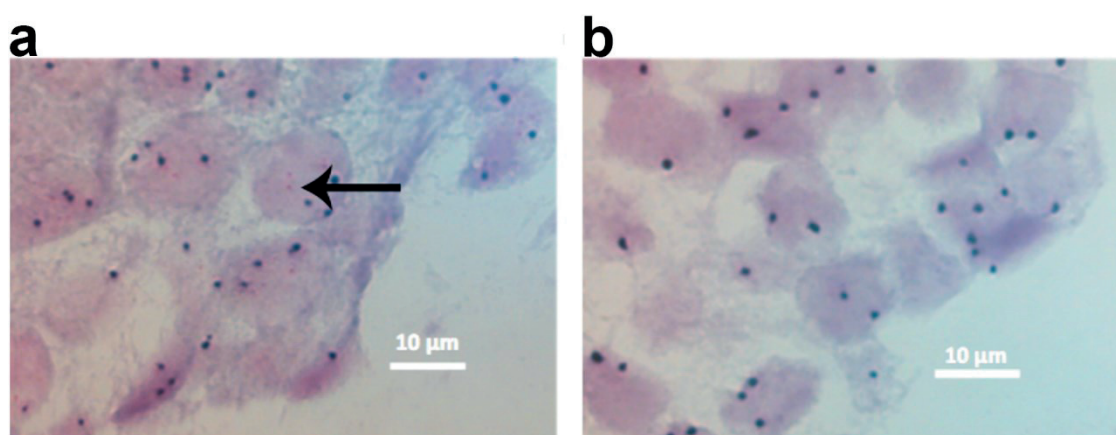
Figure 2.20 - Comparison of (a) MA-CISH (on chip) and (b) off chip CISH (using the coverslip method) performed on 2 adjacent tissue slides using the same conditions (8×dilution, 2 h hybridization). MA-CISH was implemented using a discontinuous flow regime (figure 2.5a). MA-CISH still resulted in a recognizable HER2 signal (a black arrow points to one red dot) while an off chip CISH did not give any HER2 signal in these conditions. The slides are marked with 3 colors corresponding to 2 CISH probes (HER2 in red and CEN17 in dark blue) and hematoxylin in violet for nucleus revelation.

2.5.2.2 MA-CISH tests on clinical samples

The established MA-CISH protocol (4× dilution, 2 h hybridization) was conducted on a set of 4 tissue samples. MA-CISH and standard CISH were performed for each sample on adjacent tissue slides, and the HER2 status was evaluated by assessing the average number of HER2 signals per cell and the *HER2*/CEN17 ratio. Good correlation between MA-CISH and standard CISH results was found (see figure 2.21ai,ii). No difference of HER2 classification was observed. The *HER2*/CEN17 ratio obtained from the MA-CISH SKBR3 cell line sample (3.14) is similar to the result found in the literature (3.67) and points to positivity of the HER2 classification [76].

Finally, as we obtained a fast CISH protocol, the result read-out becomes a bottle-neck for high throughput analysis. An automatic CISH scoring software was developed based on a FIJI program interface to automatically count the HER2 and CEN17 signals [65]. This program splits the single bright-field image to cyan, magenta, yellow, and key (CMYK) channels, allowing detection of dark blue dots representing the CEN17 signal in the cyan channel and quantification of the red dots representing the HER2 signal in the magenta channel. The quantification of the red dot is based on measuring the sum of pixels intensity of each of the HER2 dot in a cell. The *HER2*/CEN17 ratio and the average number of HER2 signals per cell obtained

by automatic and manual counting in the MA-CISH images are presented in figure 2.21bi,ii, showing good correlation between the two methods.
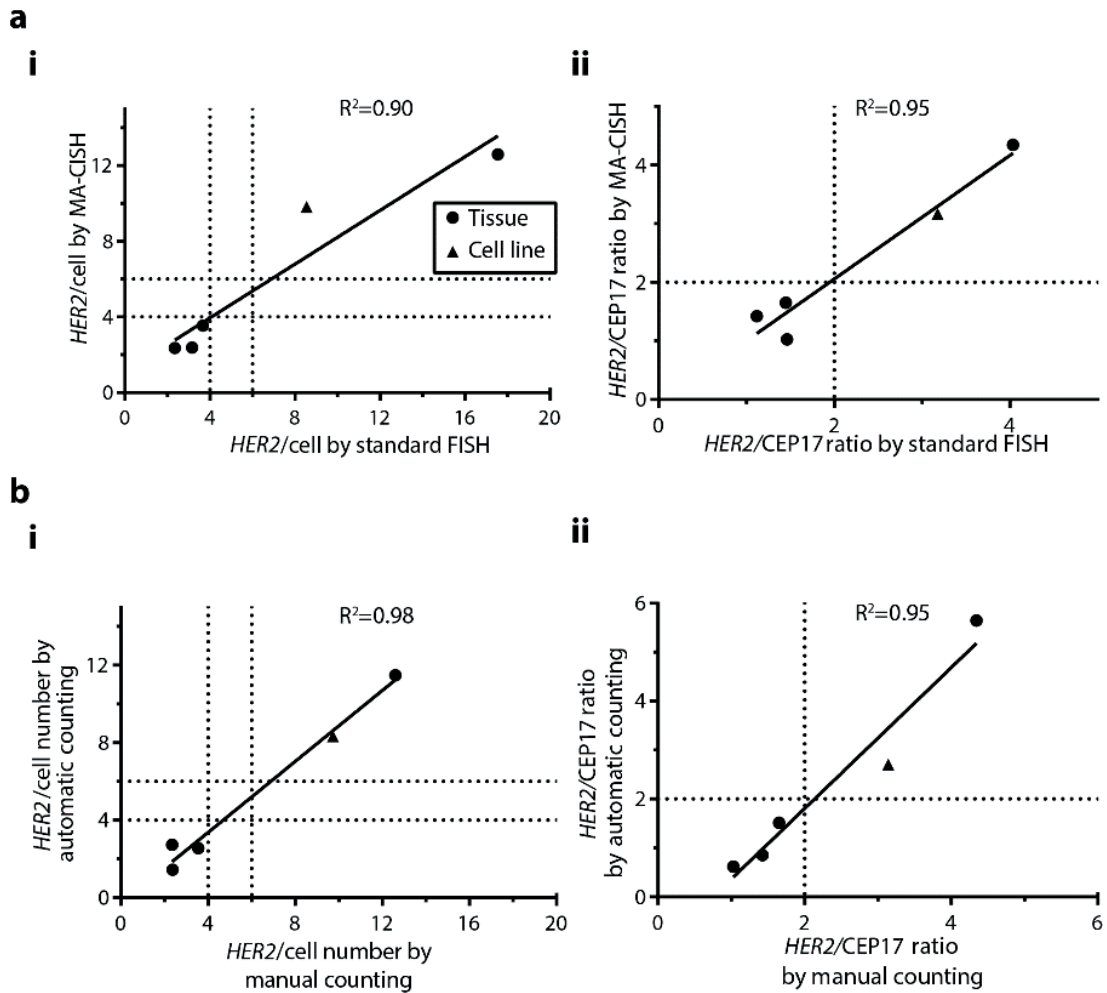
Figure 2.21 - Correlation study between the optimized MA-CISH and the standard CISH protocols for 4 tissue slides and one cell line. HER2 and CEN17 signals in a cluster of 20 cells are scored to obtain the average number of *HER2* gene copies per cell (*HER2*/cell) and the ratio between the total number of HER2 and CEN17 signals in 20 cells (*HER2*/CEN17 ratio). (a) Comparison between MA-CISH and standard CISH results. (ai) Correlation of *HER2*/cell number between MA-CISH and standard CISH performed on two slides generated from the same set of 4 clinical tissues and one cell line (SKBR3). (aii) Correlation of *HER2*/CEN17 ratio between MA-CISH and standard CISH performed using the same set of samples. (b) Correlation between automatic scoring and manual scoring using the MA-CISH images used in (a). (bi) Correlation of *HER2*/cell number (bii) Correlation of *HER2*/CEN17 ratio. Full lines show the fitting curves of a linear regression model. Dotted lines represent the threshold for negative, equivocal or positive HER2 classification.

2.5.2. Discussion

In a first approach, MA-FISH was based on a continuous flow regime, which results in a typically-weaker signal than those obtained from a standard FISH method. In this phase, we discovered that stronger signal contrast and larger signal diameter were obtained using a discontinuous flow (figure 2.5a). Compared to the standard FISH, the discontinuous MA-FISH achieves a better contrast of HER2 signal, while having 8 times shorter hybridization time and requiring only 30% of the standard probe used per experiment. The discontinuous flow possibly helps to diffuse the ISH probe in the nuclei without creating shear stress that can break the weak probe-target bond at the early stages of hybridization. For ESIMA FISH, although we cannot demonstrate the same performance improvement for the HER2 FISH signal quality using either continuous or discontinuous flows, the signals are still strong enough for an accurate detection.

MA-CISH was optimized based on the new MA-FISH protocol and proved to be reliable for the assessment of the *HER2* status in breast cancer. MA-CISH combines advantages of the standard CISH method, such as the use of a simple optical microscope, preservation of histological features and provision of stable unbleachable signals. This principle can be applied to another type of CISH probe or to the larger family of bright-field ISH techniques, such as Silver-ISH [77]. Additionally, CISH allows recording a single image for each position in the tissue instead of taking z-stack images as in FISH. This allows fast assessment of the signal using an image processing program. It should be noted that, in general, a CISH image of a high HER2-amplified cell shows a cluster of red signals (whether in standard or MA-CISH), making it hard to accurately count them individually. However, this limitation can be overcome using our image processing program that measures the cluster intensity and size to calculate the areal number of red dots inside a cluster. Moreover, automatic scoring can be applied to a large area of the tissue slide, allowing detection of possible tumor intra-heterogeneity (different scores in different tumor areas) [66]. In the future, the immunohistochemical staining procedure could easily be implemented on a chip, allowing automation of the whole protocol.

2.6. Conclusion of chapter 2

In conclusion, new techniques such as MA-FISH, ESIMA-FISH and MA-CISH have several advantages compared to their corresponding standard ISH techniques. They achieve similar performances to the standard methods, while requiring much less time and significantly reducing the consumption of the probe. The complete procedure for MA-FISH and MA-CISH can be performed in a single day, instead of 2 for the standard techniques. For ESIMA-FISH the duration of the test is only half-a-day. Using a combination of MA-CISH and automatic image analysis, more precise, faster, and cost-effective HER2 assessment in tissue samples can be obtained. Overall, the intrinsic advantages of standard ISH such as technical robustness and accurate interpretation are still retained for the microfluidic ISH techniques [57].

Beside cost and duration, two other limitations of FISH method are the complexity of the procedure and the difficulty of interpretation. The latter is mainly based on manual count directly via a microscope ocular [78, 79]. This process is long, the number of cells counted is limited and the cells counted are not traceable, i.e. lost after the scoring is done. Future developments of automatic protocols, from experimental staining procedure to signal scoring, would overcome these issues and improve the user-friendliness and reproducibility of FISH. The system used here is still a prototype. Further technical implementations could focus at tissue microarrays, automation or multiplexing to increase the MA-FISH throughput. The principle of using hydrodynamic flow for optimizing DNA hybridization provides the basis for improving further genetic investigations (DNA microarrays, RNA FISH, etc…). Last but not least, it was shown that MA-FISH

can be applied for either large centromere-targeted CEP17 probe or small locus-specific probe such as HER2 probe. Therefore, other FISH tests using small size range probes such as break apart-probes or single gene gain/loss probes could also be improved using the principle of MA-FISH [80]. Therefore, other diagnostic applications of FISH on cancer tissues, such as the analysis of *ALK* gene rearrangements in lung cancer, can also be improved using microfluidics, opening an alternative for facilitated analysis of the genetic state of the tumor. While precision medicine is opening a new era in cancer treatment, microfluidics provides the tools to decrease drastically the cost and time of genetic testing, thereby facilitating the dissemination of personalized therapy.

3. MICROFLUIDIC EXTRACTION AND MICROARRAY DETECTION OF BIOMARKERS FROM CANCER TISSUE SLIDES

In this chapter, a new microfluidic method allowing for the quantification of human epidermal growth factor receptor 2 (HER2) expression levels from formalin-fixed breast cancer tissues is described. An overview of this method is introduced as follows. After partial extraction of proteins from the tissue slide, the extract is routed to an Ab microarray for HER2 titration by fluorescence. Then the HER2-expressing cell area is evaluated by IF staining of the tissue slide and used to normalize the fluorescent HER2 signal measured from the Ab microarray. The number of *HER2* gene copies measured by FISH on an adjacent tissue slide is concordant with the normalized HER2 expression signal. This work is the first study implementing biomarker extraction and detection from cancer tissue slides using microfluidics in combination with a microarray system, paving the way for further developments towards multiplex and precise quantification of cancer biomarkers.

This chapter is adapted from the following publication:

H.T. Nguyen, L.N. Dupont, A.M. Jean, T. Gehin, Y. Chevolot, E. Laurenceau, M.A.M. Gijs. Microfluidic extraction and microarray detection of biomarkers from cancer tissue slides, Journal of Micromechanics and Microengineering (in press).

3.1. Introduction

Assessment of tissue biomarker expression is of utmost importance for diagnosis and treatment. IHC is widely used in the clinic because it represents several advantages: low complexity, assessment of biomarker levels with a small fraction of cells, and preservation of tissue morphology [81]. However, conventional IHC is not quantitative, and its assessment is often subjective. In breast cancer, for example, equivocal results in HER2 assessment by IHC require the use of an additional test such as FISH using fluorescent DNA probes to verify the presence of genetic aberrance that causes protein deregulation. Furthermore, conventional IHC can detect only a limited number of biomarkers due to few available options of adaptive chromogenic markers [59]. Other robust proteomic detection techniques, such as Western Blot, ELISA, or conventional mass spectrometry can be quantitative but are destructive, i.e., the morphological information of tissue is lost. They also have different limitations in clinical use, such as high complexity of the technique, and consumption of a relatively large amount of tissue materials [82]. An Ab microarray is a quantitative, high-throughput technique that uses Abs immobilized on a substrate (mostly a functionalized glass slide) to detect and quantify multiple proteins in a blood plasma or tissue lysate solution. The proteins captured from the solution are then directly detected by a fluorescent label, which is either directly linked to the proteins or via the use of a secondary-Ab labeling step. The main drawback of microarrays for identification of tissue biomarkers is that histological information on the tissue slide (e.g., number of cancer cells among healthy cells) is not preserved because this method requires destructive protein extraction from the tissue. Therefore, although a precise quantification can be obtained by standard proteomic techniques or microarrays, the correlation between the areal protein expression level evaluated on a tissue slide and its corresponding measured signal from extracted solutions has not been demonstrated.

We show here the proof-of-concept of protein extraction from standard clinical Formalin Fixed Paraffin Embedded (FFPE) tissue slides in a highly-controlled, reproducible manner using the MTP. First, we used

several standard techniques to optimize and benchmark this new method. More specifically, the extraction protocol was optimized based on the total protein mass obtained by a bicinchoninic acid (BCA) assay [83]. The presence of proteins was then verified by sodium dodecyl sulfate-polyacrylamide gel electrophoresis (SDS-PAGE). The detection and quantification of some protein biomarkers (vide infra) were performed by liquid chromatography tandem-mass spectrometry (LC-MS/MS) [84, 85]. Second, we connected the MTP to a detection microfluidic chip (DMC), in which Ab microarrays were integrated for HER2 detection. After performing partial protein extraction protocol, the remaining proteins allowed the tissue slide to be analyzed by IF to reveal histological information, as well as the number of cancer cells expressing HER2 proteins. In particular, as the extracted HER2 protein quantity depends on the number of cancer cells, the microarray signal related to the quantity of extracted HER2 is normalized to the surface area of cancer cell membranes. However, using only the HER2 signal, it is hard to distinguish the area of cancerous cell membranes to that of non-cancerous cells, particularly in HER2-negative-samples. Indeed, HER2 can be expressed in both cancerous and non-cancerous cells. Therefore, a CK tumor labeling technique was used for quantitative IF [62]. As epithelial cancer cells overexpress CK, this marker is used as a mask to distinguish cancer from normal cells. We proposed thus a method to calculate the HER2 biomarker density representing the average HER2 expression of a cancer cell. Finally, we demonstrated that the HER2 biomarker density was correlated with *HER2* gene copy number per cell obtained by FISH analysis of a small breast cancer tissue sample cohort, suggesting that the microfluidic-microarray technique allows discriminating HER2-positive patients from HER2-negative patients.

3.2. Materials and methods

3.2.1. Materials

3.2.1.1. Reagents

All reagents were purchased from Sigma-Aldrich (MO, USA), unless stated otherwise, and were used without further purification. All fluidic connectors, tubes, and fittings were purchased from ThermoFisher Scientific (MA, USA). Borosilicate flat glass slides (76 mm × 26 mm × 1 mm) were purchased from Schott (Mainz, Germany). All proteins used for microarray spotting were stored as aliquot at -20°C or -80°C complying with manufacturer specifications. PBS 1× (pH 7.4) was prepared by dissolving the content of one pouch of dried powder in 1 L of ultrapure water. 0.05 M carbonate buffer at pH 9.6 was prepared by dissolving the content of one pouch of dried powder in 100 mL of ultrapure water. Washing buffer contained PBS 1× and 0.1% Tween 20 (PBS-T) at pH 7.4. Blocking solution was prepared by dissolving 10 g of BSA (Bovine Serum Albumin) in 100 mL of PBS-T.

3.2.1.2. Tissue samples

FFPE breast cancer tissues were obtained from the Institute of Pathology of the University Hospital CHUV in Lausanne, according to the ethical convention BB514/2012 established with the Ethical Commission of Clinical Research of the state of Vaud. All patients did not oppose the use of their tumor sample for research purpose. 4 μm-thick tissue sections were mounted on Super Frost Plus slides (Menzel-Glazer, Germany). HER2 statuses of the tissue samples used in this study are known, according to a FISH test. The slides are named by the convention: patient number (P) - slide number (S) - extraction number (E) and successively named in an increasing order throughout the study.

3.2.2. Methods

3.2.2.1. Protein extraction by the MTP

The extraction protocol was based on the incubation of a patient tissue in an extraction solution at a high temperature (95°C during 20 min, followed by 80°C during 2 h) inside the microfluidic chamber of the MTP. The detailed protocol is as follows.

FFPE breast cancer tissue slides were heated at 65°C for 5 min on a hot plate (Scilogex MS-H280-Pro, Thomas Scientific, NJ, USA), then cooled down to room temperature (RT). Then, each slide was dipped in three different Histo-clear II (National Diagnostics, GA, USA) solutions for 5 min, and dipped successively in 5 solutions containing 100%;100%; 95%; 70%; 40% ethanol (2 min each). Then, the slide was kept at RT. A syringe was loaded with an extraction solution using a Nemesys pump (Cetoni GmbH, Germany). The extraction solution was composed of different concentrations of Tris/HCl and SDS (10, 20, 300 mM Tris/HCl and 0.5% or 2%SDS) according to table 3.1.

Table 3.1 **-** Total mass of protein recovered as a function of extraction conditions. Four different protocols were performed using 5 different breast tissue section slides obtained from the same patient (P1). Total protein mass was obtained by BCA assay. Protocol 4 (in **bold**) was chosen as the optimal protocol for further experiments.

Protocol number	Slide identification	Extraction conditions			Results
		Composition	pH	Temperature and time	Total protein mass (μg)
1	P1-S1, P1-S5 (two replicates)	10 mM Tris HCl; 100 mM NaCl; 0.5% SDS	7.5	T= 95°C t = 30 min	4.5 and 7
2	P1-S2	300 mM Tris HCl; 2% SDS	8	T=90°C t=2 h	21
3	P1-S3	20 mM Tris HCl; 2% SDS	9	T= 95°C t=20 min; Incubation T=60°C t = 2 h	18
4	**P1-S4**	**20 mM Tris HCl; 2% SDS**	**9**	**Incubation on ice 5 min; T=95°C t=20 min; T=80°C t=2 h**	**28**

The tissue slide was then clamped to the MTP half-chamber in a copper holder. The fabrication and design of the MTP and holder are described in chapter 2. The extraction chamber volume formed by the MTP and the slide has a height of 27 μm. A schematic presentation of the tissue slide in the microfluidic chamber of the

MTP is presented in figure 3.1a. During the protein extraction protocol, the assembled MTP-slide setup was placed on a hot plate and covered by a thermally insulating polystyrene chamber (figure 3.1b).
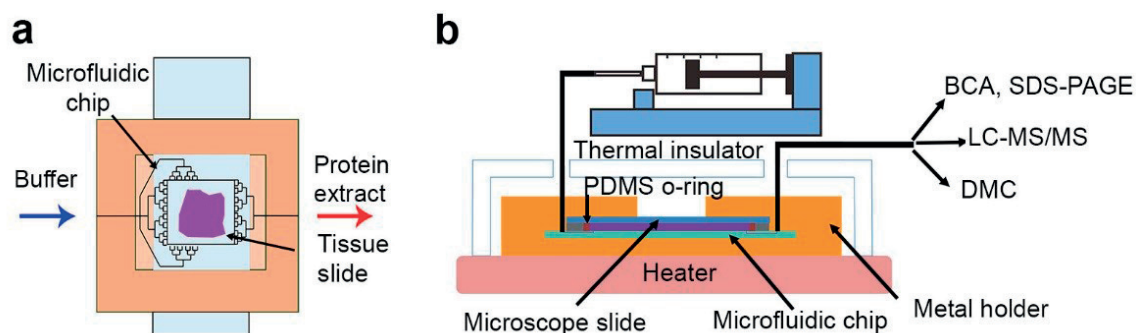
Figure 3.1 - Design of the protein extraction system. (a) Schematic view of the MTP/tissue slide stack. (b) Cross-section view of the setup during the experiment. The tissue section slide is incubated with tris(hydroxymethyl)aminomethane hydrochloride (Tris/HCl) buffer supplemented with sodium dodecyl sulfate (SDS) inside the microfluidic chamber. After incubation, the extract is either collected for standard proteomic analysis, such as a bicinchoninic acid (BCA) assay, sodium dodecyl sulfate-polyacrylamide gel electrophoresis (SDS-PAGE), liquid chromatography tandem-mass spectrometry (LC-MS/MS), or injected to the detection microfluidic chip (DMC).

The chamber was filled with the extraction solution at the flow rate of 1 μl/s. Then, bubbles were removed by a strong flow rate (20 μl/s). As soon as the extraction solution reached the outlet and the chamber was bubble-free, a blocking cap closed the fluidic system for the incubation. Then, the whole setup was cooled down to 4°C for 5 min. The temperature was controlled by an external thermometer and adjusted by an air flow. The MTP setup was then heated to 95°C using the hotplate, and the temperature was maintained for 20 min before being cooled down to 80°C by air flow. After two hour incubation at 80°C, the MTP setup was cooled down to room temperature using air flow. The blocking cap was replaced by a pipe fitting to extract the solution to either microcentrifuge tubes for standard proteomics analysis such as BCA, SDS-PAGE, LC-MS/MS or to the DMC. For LC-MS/MS analysis, successive 10 μl volumes of tissue extract were retrieved. To perform the BCA assay and SDS-PAGE analysis, 50 μl tissue extract were collected from the MTP. The slide was then removed from the MTP and received IF staining following the protocol detailed in section 3.2.2.4. This is possible because during the extraction protocol, proteins in the tissue slide are only partly dissolved in the extraction buffer. Therefore, the remaining part of proteins can be still detected by an IF staining.

The total mass protein extracted was quantified by BCA, and the presence of proteins in the protein extraction solution was verified by SDS-PAGE. Standard protocols for BCA and SDS-PAGE were used [86]. LC-MS/MS identified and quantified proteins based on peptide fragment-ion spectra [84, 85]. The LC-MS/MS protocol is detailed in section 3.2.2.6.

3.2.2.2. Ab microarray design

Capture Abs, carbonate buffer and F555-labeled streptavidin were spotted (sciFLEX-ARRAYER S3, Scienion, Germany) on N-hydroxysuccinimide (NHS)-activated silanized glass slides (Schott, Germany) as described in [87, 88]. Anti-uPA capture Ab (mouse monoclonal, Thermo Scientific, code: MON U-16-02)

and sheep polyclonal anti-HER2 capture Ab (Abcam, code: ab28324) were diluted at 4.5 μM in carbonate buffer (pH 9.6). Proteins were spotted on two areas of a slide. Each area received 15 anti-HER2 spots, 10 anti-uPA spots, 5 spots for each streptavidin concentration (4 μg/mL, 2 μg/mL, 1 μg/mL, 0.5 μg/mL, Thermo Scientific, code: S21381) and 5 carbonate buffer spots, see figure 3.2a. All spots had a diameter of 150 μm. uPA protein is expected to be absent in the extract, and is considered as a negative control, just like the carbonate buffer spots. Streptavidin-F555 was spotted as fluorescence intensity calibration and protein immobilization control. Indeed, the measured fluorescence intensity can vary depending on light intensity. Therefore, fluorescence intensity calibration using Streptavidin-F555 helped evaluate and correct possible variations of fluorescence signals. After being spotted, proteins were reacted with the glass slide surface under saturated carbonate buffer vapors overnight at 4°C.

3.2.2.3. Detection microfluidic chip (DMC)-based microarray detection

The Ab microarray slide, on which two identical Ab arrays (figure 3.2a) were spotted, was sandwiched by two in-house 3D-printed DMCs (figure 3.2b). A DMC was composed of two parts. One part was composed of a serpentine channel created by a thin soft-plastic layer (Tango Black Plus Full Cure 980, Stratasys Ltd., MN, USA) deposited on a hard-plastic substrate (VeroClear Full Cure 810, Stratasys Ltd., MN, USA). The second part (also made of VeroClear Full Cure 810) was composed of a window to observe the channel through the glass slide. Figure 3.2b shows 2 DMCs and the Ab microarrays in an upside-down configuration to visualize spot positions. After clamping the DMCs and the Ab microarrays slide, all spots should be inside the serpentine chamber created by the first part of the DMCs (figure 3.2c).
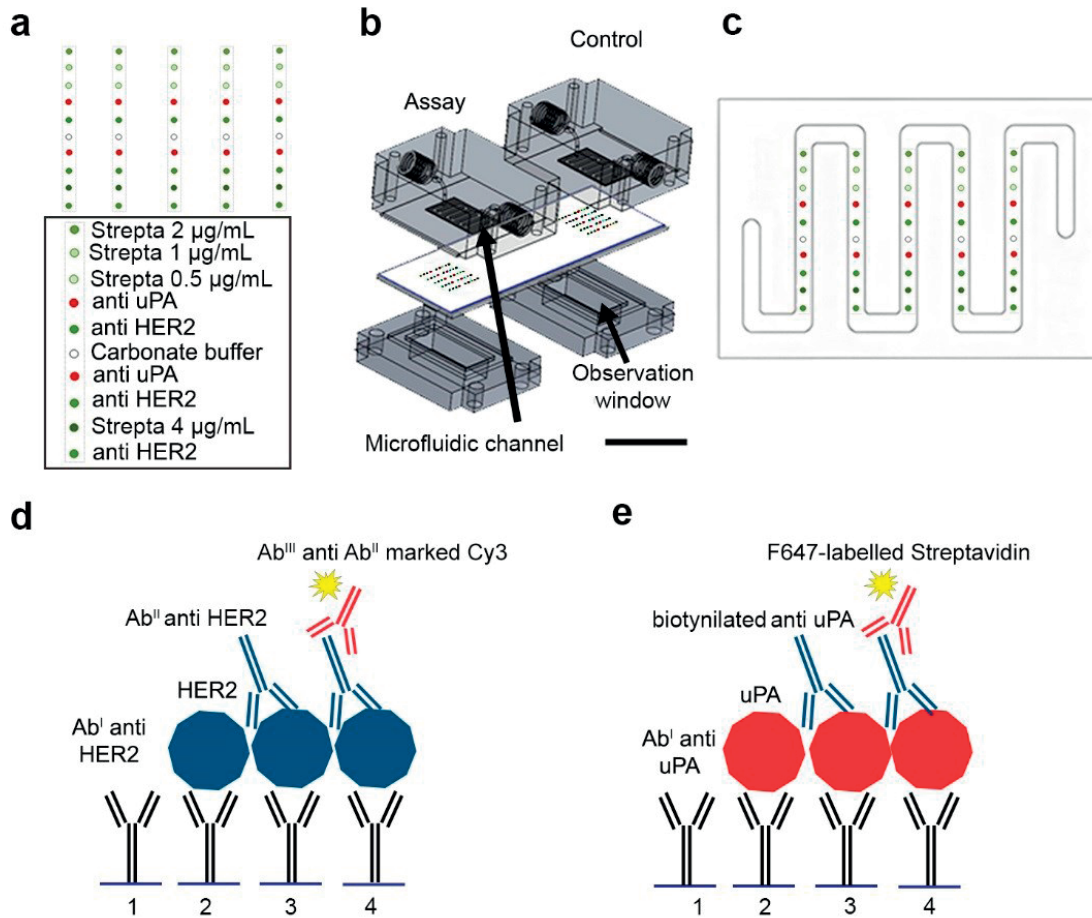
Figure 3.2 - Design of the DMC system and principle of the FISH technique. (a) Design of the Ab microarray. The array was composed of 5 replicated columns. Each column consisted of 4 spots of fluorescently F555-labeled streptavidin at 4 different concentrations (4 µg/mL, 2 µg/mL, 1 µg/mL, 0.5 µg/mL) for fluorescence signal control calibration; 2 replicated spots of anti-urokinase Plasminogen Activator (uPA) capture Ab at 4.5µM for negative control; 3 replicated spots of anti-HER2 capture Ab at 4.5 µM; and one spot of carbonate buffer for negative control. (b) Exploded view of the setup consisting of a microscope slide spotted with 2 Ab microarrays sandwiched by two DMCs. One DMC, named "assay", received the protein extract and the other DMC, named "control", received only the extraction buffer (free from proteins). Scale bar: 2 cm. Each DMC consisted of a serpentine microfluidic channel and an observation window. (c) The spotting design of one array placed inside the serpentine channel. (d) Schematic presentation of HER2 detection steps on the Ab microarray: (1) immobilization of anti-HER2-capture Ab on an NHS-activated glass slide; (2) capture of HER2 protein from the tissue extract; (3) recognition with anti-HER2 Ab (mouse anti-human HER2); (4) detection with goat anti-mouse Ab labeled with Cy3. (e) Schematic representation of uPA detection steps on the Ab microarray: (1) immobilization of anti-uPA-capture Ab; (2) capture of uPA protein; (3) recognition with biotinylated anti-uPA Ab (mouse anti-human HER2); (4) detection with F647-labeled streptavidin.

During the protein detection protocol, first, Ab microarrays were incubated with the blocking solution then washed with the washing solution PBS-T through the DMCs. Then the protein extraction solution (8 µl) from the MTP was routed to the "assay" DMC. In parallel, protein-free extraction solution (8 µl) was injected into the "control" DMC for a negative control. Discontinuous back-and-forth flows generated by a syringe pump were maintained for one hour to enhance protein- capture Ab recognition (figures 3.2d1,2 and 3.2e1,2) and avoid dead-volume issues (see figure 3.3a for the flow regime).
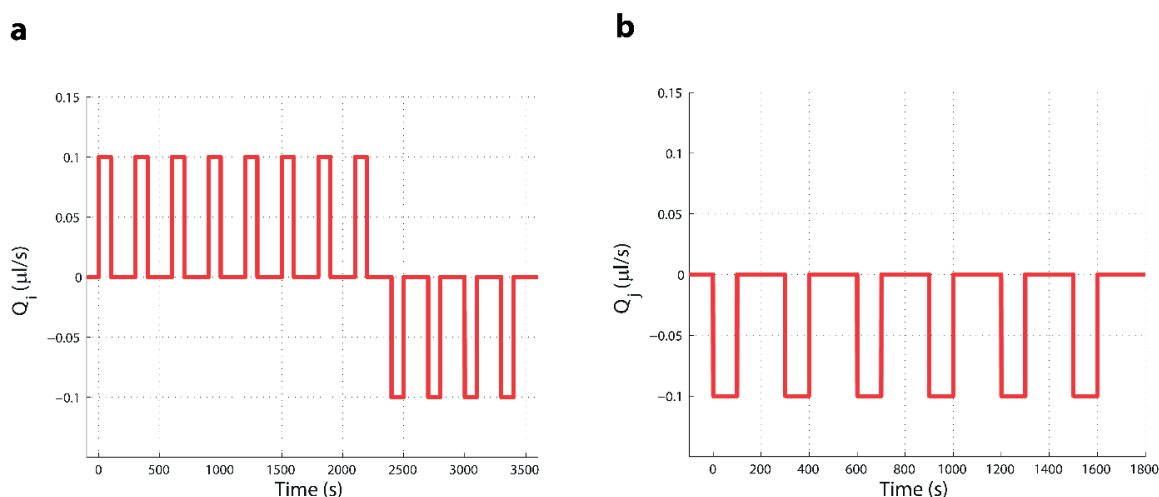
Figure 3.3 - Flow regimes used during the DMC protocols. (a) Flow regime applied during incubation of protein extraction solution with Ab microarray (b) Flow regime applied during the detection steps on the Ab microarray.

Then both DMCs and the MTP were washed with a suction flow of PBS 1× solution. The MTP setup was then disconnected to release the patient tissue slide for subsequent IF staining (see 3.2.2.5). Indeed, the protein extraction protocol leads to partial extraction of tissue proteins allowing IF staining of the remaining proteins in the patient tissue slide. Then, the DMCs ("assay" and "control") were connected directly to two syringe pumps that generated back-flows to perform the following detection (figures 3.2d3,4 and 3.2e3,4) and washing steps. First, a mixture of biotinylated anti-uPA Ab (diluted 2 times from Femtelle® kit, American Diagnostica Inc) and anti-HER2 Ab (0.05 mg/mL, Thermo Scientific, code: MA5-12998) diluted in 4% BSA/PBS-T was loaded into the chamber and incubated with the Ab microarrays during 30 min. Then, PBS-T washing solution was applied at 1 µl/s flow during 180 s. Streptavidin labeled with F647 (0.01 mg/mL diluted in 1% BSA/PBS 1×, Thermo Scientific, code: S21374) was loaded to the channel and incubated with Ab microarrays during 30 min followed by PBS-T wash (1 µl/s during 180 s). Then Cy3-labeled goat anti-mouse Ab (0.015 mg/mL diluted in 1% BSA/PBS-T, Jackson ImmunoResearch, code: 115-165-008) was incubated during 30 min followed by PBS-T wash (1 µl/s during 180 s). After removing the Ab microarray slide from DMCs, the slide was washed with PBS-T, dried and stored at -20°C until fluorescence scanning. During all incubation steps using Abs, discontinuous flows were generated (see flow regime in figure 3.3b).

Ab microarray slides were scanned using an Innopsys microarray scanner (InnoScan 1100AL) at excitation wavelengths of 532 nm and 635 nm with low laser power. Fluorescence signal acquisition and data treatment were accomplished with the Mapix 2Go software package (Innopsys). The median and the SD for

fluorescent signals were calculated from replicate spots of each Ab microarray (15 replicates for HER2, 10 replicates for uPA, 5 replicates for each streptavidin concentration and carbonate buffer, see figure 3.2a). The median background level obtained from the carbonate buffer spots was subtracted from all fluorescent signals.

3.2.2.4. Quantification of protein area by IF

IF staining for HER2 and CK was performed on the tissue slide. The slide was cover-slipped with primary Ab cocktail of rabbit anti-human c-erbB-2 oncoprotein (Code: A0485) with a concentration of 1.28 μg/mL and mouse anti-human CK (code: M3515) with a concentration of 1.02 μg/mL. The primary Abs were purchased from Agilent Technologies (Santa Clara, CA, USA). The incubation occurred at 37°C in a humid chamber for 5 min, followed by washing with PBS 1×. For fluorescent detection, secondary Ab cocktail of Alexa Fluor 594 (AF594) goat anti-rabbit IgG (Code: A-11037) and Alexa Fluor 647 (AF647) goat anti-Mouse IgG (Code: A-21236) from Life Technologies (CA, USA) with a concentration of 50 μg/mL was applied on the tissue slide, coverslipped and incubated for 5 min. After washing with PBS 1× and distilled water (DIW), SlowFade™ Gold Antifade Mountant (Life Technologies, CA, USA) containing DAPI and fluorescence-antifading agents were applied on the tissue slide for nuclear counterstaining and coverslip-mounting. The IF signal was recorded using a fluorescence microscope (Axio Imager M2m, Zeiss, Germany) with a 10× microscope objective (EC Plan-NEOFLUAR, Numerical aperture 0.3) in 2 × 2 binning mode. The IF image is used, together with obtained microarray fluorescence signal, to estimate the HER2 protein per unit surface (see section 3.2.2.7).

3.2.2.5. HER2-gene detection by FISH

The Pathvysion® HER2 FISH (ABBOTT, CA, USA) kit was used to perform FISH detection of *HER2* gene and CEN17 in breast cancer tissues. In FISH, an HER2 DNA probe labeled with spectrum orange™ fluorophore combines with its DNA target to reveal the different position of *HER2* oncogene copies inside the nucleus. The centromere of the chromosome is visualized using a DNA probe labeled with spectrum green™ fluorophore. After performing the FISH protocol, count of red and green dots allows HER2 classification. FISH was implemented in our experiment to compare the FISH score and the protein density using two slides originating from the same sample. The deparaffinization protocol for FISH was identical to that applied for protein extraction (see 3.2.2.1). After removing the paraffin and rehydrating in successive ethanol solutions from 100% to 40%, the 4-mm breast cancer sections were dipped in washing buffer, containing Tris/HCl solution (Agilent Technologies, CA, USA). Then, they were transferred to a Coplin jar containing 2-[N-morpholino] ethanesulfonic acid (MES) solution 1× buffer (Agilent Technologies, CA, USA) heated at 95-97°C for 10 min. Next, the Coplin jar was cooled down to RT for 20 min before dipping in washing buffer (twice for 3 min). Protein digestion was performed by applying protease during 10 min at 37°C. Then, the slides were washed twice with the washing buffer and dipped in post-fixation solution composing of 1% formaldehyde (Merck Millipore, Germany), PBS 1× and 20 mM MgCl$_2$, for 10 min. The slide was then washed with PBS 1×, dehydrated with ethanol 40-100% and dried. HER2 FISH probe was applied, and the slide was coverslipped, sealed with rubbers (Agilent Technologies, CA, USA) and denatured at 73°C for 5 min. Then, overnight hybridization was performed at 37°C. In the next day, the coverslip was removed, and the slide was transferred to a stringent washing buffer, containing 2× SSC, 0.3% Tween 20 (Bio Rad, CA, USA) for 2 min. Then, the slide was washed in SSC Tween (SSC 2×, 0.1% Tween 20) for 2 min, SSC 2× for 2 min, distilled water for 5 seconds and dehydrated in successive ethanol 40-100% for 2 min each before DAPI mounting medium was applied to the dried slide. Finally, the slide was

coverslipped for fluorescence microscope observation. A cluster of cancer cells was imaged using a high magnification (63×) objective (Plan-Apochromat Oil DIC) in several focal planes for scoring the number of HER2 signals per cell. *HER2* copy numbers from FISH analysis were obtained for each breast cancer patient using adjacent slides of those used in protein extraction.

3.2.2.6. Liquid chromatography tandem-mass spectrometry LC-MS/MS

10 μL of different tissue extracts were put in different gel wells (12% polyacrylamide), separated by SDS-PAGE and then stained with Coomassie blue. Each sample was excised from the gel, cut into slices and proteins were in-gel digested using trypsin as follows. Briefly, the samples were reduced in 10 mM dithioerythritol (DTE) and alkylated with 55 mM iodoacetamide (IAA), the gel pieces were dried by vacuum centrifugation. Dried samples were reconstituted in 12.5 ng/mL trypsin and incubated overnight at 37°C. Tryptic peptides were extracted in 70% ethanol, 5% formic acid from the gel slices and dried. Extracted peptides were desalted on stageTips [85] and dried again. For LC-MS/MS analysis, resuspended peptides were separated by reversed phase chromatography on a Dionex Ultimate 3000 RSLC nano UPLC system connected in-line with an Orbitrap Fusion (Thermo Fisher Scientific, Waltham, USA). Data acquisition was either performed using a data-dependent acquisition mode or using an accurate inclusion list prioritizing MS/MS sampling from a list of targets at +/- 10 ppm mass tolerances. Database search was performed using Mascot (Matrix Science, Boston, USA), MS-Amanda [84] and SEQUEST in Proteome Discoverer v.1.4. against a human Uniprot protein database (Release 2015-06). Data were further processed and inspected in Scaffold^{TM} 4. (Proteome Software, Portland, USA).

3.2.2.7. Calculation of protein density

We decomposed the ratio between the extraction signal and the control signal (ECR), which is proportional to the total concentration of HER2 protein in the extraction solution, to ECR1 and ECR2:

$$ECR = ECR1 + ECR2 \qquad (3.1)$$

where ECR1 is associated with cancer cells and ECR2 with non-cancer cells. We also suppose that the quantity of the HER2 protein extracted from one cell is proportional to the sum of all IF signal intensity of HER2 protein detected in the membrane of the cell of interest. Therefore, the ECR1 and ECR2 should be respectively proportional to the sum of all IF HER2 signals in the membranes of all cancer ($\sum I_C$) and non-cancer ($\sum I_{nc}$) cells of a tissue. We obtain the following equation:

$$\frac{ECR1}{ECR2} = \frac{\sum I_C}{\sum I_{nc}} \qquad (3.2)$$

where I_C is the intensity of one pixel of the HER2 image, located in a cancer cell membrane area (C), and I_{nc} the intensity of one pixel of the HER2 image situated in a non-cancer cell membrane area (nc). I_C and I_{nc} of all cells can be obtained using the image processing program FIJI (see section 3.2.2.8) [3].

By solving the system of equations (3.1) and (3.2), ECR1 was obtained. The HER2 protein density D, which characterizes the HER2 protein quantity in the extract per cancer cell area, is calculated by normalizing the ECR1 to the surface of the total cancer cell membrane area S:

$$D = \frac{ECR1}{S} \qquad (3.3)$$

S was obtained by applying a threshold to obtain the positive-CK cells' membranes by using the image processing program FIJI [65], see section 3.2.2.8.

3.2.2.8. Calculation of the IF HER2 intensity and area of the cancer and non-cancer cell membranes.

In this section, the image processing program for computing $\sum I_C$ and $\sum I_{nc}$ is detailed. First, after images in the 3 signal channels, corresponding to DAPI, HER2 and CK presence, were obtained using the 10× objective on the whole tissue (see main text), they were stitched into a large mosaic image. Next, the CK channel of the mosaic image was thresholded by an automatic threshold (Huang) using FIJI [89], giving the CK mask for selecting epithelial cells. Next, the HER2 channel was thresholded manually to select all membrane positions (cancer and non-cancer) where HER2 proteins are present. Note that, although non-cancer cells displayed low expression, the HER2 pixel intensity of the cell membrane could always be assessed by selecting an appropriate threshold manually. Finally, HER2 pixels inside the CK mask are originating from HER2 proteins from cancer cells, giving I_C, and HER2 pixels outside CK mask are from non-cancer cells, giving I_{nc}. Using the integrated intensity function of FIJI, $\sum I_C$ and $\sum I_{nc}$ were obtained. S was obtained by measuring the surface of the HER2 signal inside and outside the CK mask, respectively.

3.3. Results

3.3.1. Protein extraction protocol optimization

Four protocols that resulted in protein extraction from FFPE slides but preserved tissue morphology and protein activity were selected based on previous studies [86, 90-92] and were performed using the MTP. The concentrations of Tris/HCl and of SDS, the pH and the temperature were varied (see table 3.1). Five tissue slides (S1 to S5) from the same patient P1 were used for optimizing the extraction protocol. To characterize the protein extraction efficiency, the total mass of protein recovered from the FFPE slide, as measured by the BCA assay, and the molecular mass range of extracted proteins, as revealed by SDS-PAGE analysis, were evaluated. The optimal protocol was defined as recovering the highest total mass of extracted proteins. After extraction, 50 μl of protein extraction solution were retrieved from the microfluidic chip and split into two aliquots, one for BCA and one for SDS-PAGE analysis. Results are reported in table 3.1 and figure 3.4.

The total protein mass recovered varied from 4.5 μg (protocol 1) to 28 μg (protocol 4). SDS-PAGE analysis (figure 3.4a) validated the variable protein content, as could be observed by the different smear profiles. Protocol 4 led to a total of 28 μg of extracted proteins and numerous protein bands ranging from 9 to 57 kDa, as observed by SDS-PAGE analysis (see figure 3.4a). This protocol was thus selected and applied for further experiments.
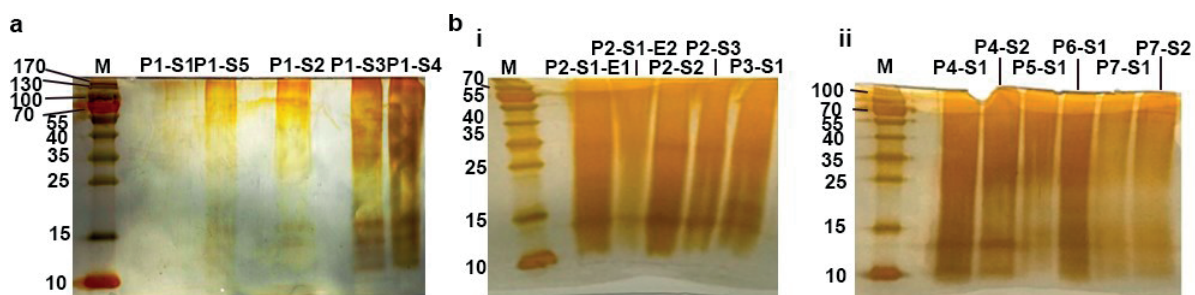
Figure 3.4 - SDS-PAGE for optimization and reproducibility analysis. (a) SDS-PAGE of protein extraction solutions obtained from different extraction protocols (S1 to S5) of the same breast cancer tissue patient (P1). M is the reference mass ladder. P1-S1 and P1-S5 are two replicates of the same protocol. (b) SDS-PAGE of protein extraction solutions obtained with protocol 4 from different breast cancer tissue patients (P2, P3, P4, P5, P6, P7). Protein extraction solutions obtained from adjacent sections of the same breast cancer tissue patient are number S1, S2, S3. Protein extraction solutions obtained from two successive extractions from the same breast cancer tissue section of the same patient are number E1 and E2, respectively. (i) Tissue slides P2-S1-E1, P2-S1-E2, P2-S2, P2-S3, P3-S1. (ii) Tissue slides P4-S1, P4-S2, P5-S1, P6-S1, P7-S1, P7-S2.

3.3.2. Reproducibility and efficiency of the protein extraction protocol

To study protein extraction reproducibility, protocol 4 (from table 3.1) was performed on tissue samples from six other breast cancer patients, named as P2 to P7. Two or three tissue slides (S1, S2, S3) from breast cancer patient P2, P4 and P7 were treated using the protocol 4 in order to study the reproducibility of the protocol. Moreover, the tissue slide S1 from patient P2 was treated twice successively (E1 and E2) using protocol 4 to check whether all proteins were extracted from the tissue slide or not (slide P2-S1-E1, P2-S1-E2). The total mass of extracted proteins obtained by BCA is reported in table 3.2. The corresponding SDS-PAGE pictures are presented in figure 3.4bi, ii.

Results from table 3.2 indicate that protocol 4 performed on different tissue slides from the same breast cancer patient (P2, P4 or P7) led to similar total protein yields. In particular, less than 10% deviation was obtained from samples P2-S1-E1, P2-S2, and P2-S3, suggesting the good reproducibility of the protein extraction protocol 4. The deviation obtained from other samples (P4-S1 and P4-S2, P7-S1 and P7-S2) was higher, but the number of replicated samples was lower than those of the P2 sample, which was a limitation for statistical study. One of the most important factors influencing the extraction yield was the possible partial evaporation of the extraction solution during the high-temperature incubation (95°C). Moreover, the presence of bubbles inside the microfluidic system could also reduce the effective extraction area. However, the total extracted protein mass depended on the area of breast cancer tissue section within the microfluidic chamber and on its cell composition. We also noticed that the second extraction of the sample P2-S1 (P2-S1-E2) yielded about half less protein mass than the first extraction (P2-S1-E1), although the protein quantity was still significant. This result indicates that not all proteins were extracted during the first extraction and remaining proteins could be further detected.

Table 3.2 - Reproducibility study of the protein extraction protocol 4. Protein extraction solutions were analyzed by BCA and the total protein mass is reported. Samples are defined with the number of the patient (P), the number of the adjacent tissue slide of the same patient (S), and the number of successive extractions from the same slide (E).

Identification	Protein mass (µg)
P2-S1-E1	15
P2-S1-E2	9
P2-S2	13
P2-S3	14
P3-S1	10
P4-S1	19
P4-S2	14
P5-S1	13
P6-S1	12
P7-S1	6
P7-S2	8

3.3.3. Identification and quantification of breast cancer biomarkers in the protein extraction solutions using targeted LC-MS/MS

Identification of breast cancer biomarkers present in the optimized protein extraction solutions was performed using a targeted LC-MS/MS technique. 5 breast cancer biomarkers were selected: HER2, PR, ER, Plasminogen activator inhibitor-1 (PAI-1), and uPA [93]. For each protein, an LC-MS/MS spectra count, defined as the total number of spectra from peptide originating from the proteins, was obtained. Among the 7 protein extraction solutions obtained from 5 different breast cancer tissue patients (P8 to P12) that were analyzed, HER2 was detected in all samples; PR was detected in only one sample (see table 3.3). The other breast cancer biomarkers (ER, PAI-1, uPA) were never detected in the protein extraction solutions obtained from the tissues, suggesting that they were probably not soluble in the extraction buffer. The analysis of the LC-MS/MS results indicated that protein concentrations highly varied in the extract. Indeed, some proteins that are abundant in the tissue such as keratin also tend to be strongly presented in the protein extraction solution. Therefore, the protein extraction efficiency depends on the presence of the proteins in the tissue and their solubility in the extraction solution. Among abundant proteins present in protein extraction solutions, the clinically interesting SERBP1 (Plasminogen activator inhibitor 1 RNA binding protein, a marker for favorable prognosis) was always detected [94]. On the contrary, uPA was detected in none of the samples by LC-MS/MS; therefore, it was chosen as a negative control for the microfluidic-microarray technique (*vide*

infra). At last, the reproducibility of our protein extraction method was confirmed with similar HER2 spectra counts recorded by the LC-MS/MS technique from 2 replicated extractions of the same breast cancer tissue patient (P12-S1 and P12-S2 in table 3.3).

Table 3.3 **-** Comparison of LC-MS/MS, microfluidic microarrays and FISH. For each protein extraction solution, the spectral counts for PR (second column) and HER2 from LC-MS/MS analysis (third column), the mean ECR obtained by microfluidic-microarray method (fourth column; with SD), and the average number of HER2 signal per cell by FISH (*HER2*/cell, fifth column) are reported. LC-MS/MS and FISH were obtained from adjacent tissue sections of the breast cancer tissue sample analyzed by the microfluidic-microarray technique. NA is "not acquired" due to the lack of human tissue sample.

	LC-MS/MS spectral counts for PR (Unity)	LC-MS/MS spectral counts for HER2 (Unity)	Mean HER2 ECR from microfluidic-microarray (Unity)	*HER2*/cell by FISH (Unity)
P8-S1	28	11	2.04(SD=0.11)	1.6
P9-S1	0	18	2.34(SD=0.18)	3.5
P9-S2			2.22(SD=0.28)	
P10-S1	NA	NA	3.99(SD=0.22)	8
P11-S1	0	37	5.36(SD=1.34)	11.4
P12-S1	0	90	NA	5.7
P12-S2	0	76	NA	5.7

3.3.4. Detection and quantification of HER2 biomarkers using the DMC

We next demonstrated a method to detect and quantify HER2 protein expression in tissue extracts using our customized Ab microarray slide combined with the DMC (figure 3.2b). First, HER2 protein was titrated from the fluorescence signals measured on Ab microarrays (figure 3.5a). Microarrays results were benchmarked with LC-MS/MS analyses obtained from adjacent sections of the same breast cancer tissue patient. Second, the global cancer cell membrane area per slide was evaluated from IF images of the breast cancer tissue slide after protein extraction. Finally, the HER2 protein density of each breast cancer tissue slide was calculated by normalizing the HER2 microarray fluorescence signal to the cancer cell membrane area obtained by IF. Results were benchmarked with FISH analyses performed on an adjacent section of the same breast cancer tissue patient.
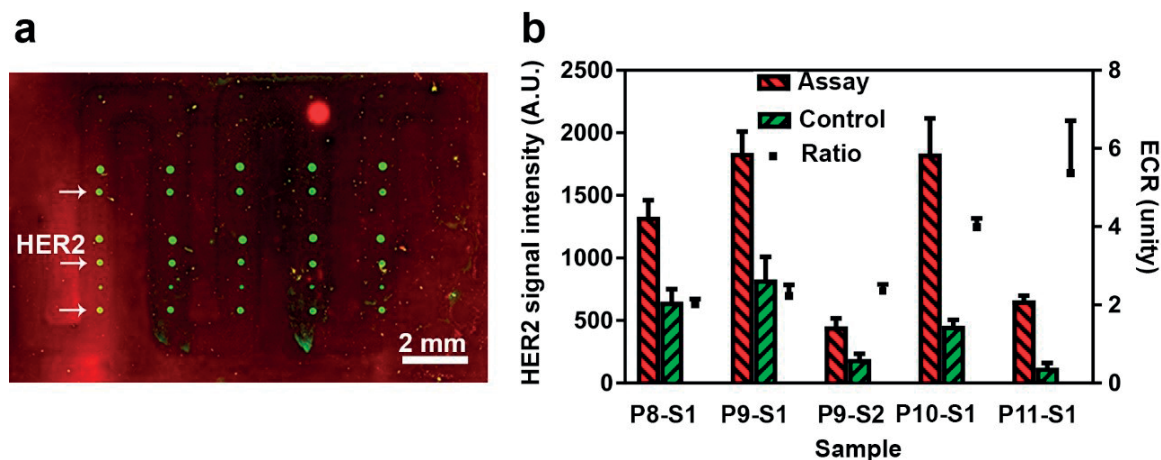
Figure 3.5 - Microarray and IF results. (a) Fluorescence image of the "assay" array of the Ab microarray after incubation of the protein extraction solution in the DMC. The positions of spots are the same as in figure 3.2a, c. In particular, positions of HER2 spots are indicated by white arrows. Fluorescence intensities from F555-streptavidin and HER2 were measured at 532-nm excitation wavelength (green channel), whereas those from uPA were measured at 635-nm excitation wavelength (red channel). The two fluorescence images were then merged into a single two-color image. (b) Fluorescence intensities (arbitrary unit, left axis) of HER2 detection signals from "control" (green bars) and "assay" (red bars) microarrays obtained from 5 protein extraction samples. These samples were prepared from 5 tissue sections of 4 different breast cancer patients (P8-11), two of them (P9-S1 and P9-S2) being adjacent sections of the same breast cancer tissue patient (P9). Fluorescence intensities from replicate spots in figure a were averaged and the SD was calculated. The ratio between "assay" and "control" signals is plotted as the extraction-to-control ratio (ECR) (dots, right axis). The error bars are obtained from the assay and control SDs.

A batch of 5 tissue sections (P8-S1, P9-S1, P9-S2, P10-S1, P11-S1) from 4 different breast cancer patients were analyzed by the microfluidic-microarray method. The HER2 statuses of these patients were assessed previously using the FISH technique. Patients P8 and P9 were HER2-negative, whereas patients P10 and P11 were HER2-positive. Ab microarrays were scanned using two excitation wavelengths: 532 nm to detect streptavidin-F555 (fluorescent calibration) and HER2 protein, and 635 nm to detect uPA (negative control). The average fluorescent signal intensities for HER2 in the "assay" and "control" DMCs are presented in figure 3.5b. For all protein extraction samples, HER2 fluorescence signals of the assays were higher than these of the controls (all t-test p values <0.01) (see figure 3.5b). No significant difference between the assay and the fluorescent control signals was obtained for uPA, which is consistent with the LC-MS results that indicated no presence of uPA. In order to estimate the quantity of extracted HER2, we normalized the signal intensity of the assay to that of the control. Indeed, low fluorescence signals were obtained in the negative control positions. First, the fluorescence intensities of the two slides P9-S1 and P9-S2 obtained from the same patient P9 displayed significantly-different HER2 signals. However, comparison of the tissue surfaces for P9-S1 and P9-S2 showed less than 10% variation suggesting that tissue size variation is not the reason for this apparent discrepancy. Second, fluorescence signals obtained from streptavidin-F555 spots indicated that protein immobilization (both streptavidin and capture Abs) on functionalized glass slides was efficient (see figure 3.6).
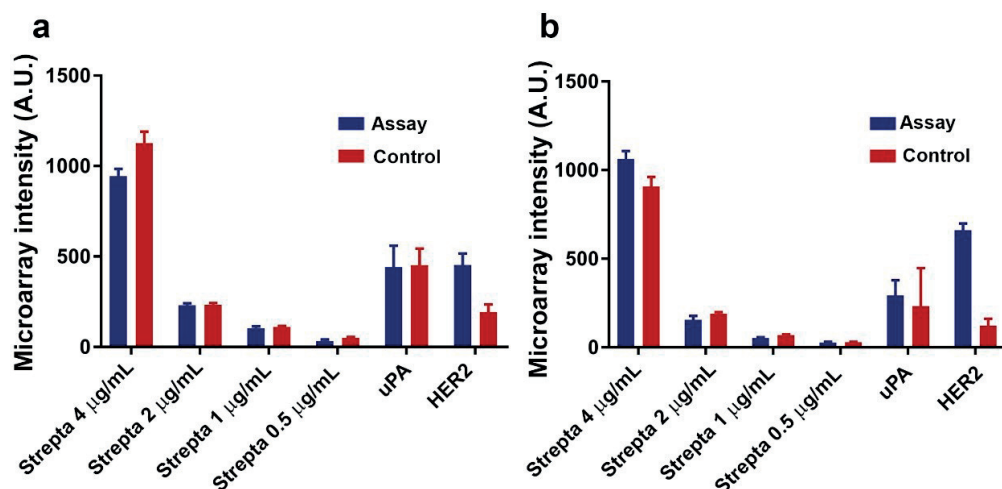
Figure 3.6 - Comparison of fluorescence intensities obtained from "assay" Ab microarray (blue bars) and "control" Ab microarray (red bars) after performing the incubation of protein extraction solution in the DMC. (a) Detection of HER2 and uPA biomarkers in protein extraction solution from breast cancer HER2-negative patient (P9-S2). (b) Detection of HER2 and uPA biomarkers in protein extraction solution from breast cancer HER2-positive patient (P11-S1). HER2 status was classified by FISH. Fluorescence intensities from various F555-labelled Streptavidin concentrations (4 μg/mL, 2 μg/mL, 1 μg/mL, 0.5 μg/mL) demonstrated that the slide–to-slide variation for 532 nm excitation wavelength was not significant (ratios of SD to mean are in the range of 0.08 to 0.3). uPA fluorescence signals displayed the same level in the "assay" and "control" microarrays while HER2 fluorescence signals were systematically higher in the "assay" microarray than in the "control" one.

Third, the HER2 fluorescence intensity of the control array representing non-specific adsorption of detection Abs and molecules, showed the same variation as the HER2 fluorescence intensity of the assay array representing the specific detection of HER2 in the protein extraction solution. Thus, we thought that the variation in the HER2 fluorescence signal between slides P9-S1 and P9-S2 could be due to variable washing efficiencies leading to variation in non-specific adsorption. Hence, in order to characterize the specific HER2 signal, the ratio between extract and control fluorescence signal (extraction-to-control ratio or ECR) was calculated. In particular, the ECR of slides P9-S1 and P9-S2 were identical as can be seen in figure 3.5b. Furthermore, ECR calculated from analysis of breast cancer patient samples (P8 to P11) displayed a good correlation (R^2=0.95) with total spectra counts obtained by LC-MS/MS analysis of adjacent sections (see figure 3.7 and table 3.3).
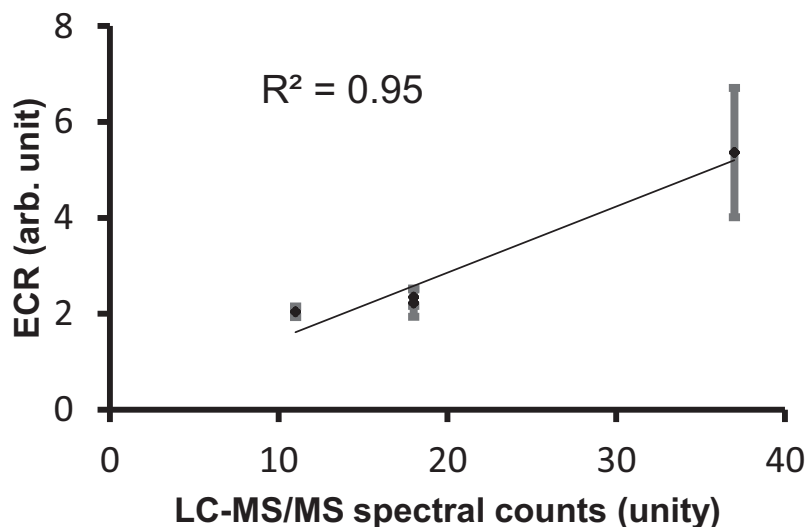
Figure 3.7 - Correlation study of four mean ratios between extract and control signals (ECR) obtained from all microfluidic-microarray spots and the LC-MS/MS analysis spectral counts. Each point represents HER2 protein quantity in the protein extraction solutions obtained from two adjacent sections from the same breast cancer tissue patient, measured by the two methods (P8-S1, P9-S1, P9-S2, P11-S1 in table 3.3).

From these results, we conclude that ECR might reflect the amount of HER2 proteins extracted from each breast cancer tissue slide. However, this amount of HER2 proteins can originate from both cancerous and non-cancerous cells: ECR=ECR1+ECR2 where ECR1 is associated with cancer cells and ECR2 with non-cancer cells. Therefore, we propose a method to obtain ECR1 from ECR, and then HER2 protein density from ECR1 normalized with the membrane surface of CK-positive cells (see section 3.2.2.7).

As shown in section 3.2, the extraction of proteins from tissue slides using the MTP was not total. Therefore, IF staining of CK and HER2 proteins could be performed to characterize the number of cancer cells and their membrane area (figure 3.8a). We assumed that the ratio ECR1/ECR2 was equal to the ratio of the total HER2 signal intensities of cancer area to non-cancer area obtained by IF (see section 3.2.2.8). Therefore, ECR1 and ECR2 could be determined by solving a 2 variables-2 equations' system (see sections 3.2.2.7 and 3.2.2.8). Then HER2 protein density was calculated by normalizing the obtained ECR1 to the area of the cancer cell membrane determined by CK marker detection. HER2 protein densities were computed for the 5 breast cancer tissue slides from patients P8 to P11 (figure 3.8b). As all standard slides used in this study have the same thickness (4 μm), HER2 protein density relates to HER2 protein expression per cell membrane volume unit. To verify if our HER2 protein density is an intrinsic characteristic of the sample which reflects the HER2 overexpression, we benchmarked it with FISH, the gold-standard for quantitative HER2 assessment [59]. Figure 3.8c is an image of a HER2-positive breast cancer tissue slide. The result presented in figure 3.8d demonstrates a good correlation between the HER2 protein density and the *HER2* copy number (R^2=0.975).
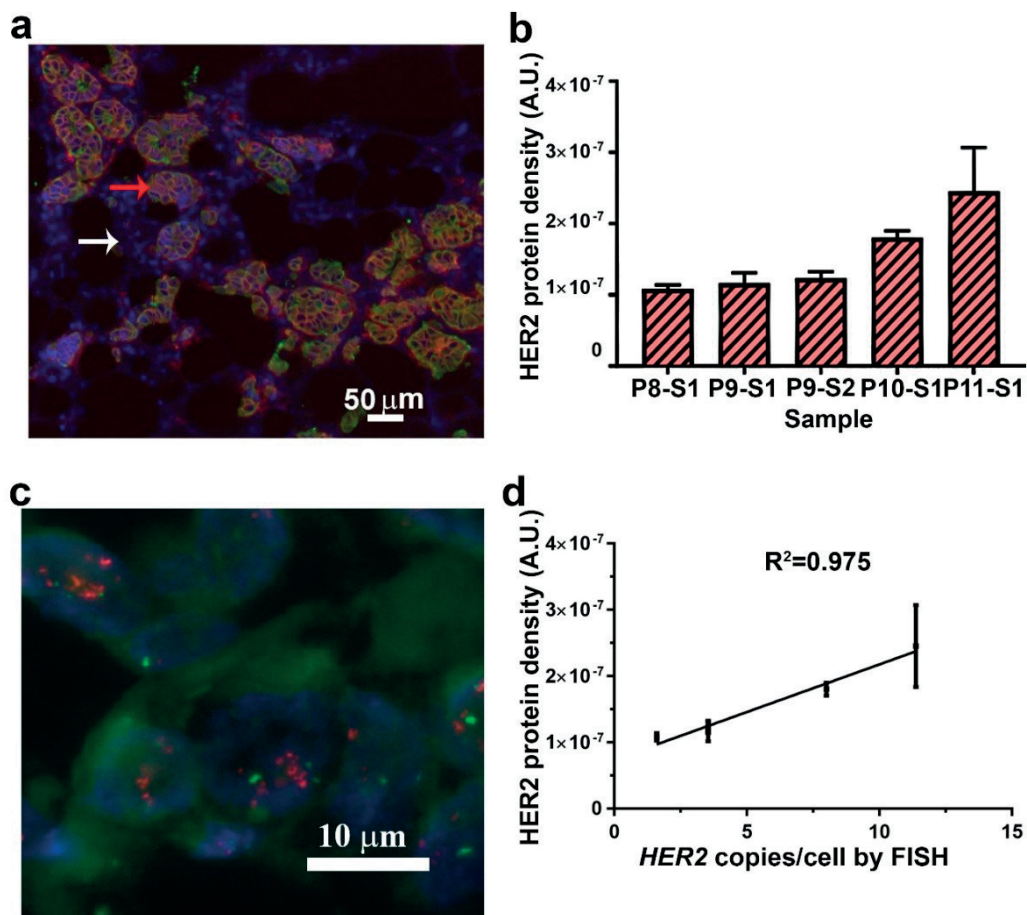
Figure 3.8 - HER2 protein density obtained from IF and FISH analysis. (a) IF image of a HER2-positive breast cancer tissue slide (P11-S1) after protein extraction and immunostaining. The red signals indicate HER2 proteins and the green signals show cytokeratin (CK), while the blue signals give the location of the nuclei. The red arrow points to cancer cells (strong expression of CK) and the white arrow indicates non-cancerous cells (weak expression of CK). (b) Normalized HER2 protein density, representing HER2 protein expression level of cancer cells, calculated from ECR obtained on DMC, per unit of cancer area obtained from IF analysis of the tissue slides. The error bars are obtained from the SD of the ECR divided by the cancer cell membrane area. (c) FISH image obtained from the HER2positive tissue slide P11-S2 adjacent to the slide P11-S1 presented in A. *HER2* gene copies are stained in red, CEN17 are stained in green and nuclei are stained in blue with DAPI counterstaining. More than six *HER2* gene copies are detected in all cancer cell nuclei indicating that the *HER2* gene was amplified. (d) Correlation study between the HER2 protein density, obtained by our microfluidic-microarray technique, and the number of *HER2* gene copies per cell, obtained by FISH analysis in a cluster of 20 cells from 5 breast cancer tissues (patients P8 to P11).

3.4. Discussion

This study offers a new method to quantify cancer biomarkers in FFPE tissue slides using microfluidics combined with protein microarrays. Although the design of the MTP was already reported [31, 62, 95], its

function is completely different in this study: it is used as a high-temperature incubator and collector of proteins. The DMC's channels were designed to have a similar microfluidic volume than the MTP (7-8 µl) for an effective Ab microarrays analysis of the protein extraction. The slides and microfluidic devices are simply assembled by scaffolding. The unique queuing of bio-chemical steps allows detection of the target molecules (HER2) with accuracy.

Compared to standard protein extraction from FFPE tissue, our microfluidic method yields lower total protein extraction mass (6-27 µg proteins per mm^3 compared to ~36 µg per mm^3 in the standard method). However, the protein concentrations of our extraction solutions display a similar range (857-4000 µg/µl) than the one obtained with the standard method (330-3440 µg/mL), as the proteins are diluted in a smaller-volume solution (7 µl compared to 50 µl) [96]. Furthermore, the microfluidic-microarray protocol is simple, uses a smaller amount of cancer tissue (1 µg instead of 2-3 µg) and does not require steps such as centrifugation, debris filtering, as in conventional extraction methods. Most importantly, the microfluidic-microarray method preserves the morphological information of the tissue sample, allowing subsequent IF analysis. In particular, the detection signal of HER2 proteins obtained with the Ab microarrays (ECR) was related to the surface of cancer cell membrane expressing HER2, as determined by IF. By combining quantitative results from Ab microarrays and morphological information from IF, we demonstrated a proof-of-concept for quantitative HER2 biomarker assessment. More specifically, HER2 protein density was correlated to *HER2* gene amplification, therefore, to *HER2* gene expression. Compared to IHC that may be more subjective to interpretation, quantitative evaluations of biomarkers can improve the accuracy and minimize errors. Moreover, the result of HER2 protein quantification could be compared to LC/MS-MS results. This method can be easily integrated into the diagnostic routine due to the simple working principle, infrastructure and automatable workflows. Comparing to the literature, this study advances the knowledge in the field of non-destructive extraction of proteins from FFPE tissues. Formalin fixation is the best method for long-term storage of clinical tissue samples, hence several studies focused on optimization of protein extraction from FFPE tissue. Chu et al. showed that it was possible to extract proteins and immune-stain the tissue after performing the extraction [90]. This pioneering study combined heat-induced antigen retrieval for fixed tissues by using Tris/HCl solution and protein extraction thanks to SDS detergents [86]. Proteins were partly extracted from the tissue surface, leaving other proteins still present in the tissue for subsequent IF analysis. The microfluidic control and standardization of the Ab microarray signals to the cell membrane surface, allow relating the microarray signals to the areal expression of the protein. Moreover, in our microfluidic method, dead-volume effects are minimum, leading to efficient quantification of the extracted proteins. Therefore, the fluorescence signal measured by the microfluidic-microarray method could reflect the total amount of biomarkers.

Despite interesting results were obtained, this investigation is still a proof-of-concept study due to the limited number of clinical samples tested. However, any generic microfluidic device could reproduce our work and perform extraction and detection on a larger clinical sample cohort to study the diagnostic accuracy. A calibration by using solutions with known protein concentrations can provide an exact concentration of proteins inside the extract. In the future, the microfluidic extraction step could be improved by increasing extraction yield for some specific biomarkers. Indeed, the extraction protocol was optimized based on the total retrieved protein mass. However, most of the extracted proteins are not exploitable for breast cancer diagnosis. Also, some interesting biomarkers such as ER or uPA, PAI-1 and ER were probably not extracted. Therefore, modifications of extraction solution, such as SDS substitution by Triton X-100 or pH alteration, are envisaged to improve the solubility of target biomarkers and increase their extraction efficiency.

3.5. Conclusion of chapter 3

In this study, a proof-of-concept of a new biomarker detection and quantification method was proposed. The microfluidic-microarray technique allows antigen retrieval of FFPE tissues, protein extraction and detection in a microfluidic chip that was combined with microarrays. The performance of this new technique is verified by standard methods. This work paves the way for implementing high-throughput, multiplex, standardized analysis of biomarkers. In future, optimization of extraction and detection protocols would give higher biomarker extraction yield and higher sensitivity of the detection. Based on our preliminary results, we anticipate that the microfluidic-microarray technique has a potential application in precision medical diagnostics.

4. HIGH-CONTENT, CELL-BY-CELL ASSESSMENT OF HER2 OVEREXPRESSION AND AMPLIFICATION IN BREAST CANCER TISSUES.

IHC and FISH are the two standard clinical methods for the assessment of Human Epidermal Growth Factor Receptor 2 (HER2) status in breast cancer, to select patients who could benefit from a HER2-targeted therapy. However, in current clinical practice, IHC is not quantitative and often subjective, while FISH is based on a quantitative evaluation of only a small part of the tissue. Therefore identification of eventual HER2 heterogeneity within the same tumor on a large scale is precluded. As HER2 heterogeneity is often associated to resistance to HER2-targeted therapy and to high relapse probability, early detection of the former can guide better treatments. In this work, we propose an experimental and analytical methodology that provides a high-content assessment of HER2 overexpression and amplification that enables for the first time the evaluation of both protein expression and gene prevalence in individual cells over a large area of a tissue slide. The technique consists of performing sequential steps: an IF assay using a microfluidic protocol, an elution step for removing the IF staining agents, a standard FISH staining protocol, and finally an automated quantitative cell-by-cell image processing over the whole tissue slide. With our method, we obtained both cancer cell's protein expression by assessing HER2 and CK proteins, and the corresponding gene amplification by scoring the number of loci of *HER2* and the number of CEP17. The image processing involved, first, the cancer area selection by filtering out the cells expressing low CK. Then, we quantified HER2 overexpression and amplification in CK-positive cells by using the ratio between HER2 protein signal and the CK signal (HER2/CK ratio), and the ratio between *HER2* loci and CEP17 (*HER2*/CEP17), respectively. We demonstrated that both parameters obtained with our method correlate with standard *HER2*/CEP17 ratios obtained from a standard FISH technique, as evaluated by a pathologist. These results demonstrate the opportunity to use the cell-by-cell *HER2*/CK ratio for quantitative HER2 assessment. Moreover, we used large-scale automatic FISH scoring to accurately detect intra-tumoral heterogeneity in both cluster and mosaic form.

4.1. Introduction

In 15-20% of breast cancer cases, HER2 is overexpressed, causing rapid progression and poor prognosis of the desease. This cancer subgroup (HER2-positive) can be treated efficiently using HER2-targeted therapies (*e.g.*, Trastuzumab and Pertuzumab). According to the 2013 ASCO recommendation [59], IHC and FISH are two validated techniques for HER2 assessment and routinely performed in clinics. With respect to IHC, HER2 protein expression in tissue and cell samples is characterized by the staining intensity in the cell membrane caused by labeled, specific Abs. For FISH, the *HER2* gene location is identified using a fluorescent DNA probe, and *HER2* gene amplification assessed by scoring the number of HER2 signals and chromosome 17 (where the *HER2* gene is placed) in each cell, for 20-100 cells. Conventional IHC is inherently subjective and qualitative, as the evaluation relies on the experience and judgment of the pathologist. Interpretation difficulty in IHC usually can be a source of diagnostic errors. Compared to IHC, FISH is more quantitative, but only a small tumor area, corresponding to 20-100 cells, can be assessed using the standard manual scoring method. More importantly, assessment of HER2 intratumoral heterogeneity (ITH) is challenging for both methods as, it is characterized by differences in HER2 status among different subclones in different regions of a tumor [97]. HER2 ITH is often associated with poor prognosis and resistance to HER2-targeted therapy [98]. Two forms of HER2 ITH exist: coexistence of discrete focal

clones of cells (*i.e.*, "cluster" heterogeneity) or individual cells placed in a dominant background of the opposite status (*i.e.*, "mosaic" heterogeneity) [66]. In clinics, the presence of "cluster" ITH can be confirmed if the proportion of the area of a minority phenotype within that of the majority is above 10 % [59]. However, the "mosaic" heterogeneity is more difficult to assess, as it is confirmed only, if the proportion of heterogeneous cells, as obtained by the manual scoring of FISH signals, is between 5-50 % of all cancer cells scored [99]. It means that in a population of 20-100 cells that were scored per patients, only a presence of 1 to 5 heterogeneous cells were enough to confirm the mosaic heterogeneity, which was not a statistically-large quantity.

To improve HER2 overexpression assessment, some recent studies have proposed using IF instead of bright-field IHC and computational analysis to quantify the HER2 protein presence [24, 31, 100]. Our group has demonstrated that digital IF quantification can improve diagnostic accuracy [31, 100]. For FISH analysis, automatic counting was developed to decrease the image analysis time and reduce human errors during FISH scoring [101-107]. However, as high magnification objectives (63×) with a small depth of focus that require z-stack images for different focal planes were used for recording FISH signals, the computational power and memory requirements were too large, still resulting in a small area analyzed.

Here, we develop a method based on microfluidics and image processing for high-content analysis of HER2 overexpression and amplification in large breast cancer tissue areas. After IF staining, tissues are imaged by a fluorescence microscope. All proteins and markers are then removed from the slide using protein digestion, followed by a standard FISH protocol, after which the slides are scanned again to obtain the FISH image. The IF and FISH images are then aligned using an image-processing software. In each cell, we quantify the HER2 protein intensity and its background, CK protein intensity (from IF), number of *HER2* gene and CEP17 (from FISH), and cell positions. We study the accuracy of these scores for HER2 classification in tissues and cell lines. As a result, the power of this method thus lies in its ability to analyze HER2 overexpression and amplification cell-by-cell, achieving unprecedented accuracy and content. Indeed, using a low magnification (20 ×) objective, the whole slide can be recorded and analyzed, allowing automated elaboration of 10^4-10^5 cells. Therefore, the presence of ITH can be detected, and its severity can be assessed using quantitative spatial analysis of protein overexpression and gene amplification. We demonstrate that both cluster and cell ITH can be detected and quantified in a large tissue area based on the local Moran's I method [37]. Finally, we achieved obtain a quantitative estimation of cluster and mosaic ITH for each patient in a cohort of 20 tissue slides. We benchmarked the mosaic ITH with a computing model to assess its significance.

4.2. Materials and methods

All cancer tissues were retrieved from the Institute of Pathology of the University Hospital CHUV in Lausanne (ethical convention BB514/2012, Ethical Commission of Clinical Research of the state of Vaud). 20 FFPE tissue samples were either primary breast cancer (16 cases) or metastatic cancer tissues in bones (2 cases) or stomach (2 cases). All breast cancer patients did not oppose the use of their tissues for research purposes. Tissue samples were anonymized and codified. Tissues were sliced using a microtome and had a thickness of 4 μm. All FFPE cell lines were purchased from AMS Biotechnology (Europe) Ltd - Switzerland. Cell lines were fixed by 10% Neutral Buffered Formalin, sliced into sections of 5-μm thickness. PBS 10× and Tween20 were acquired from Sigma-Aldrich Chemie GmbH, Buchs, Switzerland. PBS1× was obtained by diluting concentrated PBS stock in distilled DIW. For immunostaining, primary Abs: rabbit anti-human c-erbB-2 oncoprotein primary Ab (HER2, code: A0485) and mouse anti-human CK (code M3515)

were purchased from Agilent Technology Schweiz (Basel, Switzerland) and diluted from the stock in PBS supplemented with Tween 0.05 % (PBST 0.05 %) to get a final concentration 2.4 µg/ml (for HER2), CK 1.72 µg/ml (for CK). Secondary Abs AF594 goat anti-rabbit IgG (H+L, code: A-11037) and AF647 goat anti-mouse IgG (code: A-21236) were purchased from Thermo Fisher Scientific, Waltham, USA and diluted in PBST 0.05 % to get the final concentration of 50 µg/ml. FISH *HER2* Pathvysion® kit was obtained from Abbott Diagnostics (Santa Clara, CA, USA).

We focused on most-challenging cases in diagnostics, which are borderline cases in both IHC and FISH. 16 selected cases are classified as equivocal in IHC (2+), and in FISH (*HER2*/CEP17<2 and 4≤*HER2*/cell<6) [66]. 4 other cases are HER2-positive for both FISH and IHC. All FFPE tissue slides were previously assessed by a pathologist to determine the area of an invasive component of a ductal carcinoma using a HE staining. Cell lines and tissues are divided into batches; each batch had one HER2-negative (MD-MB-468), two HER2-positive cell line (SKBR3) and several tissue slides. For two SKBR3 cell line slides, one was a control slide for the staining (*i.e.*, it received only secondary Abs), and the other was processed with the same protocol as the other cell and tissue slides.

4.2.1. Microfluidic IF staining and imaging protocol

The protocol for microfluidic HER2 and CK IF staining was described previously [31, 100]. Shortly, tissue and cell slides were deparaffinized in 3 Histoclear II solutions (National Diagnostics, USA) for 5 min each. Then, they were transferred to gradual ethanol series of 100%, 100%, 95%, 70%, 40%, for 2 min each and stored in PBS 1 × until the staining process. Next, they were immuno-stained by using the MTP [31, 100] (figure 4.1ai). During the experiment, the chip was mechanically clamped to a slide together with a plastic o-ring, creating a 100 µm chamber above the slide to flush specific Abs and buffer solutions homogeneously onto the surface of the tissue section or cell pellet via the tree-like microfluidic channels. An automatic syringe pump system delivered to the slide via the microfluidic system the following solutions: PBST 0.05% (flow rate 10 µl/s during 5 second), HER2 and CK primary Ab mix (flow rate 2 µl/s during 50 second then 0.01 µl/s during 2 min), PBS 1× wash (flow rate 10 µl/s during 30 second), AF 594 and AF647 secondary Ab cocktail (flow rate 2 µl/s during 50 second then 0.01 µl/s during 2 min), PBS (flow rate 10 µl/s during 30 second) and distilled water (DIW, flow rate 10 µl/s during 30 second). After these automatic reagent flushing steps, the slide was removed from the setup and cleaned again in DIW before receiving SlowFade™ Gold Antifade mountant (Life Technologies) containing DAPI. The slide was coverslipped and stored in the fridge before imaging. All other slides in the batch were treated in the same manner. The whole microscope slide was then scanned tile by tile (10% overlap) using the microscope Axio Imager M2m (Zeiss, Germany) with a 20× objective (Plan-Apochromat, numerical aperture =0.8) in 2 × 2 binning mode. The light intensity was fixed maximum; the exposure time was first adjusted using the SKBR3 slide that received primary Abs to reach 80% of the highest non-saturated exposure time. These exposure time and light intensity were kept constant for all slides and in all batches. The control SKBR3 was checked, any non-specific signal should be reported. In each position, emissions of 3 fluorophores AF594, AF647, and DAPI, corresponding respectively to HER2, CK and nucleus signals, under adaptive excitation lights were recorded and merged into an image, see figure 4.1aii. IF images were represented by three colors (blue, green and red) corresponding respectively to the nucleus, CK and HER2 signals. After scanning, tiles were stitched using the Axiovision software.
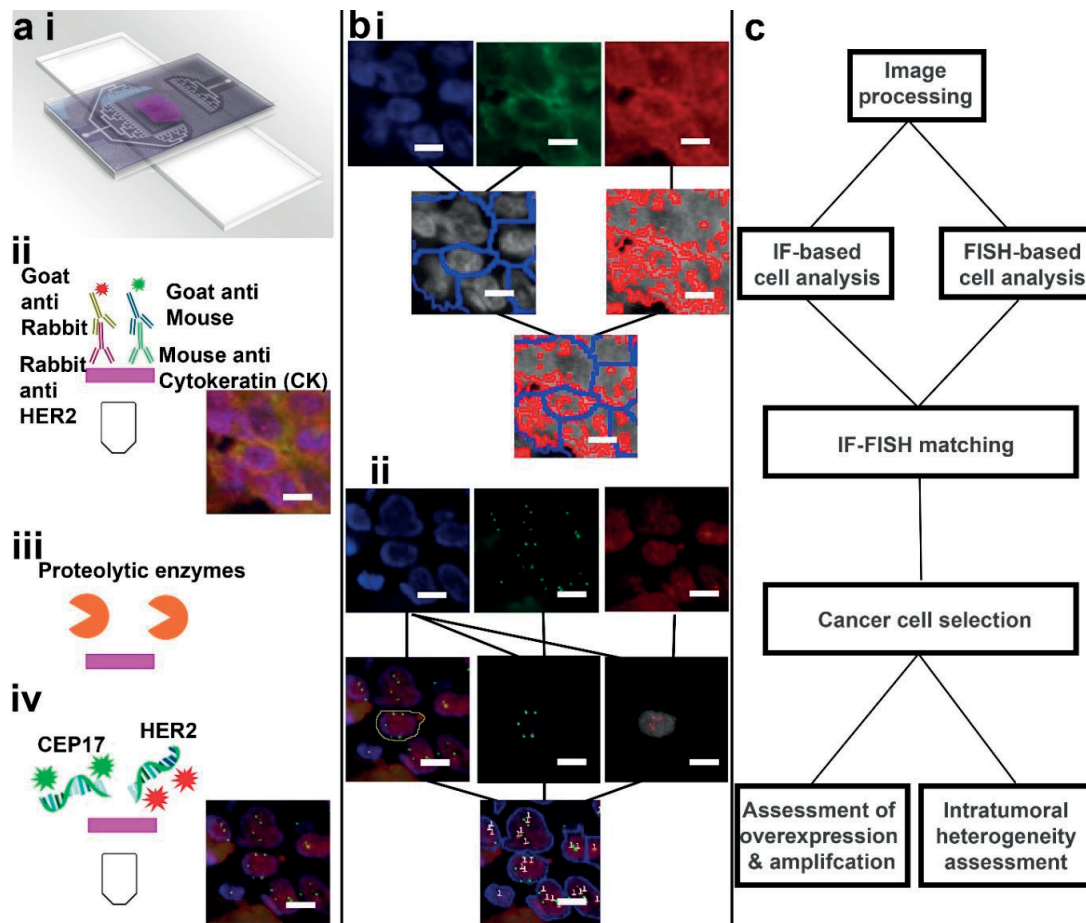
Figure 4.1 - High-content analysis of microfluidic IF and FISH. (a) Sequential IF/FISH staining. i) Immunostaining of cell pellet or tissue biopsy via the MTP (microfluidic tissue processor, see chapter 1) clamped onto the tissue-carrying glass slide to deliver the reagents in a highly-controlled fashion. ii) In the IF protocol, HER2 protein is tagged with a rabbit anti-human HER2 Ab, and CK is tagged with a mouse anti-human CK Ab. Fluorescent labeling is then achieved by using AF594-labeled goat anti-rabbit IgG Ab and AF647-labeled goat anti-mouse IgG Ab. Nuclei are marked with DAPI. The whole slide is scanned using a low magnification objective (20×). The image of a cluster of cells is presented. HER2, CK, DAPI signals are respectively displayed in red, green and blue. iii) In an elution step, staining agents are removed from the slide using proteolytic enzymes. iv) In the FISH protocol, the *HER2* loci are labelled with fluorescent HER2 probes, and centromeres of chromosome 17 are labelled with fluorescent CEP17, and nuclei are marked with DAPI. An image of the same cells as in ii is shown. *HER2* loci, CEP17 centromeres and nuclei are respectively displayed in red, green and blue. (b) Image-processing of the IF and FISH images obtained after the protocol from A. IF and FISH images, aligned using the common DAPI channel, are sequentially processed. i) For IF analysis, clusters of cells are segmented into an individual cell or a smaller group of cells based on nuclear analysis from the DAPI and CK channels. The HER2 signal also defines the membrane area in which the mean HER2 and CK intensities for each cell are measured. ii) For FISH analysis, nuclei define the area where HER2 and CEP17 signals for each cell are scored. (c) Data analysis protocol. The cell HER2 expression given by IF is merged

109

with the cell HER2 amplification obtained from FISH, followed by a filtering step that selects the cells of interest. For each sample, scores for HER2 overexpression and amplification based on the analysis of all the cells are obtained. Then, intra-tumoral heterogeneity analysis using spatial association is performed. Scale bars: 10 μm.

4.2.2. Successive FISH and imaging protocol

After IF image acquisition, the coverslip of the slide was removed. The slides were immersed in a Coplin jar containing MES 1× buffer (Agilent Technologies, Santa Clara, CA, USA) heated at 95-97°C for 10 min. Next, the Coplin jar was cooled down to RT for 20 min before dipping in washing buffer (twice for 3 min). Protein digestion was performed by applying protease (Agilent Technologies) at 37°C in 10 min (Figure 4.1aiii) then immersed in 2 washing solutions (Tris/HCl) for 2 min each. Then, the slides were dipped in post-fixation solution composing of 1% formaldehyde (Merck Millipore, Germany), PBS 1× and 20 mM MgCl2 Sigma-Aldrich (MO, USA), for 10 min. The slide was then washed with then in PBS 1×, ethanol solution with concentrations from 40-100% in 2 min each and dried. HER2 Pathvysion® FISH probe (from the FISH kit), containing a mix of DNA HER2 probe and CEP17 probes, was applied on the surface of the tissue and cell line, coverslipped and sealed with a removable rubber. The tissue and probe were denatured at 73°C for 5 min, following by an overnight incubation at 37°C. After the incubation, the rubber parts and coverslips were removed, and the tissue slide was washed in a stringent wash buffer, containing 2× SSC (Sigma-Aldrich, MO, USA), 0.3 % Tween 20 (Bio-Rad, CA, USA) for 2 min. Stringent wash buffer removed for non-specific adsorptions of DNA probes on the tissue. Then, the slide was washed in SSC Tween (SSC 2×, 0.1 % Tween 20) for 2 min, SSC 2× for 2 min, distilled water for 5 seconds and dehydrated in successive ethanol 40-100% for 2 min each before DAPI mounting medium was applied to the dried slide. Finally, the slides were coverslipped with DAPI mounting medium and sealed with a nail polishing solution. After the FISH staining, the slides were scanned tile-by-tile (10% overlap) using adaptive excitation lights and filter sets and with the same 20× objective as in the IF (without binning). The location of FISH imaging was selected based on the IF image (Figure 4.1aiv). In the end, all scanned tiles were stitched to reconstruct the large tissue area of 4 mm × 4 mm using the Axiovision software.

4.2.3. Image processing

The stitched IF and FISH images were then aligned using the common DAPI channels, sampled into small tiles having an area of 112 μm × 112 μm to decrease the computer memory requirement during the image processing process. Next, in the image processing protocol of IF signals, each IF image was segmented into cells or small clusters of cells based on nuclei and CK channels. More specifically, the CK channel was subtracted from the nucleus channel, and the local maxima were identified for determining the cell area. After this step, cells were segmented (Figure 4.1bi). In the following step, the HER2 intensity was enhanced and thresholded, defining the membrane area where HER2 and CK signals were measured. HER2 and CK protein expressions for each cell were computed by averaging the intensity of green and red pixels located in the cell membrane area. The mean background of each small tile was measured. For each cell, we calculated the (HER2 signal - mean HER2 background) / CK signal. The signals were obtained from the mean of all pixels of the selected area. Later, for short, we call this ratio the adjusted HER2/CK ratio or simply HER2/CK ratio.

In the FISH images, the nuclei were determined based on a combination of several image processing technique to enhance the signal and detect the nuclei such as edge finding, segmentation using local maxima,

and thresholding. By the end of this step, the regions of interest defining the nuclei were determined (figure 4.1bii) and associated to a cells identified in the IF image. Note that as the IF images were recorded in 2×2 binning mode, they are smaller than the FISH images. Therefore cell and nuclei coordinates in the tissue were also linked by a factor of 2. For each cell, the numbers of CEP17 and HER2 signals were scored based on local maximum detection. In particular, as CEP17 marks the alpha-satellite regions in the center of the chromosome, CEP17 dots were counted as one per local maxima position. Therefore, the total number of CEP17 for each cell was counted as the sum of local maxima in the green channel, within the area of a nucleus of a cell. For HER2, as *HER2* genes appeared as small dots, some HER2 signals could overlap and form indistinguishable clusters in the low-resolution 20×-objective images. Clusters of HER2 signals are usually brighter and larger than an individual HER2 signals. It is one of our main targets to estimate the number of *HER2* loci in each cluster to retrieve information from clustered signals. First, local maxima of the red signal within a nucleus (cluster positions) were identified. Second, in the HER2 channel, areas proportional to the full-with-half-maximum of each local maximum, corresponding to the area around the maximum, were assigned to each cluster. The cluster size and integrated intensity (sum of all signal pixels within a cluster) were measured. Last, the total number of *HER2* dots per cell was the sum of all HER2 dots in all HER2 clusters. The number of HER2 signals inside each HER2 cluster was estimated using a regression between the number of red dots counted in a higher magnification (63×) and the integrated intensity of the HER2 cluster (not shown). Note that in both red and green channels, autofluorescence was also detected together with signals, but was filtered out later, as it was detected in both channels or did not satisfiy several criteria concerning contrast and size. Also, some cells are overlapped and cannot be segmented. Therefore, the number of HER2 per nucleus was adjusted by dividing to the number of overlapped/clustered nuclei that is obtained to the mean size of cancer cells (supposed that most cells are not clustered) and rounding it to the lower integral value.

After image processing, IF and FISH signal characteristics such as immunostaining intensity, FISH scores, were obtained and merged into a single database (Figure 4.1c). For tissue analysis, the data processing was followed by a spatial analysis (*vide infra*). After the data acquisition, each nucleus defines one cell with all characteristics: HER2 protein intensity and its background, CK protein intensity (from IF), number of *HER2* loci and CEP17 (from FISH), nucleus size and cell positions in X and Y coordinates.

4.2.4.   Data analysis

To select cells of interest, we applied a series of filtering based on the following parameters: CK signals, nucleus size, the number of red and green signals. A selected nucleus has a size in the range of 50-1000 μm^2 and contains at least one HER2 and one CEP17 signal. Furthermore, it should have a relatively strong CK signal comparing to other cells in the tissue, to make sure that the cell is an epithelial cancer cell and not a normal cell. For this aim, we applied a filter based on the histogram of the CK signals in all cells. Non-epithelial cells with CK signal less than Mean - 0.5×SD were discarded. For all remained cells, we computed the mean adjusted HER2/CK ratio, the number of *HER2* loci and *HER2*/CEP17 ratio per cell and their corresponding SDs. Then, HER2 classification was performed based on the ASCO/CAP 2013 guideline for FISH assessment. We computed the ratio between the sum of all *HER2* loci and CEP17 for all cells in the tissue. This ratio, called overall *HER2*/CEP17 ratio, is slightly different to the *HER2*/CEP17 ratio per cell, which is the average of ratios. The HER2 status is determined as the follows. If an overall *HER2*/CEP17 ratio $\geq$ 2, or a number of *HER2*/cell > 6 is found, the sample was considered positive. If 4$\leq$ *HER2*/cell $\leq$6 and

overall *HER2*/CEP17 ratio < 2 are found, the sample was considered equivocal, and all scores lower than these thresholds are associated with a negative sample, following the ASCO/CAP 2013 guidelines.

4.2.5. Analysis of local indication of spatial association

Spatial heterogeneity is characterized by a local Moran's I analysis that indicates the correlation and anti-correlation between the IF or FISH scores obtained in one cell and the neighbors of this cell. We define a variable of interest X having a value x_i at each cell i that varies through a Cartesian space. Classical local Moran's I calculates a scalar product I_i at each cell i with its neighbors j as

$$I_i = z_i \times \sum_j W_{ij} z_j$$

With

$z_i = \frac{x_i - \bar{x}}{\sigma}$ is the normalized value of x_i to its mean $\bar{x}$ and SD $\sigma = \sqrt{\frac{(x_i - \bar{x})^2}{N}}$

w_{ij}: weight matrix which defines neighborhood. $w_{ij} = 0$ if i and j are not neighbors of each other. $w_{ij} = 1$ if i and j are neighbors of each other.

$\sum_j W_{ij} z_j$ is the sum of all normalized values of z_j all neighbors j

In our study, this variable X can be the adjusted HER2/CK or the *HER2*/cell number. We want to compare the cell scores with a fixed value instead of a mean and a SD of the cell population, which can vary from one tissue sample to another. Therefore, we define a variable $\tilde{z}_i$ by centering the variable X to a fixed threshold x_o (for example for the variable *HER2*/cell x_o=5), and normalizing it to the SD σ of the population.

$$\tilde{z}_i = \frac{x_i - x_o}{\sigma}$$

The sum of neighbor values becomes $\sum_j W_{ij} \tilde{z}_j$.

Cells are classified into five groups, high-high (HH), low-low (LL), high-low (HL), low-high (LH), non-classified (NC) depending on the value $\tilde{z}_i$ of the cell and the value $\sum_j W_{ij} \tilde{z}_j$ of its neighborhoods. One cell is classified as High (respectively Low) if the its variable x_i is higher (respectively lower) than a high threshold T_h (respectively low threshold T_l). This is equivalent to $\tilde{z}_i$ higher (respectively lower) than a high threshold $\frac{T_h - x_o}{\sigma}$ (respectively low threshold $\frac{T_l - x_o}{\sigma}$). The thresholds T_h and T_l of the variables such as the adjusted HER2/CK or the *HER2*/cell number are fixed for all tissues studied and have the average value equal to x_o ($\frac{T_h + T_l}{2} = x_o$). For the variable *HER2*/cell T_h=6 and T_l=4, based on the ASCO 2013 guideline [59], see the section III.3.a. For the variable HER2/CK, they are chosen based on a study on the HER2-positive cell line SKBR3 (see the section III.1.a). Neighborhood are classified as High (respectively Low) if $\sum_j W_{ij} \tilde{z}_j$ is higher (respectively lower) than 0, which means the mean of all neighborhood's values is higher (respectively lower) than x_o. An HH cell is a positive cell that is placed in a positive cluster, the analogy is applied for HL, LH, and LL cells. They are NC otherwise, i.e. the value is not high or low enough to conclude about the positivity or negativity of the cell signal. In our analysis, neighborhoods of a cell i are all cells within a distance of 100 μm to the cell i.

Finally, we define cluster heterogeneity and mosaic heterogeneity as the following. In the cluster heterogeneity, if more than 10% of all cells have a different status, for example, negative cells in positive samples or positive cells in negative samples, and form a cluster (HH or LL cells), this case is identified as cluster heterogeneity. For the mosaic heterogeneity, we calculate the proportion of HL cells in a HER2-negative sample and LH cells in a HER2 positive sample. As cells are sliced during the tissue preparation, the mosaic heterogeneity is usually confounded to the cell truncation errors of the FISH technique. Therefore the mosaic heterogeneity is only concluded, when there are more heterogeneous cells originating from biological variations than from truncation errors (see section 4.3.3.2).

4.2.6. Statistical modeling of the *HER2*-loci-per-cell number in a homogeneous cell population.

By using a statistical model, we will demonstrate that even a homogeneous cell population can display heterogeneous cells due to truncation errors. To achieve this aim, first, the geometry of a truncated cell is presented, see figure 4.2.

4.2.6.1.   Geometry of a truncated cell

A cell is modeled sphere having a radius R. Given an X axis having an origin at the center of the sphere, the cell cut has a center at x and a thickness of τ.
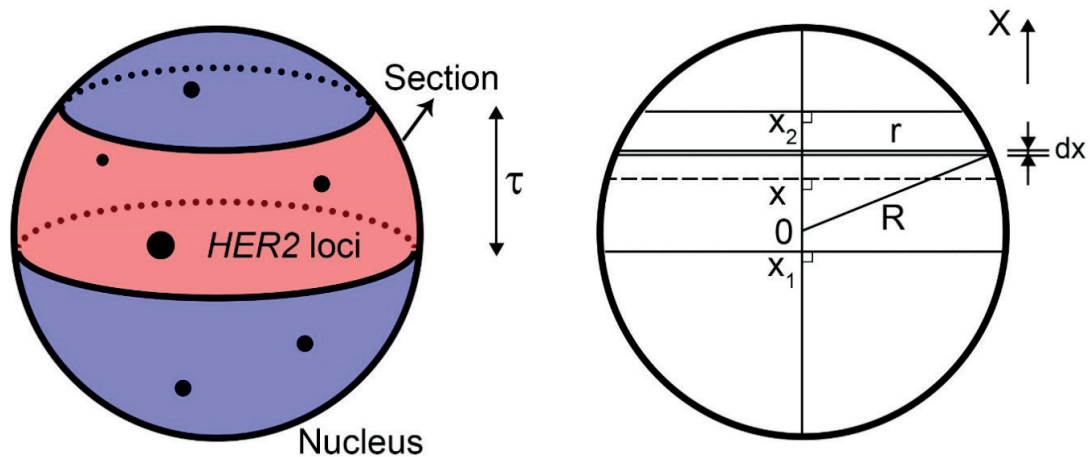
Figure 4.2 - Schematic presentation of a nucleus with several *HER2* loci. Left: section of thickness t selects only some among all *HER2* loci. Right: 2D presentation of the section and the nucleus.

The mathematical background allowing to calculate the probability density function of the HER2/cell number (the number of HER2 signals contained in the cell section) in function of the position x is presented in the following section.

Two extremities of the cut on the x axis are called x_1 and x_2 with $x_2 > x_1$. The position of the center of the cut x is arbitrary chosen, in between –R and R on the x-axis. This position x follows a uniform probability law with a probability density of f(x) with

$$f(x) = \frac{1}{2R} \quad \text{with} -R < x < R \tag{4.1}$$

For each position x, we obtain a volume $V_\tau(x)$ of the cut calculated as:

$$V_\tau(x) = \int_{x_1}^{x_2} \pi r(x)^2 dx \tag{4.2}$$

With $r(x)$ is the radius of a section of the sphere at position x, $r(x)^2 = R^2 - x^2$ (Pythagore). The calculation of $V_\tau(x)$ is detailed in Appendix C. From $V_\tau(x)$ we can calculate the probability $p(x)$ for one *HER2* locus to be placed inside the cell section. Indeed, the number of *HER2*/cell obtained in a FISH image (measured *HER2*/cell) is the number of HER2 signals that are, by "chance", placed inside the cell section. Hence, considering one *HER2* locus, it can belong to a domain inside the cut or outside the cut. Its probability to be placed inside the cut is the ratio between the volume of the cut and volume of the cell. In the Appendix C, we demonstrate that the number of number of *HER2*/cell follows a binomial law of probability. From $p(x)$ we calculate the probability mass function of the *HER2*/cell number variable used for generating a population of cell section to build truncation error model (*vide infra*).

4.2.6.2. Simulation of number of HER2/cell of a population of truncated, homogeneous cells

First, we generated a uniformly-distributed population of M elements between 0 and 1. M corresponds to the number of cells in a tissue or cell pellet. This population was used to create a set of values having a binomial distribution using the invert function of the binomial cumulative-distribution-function (cdf). The binomial cdf was the sum of all probabilities $\sum_{n=1}^{N} P(n, N, p(x))$ for n=1 to N, for a given N and $p(x)$. For N, we suppose that the theoretical number of *HER2* loci in all cells is identical and equal to N. We generated a random variable x from a continuous, uniform distribution and calculate $p(x)$ using the relation presented in [6]. In equation [6], the cut thickness τ is equal to 4 µm for tissue slides and 5 µm for cell line slides and the value of the radius of nuclei R is unknown and to be estimated from the measurements. The theoretical radius of nuclei R is supposed to be identical in all cells in the tissue.
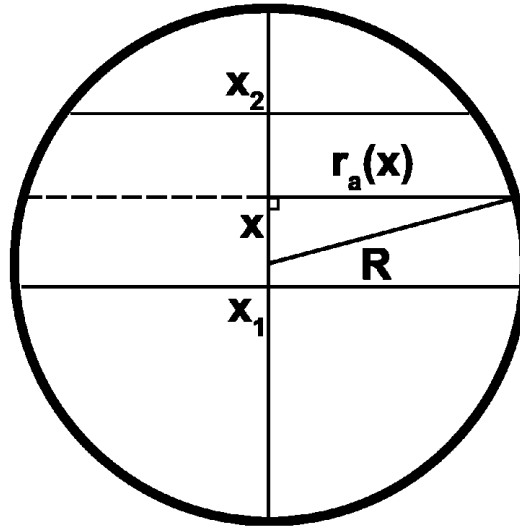
Figure 4.3 - Relation between the apparent radius r_a and true radius R. x is the center of the cut relative to the center of the nucleus. The position of the two boundaries of the cut are x_1, x_2.

In our analysis, we can measure the value of the area of a cell section that is a disk with a radius r_a (the apparent radius of a cell). Here, we will demonstrate how R can be calculated from the measured r of cell section. Indeed, these radii r_a and R are related by the Pythagore equation (Figure 4.3):

$$R^2 = x^2 + r_a(x)^2 \qquad (4.3)$$

If we consider a population of cell, x can be considered from a statistical point of view as a random variable presenting the center of the cut relative to the center of the nucleus.

As x is a uniform random variable between $-R$ and R, it has an expected value $E(x)=0$ and a variance $var(X) = \frac{[R-(-R)]^2}{12} = \frac{R^2}{3}$

By definition, the variance of x can be presented in function of expected value of x and x^2:

$$var(x) = E(x^2) - E(x)^2$$

Thus the expected value of the variable x^2 is equal to

$$[E(x^2)] = [E(x)]^2 + var(x) = 0 + \frac{R^2}{3} = \frac{R^2}{3} \qquad (4.4)$$

Therefore from the equations (4.3) and (4.4) the value of the theoretical radius of a nucleus R can be presented as a function of the expected value of r^2:

$$R^2 = E(x^2) + E(r_a(x)^2) = \frac{R^2}{3} + E(r_a(x)^2)$$

Or

$$E(r_a{}^2) \sim \frac{2R^2}{3} \qquad (4.5)$$

After measuring the apparent radius $r_a(x)$ and computing $r_a(x)^2$ for all cells in all tissues of the batch, we obtained the mean cancer cell radius $R \sim 7.0$ μm from the equation (4.5). For cell lines, R is slightly bigger and equal to 7.3 μm.

For tissue slides, we performed 10 simulations using the following set of parameters: M= 20000 (the typical number of cells in a tissue slide area), R =7 μm, τ =4 μm. For cell slides, 10 simulations were performed using the following set of parameters: M= 5000 (the typical number of cells of a cell pellet area), R =7.3 μm, τ =5 μm (the thickness of the cell pellet obtained from the supplier's specification). All simulations and calculations were performed by MATLAB (MathWorks Inc, MA, USA). For tissue slides, we performed 10 simulations using the following set of parameters: M= 20000 (the typical number of cells in a tissue slide area), R =7 μm, τ =4 μm (for example, the distribution of a truncation model having the total number of HER2 loci N=25 is presented in figure 4.4). For cell slides, 10 simulations were performed using the following set of parameters: M= 5000 (the typical number of cells of a cell pellet area), R =7.3 μm, τ =5μm the thickness of the cell pellet obtained from the supplier's specification). The mean HER2/cell of each cell population was obtained by averaging the number of HER2 loci of all truncated cells in the simulation.
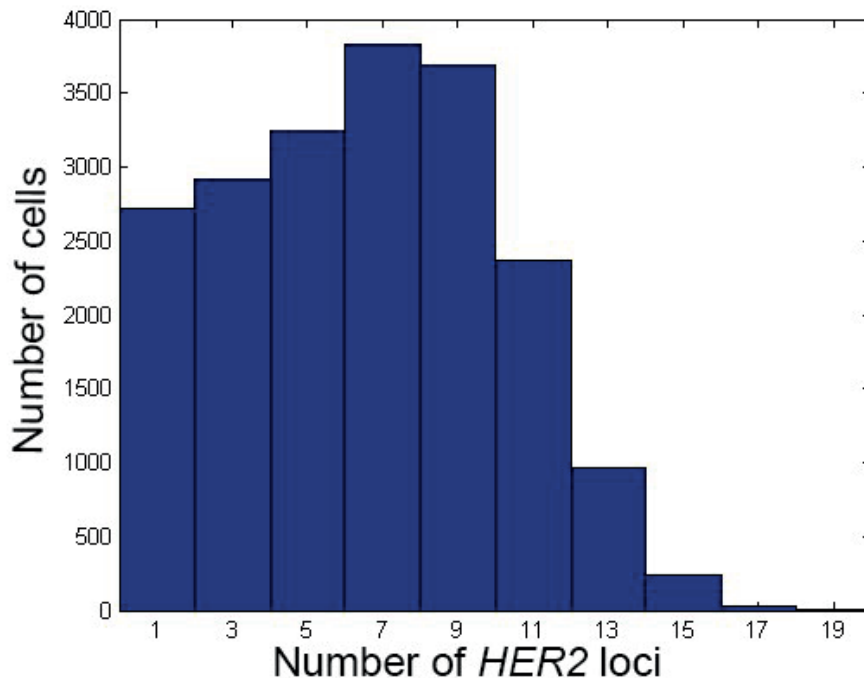
Figure 4.4 - Simulated HER2 loci histogram of a truncation model. The cell section can contain different numbers of HER2 loci varying from 1 to N, where N is the theoretical number of HER2 loci which is identical for the 20000 truncated cells generated. The x axis represents the number HER2 loci in each cell. The y axis shows the number of cells having a given number of HER2 loci. Here the total number of TC M= 20000, theoretical TC radius R =7 μm, thickness of the cut τ =4 μm and N=25.

4.2.6.3. Heterogeneity assessment in the current clinical practice.

According to ASCO 2013 guideline [59],the presence of cluster ITH is stated, if more than 10% of the total cells are strongly positive (HER2 copy/cell≥6) and clustered (equivalent to HH cells in the local Moran's I analysis of FISH HER2/cell image) in a HER2-negative sample or 10% of the total cells are negative and clustered in a HER2-positive sample (LL cells in local Moran's I image of FISH HER2/cell). For mosaic

heterogeneity, the selection criteria are less obvious. Indeed, according to the literature, the presence of cellular ITH of each patient is confirmed for a HER2-negative/equivocal sample (mean *HER2*/CEP17 ratio <2 and mean *HER2*/cell < 6) if there is a presence of heterogenous individual cells having *HER2*/cell >6 in HER2 negative clusters (HL cells in local Moran's I image of FISH signal); and for a positive sample (mean *HER2*/CEP17 ratio ≥ 2 or mean *HER2*/cell ≥ 6) with a presence of heterogeneous HER2-negative cells *HER2*/cell < 4 (equivalent to LH cells in local Moran's I image of FISH signal) [66]. According to the literature, mosaic ITH is confirmed if there is 5 to 50% heterogeneous cells [59, 79].

4.3. Results

4.3.1. High-content analysis of HER2 overexpression and amplification in cell lines and tissues

4.3.1.1. Cell line overexpression and amplification analysis
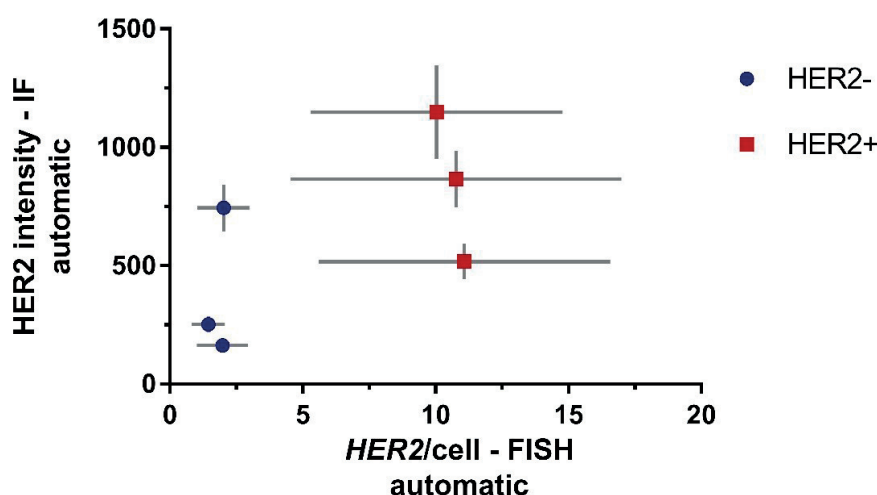
Figure 4.5 - HER2 positive- and negative- cell line characterization by both IF and FISH technique. On the horizontal axis: the mean *HER2*/cell number obtained from an automatic scoring of FISH signals. On the vertical axis, the mean HER2 intensity of an IF image. Triplicates of HER2-negative (HER2-) and HER2-positive (HER2+) samples were performed.

To assess the robustness of HER2 overexpression and amplification with our technique, we performed IF/FISH staining and analyses on well-defined HER2 controls: a HER2-positive cell line (SKBR3) and a HER2-negative cell line (MD-MB-468). Mean values of HER2 intensity from an IF image and automatic *HER2* loci per cell (*HER2*/cell) scores from FISH are plotted in figure 4.5. The automatic FISH counting scores were calculated from the total pixel intensity in clusters of red dots in a 20× image (see section 4.2.3). The horizontal and vertical error-bars are large, showing a wide range of variation of HER2 IF signals and the number of *HER2* loci among cells. When the HER2 intensity of the image's background (i.e. areas that express low HER2 signal) is substracted from the HER2 protein signal of a cell and the result is normalized to the CK signal (HER2/CK ratio) of the cell, we found that the mean ratio of all cells is similar between the replicates (see Figure 4.6a). Also, smaller variations between cells and a sharper distinction between negative and positive cell lines are observed, suggesting that HER2/CK ratio is a value characteristic of each cell line

sample, independent of between-batch variations. For FISH, the *HER2*/cell variation is explained by a "truncation error", *i.e.,* the number *HER2* loci/cell scored by FISH can take a random value between 0 to N, where N is the exact number of the *HER2* copy of this cell, because it was sliced into sections. Thus, we normalize *HER2* copy numbers to CEP17 signal numbers for each cell to limit the truncation error effects on the mean *HER2*/CEP17 score thanks to the large population of cells. Indeed, the probabilities of both HER2 and CEP17 signals contained in the cut are proportional to the thickness and size of the cell cut. Finally, the two selected parameters are the mean HER2/CK ratio and the mean *HER2*/CEP17 ratio. As SKBR3 is a weakly HER2-positive cell line [74], its IF staining intensity is closed to the HER2 negative-positive borderline. We used it to define the threshold between HER2-negative and positive tissues for quantitative IF. The analysis of SKBR3 cell slides gives a mean HER2/CK ratio of 0.316 and a SD of 0.021. A t-test to determine the confidential interval of the mean HER2/CK ratio gives a 95% confidential interval of [0.251, 0.380]. The lower bound of the 95% confidential interval 0.251 is used as the threshold for HER2 classification in tissues (*vide infra*). Control SKBR3 slides that did not receive the primary Abs did not display any specific signals, proving that the staining is specific to the biomarkers HER2 and CK.
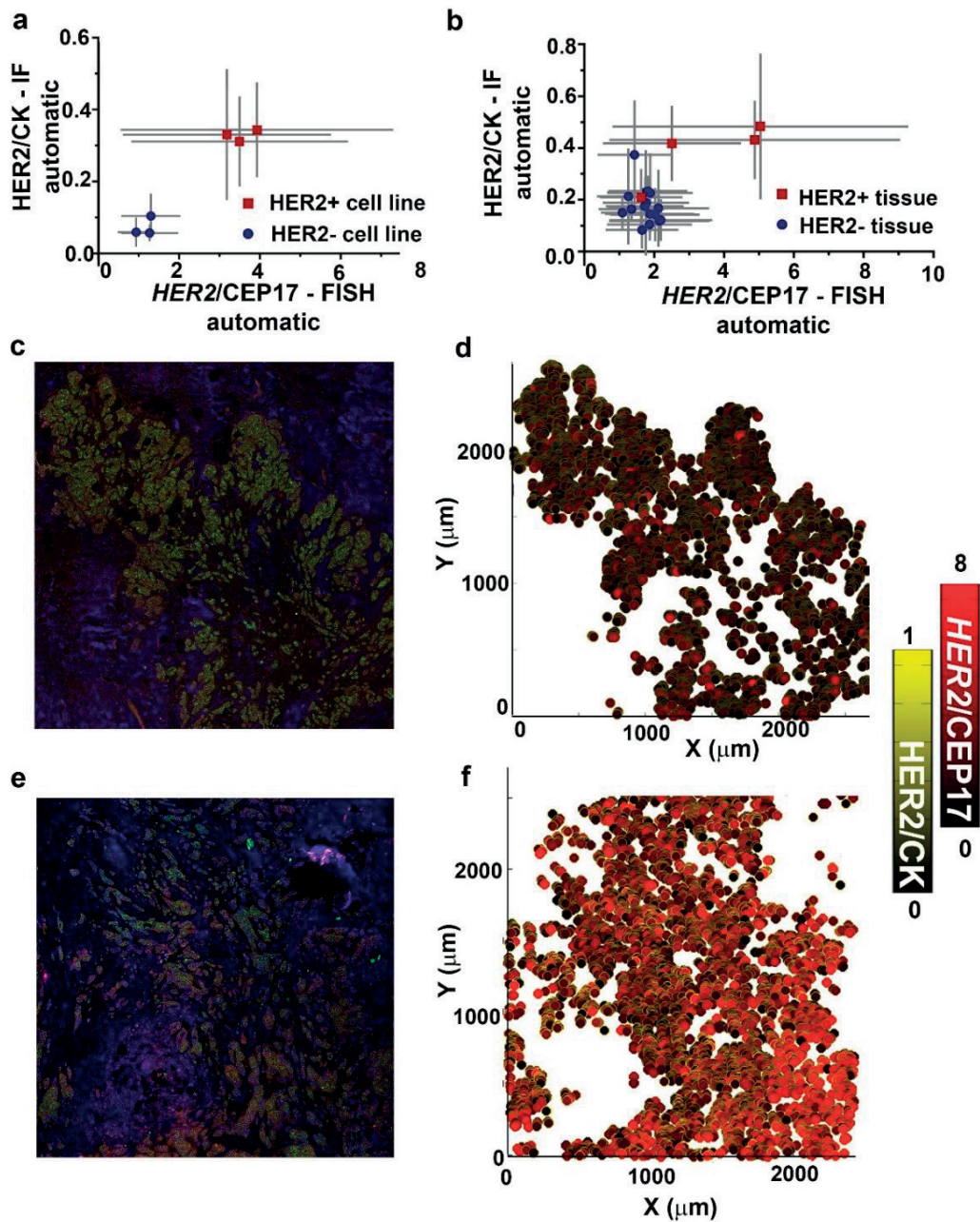
Figure 4.6 - HER2 assessment of cell lines and tissues using automatic and quantitative IF-FISH analysis. (a) HER2 overexpression (given by the cell-by-cell ratio between the HER2 and the CK signals) versus HER2 amplification (given by the cell-by-cell ratio between the number of *HER2* loci and CEP17) for HER2 positive (+) and HER2 negative (-) cell lines. Data are plotted as a mean ± SD. (b) Assessment of HER2 overexpression and amplification with the same methodology as in A for HER2+ and HER2- tissues. The HER2 status is obtained from pathological assessment by a standard FISH technique. (c) IF image of a HER2-negative tissue. (d) Cell-by-cell representation of HER2/CK. and *HER2*/CEP17 signals. Cells are represented by dots. The contours of the dots (in yellow scale) denote the

normalized HER2/CK ratio, while the inside of the dots (in red scale) indicate the *HER2*/CEP17 ratio of the cells in C. Normalization of the HER2/CK ratio (yellow scale) is obtained by allocating the value 1 to the maximum HER2/CK ratio that was obtained from all tissues. The maximum of the red scale is chosen as 8 for easy distinction between positive and negative cells. (e) IF image of a HER2-positive tissue. F) Cell-by-cell representation of the tissue in E with the same methodology as in D. Colors in IF images: Blue=DAPI, Green=CK, Red=HER2.

4.3.1.2. Tissue analysis using the high-content IF-FISH technique

Combining the IF and FISH automatic analyses, all mean HER2/CK ratios obtained from IF and *HER2*/CEP17 ratios obtained from FISH were computed for all tissues. The results are plotted in Figure 4.6b. The error bars represent the variation of these scores among cells in the tissue. In general, we observe the higher range of HER2/CK ratios and *HER2*/CEP17 ratio in the HER2-positive cases compared to that in the equivocal-negative cases, except for one positive case which has significantly lower HER2/CK ratios and *HER2*/CEP17 ratio. This is a heterogeneous case that will be discussed in the following sections. A cell-by-cell representation of a HER2-negative tissue (assessed previously by a pathologist using a standard IHC and FISH technique) is shown in Figure 4.6c. For the HER2-negative tissue (Figure 4.6c), both the HER2/CK ratios are codified in yellow scale (contours, Figure 4.6d) and the *HER2*/CEP17 ratios are codified in red scale (inside of the dots, Figure 4.6d). These parameters were lower than these same parameters for a HER2-positive tissue (Figure 4.6e,f).

4.3.2. Accurate diagnostics based on quantitative IF/FISH

Our quantitative IF/FISH method was applied to a small clinical cohort of breast cancer cases. To verify its performance compared to the conventional diagnostic method, we studied the correlation between 3 scores obtained by our method (i.e. HER2/CK, *HER2*/cell number and *HER2*/CEP17 ratios) and the pathologist's scores (i.e. standard *HER2/*cell and *HER2*/CEP17 ratios). For HER2/CK and *HER2*/CEP17 ratios, we also propose new criteria for HER2 status assessment based on these variables and compared them with the ones currently used in the clinic.

HER2/cell and *HER2*/CEP17 ratios from a pathologist were based on a count of *HER2* and CEP17 signals in a cluster of 20-100 cells, followed by dividing the number of the total *HER2* loci to the total number of cell counted, and the number of *HER2* loci in all cells to the number of CEP17 in all cells. This overall *HER2*/CEP17 ratio is different from the cell HER2/CEP17 ratio in our method, which calculates the *HER2*/CEP17 ratio for each cell first, then averages them over the complete cell population. There is a nearly perfect-correlation between these two ratios (figure 4.7). The cell-based *HER2*/CEP17 ratio is required in our high content method because normalization of HER2 signals to CEP17 signals for each cell renders less variation of the HER2 signals in the cell level.

The results from tissue analysis was pooled with the results from the HER2- and HER2+ cell line study from section 4.3.1, in which the standard *HER2*/cell and *HER2*/CEP17 ratios were obtained in our laboratory using the same manual scoring method as done by pathologists.
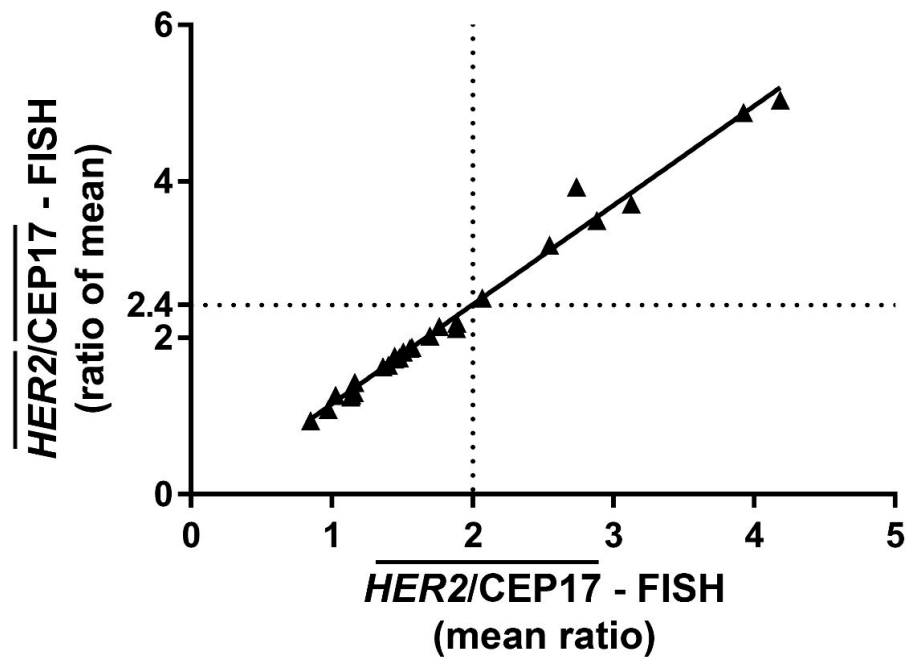
Figure 4.7 - The ratios of the mean HER2 and CEP17 signals versus the mean of *HER2*/CEP17 ratios for different tissue slides. Nearly perfect correlation is found (R^2=0.98).

We benchmarked our method with *HER2*/cell and *HER2*/CEP17 ratios instead of the IHC scores because FISH is more quantitative than IHC. In figure 4.8a, the HER2/CK ratio obtained by automatic IF analysis was compared to the standard *HER2*/CEP17 FISH scores obtained from manual counting. In figure 4.8a, the correlation between these two quantities has a sum-of-square R^2 equal of 0.64. The dotted lines are the thresholds, defined as the following. For IF, we obtained from cell line analysis a threshold of 0.273 for positivity determination. For the overall *HER2*/CEP17, we used the same threshold as in standard diagnostics routine, which is equal to 2. By using these thresholds, all but two cases are correctly classified. For the false-positive IF score, the tissue is a metastatic case of breast cancer in bones, for which the CK staining is weaker than usually, which increases the HER2/CK ratio. For the false-negative IF score, this case is a heterogeneous case, which is challenging for the decision-making. Therefore, we analyzed local indicators of spatial association (local Moran's I) for this heterogeneous case (see section 4.3.3.1). Without these two particular cases, R^2=0.80, suggesting an acceptable correlation between the two scores.
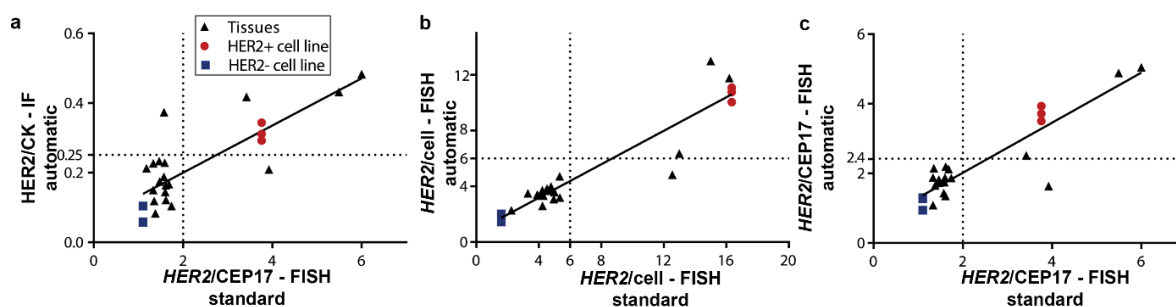
Figure 4.8 - Validation of our quantitative and automatic IF-FISH scoring method by comparison with the standard HER2 assessment for tissue and cell line samples. (a) Correlation between HER2 overexpression (HER2/CK ratio obtained from the microfluidic staining protocol and automated IF image-processing) and HER2 amplification (*HER2*/CEP17 ratio obtained from standard FISH scoring). The threshold for positivity of HER2/CK obtained by IF (horizontal dotted line) is defined as the lower bound of the 95% confidence interval obtained from a t-test on the mean HER2/CK scores of three HER2-positve cell line slides. The threshold for positivity of *HER2*/CEP17 obtained by FISH (vertical dotted line) is obtained from the ASCO 2013 guidelines. (b) Correlation between the *HER2* loci number per cell obtained from our automated counting algorithm and from the standard FISH technique. Thresholds for positivity for the variable *HER2*/cell is taken as 6 (dotted lines), obtained from the ASCO 2013 guidelines. (c) Correlation between the *HER2*/CEP17 ratio obtained from our automated counting algorithm and from the standard FISH technique. In our automatic method, the *HER2*/CEP17 ratio is calculated as the mean of the *HER2*/CEP17 ratios in all CK-positive cells of a tissue, while in the standard method it is calculated as the ratio of mean HER2 and CEP17 signals in a cluster of 20-100 cells chosen by the pathologist. The threshold for positivity for the automatic *HER2*/CEP17 ratio (horizontal dotted line) is 2.4 (see text). The threshold for positivity of *HER2*/CEP17 obtained by FISH (vertical dotted line) is obtained from the ASCO 2013 guidelines.

In figure 4.8b, the mean number of *HER2*/cell from an automatic FISH method is plotted against *HER2*/cell scores from a standard FISH scoring. For simplification, we presented only the threshold of 6 for separating positive and non-positive samples for *HER2*/cell (the equivocal class is considered as negative). A good correlation between the two scores is obtained ($R^2 = 0.88$). If the heterogeneous case is not included in the dataset $R^2 = 0.93$, which validate the use of the automatic scoring method for tissue analysis. In general, slightly smaller HER2 signals are obtained by the automatic scoring than a standard method. The difference between automatic scores and manual scores can be explained by the effect of scoring through a section of tissue that could make signals placed deep in the tissue less visible. Moreover, the automatic scoring method is based on an estimation of the number of HER2 dots, not the exact count, if two HER2 signals are closed and dim, they can be counted as one. Besides, if there are more than 2 signals per location, the obtained intensity might not be a linear function of the number of signals and often less signals are counted in this situation. However, according to ASCO 2013 guideline [59], no major misclassification (positive to negative and inversely) of HER2 status is found. Our automatic analysis gave similar scores compared to 63× z-stack scoring while having many more cells analyzed (at least two orders of magnitude). This statistical power is the basis of our high-content analysis.

Finally, in figure 4.8c, the cell *HER2*/CEP17 ratio by automatic FISH is plotted against the overall *HER2*/CEP17 ratio by the standard FISH method. This graph shows a good correlation between these two ratios R^2=0.81. If the heterogeneous case is not included, R^2=0.93. The threshold for the cell *HER2*/CEP17 ratio is obtained by adjusting the threshold of 2 in the case of overall *HER2*/CEP17 ratio, to 2.4. This adjustment is obtained from a correlation study, between the automatic cell *HER2*/CEP17 ratios of tissue samples in the cohort and their automatic overall *HER2*/CEP17 ratios (see figure 4.9). This nearly-perfect correlation (R^2=0.98) gives a regression equation linked the two ratios: cR=1.26×oR-0.105, with cR is the cell *HER2*/CEP17 ratios and oR is the overall *HER2*/CEP17 ratios. The latter has a threshold of 2 (ASCO 2013) [59]. Thus, the threshold of the cell *HER2*/CEP17 ratio is equal to 1.26×2-0.105=2.4. All three automatic scores correlate with the standard scores, thus underlining the clinical values of this method.
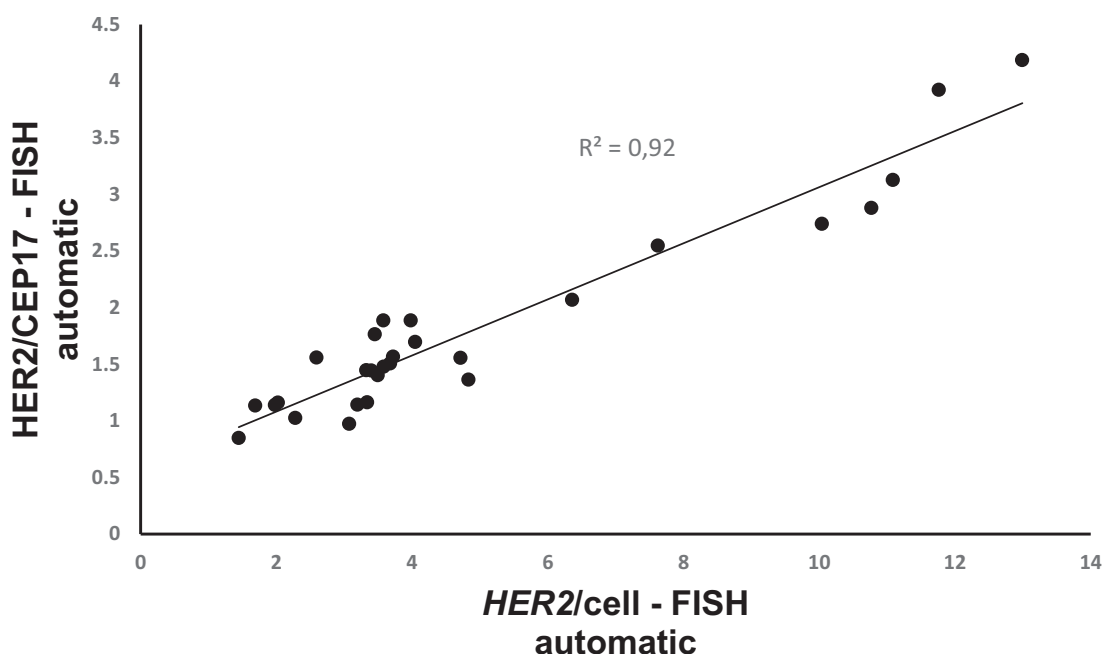
Figure 4.9 - Correlation between *HER2*/cell number and *HER2*/CEP17 ratio obtained in all tissue and cell line slides tested.

4.3.3. Spatial analysis and evaluation of ITH

4.3.3.1. Cluster heterogeneity

In this part, ITH detection and quantification using high-content analysis of IF-FISH are presented. Cluster ITH is characterized by the proportion of different tumor areas having different HER2 protein expression or gene amplification. We use the local Moran's I to characterize ITH, as this method can quantitatively discriminate cluster and mosaic ITH by comparing the variable of interest for each cell with that of its neighbors. A correlation between a cell and its neighbors reflects that they are clustered while an anti-correlation between a cell and its neighbors indicates that the cell is heterogeneous and has a different status

than its neighbors. For ITH characterization, the two parameters used are the HER2/CK ratio and *HER2*/cell number. *HER2*/CEP17 is not considered for this cell-level analysis because in addition of truncation errors from HER2 signals, it also contains the truncation errors from CEP17 signals, which requires a complicated deconvolution of the two effects. Nevertheless, *HER2*/cell number and *HER2*/CEP17 ratio are proportional (see figure 4.9); hence sole *HER2*/cell number can indicate the ITH.

As described in the section method, cells are classified into 5 groups: HH, HL, LH, LL, and NC based on the values of the considered parameter (HER2/CK and *HER2*/cell), calculated for each cell and its neighborhood, in comparison to a high and low threshold T_h and T_l. For the HER2/CK ratio, T_h is equal to T_l (single threshold) and defined as the lower boundary of the confidential interval of a t-test on SKBR3 cell lines' HER2/CK (see section 4.3.1.1). $T_h = T_l = 0.25$. Cells and neighbors having HER2/CK ≥ 0.25 are classified as H and <0.25 are L. For the parameter *HER2*/cell, as this is a standard variable, we used the current guideline for T_h and T_l, with $T_h=6$ and $T_l=4$ [66]. Cells having a *HER2* copy number>6 is unambiguously positive and if <4 is unambiguously negative. If the cell's *HER2* copy number is between 4 and 6 or equal to 4 or 6, we cannot conclude about its status (equivocal).
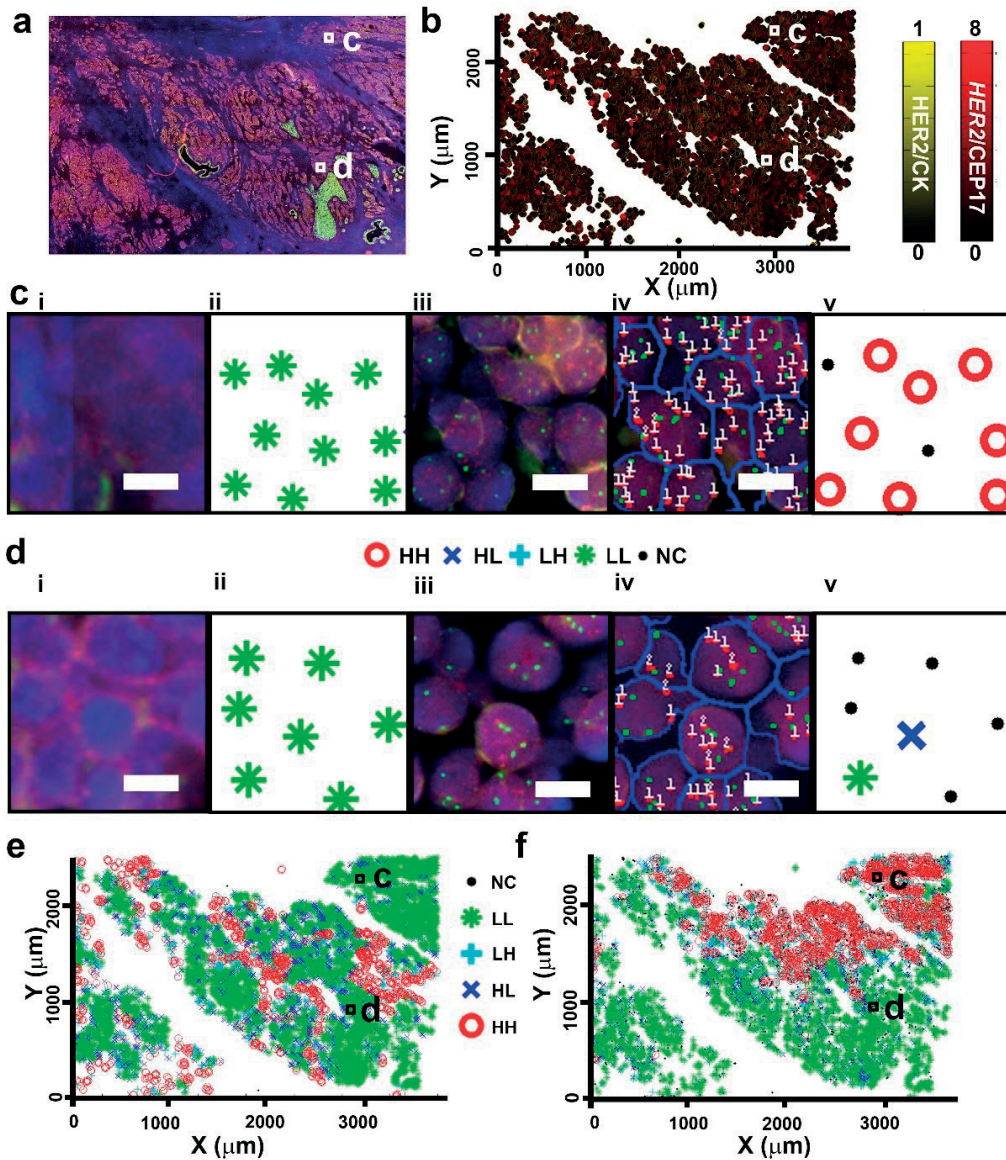
Figure 4.10 - Analysis of a heterogeneous tissue using correlation of HER2 signals of neighboring cells. (a) IF image of a tissue with definition of two regions of interest c and d, in which we will analyze the genetic heterogeneity. The red and green colors respectively representing the HER2 and Cytokeratin markers are almost colocolized, making orange in the area where tumor cells are located. Blue color represents the nuclei, equivalent to hematoxylin staining in a bright-field image. (b) Model of the tissue in a using the same cell-by-cell representation as in figure 4.6d,f. (c) Heterogeneity analysis of a HER2 FISH-positive region of the tissue in a. i) IF image: blue=nuclei, red=HER2, green=CK. ii) Correlation status of the cells in i. Cells are classified based on their own HER2 IF-status (High or Low) and on the IF-status of their neighbors (High or Low), resulting in: High-High (HH), High-Low (HL), Low-High (LH), Low-Low (LL)-type cells. Cells and their neighbors are classified as High (respectively Low) if their HER2/CK ratio is higher (respectively lower) than a threshold of 0.25. This threshold is the lower boundary of the 95% confidence interval of a t-

test on the HER2 FISH-positive cell lines' HER2/CK obtained from figure 4.6a. iii) FISH image of the region. Blue=nuclei, green=CEP17, red=HER2. iv) Automatic scoring of *HER2* loci and CEP17 of the region in iii. v) Spatial association status of the cells in iv. Cells are classified as High (respectively Low) if their *HER2* loci number is ≥6 (respectively <4).They are non-classified (NC) in the intermediate interval of *HER2* loci number from 4 to 6, where the FISH HER2 status is equivocal. (di-v) Heterogeneity analysis of a HER2 equivocal region of the region of interest d of the tissue in a, following the same procedure as in c. While the IF readout is similar, the FISH status is clearly distinct. (e) Spatial association analysis of the HER2 protein expression by IF for the whole tissue in a. (f) Spatial association analysis of HER2 amplification by FISH for the whole tissue in a, showing cluster heterogeneity, i.e. having clusters of HH cells that span in area more than 10% of the tissue. Scale bars: 10 μm.

In the following part, we demonstrate that the cluster ITH in the particular heterogeneous case mentioned in section 4.3.2 can be effectively identified and quantitatively characterized using the local Moran's I analysis. First, we observe that the IF image of the CK-positive cells in a large tissue area of the tissue displays a fairly homogeneous staining of HER2 in red and CK in green (see figure 4.10a). The co-presentation of IF overexpression by the HER2/CK ratio (contours in yellow scale) and FISH amplification by *HER2*/CEP17 ratio (inside of the dots in red scale) of CK-positive cells in the tissue do not display remarkable cluster ITH, as shown in figure 4.10b. However, this is a case having genetic heterogeneity, as proved by local Moran's I analysis (*vide infra*). In figure 4.10ci, IF image of a FISH-positive cluster of the tissue is displayed. local Moran's I analysis of the parameter HER2/CK from the IF image shows only LL cells are in this region, confirming that the HER2 expression is clustered and homogeneously negative in this area (figure 4.10cii). However, in the FISH image (figure 4.10ciii) this cluster is displayed with a majority of positive cells, as highlighted by the automatic analysis of FISH signal (figure 4.10civ). In figure 4.10cv, the local Moran's I map for FISH indicates that most cells are HH, meaning that they are amplified (*HER2*/cell number>6) and clustered, while two other cells are non-classified (4≤*HER2*/cell number≤6). In figure 4.10di, IF image of a FISH-equivocal cluster (*HER2*/cell in between 4 and 6) of the tissue is displayed. While the cell's IF signal is still classified as negative and clustered (figure 4.10di, ii), FISH image (figure 4diii) shows most are non-classified cells, except one cell that is highly amplified. The automatic scoring of FISH signal and local Moran's I analysis both confirm that this area has the majority of FISH-equivocal cells and one heterogeneous HL cell (figure 4.10div, v). In figure 4.10e, a local Moran's I map of the IF HER2/CK ratios of CK-positive cells in the tissue area is presented, indicating that the staining is fairly homogeneous, except in some areas where there is cluster ITH. In 4.10f, local Moran's I maps of the *HER2*/cell from the FISH image of the tissue area are plotted. We observe the presence of a FISH-positive area and a FISH-negative/equivocal area. Finally, the proportion of HH, HL, LH and LL cells among all CK-positive cells are obtained for heterogeneity quantification (*vide infra*).

4.3.3.2. Mosaic heterogeneity

The second objective of the study is quantitative assessment of mosaic ITH that is represented by the proportion of individual heterogeneous cell (positive/negative) in a cluster of cells having a different status (negative/positive). In our study, after the local Moran's I analysis, the mosaic ITH is the proportion of HL cells (for a HER2-negative patient) or LH cells (for a HER2-positive patient) in all CK-positive cells. However, this proportion can be biased by the truncation errors, because a positive cell can also display a small number of *HER2*/cell depending on the position of the cut and the probability that the HER2 signals are placed inside the cut. Therefore, we simulated the truncation errors from a homogeneous cell population in function of the number of *HER2*/cell to distinguish these errors to the real mosaic ITH. We assumed that

the cells were randomly scattered in the space. Therefore, the truncation errors that are presented by the number of cells having different status in the whole cell population are also considered as heterogeneous cell (HL cells in case of negative FISH HER2 and LH cells in case of positive FISH HER2). In figure 4.11a, we present both the truncation error model (dots) and the measured mosaic ITH in all tissues and cell lines (lines). The mosaic ITH of cell lines is certainly linked to the truncation error, hence used as a benchmark for the tissue analysis. The theoretical curve representing the truncation error is explained as follows. First, there is no highly amplified cell for the low HER2/cell value. When the number of HER2/cell increases, the HER2 loci population shifts to a higher value, thus more cells are recognized as positive. Using a fitting function, we found that the truncation errors increases following a polynomial function if the mean HER2/cell still inferior 6. The population passes at peak at around 6 when a large amount of cells are positive but the mean value is still less than 6. After the mean passes 6, the criterion for selecting heterogeneous cells changes to LH cells, resulting on a sharp reduction of the proportion of heterogeneous cells. When the mean increases further, the truncation errors decreases drastically following an exponential function. We compare now our truncation model with the mosaic ITH obtained after local Moran's I analysis in all tissue slides. The mosaic ITH fits well to the truncation error model for most cases. Moreover, when the cell line's homogeneous population was analyzed by local Moran's I analysis, we found that positive cell lines also have a strong mosaic ITH (6.2-10.8%), which can also be explained by the truncation error model for cell lines. Therefore, if the apparent mosaic ITH is lower or similar than the model, we can thus associate the measured mosaic ITH to the truncation errors. Lower mosaic ITH compared to the model are observed in two tissues and 2 HER2-positive cell slides. For the tissues, we obtained a lower mosaic ITH because these two tissue display highest percentage of the clustered heterogeneous cells (7.7 and 11.7%) among all tissues analyzed (all are other are less than 4%), see table 4.1. In these two tissues, the mosaic heterogeneity cells were only considered in the dominant parts of the tissues, hence decreasing the overall percentage of the mosaic heterogeneous cells in the whole cell population. For positive cell lines, the difference between the mosaic ITH and the model is larger than that of most tissues. We could explain that by the smaller number of cells considered in cell line slides (usually 2-5 times less). Furthermore, the mean HER2/cell of positive cell lines measured by the automatic scoring is slightly smaller than that of the manual counting technique. The measured mosaic ITH of the HER2-positive cell line having a high value of mean HER2/cell, corresponds now with a smaller value of mean HER2/cell that is affiliated with higher theoretical truncation errors. Finally, one tissue sample with much higher mosaic ITH than the model is suspected having a real mosaic ITH (figure 4.11a, the triangle marked with b). Indeed, we can observe in the automatic scoring FISH image in one tissue position that the presence of heterogeneous cells of the true mosaic ITH tissue (figure 4.11b) is more important than that of a homogeneous tissue (figure 4.11c). Therefore, we can conclude that our method has successfully confirmed the presence of cluster and mosaic ITH in all cases. Finally, a simple graph recapitulating the HER2 phenotypic and genotypic characteristics of each tissue as well as their cluster and mosaic heterogeneity can be plotted (figure 4.11d). We can distinguish one case with mosaic heterogeneity and one case with cluster heterogeneity among all tissues tested. In the future, this graph can be later used to assist the clinical decision.
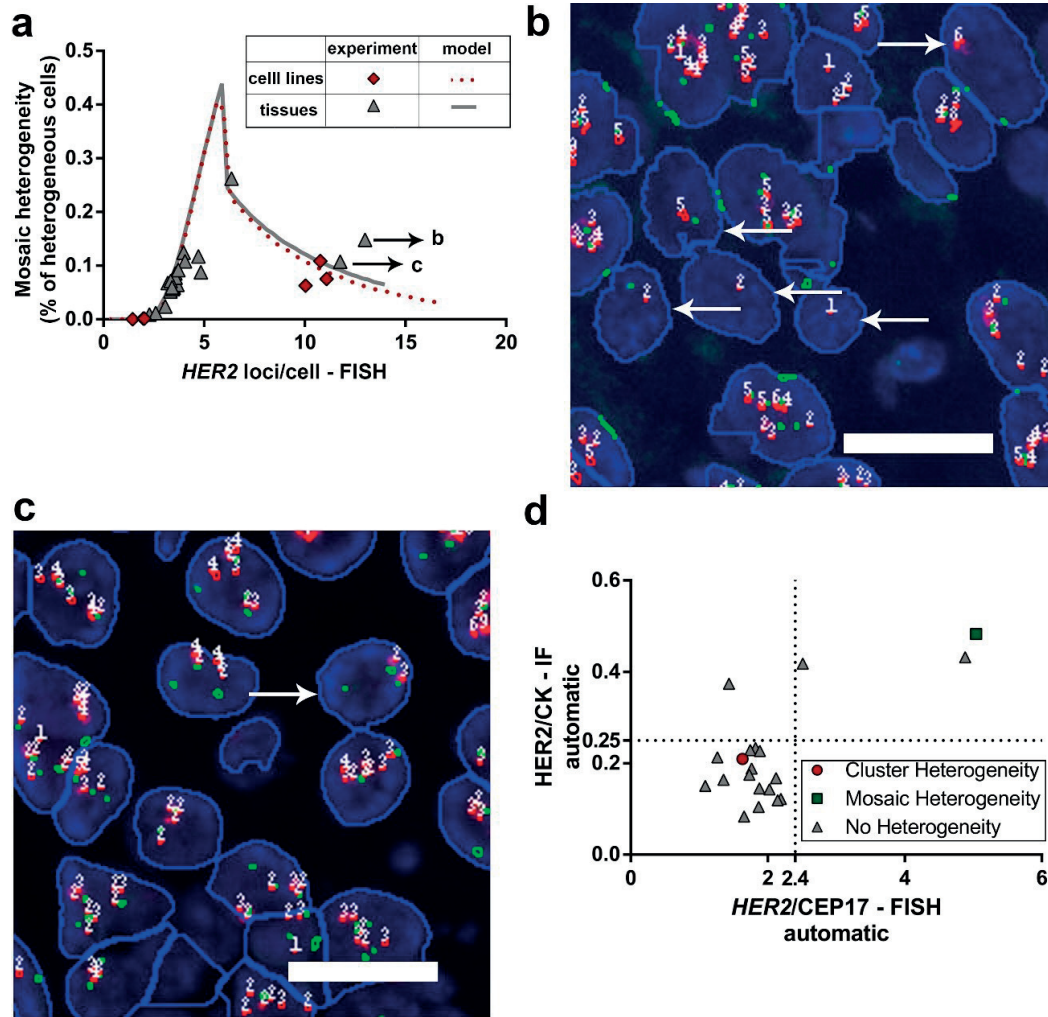
Figure 4.11 - Interpretation of mosaic intratumoral heterogeneity (ITH) by comparison to a statistical truncation model. (a) The mosaic ITH is measured in all tissue samples and benchmarked with the readout of the two cell lines: it is defined as the ratio of the number of individual heterogeneous cells (i.e. cells with positive/negative FISH status in a cluster of cells of negative/positive FISH status), divided by the total number of cancer cells in a tissue. For a HER2 positive sample (mean $HER2$/cell≥6 or $HER2$/CEP17≥2), mosaic ITH cells correspond specifically to LH cells of a spatial association analysis, like the ones marked by the + symbol in figure 4.10f. For a HER2- negative and equivocal sample (mean $HER2$/cell<6 and $HER2$/CEP17<2), mosaic ITH cells correspond to HL cells of a spatial association analysis, like the ones marked by the × symbol in figure 4.10f. For each cell line and tissue, the apparent mosaic ITH of a homogeneous population can be artificial when it is due to truncation errors. Indeed, truncated cells having random position of the nucleus with respect to the cut contain a number of HER2 dots that follows a binomial law of probability. The full line represents a model simulation that describes such truncation errors in a homogeneous population of cells as a function of varying $HER2$ loci number. Data points lying above the model curve can be considered as exhibiting true mosaic ITH (figure 4.10b), while points on the curve

represent a false apparent mosaic ITH, as due to truncation errors (figure 4.10c). (b) The automatic scoring FISH image of a true mosaic ITH. Heterogeneous cells are indicated by white arrows (c) The automatic scoring FISH image of a false mosaic ITH case. Less heterogeneous cells are observed. Scale bars: 20 μm. (d) HER2 overexpression versus HER2 amplification for all tissues with additional heterogeneity information. It shows one patient with true mosaic ITH (the same than in figure 4. 11b) and one patient with cluster heterogeneity (data of figure 4.10f) among the 20 patients tested. Thresholds for positivity are defined as before and indicated by the dotted lines.

Table 4.1 - High-content, automatic analysis IF/FISH results for all tissues, positive and negative cell lines. In columns (left to right): identification number (ID) of the samples; mean of the scores HER2/CK ratio, *HER2*/CEP17 ratio, *HER2*/cell; proportion of cluster and mosaic heterogeneous cells.

	ID	HER2/CK-IF	Cell *HER2*/CEP17-FISH	*HER2*/cell-FISH	Cluster heterogeneity (%)	Mosaic heterogeneity (%)
Tissue	1	0.21	1.63	4.83	0.17	0.09
	2	0.19	1.77	3.33	0.00	0.05
	3	0.15	1.09	3.08	0.00	0.02
	4	0.43	4.88	11.76	0.00	0.11
	5	0.21	1.27	2.28	0.00	0.01
	6	0.08	1.65	3.50	0.00	0.06
	7	0.16	1.35	3.20	0.01	0.07
	8	0.23	1.82	3.68	0.00	0.06
	9	0.12	2.19	3.58	0.00	0.09
	10	0.42	2.51	6.36	0.04	0.26
	11	0.23	1.75	3.58	0.00	0.08
	12	0.17	2.12	3.98	0.03	0.12
	13	0.10	1.87	4.72	0.08	0.12
	14	0.12	2.15	3.45	0.00	0.06
	15	0.14	2.03	4.05	0.01	0.11
	16	0.23	1.88	3.72	0.00	0.09
	17	0.37	1.43	3.34	0.00	0.07
	18	0.14	1.88	2.59	0.00	0.01
	19	0.48	5.04	12.99	0.00	0.15
	20	0.17	1.73	3.40	0.01	0.06
HER2-positive cell line	1	0.29	3.71	11.09	0.00	0.08
	2	0.34	3.93	3.93	0.00	0.06
	3	0.31	3.50	10.77	0.00	0.11
HER2-negative cell line	1	0.10	1.30	1.30	0.00	0.00
	2	0.06	0.94	1.45	0.00	0.00
	3	0.06	1.27	1.98	0.00	0.00

4.4. Discussion

In this work, we proposed an experimental and analytical method for quantitative assessment of both HER2 amplification and overexpression of the same breast cancer tissue slide. This technique can overcome inherent drawbacks of classical IF and FISH techniques by performing a controlled staining using the MTP and cell-by-cell computation of IF signals. Indeed, by using a short flushing of Abs, the microfluidic system keeps the IF signal in a non-saturated mode, favoring the discrimination of HER2-positive and negative cases. This advantage of microfluidic IF staining was already reported. The novelty of this method is in the unique queuing of (bio-chemical/computational) steps used for protein and gene biomarker quantification, with application to diagnostics and heterogeneity assessment. First, this research shows an improvement of quantification of the IF signals. Indeed, in previous reports on microfluidic IF for HER2 quantification, IF scoring was based on the histogram of HER2 signals [62]. Thus, the relation between the IF scores and the ISH scores was not a directly a linear relation. Moreover, the scores proposed there were not standardized because the obtained scores were not stand-alone as a variable but needed to be normalized to a reference signal, for example, a known positive tissue slide. We show here that the adjusted HER2/CK ratio averaged in segmented cells is a quantitative indication of HER2 overexpression, demonstrated by its linear correlation with the standard *HER2*/CEP17 ratio. Besides, this new IF quantification method does not require the use of benchmark tissues with a known status for staining comparison.

On the side of FISH quantification, our imaging technique uses a 20× objective with a ~5µm depth-of-focus, which is larger than the thickness of a tissue slide. This avoids extensive high-resolution z-stack imaging by a 63× objective, which allows acquiring a large region of interest of a tissue or cell sample of 4mm × 4mm. We can also perform analysis in a large area of 16 mm × 16 mm, defined by the microfluidic chamber of the MTP, but the excess number of cells usually does not change the clinical conclusion. If heterogeneity is detected, more areas can be analyzed to confirm the state of the disease. By using both quantitative IF and automatic FISH scoring at a cell level, accurate HER2 clinical assessments can be obtained based on the high number of analyzed cells.

More importantly, this research paves the way to study ITH quantitatively. We highlight that the mechanism responsible for the presence of ITH and its biological consequences are not well understood [10]. The main challenge is the lack of a suitable analysis tool that can record and analyze a large number of cells. To address this need, quantitative assessment of ITH has been recently developed, principally based on imaging of IHC and bright-field ISH staining [108-110]. However, limitations of the number of markers used, difficulty of cell segmentation, non-linearity of IHC signal impede cell-by-cell analysis of both protein expression and gene amplification. In this study, by using local Moran's I analysis of IF/FISH images, the occurrence of cluster and mosaic ITH can be quantitatively assessed. One cluster ITH was successfully identified using the local Moran's I analysis. In general, IF and FISH status in cluster heterogeneous cases are usually concordant [111], but in this case the IF staining is fairly homogeneous, only the gene amplification can reveal heterogeneity. Thus, both overexpression and amplification analyses are needed to fully assess the two types of heterogeneity (cluster and mosaic). Without a high-content analysis of the FISH image, it is very challenging to conclude about the cluster heterogeneity in this case. Heterogeneity assessments using both IF and FISH give thus a reliable and robust conclusion about heterogeneity which can be considered during a clinical decision. For mosaic heterogeneity, we demonstrated that in most cases, truncation errors caused coexistence of cells with different status. However, one real mosaic heterogeneous case was successfully identified, as it had an unambiguously higher heterogeneous cell proportion than the one corresponding to truncation error. In the future, based on the results of this heterogeneity analysis, more

retrospective studies for ITH analysis can be done to establish better the link between ITH and cancer prognostics. Therefore, cases currently identified with ITH (estimated to be one fourth of all breast cancer cases [111]) could be reassessed to determine their true heterogeneity nature.

Nevertheless, the number of *HER2*/cell scored are different than that of a standard technique depending on computational estimation of the number of signals (figure 4.8b). Moreover, the standard method is biased by under-sampling. For borderline cases (*HER2*/cell in between 4 and 6), this can change the assessment, for example from equivocal to negative (*HER2*/cell less than 4). In the whole tissue, the proportion of cells' HER2 classification errors due to the small changes in the *HER2*/cell scored is small. Therefore, for all non-cluster-heterogeneous cases, no major change from positive to negative status or vice versa is recorded. We also expect that the local Moran's I analysis give a very high accuracy of ITH status. Finally, we highlight that the aim of this study is not to replace the standard scoring technique, but to (1) provide a quantitative method for IF scoring, (2) verify the quantitative assessment in a large number of cells (3) detect ITH with local Moran's I analysis. In the future, larger clinical cohort may be studied to further explore the power of this technique to identify ITH.

4.5. Conclusion of chapter 4

In conclusion, we successfully established a new method for accurate HER2 assessment in breast cancer tissue using high-content analysis of microfluidic IF and automatic FISH scoring. The study has shown that quantitative evaluation of HER2 IF signal can be obtained by calculating the HER2/CK in all cells on the tissue slide. By combining quantitative IF and automatic scoring FISH, this powerful method characterizes the whole tissue by its cell-by-cell HER2 overexpression and amplification. Indeed, the mean HER2/CK and *HER2*/CEP17 ratio of all cancer cells correlate with the *HER2*/CEP17 ratio obtained from a standard FISH technique, underlining the capability of taking into account a large number of cells to obtain an adequate sampling statistics. Finally, using local Moran's I analysis, ITH was detected in both cluster and mosaic form, by excluding truncation errors with numerical simulations. Cases currently identified with mosaic heterogeneity (~1/4 of all cases) can be reviewed using our method for determining those having true mosaic heterogeneity. It is our perspective that cancer treatment in the future can be more personalized, as we can analyze tumors at an individual cancer cell level using automatic, high-content methods.

5. CONCLUSION AND PERSPECTIVE

5.1. Conclusion

In this dissertation, several new methods related to microfluidic technology for improving cancer diagnosis were presented. In chapter 1, an overview of breast cancer and some diagnostic tests was introduced. We knew that fast, inexpensive and accurate assessment of onco-genes or proteins is of utmost important in modern cancer treatment. We also understand the theoretical background of convection-diffusion-reaction mechanism in a microfluidic system, which explains the role of flows in a reaction-limited system. Moreover, literature reviews related to general microfluidic technologies as well as the particular chip used were presented. Finally, the reliability of the microfluidic chip was carefully studied to ensure that it can resist to high-temperature and solvents.

Chapter 2 described three methods: MA-FISH, ESIMA-FISH and MA-CISH that uses the microfluidic-assistance principle for *HER2* gene assessment. These methods are the first microfluidic FISH tests for tissue analysis that offer an improvement of both processing time and cost. These methods are based on probe recirculation and reaction acceleration using back-and-forth flows, which are technically innovative. We performed protocol optimization for each FISH or CISH probes and applied the parameter sets obtained on several clinical samples for validation. We concluded that microfluidic flows help decreasing the time and reagent needed for FISH or CISH tests. In addition, we proved that discontinuous flows were more efficient for hybridization acceleration for a formamide-based probe. Briefly, we achieved faster and cheaper in-situ hybridization tests while keeping the same diagnostic accuracy than the standard techniques. An additional cost due to the microfluidic setup (the microfluidic chip and the syringe pumps) is estimated to be around 10000$). Nevertheless, this cost can be recompensed in a long term. Another solution to decrease the hardware cost is to replace the micro-fabricated silicon chip by a plastic–based chip, in the condition that the melting temperature of the plastic chip is higher than the denaturation temperature of a FISH protocol (~ 73-75°C).

In chapter 3, we described a new HER2 protein quantification method, using protein a microfluidic-microarray setup combined with IF staining. The particularity of this method compared to the literature is that proteins in a tissue slide are partly extracted and routed into a microfluidic chip containing Ab-microarrays for detection of HER2 proteins. A study on a small tissue cohort shows that HER2 protein mass quantified by this technique correlates with the LC/MS-MS spectral counts reflecting the number of HER2 protein present in the extraction solution. We also demonstrated that HER2 protein overexpression estimated by the microfluidic-microarray method agrees with the FISH scores that is an indication of HER2 amplification. This proof-of-concept study paves the way for high-throughput tissue biomarker quantification that can be used in the clinics.

The chapter 4 showed a new approach for HER2 assessment using quantitative IF combined with high-content, automatic FISH analysis for evaluating cancer heterogeneity. This is the first method using image processing to analyze both IF and FISH signals cell by cell. This method successfully identified cases with cluster and mosaic heterogeneity in a batch of 20 tissue samples with unprecedented accuracy. In particular, true mosaic heterogeneity is distinguished to that due to truncation errors originating from the sample preparations. These achievements could pave the way to further retrospective study of heterogeneity and its link to clinical outcomes, guiding pathologist to identify cases having true heterogeneity.

Brief, through diverse microfluidic techniques, our research provided a framework for the applications of microfluidics in cancer diagnosis. Faster, cheaper, simpler, and more-accurate HER2 assessment can be performed using a microfluidics device. In my opinion, microfluidics can become a part of clinical routine, if this technology gets enough support from pharmaceutical companies and governments. To realize this perspective, we need collaborations between research laboratories and industries to promote and commercialize this technology.

5.2. Future research directions

At the moment, MA-FISH is performed by a simple setup that requires several manual assembling-disassembling steps. To improve the test's user-friendliness, automatic MA-FISH can be envisaged. To achieve that aim, more inlets and outlets and junctions can be added in the setup holder to separate the probe and flanking oil solution. Moreover, sophisticate pumping system that can deliver multiple reagents can be integrated. Automatization of the MA-FISH protocol will be the next step to apply this technique to clinical diagnostics.

The microfluidic-microarray technique is very advantageous to achieve a fast and complete tissue diagnostics using standard slides. Indeed, as we demonstrated the feasibility of HER2 assessment, other tissue biomarkers such as ER and PR can also be quantified using the same principle. The only requirement is that these proteins are presented and not denatured in the chosen extraction solution. We anticipate that this simple, quantitative cancer screening method can accurately classify tissue samples into their molecular subgroups.

As our high-content analysis method is principally based on an image processing program allowing fluorescence scoring and signal quantification, this technique can be applied in all other fields, such as quantification of RNA FISH or live-imaging IF image. We can also apply the IF heterogeneity analysis to evaluate ITH of ER or PR biomarkers.

APPENDIX

Appendix A

Here is an example of Local's Moran I computation. Given 5 points x_1, x_2, x_3, x_4, x_5 with x_1 is in the center of figure A.1. The point with the value x_1 is placed at the center of the figure (marked in red dot), where we calculate the Local's Moran I. The threshold distance marked by the large red circle. There are two point x_3 and x_4 that are inside the circle and x_2 and x_5 are outside.
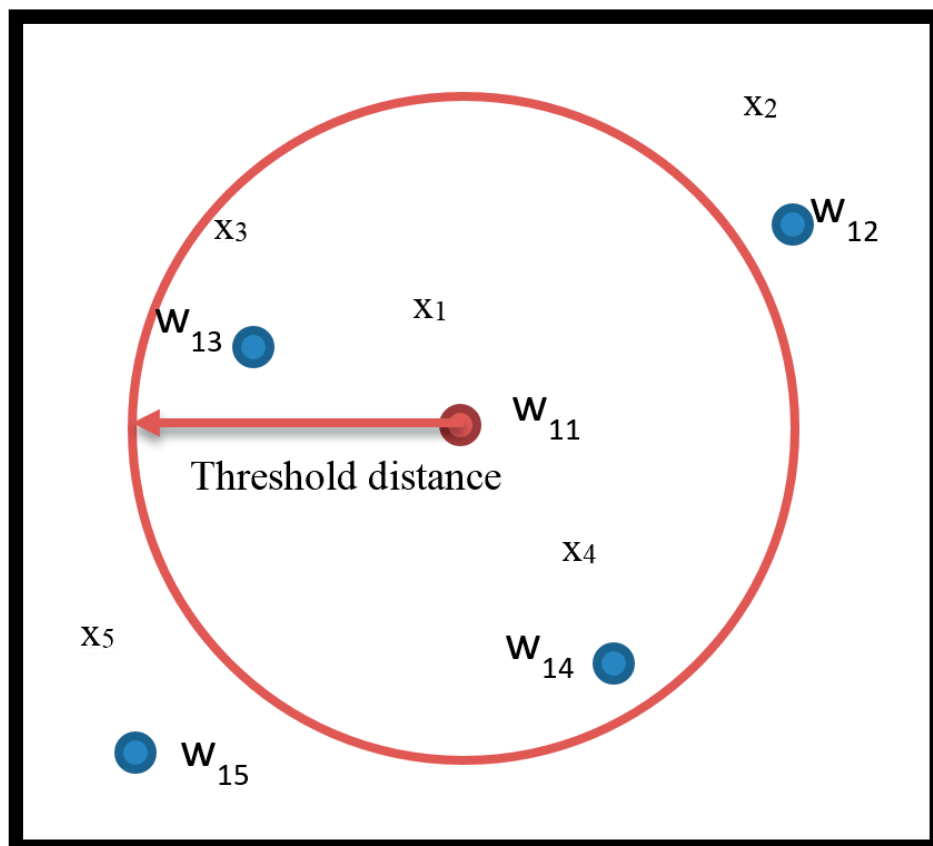
Figure A.1 - Example of weight matrix calculation

Thus, Local's Moran I at unit 1 is calculated as follows

$$I_1 = z_1 \times [(w_{12} \times z_2) + (w_{13} \times z_3) + (w_{14} \times z_4) + (w_{15} \times z_5)] \tag{A.1}$$

where

$$N = 5$$

$$\bar{x} = \frac{x_1 + x_2 + x_3 + x_4 + x_5}{5}$$

$$\sigma = \sqrt{\frac{(x_1 - \bar{x})^2 + (x_2 - \bar{x})^2 + (x_3 - \bar{x})^2 + (x_4 - \bar{x})^2 + (x_5 - \bar{x})^2}{5}}$$

$$z_1 = \frac{x_1 - \bar{x}}{\sigma}$$

$$z_2 = \frac{x_2 - \bar{x}}{\sigma}$$

$$z_3 = \frac{x_3 - \bar{x}}{\sigma}$$

$$z_4 = \frac{x_4 - \bar{x}}{\sigma}$$

$$z_5 = \frac{x_5 - \bar{x}}{\sigma}$$

According to the threshold distance, the points with j = 3,4 are neighbors of i = 1

$$w_{12} = 0; \; w_{13} = 1; \; w_{14} = 1; \; w_{15} = 0$$

Thus, Local's Moran I at unit 1 becomes

$$I_1 = z_1 \times (z_1 + z_4)$$

The classification of the point i=1 depends on the sign of z_1 and $z_1 + z_4$. The latter is the sum of all normalized value of all neighboring elements within a given distance.

However, the local Moran's I value would be a result of randomness. To test whether spatial association comes from random distribution or actual spatial autocorrelation, the significance of local Moran's I at each I is computed as follow.

$$p \; value = \; Probability \; [I_i > \delta_i] < \alpha_i$$

One generates n permutations where values of neighbors j of the unit I are assigned randomly. Then, one calculates I_i at each permutation. After that, the percentage of I_i over δ_i (original local Moran's I value at unit i) is the probability of random spatial association. This probability should be less than α_i which is the chosen significance or pseudo significance level. In the tumor heterogeneity analysis performed in chapter 4, we will not run permutations to verify local Moran's I significance because we define high/low values using fixed threshold values.

In fact, Moran's I is a summation of individual local Moran's I at each unit i. Thus, the relationship between Moran's I and local Moran's I are as follows.

$$I = \sum_i \frac{I_i}{N} \tag{A.2}$$

where

I= Moran's I measure of global autocorrelation

I_i= Local Moran's I measure of local autocorrelation

N= number of analysis units in the map

Appendix B

Pearson coefficient represents the linear correlation between two variables. Given two variables X_1, X_2, the Pearson correlation is defined as

$$r = \frac{cov(X_1, X_2)}{\sigma_1 \sigma_2}$$

Where $cov(X_1, X_2)$ is the covariance of X_1 and X_2, σ_1 and σ_2 are respectively the standard deviation of X_1 and X_2.

If the Pearson coefficient is positive, the two variables are positively correlated. If the Pearson coefficient is negative, negative correlation is expected. A Pearson coefficient close having an absolute value close to 1 means the correlation is strong and close to 0 means that there is no linear correlation between the two variables.

Appendix C

In this section, we calculate the volume of a truncated cell section, depending on the position x of the center of the cut. From the equation (4.2) in chapter 4, we have:

$$V_\tau(x) = \pi \int_{x_1}^{x_2} (R^2 - x^2) dx = \pi (R^2 x|_{x_1}^{x_2} - \frac{x^3}{3}|_{x_1}^{x_2}) = \pi[R^2(x_2 - x_1) - \frac{x_2^3 - x_1^3}{3}] \qquad (A.3)$$

If $x_2 > R$, we have $x_2 = R, x_1 = x - \tau/2$, we obtain:

$$V_\tau(x) = \frac{\pi \left[2R^3 - 3R^2\left(x - \frac{\tau}{2}\right) + \left(x - \frac{\tau}{2}\right)^3\right]}{3} if\ x \epsilon \left[R - \frac{\tau}{2}, R\right] \qquad (A.4)$$

If $x_1 < -R$, we have $x_1 = -R, x_2 = x + \tau/2$, we obtain:

$$V_\tau(x) = \frac{\pi[-2R^3 + 3R^2\left(x + \frac{\tau}{2}\right) - \left(x + \frac{\tau}{2}\right)^3]}{3}, if\ x \epsilon \left[-R, -R + \frac{\tau}{2}\right] \qquad (A.5)$$

If $x_1 > -R$ and $x_2 < R$, we have $x_1 = x - \tau/2$ and $x_1 = x + \tau/2$, we have:

$$V_\tau(x) = \frac{\pi\tau(3R^2 - \frac{\tau^2}{4} - 3x^2)}{3}, if\ x \epsilon \left[-R + \frac{\tau}{2}, R - \frac{\tau}{2}\right] \qquad (A.6)$$

$p(x)$ is the probability for one *HER2* locus to be placed inside the cut and it-self a random variable. $p(x)$ can be computed from the volume of cut $V_\tau(x)$:

$$p(x) = \frac{V_\tau(x)}{V_{cell}} = \frac{2R^3 - 3R^2\left(x - \frac{\tau}{2}\right) + \left(x - \frac{\tau}{2}\right)^3}{4R^3}, if\ x \in \left[R - \frac{\tau}{2}, R\right] \tag{A.7}$$

$$p(x) = \frac{-2R^3 + 3R^2\left(x + \frac{\tau}{2}\right) - \left(x + \frac{\tau}{2}\right)^3}{4R^3}, if\ x \in \left[-R, -R + \frac{\tau}{2}\right] \tag{A.8}$$

$$p(x) = \frac{\tau\left(3R^2 - \frac{\tau^2}{4} - 3x^2\right)}{4R^3}, if\ x \in \left[-R + \frac{\tau}{2}, R - \frac{\tau}{2}\right] \tag{A.9}$$

$$p(x) = 0, if\ x < -R\ or\ x > R \tag{A.10}$$

Therefore, the locus has a probability of $p(x)$ to be placed in the domain of the cut and a probability of $q(x) = 1 - p(x)$ to be placed outside the domain. Therefore, the random variable "the locus belongs to the cut" follows a Bernoulli distribution. The sum of all loci in a cut follows thus a binomial distribution, i.e. a sum of variables following a Bernoulli distribution. The probability of a cell section having a number of dots n is written as

$$P[n, N, p(x)] = \frac{N!}{n!\,(N-n)!} p(x)^n (1 - p(x))^{N-n} \tag{A.11}$$

This is also the probability mass function of the *HER2*/cell number used for generating a population of cell section to build truncation error model.

References

[1]   L.A. Torre, F. Bray, R.L. Siegel, J. Ferlay, J. Lortet-Tieulent, A. Jemal, Global cancer statistics, 2012, CA Cancer J. Clin. 65 (2015) 87-108

[2]   F.A. Tavassoli, P. Devilee, I.A.f.R.o. Cancer, W.H. Organization, Pathology and Genetics of Tumours of the Breast and Female Genital Organs, IARC Press, 2003.

[3]   G.N. Sharma, R. Dave, J. Sanadya, P. Sharma, K.K. Sharma, Various types and management of breast cancer: An overview, J. Adv. Pharm. Technol. Res. 1 (2010) 109-126

[4]   A.G. Rivenbark, S.M. O'Connor, W.B. Coleman, Molecular and cellular heterogeneity in breast cancer: challenges for personalized medicine, Am J Pathol 183 (2013) 1113-1124

[5]   H.-P. Sinn, H. Kreipe, A Brief Overview of the WHO Classification of Breast Tumors, 4th Edition, Focusing on Issues and Updates from the 3rd Edition, Breast Care 8 (2013) 149-154

[6]   J. Albanell, J. Codony, A. Rovira, B. Mellado, P. Gascón, Mechanism of Action of Anti-HER2 Monoclonal Antibodies: Scientific Update on Trastuzumab and 2C4, New Trends in Cancer for the 21st Century, Springer, Boston, MA, 2003, pp. 253-268

[7]   S. Farkona, E.P. Diamandis, I.M. Blasutig, Cancer immunotherapy: the beginning of the end of cancer?, BMC Med. 14 (2016)

[8]   R. Nanda, L.Q.M. Chow, E.C. Dees, R. Berger, S. Gupta, R. Geva, L. Pusztai, K. Pathiraja, G. Aktan, J.D. Cheng, V. Karantza, L. Buisseret, Pembrolizumab in Patients With Advanced Triple-Negative Breast Cancer: Phase Ib KEYNOTE-012 Study, J. Clin. Oncol. 34 (2016) 2460-2467

[9]   N. McGranahan, C. Swanton, Clonal Heterogeneity and Tumor Evolution: Past, Present, and the Future, Cell 168 (2017) 613-628

[10]   A. Marusyk, K. Polyak, Tumor heterogeneity: causes and consequences, Biochim. Biophys. Acta 1805 (2010) 105-117

[11]   A. Marusyk, D.P. Tabassum, P.M. Altrock, V. Almendro, F. Michor, K. Polyak, Non-cell-autonomous driving of tumour growth supports sub-clonal heterogeneity, Nature 514 (2014) 54-58

[12]   N.A. Saunders, F. Simpson, E.W. Thompson, M.M. Hill, L. Endo-Munoz, G. Leggatt, R.F. Minchin, A. Guminski, Role of intratumoural heterogeneity in cancer drug resistance: molecular and clinical perspectives, EMBO Mol. Med. 4 (2012) 675-684

[13]   P. Ramos, M. Bentires-Alj, Mechanism-based cancer therapy: resistance to therapy, therapy for resistance, Oncogene 34 (2015) 3617-3626

[14]   N. McGranahan, A.J.S. Furness, R. Rosenthal, S. Ramskov, R. Lyngaa, S.K. Saini, M. Jamal-Hanjani, G.A. Wilson, N.J. Birkbak, C.T. Hiley, T.B.K. Watkins, S. Shafi, N. Murugaesu, R. Mitter, A.U. Akarca, J. Linares, T. Marafioti, J.Y. Henry, E.M.V. Allen, D. Miao, B. Schilling, D. Schadendorf, L.A. Garraway, V. Makarov, N.A. Rizvi, A. Snyder, M.D. Hellmann, T. Merghoub, J.D. Wolchok, S.A. Shukla, C.J. Wu, K.S. Peggs, T.A. Chan, S.R. Hadrup, S.A. Quezada, C. Swanton, Clonal neoantigens elicit T cell immunoreactivity and sensitivity to immune checkpoint blockade, Science 351 (2016) 1463-1469

[15]   M.J. Duffy, P.M. McGowan, N. Harbeck, C. Thomssen, M. Schmitt, uPA and PAI-1 as biomarkers in breast cancer: validated for clinical use in level-of-evidence-1 studies, Breast Cancer Res 16 (2014)

[16]   N. Patani, L.-A. Martin, M. Dowsett, Biomarkers for the clinical management of breast cancer: International perspective, Int. J. Cancer 133 (2013) 1-13

[17]   J. Zhou, L. Belov, N. Armstrong, R. Christopherson, Antibody Microarrays and Multiplexing, Bioinform Hum Proteomics, 2013, pp. 331-359

[18]   R. Bumgarner, DNA microarrays: Types, Applications and their future, Curr. Protoc. Mol. Biol. 0 22 (2013) Unit-22.1.

[19]   B.S. Wittner, D.C. Sgroi, P.D. Ryan, T.J. Bruinsma, A.M. Glas, A. Male, S. Dahiya, K. Habin, R. Bernards, D.A. Haber, L.J. Van't Veer, S. Ramaswamy, Analysis of the MammaPrint Breast Cancer Assay in a Predominantly Postmenopausal Cohort, Clinical cancer research : an official journal of the American Association for Cancer Research 14 (2008) 2988-2993

[20]   E. Ayad, M. Mansy, D. Elwi, M. Salem, M. Salama, K. Kayser, Comparative study between quantitative digital image analysis and fluorescence in situ hybridization of breast cancer equivocal human epidermal growth factor receptors 2 score 2+ cases, J. Pathol. Inform. 6 (2015)

[21]   D.C. Zaha, Significance of immunohistochemistry in breast cancer, World J. Clin. Oncol. 5 (2014) 382-392

[22]   S.-W. Kim, J. Roh, C.-S. Park, Immunohistochemistry for Pathologists: Protocols, Pitfalls, and Tips, Journal of Pathology and Translational Medicine 50 (2016) 411-418

[23]   H. Nitta, B. Kelly, M. Padilla, N. Wick, P. Brunhoeber, I. Bai, S. Singh, J. Ranger-Moore, C. Bieniarz, H. Tsuda, T. M Grogan, A gene-protein assay for human epidermal growth factor receptor 2 (HER2): brightfield tricolor visualization of HER2 protein, the HER2 gene, and chromosome 17 centromere (CEN17) in formalin-fixed, paraffin-embedded breast cancer tissue sections, Diagn. Pathol. 7 (2012) 60

[24]   M.I. Toki, F. Cecchi, T. Hembrough, K.N. Syrigos, D.L. Rimm, Proof of the quantitative potential of immunofluorescence by mass spectrometry, Lab. Invest. 97 (2017) 329-334

[25]   H. Nitta, B. Hauss-Wegrzyniak, M. Lehrkamp, A.E. Murillo, F. Gaire, M. Farrell, E. Walk, F. Penault-Llorca, M. Kurosumi, M. Dietel, L. Wang, M. Loftus, J. Pettay, R.R. Tubbs, T.M. Grogan, Development of automated brightfield double In Situ hybridization (BDISH) application for HER2 g ene and chromosome 17 centromere (CEN 17) for breast carcinomas and an assay performance comparison to manual dual color HER2 fluorescence In Situ hybridization (FISH), Diagn. Pathol. 3 (2008) 41

[26]   I.V. Jani, T.F. Peter, How point-of-care testing could drive innovation in global health, The New England Journal of Medicine 368 (2013) 2319-2324

[27]   S. Prakash, M. Pinti, B. Bhushan, Theory, fabrication and applications of microfluidic and nanofluidic biosensors, Phil. Trans. R. Soc. A 370 (2012) 2269-2303

[28]   T.M. Squires, R.J. Messinger, S.R. Manalis, Making it stick: convection, reaction and diffusion in surface-based biosensors, Nat. Biotechnol. 26 (2008) 417

[29]   S.-J.J. Lee, N. Sundararajan, Microfabrication for Microfluidics, Artech House, 2010.

[30]   L.R. Volpatti, A.K. Yetisen, Commercialization of microfluidic devices, Trends Biotechnol. 32 (2014) 347-350

[31]   A.T. Ciftlik, H.-A. Lehr, M.A.M. Gijs, Microfluidic processor allows rapid HER2 immunohistochemistry of breast carcinomas and significantly reduces ambiguous (2+) read-outs, Proc. Natl. Acad. Sci. U.S.A. 110 (2013) 5363-5368

[32]   A.T. Ciftlik, M.A.M. Gijs, Parylene to silicon nitride bonding for post-integration of high pressure microfluidics to CMOS devices, Lab. Chip. 12 (2011) 396-400

[33]   A. Pinato, Reliability and parylene encapsulation of organic devices, Universita Degli Studi Di Padova, Italy, 2011.

[34]   Y. Cai, L. Yang, H. Zhang, Y. Wang, Laser cutting silicon-glass double layer wafer with laser induced thermal-crack propagation, Optics and Lasers in Engineering 82 (2016) 173-185

[35]   F. Östlund, K. Rzepiejewska-Malyska, K. Leifer, L.M. Hale, Y. Tang, R. Ballarini, W.W. Gerberich, J. Michler, Brittle-to-Ductile Transition in Uniaxial Compression of Silicon Pillars at Room Temperature, Adv. Funct. Mater. 19 (2009) 2439-2444

[36]   P. Moran, The Interpretation of Statistical Maps, Journal of the Royal Statistical Society Series B-Statistical Methodology 10 (1948) 243-251

[37]   L. Anselin, Local Indicators of Spatial Association—LISA, Geographical Analysis 27 (1995) 93-115

[38]   D.E. Impoinvil, T. Solomon, W.W. Schluter, A. Rayamajhi, R.P. Bichha, G. Shakya, C. Caminade, M. Baylis, The Spatial Heterogeneity between Japanese Encephalitis Incidence Distribution and Environmental Variables in Nepal, PLoS One 6 (2011) e22192

[39]   D. Pinkel, T. Straume, J.W. Gray, Cytogenetic analysis using quantitative, high-sensitivity, fluorescence hybridization., Proc. Natl. Acad. Sci. U. S. A. 83 (1986) 2934-2938

[40]   D.C. Tkachuk, D. Pinkel, W.L. Kuo, H.U. Weier, J.W. Gray, Clinical applications of fluorescence in situ hybridization, Genet. Anal. Tech. Appl. 8 (1991) 67-74

[41]   D.O. Wang, A. Okamoto, ECHO probes: Fluorescence emission control for nucleic acid imaging, Journal of Photochemistry and Photobiology C-Photochemistry Reviews 13 (2012) 112-123

[42]   B.J. Beliveau, E.F. Joyce, N. Apostolopoulos, F. Yilmaz, C.Y. Fonseka, R.B. McCole, Y. Chang, J.B. Li, T.N. Senaratne, B.R. Williams, J.-M. Rouillard, C.-t. Wu, Versatile design and synthesis platform for visualizing genomes with Oligopaint FISH probes, Proc. Natl. Acad. Sci. U.S.A. 109 (2012) 21301-21306
[43]   Y. Saito, K. Imai, R. Nakamura, H. Nanjo, K. Terata, H. Konno, Y. Akagami, Y. Minamiya, Novel method for rapid in-situ hybridization of HER2 using non-contact alternating-current electric-field mixing, Sci. Rep. 6 (2016)
[44]   S.H. Matthiesen, C.M. Hansen, Fast and Non-Toxic In Situ Hybridization without Blocking of Repetitive Sequences, PLoS One 7 (2012) e40675
[45]   V.J. Sieben, C.S. Debes Marun, P.M. Pilarski, G.V. Kaigala, L.M. Pilarski, C.J. Backhouse, FISH and chips: chromosomal analysis on microfluidic platforms, IET nanobiotechnology 1 (2007) 27-35
[46]   V.J. Sieben, C.S. Debes-Marun, L.M. Pilarski, C.J. Backhouse, An integrated microfluidic chip for chromosome enumeration using fluorescence in situ hybridization, Lab. Chip. 8 (2008) 2151-2156
[47]   D. Huber, J. Autebert, G.V. Kaigala, Micro fluorescence in situ hybridization (µFISH) for spatially multiplexed analysis of a cell monolayer, Biomed. Microdevices 18 (2016) 40
[48]   K. Perez-Toralla, G. Mottet, E.T. Guneri, J. Champ, F.-C. Bidard, J.-Y. Pierga, J. Klijanienko, I. Draskovic, L. Malaquin, J.-L. Viovy, S. Descroix, FISH in chips: turning microfluidic fluorescence in situ hybridization into a quantitative and clinically reliable molecular diagnosis tool, Lab. Chip. 15 (2015) 811-822
[49]   A. Zanardi, D. Bandiera, F. Bertolini, C.A. Corsini, G. Gregato, P. Milani, E. Barborini, R. Carbone, Miniaturized FISH for screening of onco-hematological malignancies, Biotechniques 49 (2010) 497-504
[50]   S.S.Y. Ho, C. Chua, L. Gole, A. Biswas, E. Koay, M. Choolani, Same-day prenatal diagnosis of common chromosomal aneuploidies using microfluidics-fluorescence in situ hybridization, Prenat. Diagn. 32 (2012) 321-328
[51]   I. Vedarethinam, P. Shah, M. Dimaki, Z. Tumer, N. Tommerup, W.E. Svendsen, Metaphase FISH on a chip: miniaturized microfluidic device for fluorescence in situ hybridization, Sensors (Basel) 10 (2010) 9831-9846
[52]   P. Liu, R.J. Meagher, Y.K. Light, S. Yilmaz, R. Chakraborty, A.P. Arkin, T.C. Hazen, A.K. Singh, Microfluidic fluorescence in situ hybridization and flow cytometry (µFlowFISH), Lab. Chip. 11 (2011) 2673-2679
[53]   M. Wu, M. Piccini, C.-Y. Koh, K.S. Lam, A.K. Singh, Single Cell MicroRNA Analysis Using Microfluidic Flow Cytometry, PLoS One 8 (2013) e55044
[54]   K. Sato, Microdevice in Cellular Pathology: Microfluidic Platforms for Fluorescence *in situ* Hybridization and Analysis of Circulating Tumor Cells, Anal. Sci. 31 (2015) 867-873
[55]   C.L. Vogel, M.A. Cobleigh, D. Tripathy, J.C. Gutheil, L.N. Harris, L. Fehrenbacher, D.J. Slamon, M. Murphy, W.F. Novotny, M. Burchmore, S. Shak, S.J. Stewart, M. Press, Efficacy and safety of trastuzumab as a single agent in first-line treatment of HER2-overexpressing metastatic breast cancer, J. Clin. Oncol. 20 (2002) 719-726
[56]   C. Helwick, Repeat FISH Testing Not Cost-Effective for Her-2/neu Determination, in: M.M. News (Ed.) American Society for Clinical Pathology (ASCP) 2009 Annual Meeting, Medscape Medical News, Chicago, Illinois, 2009, p. Abstract 86.
[57]   B. Carlson, HER2 TESTS: How Do We Choose?, Biotechnology healthcare 5 (2008) 23-27
[58]   N. Dendukuri, K. Khetani, M. McIsaac, J. Brophy, Testing for HER2-positive breast cancer: a systematic review and cost-effectiveness analysis, Can. Med. Assoc. J. 176 (2007) 1429-1434
[59]   A.C. Wolff, M.E.H. Hammond, D.G. Hicks, M. Dowsett, L.M. McShane, K.H. Allison, D.C. Allred, J.M.S. Bartlett, M. Bilous, P. Fitzgibbons, W. Hanna, R.B. Jenkins, P.B. Mangu, S. Paik, E.A. Perez, M.F. Press, P.A. Spears, G.H. Vance, G. Viale, D.F. Hayes, Recommendations for Human Epidermal Growth Factor Receptor 2 Testing in Breast Cancer: American Society of Clinical Oncology/College of American Pathologists Clinical Practice Guideline Update, J. Clin. Oncol. 31 (2013) 3997-4013
[60]   F. Penault-Llorca, A. Vincent-Salomon, G. MacGrogan, P. Roger, I. Treilleux, A. Valent, M.-C. Mathieu, M. Antoine, V. Becette, C. Bor, E. Brabencova, E. Charafe-Jauffret, M.-P. Chenard, M.-M. Dauplat, P. Delrée, M. Devouassoux, M. Fiche, M.-E. Fondrevelle, V. Fridman, C. Garbar, P. Genin, J.-P.

Ghnassia, J. Haudebourg, S. Laberge-Le Couteulx, D. Loussouarn, A. Maran-Gonzalez, M. Marcy, P. Michenet, B. Poulet, C. Sagan, M. Trassard, V. Verriele, L. Arnould, M. Lacroix-Triki, Mise à jour 2014 des recommandations du GEFPICS pour l'évaluation du statut HER2 dans les cancers du sein en France, Ann. Pathol. 34 (2014) 352-365

[61] K.-J. Kao, C.-H. Tai, W.-H. Chang, T.-S. Yeh, T.-C. Chen, G.-B. Lee, A fluorescence in situ hybridization (FISH) microfluidic platform for detection of HER2 amplification in cancer cells, Biosens. Bioelectron. 69 (2015) 272-279

[62] D.G. Dupouy, A.T. Ciftlik, M. Fiche, D. Heintze, B. Bisig, L. de Leval, M.A.M. Gijs, Continuous quantification of HER2 expression by microfluidic precision immunofluorescence estimates HER2 gene amplification in breast cancer, Sci. Rep. 6 (2016) 20277

[63] R.S. Sirohi, Introduction to Optical Metrology, CRC Press, 2015.

[64] A.E. Carpenter, T.R. Jones, M.R. Lamprecht, C. Clarke, I. Kang, O. Friman, D.A. Guertin, J. Chang, R.A. Lindquist, J. Moffat, P. Golland, D.M. Sabatini, CellProfiler: image analysis software for identifying and quantifying cell phenotypes, Genome Biol. 7 (2006) R100

[65] J. Schindelin, I. Arganda-Carreras, E. Frise, V. Kaynig, M. Longair, T. Pietzsch, S. Preibisch, C. Rueden, S. Saalfeld, B. Schmid, J.-Y. Tinevez, D.J. White, V. Hartenstein, K. Eliceiri, P. Tomancak, A. Cardona, Fiji: an open-source platform for biological-image analysis, Nat. Methods 9 (2012) 676-682

[66] W.M. Hanna, J. Rüschoff, M. Bilous, R.A. Coudry, M. Dowsett, R.Y. Osamura, F. Penault-Llorca, M. van de Vijver, G. Viale, HER2 in situ hybridization in breast cancer: clinical implications of polysomy 17 and genetic heterogeneity, Mod. Pathol. 27 (2014) 4-18

[67] J. Vanderhoeven, K. Pappaert, B. Dutta, P. Van Hummelen, G. Desmet, DNA microarray enhancement using a continuously and discontinuously rotating microchamber, Anal. Chem. 77 (2005) 4474-4480

[68] L.P. Middleton, K.M. Price, P. Puig, L.J. Heydon, E. Tarco, N. Sneige, K. Barr, M.T. Deavers, Implementation of American Society of Clinical Oncology/College of American Pathologists HER2 Guideline Recommendations in a Tertiary Care Facility Increases HER2 Immunohistochemistry and Fluorescence In Situ Hybridization Concordance and Decreases the Number of Inconclusive Cases, Arch. Pathol. Lab. Med. 133 (2009) 775-780

[69] J.T. Jørgensen, S. Møller, B.B. Rasmussen, H. Winther, A. Schønau, A. Knoop, High Concordance Between Two Companion Diagnostics Tests, Am. J. Clin. Pathol. 136 (2011) 145-151

[70] H. Yaziji, L.C. Goldstein, T.S. Barry, R. Werling, H. Hwang, G.K. Ellis, J.R. Gralow, R.B. Livingston, A.M. Gown, HER-2 testing in breast cancer using parallel tissue-based methods, JAMA 291(16) (2004) 1972-7

[71] N. Dybdal, G. Leiberman, S. Anderson, B. McCune, A. Bajamonde, R.L. Cohen, R.D. Mass, C. Sanders, M.F. Press, Determination of HER2 gene amplification by fluorescence in situ hybridization and concordance with the clinical trials immunohistochemical assay in women with metastatic breast cancer evaluated for treatment with trastuzumab, Breast Cancer Res. Treat. 93 (2005) 3-11

[72] J. Cohen, A coefficient of agreement for nominal scales, Educ. Psychol. Meas. 20 (1960) 37-46

[73] G.L. Lukacs, P. Haggie, O. Seksek, D. Lechardeur, N. Freedman, A.S. Verkman, Size-dependent DNA mobility in cytoplasm and nucleus, The Journal of Biological Chemistry 275 (2000) 1625-1629

[74] D.L. Holliday, V. Speirs, Choosing the right cell line for breast cancer research, Breast Cancer Res 13 (2011) 215

[75] G.E.P. Box, J.S. Hunter, W.G. Hunter, Statistics for Experimenters: Design, Innovation, and Discovery, 2nd Edition, 2nd edition ed., Wiley-Interscience, Hoboken, N.J, 2005.

[76] J.M.S. Bartlett, M. Ibrahim, B. Jasani, J.M. Morgan, I. Ellis, E. Kay, Y. Connolly, F. Campbell, A. O'Grady, S. Barnett, K. Miller, External Quality Assurance of HER2 FISH and ISH TestingThree Years of the UK National External Quality Assurance Scheme, Am. J. Clin. Pathol. 131 (2009) 106-111

[77] W.M. Hanna, K. Kwok, Chromogenic in-situ hybridization: a viable alternative to fluorescence in-situ hybridization in the HER2 testing algorithm, Mod. Pathol. 19 (2006) 481-487

[78] J.M.S. Bartlett, J. Starczynski, N. Atkey, E. Kay, A. O'Grady, M. Gandy, M. Ibrahim, B. Jasani, I.O. Ellis, S.E. Pinder, R.A. Walker, HER2 testing in the UK: recommendations for breast and gastric in-situ hybridisation methods, J. Clin. Pathol. 64 (2011) 649-653

[79]   E.A. Perez, J. Cortés, A.M. Gonzalez-Angulo, J.M.S. Bartlett, HER2 testing: Current status and future directions, Cancer Treat. Rev. 40 (2014) 276-284

[80]   K.M. Heselmeyer-Haddad, L.Y. Berroa Garcia, A. Bradley, L. Hernandez, Y. Hu, J.K. Habermann, C. Dumke, C. Thorns, S. Perner, E. Pestova, C. Burke, S.A. Chowdhury, R. Schwartz, A.A. Schäffer, P.L. Paris, T. Ried, Single-Cell Genetic Analysis Reveals Insights into Clonal Development of Prostate Cancers and Indicates Loss of PTEN as a Marker of Poor Prognosis, Am J Pathol 184 (2014) 2671-2686

[81]   L.L.d. Matos, D.C. Trufelli, M.G.L. de Matos, M.A. da Silva Pinhal, Immunohistochemistry as an important tool in biomarkers detection and clinical practice, Biomark Insights 5 (2010) 9-20

[82]   C. Ericsson, B. Franzén, M. Nistér, Frozen tissue biobanks. Tissue handling, cryopreservation, extraction, and use for proteomic analysis, Acta Oncol. 45 (2006) 643-661

[83]   Z. Yang, Y. Chevolot, T. Géhin, J. Solassol, A. Mange, E. Souteyrand, E. Laurenceau, Improvement of protein immobilization for the elaboration of tumor-associated antigen microarrays: application to the sensitive and specific detection of tumor markers from breast cancer sera, Biosens. Bioelectron. 40 (2013) 385-392

[84]   V. Dorfer, P. Pichler, T. Stranzl, J. Stadlmann, T. Taus, S. Winkler, K. Mechtler, MS Amanda, a Universal Identification Algorithm Optimized for High Accuracy Tandem Mass Spectra, J. Proteome Res. 13 (2014) 3679-3684

[85]   J. Rappsilber, M. Mann, Y. Ishihama, Protocol for micro-purification, enrichment, pre-fractionation and storage of peptides for proteomics using StageTips, Nat. Protoc. 2 (2007) 1896-1906

[86]   H. Guo, W. Liu, Z. Ju, P. Tamboli, E. Jonasch, G.B. Mills, Y. Lu, B.T. Hennessy, D. Tsavachidou, An efficient procedure for protein extraction from formalin-fixed, paraffin-embedded tissues for reverse phase protein arrays, Proteome Sci. 10 (2012) 56

[87]   Z. Yang, Y. Chevolot, Y. Ataman-Önal, G. Choquet-Kastylevsky, E. Souteyrand, E. Laurenceau, Cancer biomarkers detection using 3D microstructured protein chip: Implementation of customized multiplex immunoassay, Sensors Actuators B: Chem. 175 (2012) 22-28

[88]   L. Shi, T. Gehin, Y. Chevolot, E. Souteyrand, A. Mangé, J. Solassol, E. Laurenceau, Anti-heat shock protein autoantibody profiling in breast cancer using customized protein microarray, Anal. Bioanal. Chem. 408 (2016) 1497-1506

[89]   L.-K. Huang, M.-J.J. Wang, Image thresholding by minimizing the measures of fuzziness, Pattern Recognit. 28 (1995) 41-51

[90]   W.-S. Chu, Q. Liang, J. Liu, M.Q. Wei, M. Winters, L. Liotta, G. Sandberg, M. Gong, A nondestructive molecule extraction method allowing morphological and molecular analyses using a single tissue section, Lab. Invest. 85 (2005) 1416-1428

[91]   Y. Kawashima, Y. Kodera, A. Singh, M. Matsumoto, H. Matsumoto, Efficient extraction of proteins from formalin-fixed paraffin-embedded tissues requires higher concentration of tris(hydroxymethyl)aminomethane, Clin. Proteomics 11 (2014) 4

[92]   S.-R. Shi, C. Liu, B.M. Balgley, C. Lee, C.R. Taylor, Protein Extraction from Formalin-fixed, Paraffin-embedded Tissue Sections: Quality Evaluation by Mass Spectrometry, J. Histochem. Cytochem. 54 (2006) 739-743

[93]   N.F. Dovnik, I. Takac, Prognostic significance of uPA/PAI-1 level, HER2 status, and traditional histologic factors for survival in node-negative breast cancer patients, Radiol Oncol. 51 (2016) 65-73

[94]   N.B. Serce, A. Boesl, I. Klaman, S. von Serényi, E. Noetzel, M.F. Press, A. Dimmler, A. Hartmann, J. Sehouli, R. Knuechel, M.W. Beckmann, P.A. Fasching, E. Dahl, Overexpression of SERBP1 (Plasminogen activator inhibitor 1 RNA binding protein) in human breast cancer is correlated with favourable prognosis, BMC Cancer 12 (2012) 597

[95]   H.T. Nguyen, R. Trouillon, S. Matsuoka, M. Fiche, L. de Leval, B. Bisig, M.A. Gijs, Microfluidics-assisted fluorescence in situ hybridization for advantageous human epidermal growth factor receptor 2 assessment in breast cancer, Laboratory Investigation; a Journal of Technical Methods and Pathology 97 (2017) 93-103

[96]   F. Pauly, L. Dexlin-Mellby, S. Ek, M. Ohlin, N. Olsson, K. Jirström, M. Dictor, S. Schoenmakers, C.A.K. Borrebaeck, C. Wingren, Protein Expression Profiling of Formalin-Fixed Paraffin-Embedded Tissue Using Recombinant Antibody Microarrays, J. Proteome Res. 12 (2013) 5943-5953

[97]   R. Fisher, L. Pusztai, C. Swanton, Cancer heterogeneity: implications for targeted therapeutics, Br. J. Cancer 108 (2013) 479-485

[98]   H. Seol, H.J. Lee, Y. Choi, H.E. Lee, Y.J. Kim, J.H. Kim, E. Kang, S.-W. Kim, S.Y. Park, Intratumoral heterogeneity of HER2 gene amplification in breast cancer: its clinicopathological significance, Mod. Pathol. 25 (2012) 938-948

[99]   N.E. Buckley, C. Forde, D.G. McArt, D.P. Boyle, P.B. Mullan, J.A. James, P. Maxwell, S. McQuaid, M. Salto-Tellez, Quantification of HER2 heterogeneity in breast cancer-implications for identification of sub-dominant clones for personalised treatment, Sci. Rep. 6 (2016) 23383

[100]   D.G. Dupouy, A.T. Ciftlik, M. Fiche, D. Heintze, B. Bisig, L.d. Leval, M.A.M. Gijs, Continuous quantification of HER2 expression by microfluidic precision immunofluorescence estimates *HER2* gene amplification in breast cancer, Sci. Rep. 6 (2016) srep20277

[101]   H. Netten, I.T. Young, L.J. van Vliet, H.J. Tanke, H. Vroljik, W.C.R. Sloos, FISH and chips: Automation of fluorescent dot counting in interphase cell nuclei, Cytometry 28 (1997) 1-10

[102]   G. Kiszler, L. Krecsák, A. Csizmadia, T. Micsik, D. Szabó, V. Jónás, V. Prémusz, T. Krenács, B. Molnár, Semi-automatic FISH quantification on digital slides, Diagn. Pathol. 8 (2013) S21

[103]   M. Daniely, T. Kaplan, E. Kaplan, A. Freiberger, Methods of detecting cancer cells in biological samples, Bioview Ltd., 2004.

[104]   R.A. Knudson, B.M. Shearer, R.P. Ketterling, Automated Duet spot counting system and manual technologist scoring using dual-fusion fluorescence in situ hybridization (D-FISH) strategy: comparison and application to FISH minimal residual disease testing in patients with chronic myeloid leukemia, Cancer Genet. Cytogenet. 175 (2007) 8-18

[105]   D. Furrer, S. Jacob, C. Caron, F. Sanschagrin, L. Provencher, C. Diorio, Validation of a new classifier for the automated analysis of the human epidermal growth factor receptor 2 (HER2) gene amplification in breast cancer specimens, Diagn. Pathol. 8 (2013) 17

[106]   C. Öhlschlegel, D. Kradolfer, M. Hell, W. Jochum, Comparison of automated and manual FISH for evaluation of HER2 gene status on breast carcinoma core biopsies, BMC Clin. Pathol. 13 (2013) 13

[107]   E.M.J. van der Logt, D.A.J. Kuperus, J.W. van Setten, M.C. van den Heuvel, J.E. Boers, E. Schuuring, R.E. Kibbelaar, Fully automated fluorescent in situ hybridization (FISH) staining and digital analysis of HER2 in breast cancer: a validation study, PLoS One 10 (2015) e0123201

[108]   Q. Zhong, J.H. Rüschoff, T. Guo, M. Gabrani, P.J. Schüffler, M. Rechsteiner, Y. Liu, T.J. Fuchs, N.J. Rupp, C. Fankhauser, J.M. Buhmann, S. Perner, C. Poyet, M. Blattner, D. Soldini, H. Moch, M.A. Rubin, A. Noske, J. Rüschoff, M.C. Haffner, W. Jochum, P.J. Wild, Image-based computational quantification and visualization of genetic alterations and tumour heterogeneity, Sci. Rep. 6 (2016) srep24146

[109]   S.J. Potts, J.S. Krueger, N.D. Landis, D.A. Eberhard, G.D. Young, S.C. Schmechel, H. Lange, Evaluating tumor heterogeneity in immunohistochemistry-stained breast cancer tissue, Laboratory Investigation; a Journal of Technical Methods and Pathology 92 (2012) 1342-1357

[110]   M.E. Vandenberghe, M.L.J. Scott, P.W. Scorer, M. Söderberg, D. Balcerzak, C. Barker, Relevance of deep learning to facilitate the diagnosis of HER2 status in breast cancer, Sci. Rep. 7 (2017) 45938

[111]   S. Kurozumi, M. Padilla, M. Kurosumi, H. Matsumoto, K. Inoue, J. Horiguchi, I. Takeyoshi, T. Oyama, J. Ranger-Moore, D.C. Allred, E. Dennis, H. Nitta, HER2 intratumoral heterogeneity analyses by concurrent HER2 gene and protein assessment for the prognosis of HER2 negative invasive breast cancer patients, Breast Cancer Res. Treat. 158 (2016) 99-111

List of abbreviations

Ab: antibody

Abs: antibodies

AF594: Alexa Fluor 594

AF647: Alexa Fluor 647

AP: alkaline phosphatase

ANOVA: analysis of variance

BCA: bicinchoninic acid

CEN17: centromere of chromosome 17

CEP17: centromere enumeration probe 17

CK: cytokeratin

CVD: chemical vapor deposition

CSC: cancer stem cell

DAB: 3,3'-diaminobenzidine

DAPI: 4, 6-diamidino-2-phenylindole

DCIS: ductal carcinoma in situ

DMC: detection microfluidic chip

DNA: Deoxyribonucleic acid

DRIE: deep reactive ion etching

ECR: extraction-to-control ratio

ELISA: enzyme-linked immunosorbent assay

ESIMA-FISH: extra-short incubation microfluidic-assisted fluorescence in situ hybridization

ER: estrogen receptor

FFPE: formalin-fixed paraffin-embedded

FITC: fluorescein isothiocyanate

FISH: fluorescence in situ hybridization

HE: hematoxylin & eosin

HER2: human epithelial growth factor receptor

HH: High - High

HL: High - Low

HRP: Horseradish peroxidase

IF: immunofluorescence

IHC: Immunohistochemistry

IQ-FISH: instant-quality fluorescence in situ hybridization

ITH: intratumoral heterogeneity

ISH: in situ hybridization

LC-MS/MS: liquid chromatography tandem-mass spectrometry

LH: Low - High

LL: Low - Low

MA-CISH: microfluidic-assistance chromogenic in situ hybridization

MA-FISH: microfluidic-assistance fluorescence in situ hybridization

MES: 2-[N-morpholino] ethanesulfonic acid

MTP: microfluidic tissue processor

PAI1: plasminogen activator inhibitor 1

PBS: phosphate buffer saline

PDMS: polydimethylsiloxane

PR: progesterone receptor

PVD: physical vapor deposition

RNA: ribonucleic acid

ROI: region of interest

TC: tumor cell

TCs: tumor cells

TME: tumor microenvironment

uPA: urokinase plasminogen activator

SD: standard deviation

SDS-PAGE: sodium dodecyl sulfate-polyacrylamide gel electrophoresis

SSC: sodium-saline citrate

Huu Tuan Nguyen

EPFL	Tel. :	+41 (0)21 693 65 85
STI / IMT / LMIS 2	Fax :	+41 (0)21 693 59 50
Station 17	E-mail :	Huu.nguyen@epfl.ch
CH – 1015 Lausanne	Office:	BM3131 (bâtiment BM)
	ORCHID ID:	0000-0001-6130-2828

CURRICULUM VITAE

RESEARCH INTERESTS

Microfluidic technology for cancer diagnostics and treatment

EDUCATION

10.2013-present   École Polytechnique Fédérale de Lausanne - EPFL, Switzerland

Ph.D., microsystems et microelectronics

Thesis: Improvement of breast cancer diagnosis through microfluidics

Advisor: Prof. Martin A.M. Gijs

09.2012-09.2013   INSA (Institut national des sciences appliquées) de Lyon – INSA Lyon, École Central de Lyon, Université Claude Bernard Lyon 1, France

Joint M.Sc. program in micro and nanotechnology

Thesis: Development of microfluidic components for biological detection

Advisor: Prof. Pascal Perriat (INSA de Lyon, France) and Dr. Wu Ruige (Simtech, Singapore)

09.2010-09.2013   INSA de Lyon, France

French diploma of Engineering (French-"diplôme d'ingénieur") in materials science and engineering

09.2008-09.2010   INSA de Rennes, France

General science courses (French -"classe préparatoire") for French diploma of Engineering

INSTITUTIONAL RESPONSIBILITIES

09.2014-09.2016   Faculty council member of School of Engineering (STI), EPFL

WORK EXPERIENCES

09.2014-01.2017   Teaching assistant for clean room practical section (Micro-332), EPFL, Switzerland

04.2013-09.2013	Master thesis - Singapore Institute of Manufacturing Technology, Singapore
09.2012-03.2013	Semester project - Lyon Institute of Nanotechnology, France
06.2012-08.2012	Research assistant - MATEIS laboratory (Material sciences), INSA de Lyon, France
06.2009-07.2009	Intern – Laboratory of civil and mechanical engineering, INSA de Rennes, France

SKILLS

| Languages | Vietnamese (mother tongue), French (fluent), English (fluent) |
| Engineering | Image processing (FIJI, CellProfiler); data Analysis (WEKA data mining); computer programming (Matlab, JAVA, Labview); mechanical design (Solidworks, Auto CAD); microfabrication in cleanroom; fluorescence microscope |

SUPERVISION OF STUDENTS/JUNIOR RESEARCHERS

02.2017-06.2017	Antoine J. Maxime, full-time intern
03.2016-07.2016	Laurène N. Dupont, master thesis student
02.2016-06.2016	Léa S. Bernier, semester project master student
02.2016-06.2016	Estelle A. Cuttaz, semester project bachelor student
09.2015-12.2015	Seiya Matsuoka, full-time intern

PRIZES, AWARDS, FELLOWSHIPS

05.2018	Swiss national science foundation post-doctoral fellowship at MIT, USA
09.2013	Master in nanoscale engineering with high honors
09.2011-09.2013	Odon Vallet scholarship for excellent engineering students
09.2009-09.2011	Among top 10% of the 2nd and 3rd year of University
09.2008-09.2009	Rank 1st of the 1st year of University
06.2008	French Baccalaureate (Sciences) with high honors
	Highest score at Hue University entrance exam (Math, Chemistry, Biology)
05.2007&05.2008	First and second prize in the math competition of Danang city, Vietnam

EXTRA-CURRICULUM ACTIVITIES

2013-15	Vice- and president of Vietnam student community in Lausanne (VNLausanne)
2011-12	Program director in Asian Week festival in INSA de Lyon
	Liaison officer in Rhône-Alpes Recruitment showroom (France)

PUBLISHED JOURNAL ARTICLES

- **Nguyen HT,** Dupont LN, Jean AM, Gehin T, Chevolot Y, Laurenceau E, Gijs MAM. Microfluidic extraction and microarray detection of biomarkers from cancer tissue slides, Journal of Micromechanics and Microengineering. http://iopscience.iop.org/article/10.1088/1361-6439/aaa7a1

- **Nguyen HT**, Dupont LN, Cuttaz EA, Jean AM, Trouillon R, Gijs MAM. Breast cancer HER2 analysis by extra-short incubation microfluidics-assisted fluorescence in situ hybridization (ESIMA FISH). Microelectron Eng. 2018. https://www.sciencedirect.com/science/article/pii/S0167931717303477
- **Nguyen HT**, Bernier LS, Jean AM, Trouillon R, Gijs MAM. Microfluidic-assisted chromogenic in situ hybridization (MA-CISH) for fast and accurate breast cancer diagnosis. Microelectron Eng. 2017. https://www.sciencedirect.com/science/article/pii/S0167931717304057
- **Nguyen HT**, Trouillon R, Matsuoka S, Fiche M, de Leval L, Bisig B, Gijs MAM. Microfluidics-assisted fluorescence in situ hybridization for advantageous human epidermal growth factor receptor 2 assessment in breast cancer. Lab Invest.2016. https://www.nature.com/articles/labinvest2016121
- Shaegh SAM, Wang Z, Ng SH, Wu R, **Nguyen HT**, Chan LCZ, Toh AGG & Wang Z. Plug-and-play microvalve and micro pump for rapid integration with microfluidic chips. Microfluid. Nanofluid. 2015. https://link.springer.com/article/10.1007/s10404-015-1582-4

UNPUBLISHED WORKS
- **Nguyen HT**, Migliozzi D, Bisig B, de Leval L, Gijs MAM. High-content, cell-by-cell assessment of HER2 overexpression and amplification in breast cancer tissues).

CONFERENCES
- **Nguyen HT**, Trouillon R, Matsuoka S, Fiche M, de Leval L, Bisig B, Gijs MAM. Fluorescence in situ hybridization (FISH) enhancement using microfluidic flow for an accurate, fast and economical assessment of her2 status in breast cancer. Microtas conference; Dublin, Ireland; 2016. Poster presentation.
- **Nguyen HT**, Bisig B, Dupont LN, Cuttaz EA, Trouillon R, de Leval L, Gijs MAM. Extra short incubation microfluidic assisted – fluorescence in situ hybridization (ESIMA-FISH). NanoBioTech; Montreux, Switzerland; 2016. Poster presentation.
- **Nguyen HT**, Dupont LN, Cuttaz EA, Jean AM, Trouillon R, Gijs MAM, Using microfluidics for advanced Fluorescence In-Situ Hybridization (FISH) in cancer diagnosis (MNE 2017). 43rd International Conference on Micro and NanoEngineering; Braga, Portugal; September 2017. Poster presentation.
- **Nguyen HT,** Bernier LS, Jean AM, Trouillon R, Gijs MAM, Microfluidics-assisted Chromogenic In Situ Hybridization (MA-CISH) for HER2 gene detection in breast cancer diagnosis. 43rd International Conference on Micro and NanoEngineering (MNE 2017); Braga, Portugal; September 2017. Poster presentation.
- Migliozzi D*, **Nguyen HT***, Gijs MAM, Cell-based quantification of the fluorescence signal from an ultra-fast microfluidic immunostaining: application to human breast cancer cell lines. Microfluidics, BioMEMS, and Medical Microsystems XVI conference. January 2018. Oral presentation. (* co-first author).

THESES
- **Nguyen HT**. Improvement of breast cancer diagnosis through microfluidics, Ph.D Thesis, April 2018, Lausanne, Switzerland (in preparation).
- **Nguyen HT**. Development of microfluidic components for biological detection, M.Sc Thesis, September 2013, SIMTech, Singapore.